The Versatile Chemistry of As_n Ligand Complexes

- Synthesis and Reactivity -

Dissertation

zur Erlangung des
DOKTORGRADES DER NATURWISSENSCHAFTEN
(Dr. rer. nat.)
der Naturwissenschaftlichen Fakultät IV – Chemie und Pharmazie
der Universität Regensburg

vorgelegt von
Monika Schmidt
aus Wenzenbach
Regensburg 2016

Diese Arbeit wurde von Prof. Dr. Manfred Scheer angeleitet.

Das Promotionsgesuch wurde am 9. September 2016 eingereicht.

Tag des wissenschaftlichen Kolloquiums: 18. November 2016

Prüfungskommission:

Vorsitzender: Prof. Dr. Arnd Vogler

1. Gutachter: Prof. Dr. Manfred Scheer

2. Gutachter: Prof. Dr. Henri Brunner

Weitere Prüfer: Prof. Dr. Frank-Michael Matysik

Universität Regensburg

Eidesstattliche Erklärung

Ich erkläre hiermit an Eides statt, dass ich die vorliegende Arbeit ohne unzulässige Hilfe Dritter und ohne Benutzung anderer als der angegebenen Hilfsmittel angefertigt habe; die aus anderen Quellen direkt oder indirekt übernommenen Daten und Konzepte sind unter Angabe des Literaturzitats gekennzeichnet.

…….

Monika Schmidt

This thesis was elaborated within the period from November 2011 till September 2016 at the Institute of Inorganic Chemistry at the University of Regensburg under the supervision of Prof. Dr. Manfred Scheer.

Results from collaborations, which are not mentioned within this work, have been published during the thesis:

M. Fleischmann, S. Welsch, H. Krauss, M. Schmidt, M. Bodensteiner, E. V. Peresypkina, M. Sierka, C. Gröger, M. Scheer, *Chem. Eur. J.* 2014, *20*, 3759-3768.

C. Schoo, S. Bestgen, M. Schmidt, S. N. Konchenko, M. Scheer, P. W. Roesky, *Chem. Commun.* 2016, *52*, 13217-13220.

“Our heads are round so our thoughts can change direction.“

Francis-Marie Martinez Picabia

To my family

Preface

A general introduction about As_n ligand complexes and their relevance in organometallic chemistry is given at the beginning of this thesis. In this context, the research objectives and some general considerations about the Cp^{Bn} ligand, which is frequently used in this work, are also described. As each chapter presents a topic on its own, a short introduction is included at the beginning of each to present the current state of research. The results of these chapters are suitable for publication in the future or are on the brink of being published. Moreover, each chapter contains the section author contribution, in which the extent of involvement is described. Here, results from collaborations are also stated. For a uniform design of this thesis, all chapters possess the same layout (text settings, pictures, subchapters) and the numbering for compounds, figures, schemes and tables begins anew each chapter. In addition, a graphical abstract has been created for each chapter and a comprehensive summary on the topics is presented at the end of the thesis.

Table of Contents

1. Introduction

1.1 Arsenic and its Relevance in Organometallic Chemistry

Arsenic is a Janus faced element. On the one hand, arsenic and its derivatives have found many applications in pharmaceutical industry, agriculture (herbicides and insecticides) and forestry as well as in the semiconductor industry (e.g. GaAs semiconductors) (Figure 1.1).[1] On the other hand, especially the so called white arsenic (As_2O_3) caused many murders and harm through the centuries.[2]

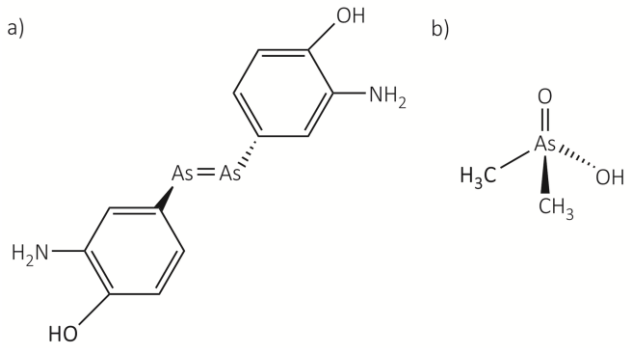

Figure 1.1 Historically important arsenic derivatives. a) Arsphenamine[1a] (Salvarsan®, medication for syphilis) and b) dimethylarsinic acid[1b] (used as a total herbicide and desiccant in agriculture).

Although the poisonous nature of arsenic minerals has been known since the Greeks, the element arsenic itself was first identified by Albertus Magnus around 1250.[3] Grey or metallic arsenic (As_{grey}) consists of undulated layers, which are held together by condensed As_6 rings (Figure 1.2). Therefore, As_{grey} is structurally related to the rhombohedral form of black phosphorus at high pressure. In addition, two further allotropic modifications of arsenic exist: black arsenic and yellow arsenic. The latter was first described by Bettendorf in 1867.[4] Gaseous yellow arsenic can be obtained by heating grey arsenic up to 616°C[3,4,5] and is built up by discrete tetrahedral As_4 molecules (Figure 1.2).[6] Similar to white phosphorus (P_4), it represents the most reactive allotrope, but also the most toxic and least stable one. Nowadays, several modifications of As_4 (crystalline and amorphous) are known, but especially its light sensitivity and therefore its fast decomposition to amorphous grey arsenic makes its investigation and also its use as a starting material difficult.

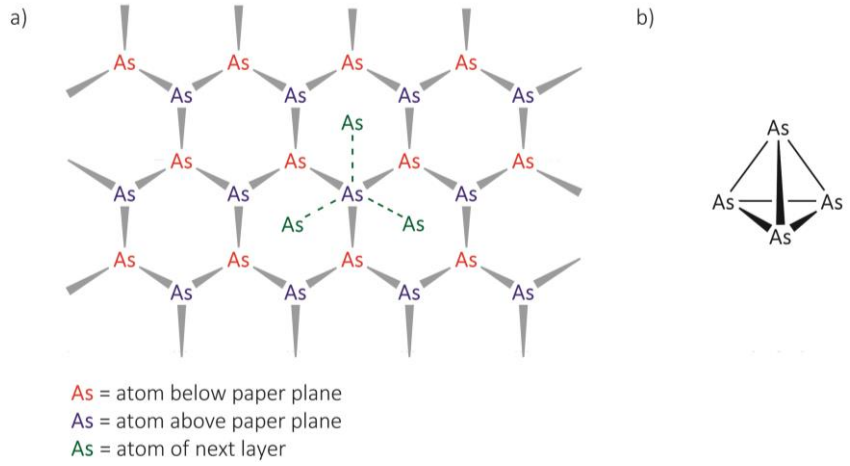

Figure 1.2 Structures of a) grey arsenic and b) yellow arsenic.[3]

The latest allotrope is black arsenic. It has first been mentioned in 1957[7] and can be divided into two subgroups, amorphous and orthorhombic black arsenic. The orthorhombic form is closely related to black phosphorus at atmospheric pressure. Furthermore, the orthorhombic black arsenic is also known as the mineral arsenolamprite in nature.[3]

In addition to the well-known allotropic modifications, especially theoretical studies predict elemental nanostructures of arsenic. Thereby, icosahedral and ring shaped arsenic cages[8] as well as nanotubes[9] are discussed. However, this is only mentioned for completeness and will not be further discussed.

Due to its high reactivity, particularly yellow arsenic found application in organometallic chemistry. Nevertheless, the first As_n ligand complexes were synthesised by using uncommon arsenic sources like $AsCl_3$ and *cyclo*-$(AsMe)_5$, respectively.[10] Hence, $[Co_2(CO)_5(PPh_3)(\mu,\eta^{2:2}\text{-}As_2)]$ ($PPh_3 = P(C_6H_5)_3$) and $[Co(CO)_3(\eta^3\text{-}As_3)]$ opened the new era of unsubstituted naked group 15 element ligand complexes in the late 1960s (Figure 1.3).[11]

About ten years later, Hoffmann postulated the isolobal analogy. The message of this concept is that:

> *'…we will call two fragments isolobal if the number, symmetry properties, approximate energy and shape of the frontier orbitals and the number of electrons in them are similar – not identical, but similar.'*[12]

Therefore, a methine group, for example, can be considered to be isolobal with arsenic and with a $d^9\text{-}ML_3$ fragment, respectively (Figure 1.3). Since that time, this fact has extensively been used to explain and to predict new compounds and represents a connection between inorganic

and organic chemistry. Accordingly, the cyclopentadienyl anion $[C_5H_5]^-$ is formally isolobal with the pentaarsolyl anion [*cyclo*-$As_5]^-$. In this context, $[Cp^RFe(\eta^5\text{-}As_5)]$ (Cp^R = Cp*(η^5-C_5Me_5) (**I**), Cp' (η^5-C_5EtMe_4))[13] can be described as the heavier analogue of the well-known ferrocene $[Cp_2Fe]$ (Cp = η^5-C_5H_5) (Figure 1.3).

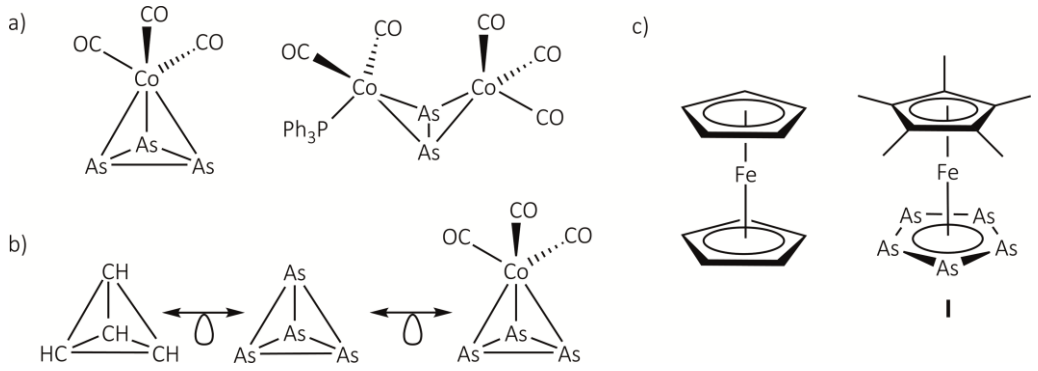

Figure 1.3 Illustration of a) $[Co(CO)_3(\eta^3\text{-}As_3)]$ (left) and $[Co_2(CO)_5(PPh_3)(\mu,\eta^{2:2}\text{-}As_2)]$ (right). b) Isolobal analogy between 'CH', 'As' and d^9-ML_3 fragments. c) $[Cp_2Fe]$ (left) and its heavier analogue $[Cp^*Fe(\eta^5\text{-}As_5)]$ (**I**) (right).

Since 1985, As_n ligand complexes have attracted more and more organometallic chemists and a variety of complexes with different coordination modes were obtained (Figure 1.4).[14] Generally, the As_4 tetrahedron often undergoes degradation, and complexes containing smaller As_n units can be isolated. However, also a subsequent aggregation to larger arsenic frameworks can take place, as it will be shown later on. Usually, cyclopentadienyl containing transition metal carbonyl complexes of the type $[Cp^RM(CO)_x]_y$ are suitable precursors for this purpose. Recently, the use of transition metal complexes with labile ligands, e.g. compounds of the general formula $[Cp^R_xM_y(L)_z]$ (L = e.g. toluene), got popular. To date, the largest fully characterised neutral As_n ligand complex $[(Cp'''Co)_3(\mu_3,\eta^{4:4:2:1}\text{-}As_{12})]$ (Cp''' = η^5-1,2,4-$C_5H_2{}^tBu_3$) was prepared by this way. It was obtained by the reaction of As_4 with $[(Cp'''Co)_2(\mu,\eta^{4:4}\text{-toluene})]$ at room temperature (Figure 1.4).[15]

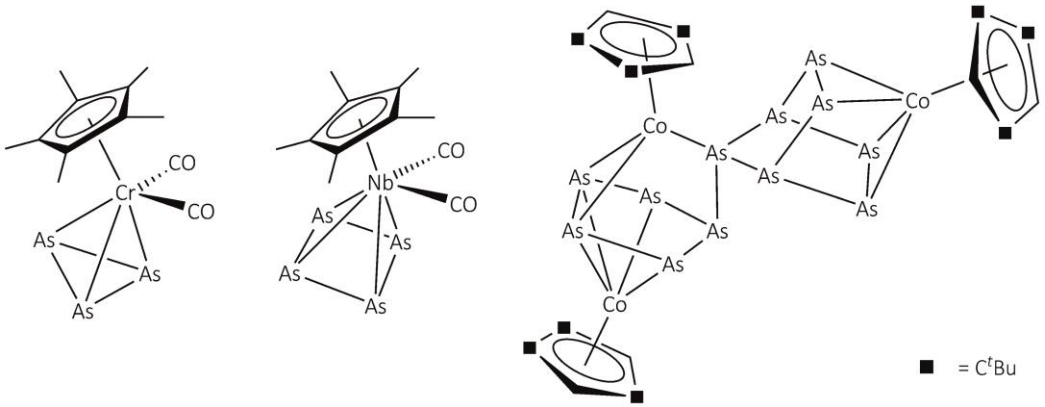

Figure 1.4 Selected neutral As_n ligand complexes (n = 3,[16] 4,[17] 12[15]).

In contrast, the smallest possible arsenic unit with only one arsenic atom can be realised in $[(N_3N)W{\equiv}As]$ ($N_3N = N(CH_2CH_2NSiMe_3)_3$).[18] However, in this reaction $LiAs(SiMe_3)_2$ is used as the arsenic source.

While the discussed complexes derive from degradation and aggregation, respectively, the stabilisation of the intact As_4 tetrahedron seems to be an insuperable challenge in the past. But quite recently, the synthesis of $[Ag(\eta^2\text{-}As_4)_2][TEF]$ (**II**) ($[TEF]^- = [Al\{OC(CF_3)_3\}_4]^-$) was presented by reacting the weakly coordinated silver (I) complex $[Ag(CH_2Cl_2)][TEF]$ with yellow arsenic.[19] Thereby, two As_4 units are coordinated in a η^2-fashion by one Ag^+ cation. Surprisingly, the As_4 unit can be transferred unscathed from **II** to a $[(PPh_3)Au]^+$ or a $[Cp^*Ru(dppe)]^+$ fragment (dppe = 1,2-bis(diphenylphosphino)ethane), respectively (Figure 1.5).[20] The latter reaction leads to the formation of $[Cp^*Ru(dppe)(\eta^1\text{-}As_4)][TEF]$, the first complex containing a monohapto coordinated As_4 ligand. At the same time, the arsenic tetrahedron still remains intact.

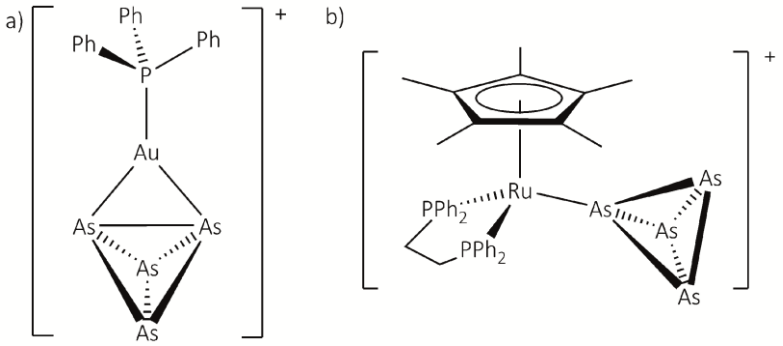

Figure 1.5 Schematic illustration of a) $[(PPh_3)Au(\eta^2\text{-}As_4)]^+$ and b) $[Cp^*Ru(dppe)(\eta^1\text{-}As_4)]^+$.

Hitherto, different transition metal precursors have been discussed. Thereby, the majority of the mentioned arsenic complexes carry Cp^R ligands. However, recently it could be shown that yellow arsenic can also be activated by unsaturated transition metal complexes bearing β-diketiminato ligands (Figure 1.6).[21]

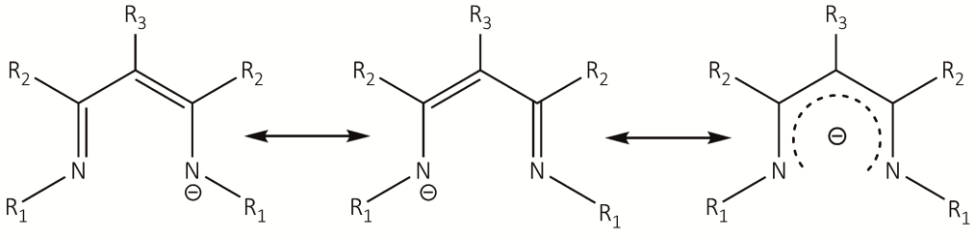

Figure 1.6 General formulas of the β-diketiminato ligands. Substituents R_1, R_2 and R_3 can be chosen depending on the required steric demand and electronic properties.

These ligands formally represent a five electron ligand like the Cp^R ligand. Due to the possible variation of the substituents, a novel group of complexes was born. Several small molecules like

N_2, P_4, S_8, Se_{red} and α-Te, respectively, could be activated by such complexes.[22] Recently, we reported on the fixation and release of E_4 (E = P, As) by [({N($C_6H_3^{i}Pr_2$-2,6)C(Me)}$_2$CH)Cu(CH_3CN)], carrying a labile acetonitrile ligand, which can easily be replaced by the E_4 unit.[23] Thereby, astonishingly, the E_4 tetrahedron still remains intact. By the addition of pyridine, the release of white phosphorus or yellow arsenic can be observed. To date, this feature is only observed for complex **II**.[19,20,24]

In principle, the activation of yellow arsenic can also be achieved by main group complexes[25] and therefore also by carbenes. During his Ph.D. thesis, Christoph Schwarzmaier succeeded in stabilising As_n units resulting from the degradation of As_4 with cyclic (alkyl)(amino)carbenes (CAAC) by an one step reaction (Figure 1.7).[26] Such complexes are usually synthesised by a multistep reaction starting from $AsCl_3$ and the correlating carbene.[27]

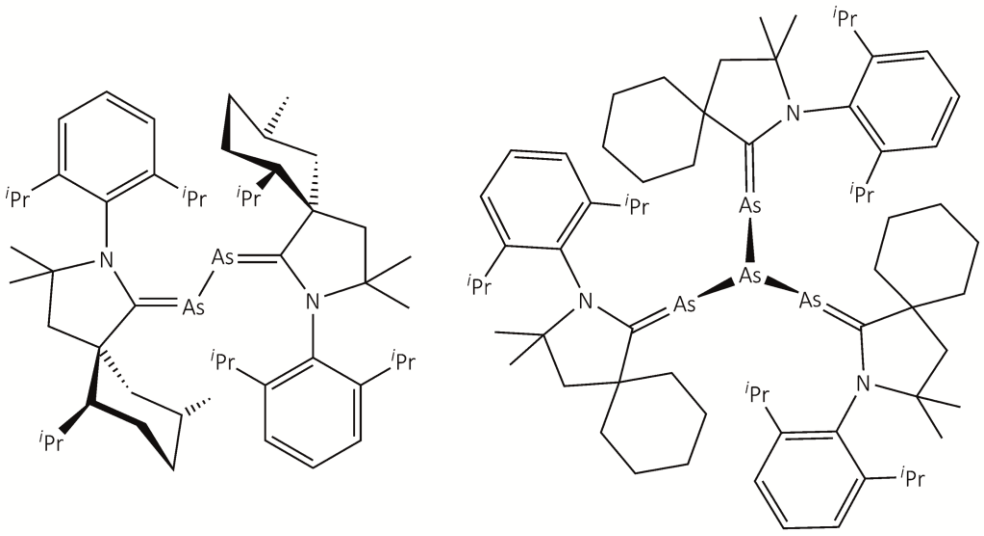

Figure 1.7 Illustration of [(^{Menthyl}CAAC)$_2$As$_2$] (left) and [(^{cHex}CAAC)$_3$As$_4$] (right).

While the use of yellow arsenic as a starting material leads to the formation of neutral complexes most of the time, other common arsenic sources like the Zintl anion $[As_7]^{3-}$ afforded polyarsenides. Here, the formation of larger arsenic clusters is particularly favoured. Eichhorns accomplishments deserve a special mention, regarding several publications in this field during the 1990s.[28] One outstanding example is the synthesis of $[As@Ni_{12}@As_{20}]^{3-}$ (**III**), which could be prepared by reacting K_3As_7 with $Ni(COD)_2$ (COD = cycloocta-1,5-diene) in the presence of $^{n}Bu_4PBr$.[29] The resulting cluster **III** has an onion like structure and can be interpreted as an As_{20} pentagonal dodecahedron which encapsulates a Ni_{12}^{-} icosahedron. In addition, an arsenic atom is enclosed in the centre of the Ni_{12}^{-} subunit (Figure 1.8).

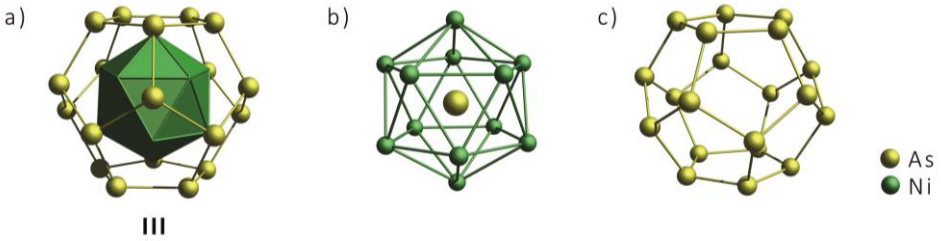

III

Figure 1.8 Molecular structure of a) the intermetalloide cluster $[As@Ni_{12}@As_{20}]^{3-}$ (**III**). The $[Ni_{12}(\mu_{12}\text{-}As)]^{3-}$ core is depicted as icosahedron and bonds between the As_{20} shell and the Ni_{12} unit are omitted for clarity. b) The $[Ni_{12}(\mu_{12}\text{-}As)]^{3-}$ subunit. c) The exterior As_{20} cage.[29]

Up to date, **III** represents one of the largest anionic, arsenic containing complexes and is the only known example for a fullerene like intermetalloide cluster. As already mentioned, icosahedral allotropes of arsenic have been predicted[8] and therein, the As_{20} fullerene seems to be a promising candidate. Nowadays, especially the Goicoechea group is interested in Zintl anions and their coordination chemistry.[30] In contrast, the neutral species $[As_7(SiMe_3)_3]$ is definitely less common for the synthesis of polyarsenides. Therefore, only few examples are known in literature.[31]

As already discussed above, other arsenic sources can also be taken in account. In the early stages of As_n ligand complexes, cyclic organo arsenic derivatives, e.g. *cyclo*-$(AsMe)_5$ or *cyclo*-$(AsPh)_6$, have been often used.[10b,32] Far less used arsenic precursors are metallic arsenic,[33] As_4S_4,[34] $AsCl_3$,[35] $As(SiMe_3)_3$,[36] and $PhAs(SiMe_3)_2$,[37] respectively.

1.2 As_n Ligand Complexes in Coordination Chemistry

Reactivity of As_n Ligand Complexes

Taking a look into the literature, one can notice that especially the Scherer group studied the reactivity of As_n ligand complexes. Particular attention is paid to the reactivity of $[Cp^*Fe(\eta^5\text{-}As_5)]$ (**I**) towards other transition metal complexes.[38] Unlike $[Cp_2Fe]$, complex **I** should show a different reactivity due to the available lone pair of each arsenic atom and a possibility for coordination to metal fragments. Thereby, the reactivity pattern of **I** ranges from simple coordination over transfer reaction to complete rearrangement (Scheme 1.1). In addition, the Scherer group succeeded in the oxidation of **I** with $[CpFe(C_6H_6)][PF_6]$ to yield the 30 VE triple decker complex $[(CpFe)(\mu,\eta^{5:5}\text{-}As_5)(Cp^*Fe)][PF_6]$.[13] To get an insight into the charge distribution and coordination features of **I**, ^{57}Fe Mössbauer spectroscopy and differential scanning calorimetry (DSC) as well as DFT calculations were carried out.[39] Based on these results, **I** is comparable to its lighter congener $[Cp^*Fe(\eta^5\text{-}P_5)]$ (**IV**). However, the DFT results reveal a reversed energy distribution of the unoccupied orbitals (LUMO, LUMO+1) for **I** compared to **IV**, while the HOMO is localised at

the *cyclo*-E_5 ring in both cases. In contrast, ^{57}Fe Mössbauer spectroscopy results show similar quadrupole hyperfine interactions for **I** and **IV**, but different isomeric shifts (at 90 K) for **I** and **IV**.

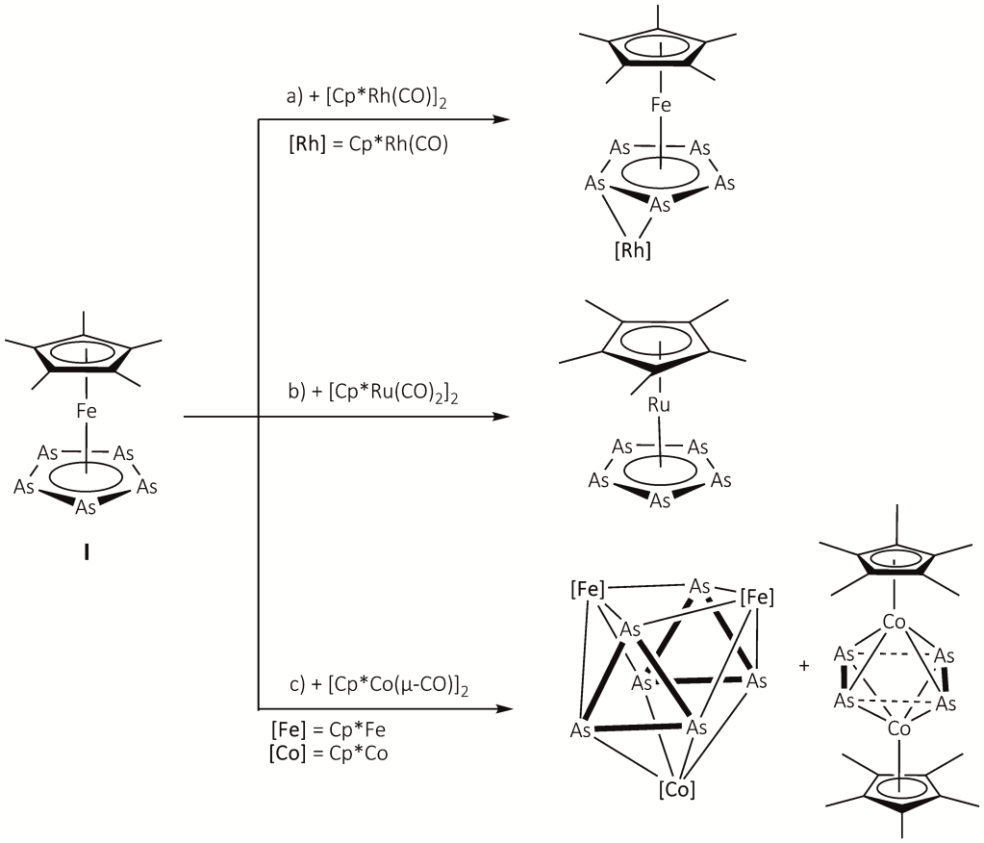

Scheme 1.1 Reactivity pattern of [Cp*Fe(η^5-As_5)] (**I**) towards transition metal complexes. a) Side-on coordination of a [Cp*Rh(CO)] fragment.[38c] b) Transfer of the *cyclo*-As_5 ligand to the $[Cp^*Ru]^+$ unit.[38b] c) Rearrangement of **I** during the reaction with $[Cp^*Co(\mu\text{-}CO)]_2$.[38d]

Nowadays, the interest for As_n ligand complexes has slightly been diminished. Especially the difficult handling and challenging synthesis as well as low yields and the lack of characteristic analytical tools (e.g. NMR spectroscopy) make arsenic complexes much more challenging in comparison to P_n ligand complexes. For this reason, only a small number of publications concerning the reactivity of As_n ligand complexes can be found in literature up to date. Nevertheless, it is worth to investigate arsenic compounds, since E_n ligand complexes (E = P, As) are usually known for their different reactivity.[39b,40,41] This is exemplary emphasised in the reactivity of **I** and [Cp*Fe(η^5-P_5)] (**IV**) towards divalent samarium complexes. Depending on the solvent used, different polyarsenides, [(Cp''$_2$Sm)(μ,$\eta^{4:4}$-As_4)(Cp*Fe)] or the norbornadiene scaffold containing complex [(Cp''$_2$Sm)$_2$As$_7$(Cp*Fe)], can be isolated by reacting **I** with [Cp''$_2$Sm(thf)] (Cp'' = η^5-1,3-$C_5H_3{}^tBu_2$) (Figure 1.9).[42]

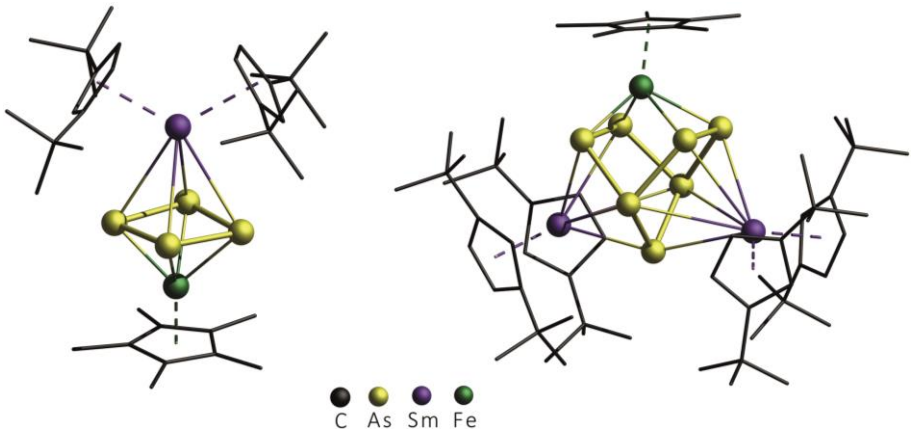

Figure 1.9 Molecular structure of $[(Cp''_2Sm)(\mu,\eta^{4:4}\text{-}As_4)(Cp^*Fe)]$ (left) and $[(Cp''_2Sm)_2As_7(Cp^*Fe)]$ (right).[42] Cp* and Cp'' ligands are represented in the wire or frame model and H atoms are omitted for clarity.

In contrast, the reaction of the phosphorus derivative **IV** with $[Cp^R{}_2Sm(thf)_2]$ (Cp^R = Cp*, Cp^{Pr} (η^5-$C_5Me_4{}^nPr$)) results formally in a dimerisation to $[(Cp^R{}_2Sm)_2P_{10}(Cp^*Fe)_2]$.[43] In addition, changing the samarium precursor to $[(DIP_2pyr)SmI(thf)_3]$ (DIP_2pyr = 2,5-bis{N-(2,6-diiso-propylphenyl)iminomethyl}pyrrolyl) afforded $[Cp^*Fe(\mu_3,\eta^{4:2:2:1}\text{-}P_5)Sm(DIP_2pyr)]_2$ as well as $[Cp^*Fe(\mu,\eta^{4:2:1}\text{-}P_5)Sm(DIP_2pyr)(thf)_2]$.[44] Related arsenic complexes originating from this samarium complex are unknown so far.

Moreover, the reactivity of $[\{CpMo(CO)_2\}_2(\mu,\eta^{2:2}\text{-}As_2)]$ (**V**) and $[(Cp^*Mo)_2(\mu,\eta^{6:6}\text{-}As_6)]$ towards $[o\text{-}(HgC_6F_4)_3]$ and $AgBF_4$, respectively, has been investigated by the Scheer group.[41] Recently, the butterfly complex $[\{Cp'''Fe(CO)_2\}_2(\mu,\eta^{1:1}\text{-}As_4)]$ could also be introduced as a chelating ligand.[45] In combination with $[Cu(CH_3CN)_4][BF_4]$ the reaction leads to the formation of $[\{\{Cp'''Fe(CO)_2\}_2(\mu,\eta^{1:1}\text{-}As_4)\}_2Cu][BF_4]$. The latter is expected to be a promising co-ligand for catalysis, due to its small bite angle and the sterically demanding Cp''' ligand.

As_n Ligand Complexes in Supramolecular Chemistry

As already mentioned, the reactivity of As_n ligand complexes in comparison to their lighter P_n homologues is only poorly investigated. Hence, it is not surprising that the potential of arsenic complexes in supramolecular chemistry is underestimated so far. In contrast, several P_n ligand complexes have found application in supramolecular chemistry up to now.[46] An extraordinary position is occupied by $[Cp^RFe(\eta^5\text{-}P_5)]$ (Cp^R = Cp* (**IV**), Cp^{Bn} (η^5-$C_5\{CH_2(C_6H_5)\}_5$) (**VI**), Cp^{BIG} (η^5-$C_5\{4\text{-}{}^nBuC_6H_4\}_5$) (**VII**)). In combination with coinage metal salts, one and two dimensional polymers as well as fullerene like molecules or nano capsules are obtained.[46a,47] Although DFT calculations suggest a similar coordination behaviour for the Cp* pentaarsaferrocene derivative **I**, it reacts with Cu^I halides to form one dimensional polymers.[39b] The formation of fullerene like

molecules has not been observed. This might be attributed to the preference for π-coordination of **I** through As-As bonds (η^2-coordination), while **IV**, **VI** and **VII** prefer σ-coordination (η^1-coordination) *via* the phosphorus lone pairs. For a long time, the σ-coordination for As_n ligand complexes seemed to be out of reach, but recently the first 1,3-σ-coordination of **I** to a Lewis acid could be realised in the one dimensional polymer $[Cu_3(\mu\text{-}Cl)_2(dpmp)_2\{(\mu,\eta^{1:1:5}\text{-}As_5)FeCp^*\}]_n[BF_4]_n$ (dpmp = bis(diphenylphosphinomethyl)phenylphosphine) (Figure 1.10).[48] Moreover, the identical coordination mode is also achieved for **V**, however, just as a discrete dimeric complex.

In addition to the first 1,3-coordination, we could also observe an unexpected η^5-coordination of **I** in $[M(\{Cp^*Fe\}\{\mu,\eta^{5:1}\text{-}As_5\})_3]_n[TEF]_n$ (Figure 1.10).[40a] Due to weak σ-interactions, an alignment to columns is obtained in the solid state. In contrast, the reaction of **I** with [Ag][FAL] ($[FAL]^- = [FAl\{OC_6F_{10}(C_6F_5)\}_3]^-$) did not afford polymeric products. However, depending on the stoichiometry dimeric and trimeric coordination compounds are formed.[41] Similar coordination products are also predicted for using [Ag][TEF] instead of [Ag][FAL].[41]

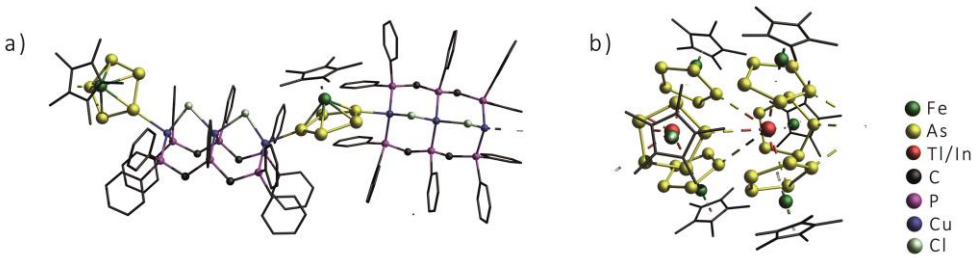

Figure 1.10 Sections of the one dimensional polymers (ball and stick representation) of a) $[Cu_3(\mu\text{-}Cl)_2(dpmp)_2\{(\mu,\eta^{1:1:5}\text{-}As_5)FeCp^*\}]_n[BF_4]_n$[48] and b) $[M(\{Cp^*Fe\}\{\mu,\eta^{5:1}\text{-}As_5\})_3]_n[TEF]_n$ (M = In, Tl).[40b] Cp* ligands and phenyl substituents of dpmp ligands are drawn in the wire or frame model. H atoms and counterions are omitted for clarity.

A further well established building block for supramolecular chemistry is $[Cp^*Mo(CO)_2(\eta^3\text{-}As_3)]$ (**VIII**). The reaction of **VIII** with Cu^I halides leads to the formation of $\{Cu(\mu\text{-}X)\}_2$ bridged dimers. In contrast, the use of [Ag][TEF] bearing a weakly coordination anion provides the dimer $[Ag_2\{Cp^*Mo(CO)_2(\mu,\eta^{3:2}\text{-}As_3)\}_2\{Cp^*Mo(CO)_2(\mu,\eta^{3:2:2}\text{-}As_3)\}_2][TEF]_2$ (**IX**).[49] Thereby, **IX** represents one of the first examples of arsenic based oligomers in literature. Hereby, the general preference for η^2-coordination is already illustrated. Surprisingly, ESI MS spectra indicate dissociation of **IX** to $[Ag\{Cp^*Mo(CO)_2As_3\}_2]^+$. Therefore, equilibrium is discussed to occur in solution, which is also confirmed by DFT calculations. In contrast to **IX**, its Tl derivative forms a columnar structure in the solid state, which is dominated by π-coordination of the As_3 ligands through As-As bonds.[50]

1.3 The Cp^R Ligand in Organometallic Chemistry

The Cp^R ligand influences the development in organometallic chemistry like no other ligand. Since the structural determination of ferrocene [Cp_2Fe],[51] the cyclopentadienyl anion and its derivatives are the most frequently used ligands in organometallic chemistry. This effect is certainly based on the versatile coordination modes reaching from η^1 to the maximum of η^5. Up to date, a big library of Cp^R derivatives has been established as a result of the easy substitution of H atoms at the Cp ligand (Figure 1.11). Thereby, the electronic structure, the degree of substitution as well as the steric demand can be controlled. A trend for using larger Cp^R ligands can especially be observed in the last years, since they are known to stabilise unprecedented structural motifs and kinetically favoured complexes, respectively.[52] Additionally, the increased solubility of the resulting complexes cannot be neglected.

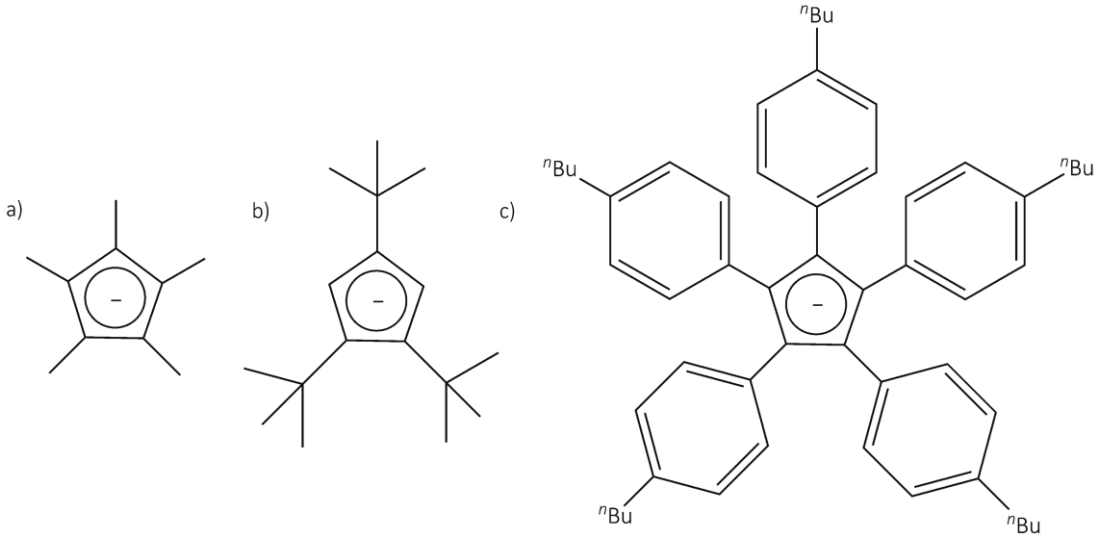

Figure 1.11 Representation of selected Cp^R ligands with an increasing steric demand from left to right. a) Cp* ligand, b) Cp''' ligand and c) Cp^{BIG} ligand.

The consequences of substitution are impressively revealed in the reaction of $[Cp^RFe(CO)_2]_2$ with As_4 (Cp^R = Cp, Cp*, Cp^{BIG} (**X**)). While the reaction of the parent compound leads to the formation of $[Cp_4Fe_4(As_2)_2]$,[53] the stepwise increase of the steric demand results in the formation of $[Cp^*Fe(\eta^5\text{-}As_5)]$[13] and the butterfly complex $[\{Cp^{BIG}Fe(CO)_2\}_2(\mu,\eta^{1:1}\text{-}As_4)]$ (**XI**),[54] respectively. Remarkably, **XI** is already obtained at room temperature, whereas the other reactions take place at 190 °C. This is caused by dissociation of **X** in solution at room temperature to highly reactive $[Cp^{BIG}Fe(CO)_2]^{\cdot}$ radicals.[55] Nevertheless, further co-thermolysis of **XI** with As_4 provides $[Cp^{BIG}Fe(\eta^5\text{-}As_5)]$, $[(Cp^{BIG}Fe)_2(\mu,\eta^{4:4}\text{-}As_4)]$ and $[(Cp^{BIG}Fe)_3(\mu_3,\eta^{4:4:4}\text{-}As_6)]$.[56]

In addition to the mentioned aspects, Cp ligands containing functional groups are also of current interest. An outstanding example seems to be the pentacyanocylcopentadienide anion $[C_5(CN)_5]^-$ (**XII**), which shows a fivefold symmetric moiety in the solid state (Figure 1.12).[57] In combination with sodium carbonate, metal organic frameworks (MOFs) can be isolated.[58] Thereby, each cyanide substituent coordinates to one sodium cation, which results in a clathrate type structure, possessing fullerene like topology (Figure 1.12).

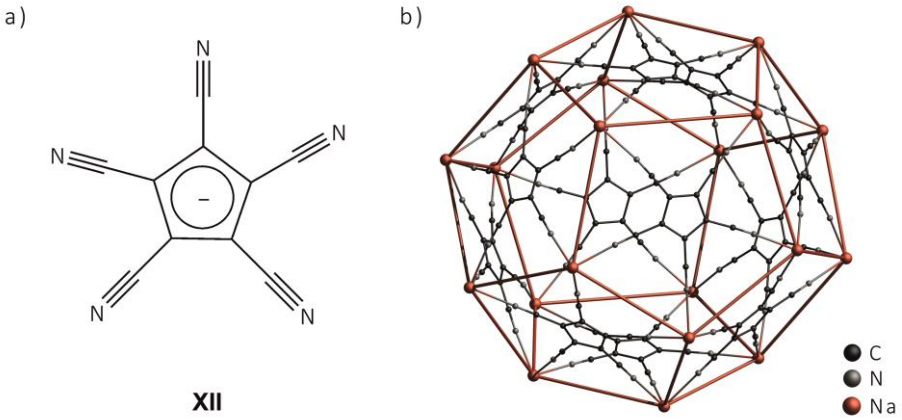

XII

Figure 1.12 a) Illustration of $[C_5(CN)_5]^-$ (**XII**) and b) simplified representative unit of the dodecahedral $[Na_{46}\{C_5(CN)_5\}_{48}]^{2-}$ dianion.[58]

A further representative of the class of Cp^R ligands with increasing steric demand in comparison to the Cp ligand is the pentabenzylcylcopentadienyl derivative Cp^{Bn}.[59] Several main group complexes[60] as well as transition metal complexes[61] bearing the Cp^{Bn} ligand are reported in literature. Since the benzyl substituents are very flexible and the electronic features are comparable to the Cp* derivative, it can be generally viewed as a synthon for the Cp* ligand. Moreover, the good solubility in almost all common solvents can be considered as an advantage. Although the Cp^{Bn} ligand has a high potential due to advantageous features (solubility, possible detection of novel structural motifs, etc.), investigations are limited to the synthesis of metallocenes or metal containing complexes. During his Ph.D. thesis, Fabian Dielmann introduced the Cp^{Bn} ligand in the field of P_4 activation. In addition, the resulting P_n ligand complexes were used as building blocks in supramolecular chemistry.[62] Thereby, the pentaphosphaferrocene derivative **VI** represents a first example (Figure 1.13). Due to an available lone pair at each phosphorus atom, it contains fivefold symmetry similar to **XII**. Consequently, **VI** has the possibility for quintuple coordination since the Cp* derivative **IV** is

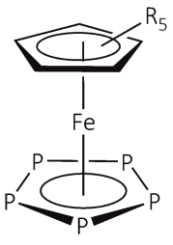

IV (R = Cp*)
VI (R = Cp^{Bn})

Figure 1.13 General formula of $[Cp^RFe(\eta^5\text{-}P_5)]$ (Cp^R = Cp* (**IV**), Cp^{Bn} (**VI**)).

known to form spherical aggregates in reactions with CuX (X = Cl, Br, I). Thus, it is not unexpected that **VI** shows similar reactivity towards Cu^{I} halides. In addition to fullerene like macromolecules, also a self-assembled rugby ball like compound arising from **VI** and $CuBr_2$ as well as one and two dimensional polymers have been synthesised (Figure 1. 14).[47c-e,62,63]

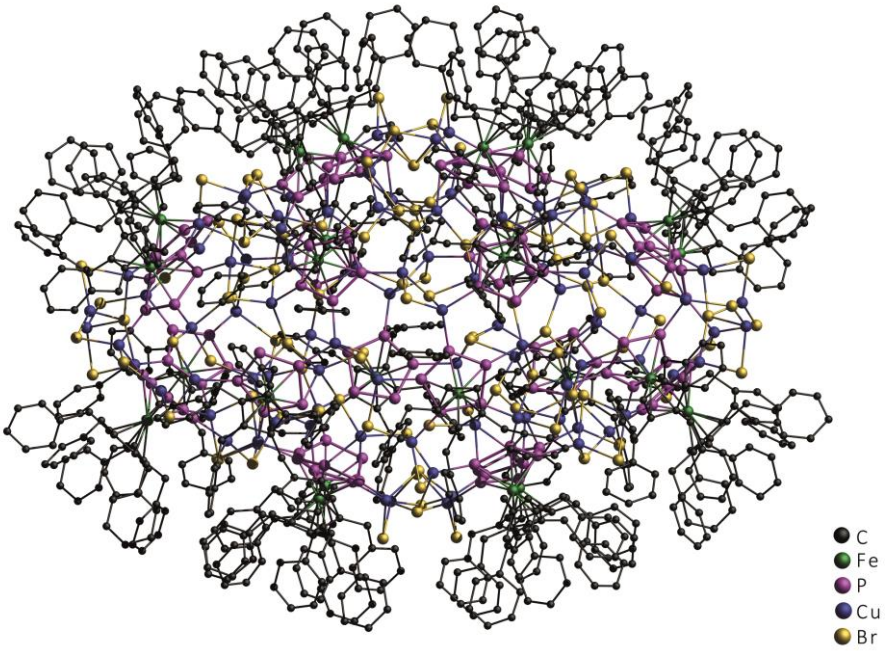

Figure 1. 14 Ball and stick representation of the rugby ball $[\{Cp^{Bn}Fe(\eta^5\text{-}P_5)\}_{24}Cu_{96}Br_{96}]$.[47e] H atoms, solvent molecules as well as disorder are omitted for clarity.

1.4 References

[1] a) S. C. Grund, K. Hanusch, H. U. Wolf, *Ullmann's Encyclopedia of Industrial Chemistry*, Wiley-VCH Verlag GmbH & Co. KGaA 2000, 1-43; b) S. Gibaud, G. Jaouen, *Organomet. Chem.* 2010, *32*, 1-20;

[2] G. Süss-Fink, *Chem. unserer Zeit* 2012, *46*, 100-109.

[3] A. F. Holleman, E. Wiberg, N. Wiberg, *Lehrbuch der Anorganischen Chemie, Vol. 102*, Walter de Gruyter, Berlin, 2007, 822-826.

[4] A. Bettendorff, *Liebigs Ann. Chem.* 1867, *144*, 110-114.

[5] H. Erdmann, M. V. Unruh, *Z. Anorg. Chem.* 1902, *32*, 437-452.

[6] Y. Morino, T. Ukaji, T. Ito, *Bull. Chem. Soc. Jpn.* 1966, *39*, 64-71.

[7] H. Krebs, W. Holz, K. H. Worms, *Chem. Ber.* 1957, *90*, 1031-1037.

[8] A. J. Karttunen, M. Linnolahti, T. A. Pakkanen, *Chem. Phys. Chem.* 2007, *8*, 2373-2378.

[9] S. Zamfira, M. Popescu, F. Sava, *Chalcogenide Letters* 2005, *2*, 55-61.

[10] a) A. S. Foust, M. S. Foster, L. F. Dahl, *J. Am. Chem. Soc.* 1969, *91*, 5631-5633; b) A. S. Foust, M. S. Foster, L. F. Dahl, *J. Am. Chem. Soc.* 1969, *91*, 5633-5635.

[11] Group 15 element ligand complexes contain substituent-free pnictogen atoms, binding directly to the transition metal without any organic moieties or similar groups like $SiMe_3$ or NR_2.

[12] R. Hoffmann, *Angew. Chem. Int. Ed.* 1982, *21*, 711-724.

[13] O. J. Scherer, C. Blath, G. Wolmershäuser, *J. Organomet. Chem.* 1990, *387*, C21-C24.

[14] a) O. J. Scherer, *Angew. Chem. Int. Ed. Engl.* 1985, *24*, 924-943; b) O. J. Scherer, *Angew. Chem. Int. Ed. Engl.* 1990, *29*, 1104-1122; c) O. J. Scherer, *Acc. Chem. Res.* 1999, *32*, 751-762.

[15] C. Graßl, M. Bodensteiner, M. Zabel, M. Scheer, *Chem. Sci.* 2015, *6*, 1379-1382.

[16] O. J. Scherer, W. Wiedemann, G. Wolmershäuser, *Chem. Ber.* 1990, *123*, 3-6.

[17] O. J. Scherer, J. Vondung, G. Wolmershäuser, *J. Organomet. Chem.* 1989, *376*, C35-C38.

[18] M. Scheer, J. Müller, M. Häser, *Angew. Chem. Int. Ed. Engl.* 1996, *35*, 2492-2496.

[19] C. Schwarzmaier, M. Sierka, M. Scheer, *Angew. Chem. Int. Ed.* 2013, *52*, 858-861.

[20] C. Schwarzmaier, A. Y. Timoshkin, M. Scheer, *Angew. Chem. Int. Ed.* 2013, *52*, 7600-7603.

[21] C. Graßl, *Ph.D. thesis*, Universität Regensburg, 2013.

[22] selected publications: a) Y. Peng, H. Fan, H. Zhu, H. W. Roesky, J. Magull, C. E. Hughes, *Angew. Chem. Int. Ed.* 2004, *43*, 3443-3445; b) Y. Xiong, S. Yao, M. Brym, M. Driess, *Angew. Chem. Int. Ed.* 2007, *46*, 4511-4513; c) S. Yao, C. Milsmann, E. Bill, K. Wieghardt, M. Driess,

J. Am. Chem. Soc. 2008, *130*, 13536-13537; d) S. Yao, Y. Xiong, X. Zhang, M. Schlangen, H. Schwarz, C. Milsmann, M. Driess, *Angew. Chem. Int. Ed.* 2009, *48*, 4551-4555; e) G. Prabusankar, A. Doddi, C. Gemel, M. Winter, R. A. Fischer, *Inorg. Chem.* 2010, *49*, 7976-7980.

[23] F. Spitzer, M. Sierka, M. Latronico, P. Mastrorilli, A. V. Virovets, M. Scheer, *Angew. Chem. Int. Ed.* 2015, *54*, 4392-4396.

[24] C. Schwarzmaier, A. Schindler, C. Heindl, S. Scheuermayer, E. V. Peresypkina, A. V. Virovets, M. Neumeier, R. Gschwind, M. Scheer, *Angew. Chem. Int. Ed.* 2013, *52*, 10896-10899.

[25] R. P. Tan, N. M. Comerlato, D. R. Powell, R. West, *Angew. Chem. Int. Ed. Engl.* 1992, *31*, 1217-1218.

[26] C. Schwarzmaier, *Ph.D. thesis*, Universität Regensburg, 2012.

[27] M. Y. Abraham, Y. Wang, Y. Xie, P. Wei, H. F. Schaefer, P. v. R. Schleyer, G. H. Robinson, *Chem. Eur. J.* 2010, *16*, 432-435.

[28] a) R. C. Haushalter, B. W. Eichhorn, A. L. Rheingold, S. J. Geib, *J. Chem. Soc., Chem. Commun.* 1988, 1027-1028; b) B. W. Eichhorn, R. C. Haushalter, J. C. Huffman, *Angew. Chem. Int. Ed. Engl.* 1989, *28*, 1032-1033; c) B. W. Eichhorn, S. P. Mattamana, D. R. Gardner, J. C. Fettinger, *J. Am. Chem. Soc.* 1998, *120*, 9708-9709.

[29] M. J. Moses, J. C. Fettinger, B. W. Eichhorn, *Science* 2003, *300*, 778-780.

[30] a) C. Knapp, B. Zhou, M. S. Denning, N. H. Rees, J. M. Goicoechea, *Dalton Trans.* 2010, *39*, 426-436; b) C. M. Knapp, J. S. Large, N. H. Rees, J. M. Goicoechea, *Dalton Trans.* 2011, *40*, 735-745; c) C. M. Knapp, B. H. Westcott, M. A. C. Raybould, J. E. McGrady, J. M. Goicoechea, *Chem. Commun.* 2012, *48*, 12183-12185; d) R. S. P. Turbervill, J. M. Goicoechea, *Chem. Commun.* 2012, *48*, 6100-6102; e) R. S. P. Turbervill, A. R. Jupp, P. S. B. McCullough, D. Ergöçmen, J. M. Goicoechea, *Organometallics* 2013, *32*, 2234-2244.

[31] a) R. Ahlrichs, D. Fenske, K. Fromm, H. Krautscheid, U. Krautscheid, O. Treutler, *Chem. Eur. J.* 1996, *2*, 238-244; b) C. von Hänisch, D. Fenske, F. Weigend, R. Ahlrichs, R. Ahlrichs, F. Weigend, *Chem. Eur. J.* 1997, *3*, 1494-1498; c) C. v. Hänisch, D. Fenske, *Z. Anorg. Allg. Chem.* 1998, *624*, 367-369.

[32] a) P. J. Sullivan, A. L. Rheingold, *Organometallics* 1982, *1*, 1547-1549; b) P. Mercando, A.-J. DiMaio, A. L. Rheingold, *Angew. Chem. Int. Ed. Engl.* 1987, *26*, 244-245; c) K. Mast, O. J. Scherer, G. Wolmershäuser, *Z. Anorg. Allg. Chem.* 1999, *625*, 1475-1478.

[33] L. Y. Goh, R. C. S. Wong, W. H. Yip, T. C. W. Mak, *Organometallics* 1991, *10*, 875-879.

[34] I. Bernal, H. Brunner, W. Meier, H. Pfisterer, J. Wachter, M. L. Ziegler, *Angew. Chem. Int. Ed. Engl.* 1984, *23*, 438-439.

[35] B. Sigwarth, L. Zsolnai, H. Berke, G. Huttner, *J. Organomet. Chem.* **1982**, *226*, C5-C8.

[36] a) D. Fenske, H. Fleischer, C. Persau, *Angew. Chem. Int. Ed. Engl.* **1989**, *28*, 1665-1667; b) J. Besinger, D. Fenske, *Z. Anorg. Allg. Chem.* **2001**, *627*, 1487-1494.

[37] a) D. Fenske, J. Hachgenei, *Angew. Chem. Int. Ed. Engl.* **1986**, *25*, 175-177; b) D. Fenske, K. Merzweiler, J. Ohmer, *Angew. Chem. Int. Ed. Engl.* **1988**, *27*, 1512-1513.

[38] a) B. Rink, O. J. Scherer, G. Heckmann, G. Wolmershäuser, *Chem. Ber.* **1992**, *125*, 1011-1016; b) B. Rink, O. J. Scherer, G. Wolmershäuser, *Chem. Ber.* **1995**, *128*, 71-73; c) M. Detzel, G. Friedrich, O. J. Scherer, G. Wolmershäuser, *Angew. Chem. Int. Ed. Engl.* **1995**, *34*, 1321-1323; d) G. Friedrich, O. J. Scherer, G. Wolmershäuser, *Z. Anorg. Allg. Chem.* **1996**, *622*, 1478-1486.

[39] a) R. H. Herber, O. J. Scherer, *Eur. J. Inorg. Chem.* **2000**, *12*, 2451-2453; b) H. Krauss, G. Balázs, M. Bodensteiner, M. Scheer, *Chem. Sci.* **2010**, *1*, 337-342.

[40] a) M. Fleischmann, S. Welsch, H. Krauss, M. Schmidt, M. Bodensteiner, E. V. Peresypkina, M. Sierka, C. Gröger, M. Scheer, *Chem. Eur. J.* **2014**, *20*, 3759-3768; b) M. Fleischmann, J. S. Jones, F. P. Gabbai, M. Scheer, *Chem. Sci.* **2015**, *6*, 132-139.

[41] M. Fleischmann, *Ph.D. thesis*, Universität Regensburg, **2015**.

[42] N. Arleth, M. T. Gamer, R. Köppe, S. N. Konchenko, M. Fleischmann, M. Scheer, P. W. Roesky, *Angew. Chem. Int. Ed.* **2016**, *55*, 1557-1560.

[43] T. Li, M. T. Gamer, M. Scheer, S. N. Konchenko, P. W. Roesky, *Chem. Commun.* **2013**, *49*, 2183-2185.

[44] T. Li, J. Wiecko, N. A. Pushkarevsky, M. T. Gamer, R. Köppe, S. N. Konchenko, M. Scheer, P. W. Roesky, *Angew. Chem. Int. Ed.* **2011**, *50*, 9491-9495.

[45] C. Schwarzmaier, S. Heinl, G. Balázs, M. Scheer, *Angew. Chem. Int. Ed.* **2015**, *54*, 13116-13121.

[46] selected publications: a) M. Scheer, *Dalton Trans.* **2008**, *33*, 4321-4524; b) B. Attenberger, E. V. Peresypkina, M. Scheer, *Inorg. Chem.* **2015**, *54*, 7021-7029; c) M. Fleischmann, S. Welsch, E. V. Peresypkina, A. V. Virovets, M. Scheer, *Chem. Eur. J.* **2015**, *21*, 14332-14336; d) C. Heindl, A. Kuntz, E. V. Peresypkina, A. V. Virovets, M. Zabel, D. Ludeker, G. Brunklaus, M. Scheer, *Dalton Trans.* **2015**, *44*, 6502-6509.

[47] selected publications: a) S. Welsch, C. Gröger, M. Sierka, M. Scheer, *Angew. Chem. Int. Ed.* **2011**, *50*, 1435-1438; b) F. Dielmann, A. Schindler, S. Scheuermayer, J. Bai, R. Merkle, M. Zabel, A. V. Virovets, E. V. Peresypkina, G. Brunklaus, H. Eckert, M. Scheer, *Chem. Eur. J.* **2012**, *18*, 1168-1179; c) F. Dielmann, C. Heindl, F. Hastreiter, E. V. Peresypkina, A. V. Virovets, R. M. Gschwind, M. Scheer, *Angew. Chem. Int. Ed.* **2014**, *53*, 13605-13608; d) F.

Dielmann, M. Fleischmann, C. Heindl, E. V. Peresypkina, A. V. Virovets, R. M. Gschwind, M. Scheer, *Chem. Eur. J.* 2015, *21*, 6208-6214; e) C. Heindl, E. V. Peresypkina, A. V. Virovets, W. Kremer, M. Scheer, *J. Am. Chem. Soc.* 2015, *137*, 10938-10941; f) S. Heinl, E. Peresypkina, J. Sutter, M. Scheer, *Angew. Chem. Int. Ed.* 2015, *54*, 13431-13435.

[48] M. Fleischmann, L. Dütsch, M. E. Moussa, A. Schindler, G. Balazs, C. Lescop, M. Scheer, *Chem. Commun.* 2015, *51*, 2893-2895.

[49] L. J. Gregoriades, H. Krauss, J. Wachter, A. V. Virovets, M. Sierka, M. Scheer, *Angew. Chem. Int. Ed.* 2006, *45*, 4189-4192.

[50] H. Krauss, *Ph.D. thesis*, Universität Regensburg, 2011.

[51] a) T. J. Kealy, P. L. Pauson, *Nature* 1951, *168*, 1039-1040; b) S. A. Miller, J. A. Tebboth, J. F. Tremaine, *J. Chem. Soc.* 1952, 632-635.

[52] C. Janiak, H. Schuhmann, *Adv. Organomet. Chem.* 1991, *33*, 291-393.

[53] O. J. Scherer, G. Kemény, G. Wolmershäuser, *Chem. Ber.* 1995, *128*, 1145-1148.

[54] S. Heinl, M. Scheer, *Chem. Sci.* 2014, *5*, 3221-3225.

[55] S. Heinl, M. Scheer, *Dalton Trans.* 2014, *43*, 16139-16142.

[56] S. Heinl, *Ph.D. thesis*, Universität Regensburg, 2014.

[57] R. J. Less, M. McPartlin, J. M. Rawson, P. T. Wood, D. S. Wright, *Chem. Eur. J.* 2010, *16*, 13723-13728.

[58] R. J. Less, T. C. Wilson, B. Guan, M. McPartlin, A. Steiner, P. T. Wood, D. S. Wright, *Eur. J. Inorg. Chem.* 2013, *2013*, 1161-1169.

[59] S. S. Hirsch, W. J. Bailey, *J. Org. Chem.* 1978, *43*, 4090-4094.

[60] a) H. Schumann, C. Janiak, *J. Organomet. Chem.* 1988, *354*, 7-13; b) H. Schumann, C. Janiak, F. Görlitz, J. Loebel, A. Dietrich, *J. Organomet. Chem.* 1989, *363*, 243-251; c) C. Dohmeier, E. Baum, A. Ecker, R. Köppe, H. Schnöckel, *Organometallics* 1996, *15*, 4702-4706.

[61] a) J. W. Chambers, A. J. Baskar, S. G. Bott, J. L. Atwood, M. D. Rausch, *Organometallics* 1986, *5*, 1635-1641; b) M. D. Rausch, W. M. Tsai, J. W. Chambers, *Organometallics* 1989, *8*, 816-821; c) W. M. Tsai, M. D. Rausch, *Organometallics* 1996, *15*, 2591-2594; d) G. Schmid, U. Thewalt, P. Sedmera, V. Hanus, K. Mach, *Collect. Czech. Chem. Commun.* 1998, *63*, 636-645; e) S. Namorado, J. Cui, C. G. d. Azevedo, M. A. Lemos, M. T. Duarte, J. R. Ascenso, A. R. Dias, A. M. Martins, *Eur. J. Inorg. Chem.* 2007, *8*, 1103–1113.

[62] F. Dielmann, *Ph.D. thesis*, Universität Regensburg 2011.

[63] a) B. Krämer, *master thesis*, Universität Regensburg, 2014; b) C. Heindl, *Ph.D. thesis*, Universität Regensburg, 2015.

2. Research Objectives

As presented in the introduction, As_n ligand complexes are rare in organometallic chemistry and especially in coordination chemistry. Moreover, the influence of the Cp^{Bn} ligand (Cp^{Bn} = η^5-$C_5(CH_2\{C_6H_5\})_5$) on the reactivity and stability of As_n ligand complexes has not been studied yet, since only preliminary investigations on the lighter congener phosphorus exist. At the same time, the Cp^{Bn} ligand offers good solubility of the obtained arsenic compounds and the hope that unprecedented structural motifs might be obtained. Consequently, the research objectives for this work are:

- Preparation of transition metal complexes bearing the Cp^{Bn} ligand as starting materials for the synthesis of As_n ligand complexes.
- Synthesis of novel As_n ligand complexes and investigation of two different synthetic methods: i) thermolysis involving the reaction of transition metal precursors with As_4 at elevated temperatures and ii) transfer reactions using [Cp''$_2$Zr($\eta^{1:1}$-As_4)] (Cp'' = η^5-1,3-$C_5H_3{}^tBu_2$) as an arsenic source under mild reaction conditions.

It was also demonstrated that As_n ligand complexes are suitable building blocks for supramolecular chemistry. In combination with Lewis acids, both oligomeric as well as polymeric products are observed. However, the variety of Lewis acids is mainly limited to Cu^I halides and other monovalent metal salts have scarcely been used for this purpose so far. Moreover, mostly Cp* substituted arsenic precursors play a key role, although the Cp^{Bn} ligand displays promising properties for spherical aggregates as observed for [Cp^{Bn}Fe(η^5-P_5)]. Thus, the objectives are as follows:

- Investigation of the reactivity of [Cp*Fe(η^5-As_5)] towards coinage metal salts.
- Introduction of Cp^{Bn} substituted As_n ligand complexes in supramolecular chemistry.

As mentioned in chapter 1.2 and 1.3, the reactivity of [Cp*Fe(η^5-As_5)] has been of great interest, but redox chemistry has not been studied yet. In 2015, David Konieczny was able to briefly explore the reduction of [Cp*Fe(η^5-As_5)] in the presence of KH during his master thesis. Therefore, a further task is:

- Investigation of the redox properties of [Cp*Fe(η^5-As_5)].

3. General Considerations for the Cp^{Bn} Ligand

The intention of this chapter is to give a brief overview of general features of the Cp^{Bn} ligand. Accordingly, the subsequent subchapters summarise observations concerning complexes bearing the Cp^{Bn} ligand. All these observations are based on personal experience and do not refer to specific compounds.

3.1 Solubility

In general, the discussed complexes show a good solubility in CH_2Cl_2 and toluene and in some cases in thf. While the complexes dissolve only in the heat in *n*-hexane or *n*-pentane, most compounds are insoluble in CH_3CN. However, this fact can be exploited for crystallisation. The majority of the described complexes are crystallised by layering a CH_2Cl_2 or toluene solution with CH_3CN. Moreover, especially (cold) *n*-hexane or *n*-pentane can be used several times for washing the obtained crystals before drying *in vacuo*.

Since the Cp^{Bn} ligand dominates the solubility of the complexes, the isolation of reaction products can be difficult. Therefore, purification often takes place by column chromatography, which is sometimes difficult due to similar retention factors R_f of the products. Thus, long chromatographic columns and/or a high percentage of *n*-hexane in the eluent mixture are required.

3.2 Geometrical Considerations and Crystal Structures

As mentioned in the introductory chapter 1.3, the Cp^{Bn} ligand can be considered as a synthon for the Cp* ligand. Due to the flexibility of the benzyl ligands, which can be oriented in the direction pointing away from the transition metal centre, the steric demand is comparable to the Cp* derivative. This can be visualised by evaluating the angle between the Cp^{R} ligand and the metal atom (Figure 3.1). However, the orientation of the benzyl substituents can change due to incorporation of solvent molecules (e.g. toluene) in the crystal. As a result, one benzyl substituent is sometimes pointing in the direction of the transition metal atom. Furthermore, disorder of the substituents is often enhanced by the flexibility of the benzyl groups and leads to poor refinement in single crystal X-ray structure determination.

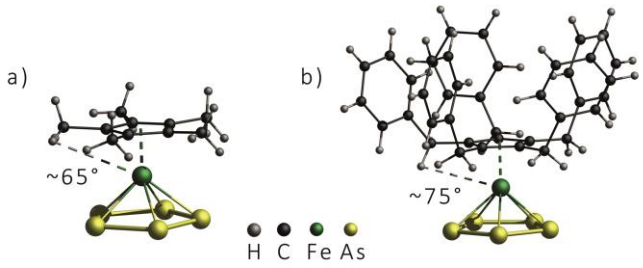

Figure 3.1 Comparison of the angle between the Cp^{R} ligand and the metal atom. a) [Cp*Fe(η^5-As$_5$)] and b) [Cp^{Bn}Fe(η^5-As$_5$)].

Moreover, the Cp^{Bn} derivatives generally form both intra- and intermolecular π-stacking interactions, while complexes bearing the Cp* ligand exhibit most of the time no specific arrangement in the crystal. Accordingly, the benzyl substituents are orientated towards each other (intermolecular interactions), often resulting in a pseudo one dimensional arrangement within the crystal (Figure 3.2). These intermolecular π-π interactions are also responsible for the poor solubility in aliphatic solvents and the insolubility in CH_3CN, respectively (see chapter 3.1). As a result, even toluene proved to be a poor solvent in some cases.

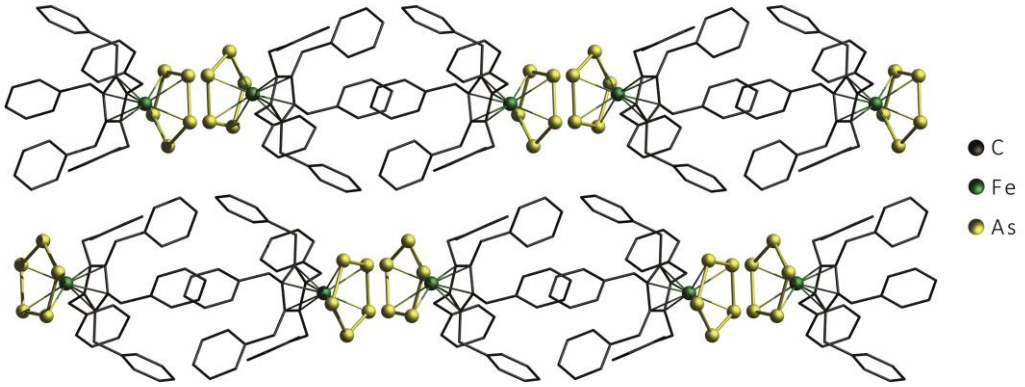

Figure 3.2 Representation of [Cp^{Bn}Fe(η^5-As$_5$)] in the solid state. View along the crystallographic b-axis. Cp^{Bn} ligands are depicted in wire or frame model and H atoms are omitted for clarity.

Furthermore, pixel calculations predict several different assemblies for benzene dimers in the gas phase with similar energy minima.[1] In Figure 3.3, favoured orientations of benzene dimers, T-shaped (**I**) or parallel (**II**) arrangement, are illustrated. Correspondingly, the orientation **I** and **II** are also realised in the benzyl substituents as intramolecular interactions in the solid state (Figure 3.3).

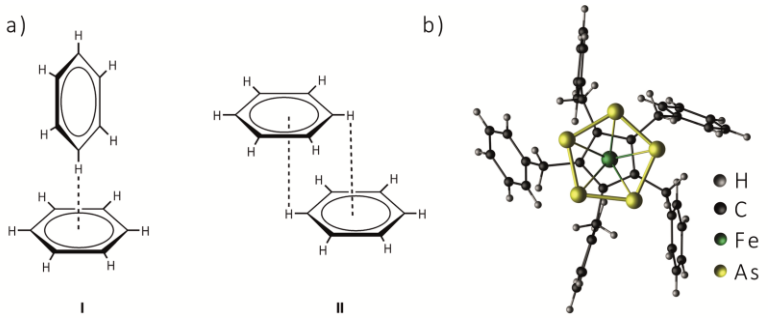

Figure 3.3 Illustration of a) benzene dimers in the gas phase with favoured arrangement (type **I** or **II**) and b) intramolecular interaction of the phenyl rings within $[Cp^{Bn}Fe(\eta^5\text{-}As_5)]$.

3.3 Spectroscopic and Spectrometric Investigations

Generally, all synthesised complexes show similar ^1H NMR spectra for the Cp^{Bn} ligand(s). Since the benzyl substituents can be seen as chemically and magnetically equivalent, one set of signals is received most of the time. The corresponding singlet for the methylene groups is obtained in the range of 3.37 ppm to 4.24 ppm and for the phenyl groups a multiplet between 6.12 ppm and 7.09 ppm is detected.[2] Sometimes, even the phenyl rings are equivalent on the NMR timescale and a doublet (H^{ortho}), a doublet of doublets (H^{meta}) and a triplet (H^{para}) can be assigned. The same applies to the $^{13}C\{^1H\}$ NMR spectroscopy. Generally, one signal for the methylene group (30.99 ppm to 36.48 ppm) and the Cp ring (89.26 ppm to 108.47 ppm) can be found. For the phenyl ring four signals at the corresponding δ values (125.15 ppm to 140.41 ppm) can be obtained.

In addition, all compounds have been studied by mass spectrometry. Thereby, fragments of the Cp^{Bn} ligand often represent the base peak in the EI MS spectra (e.g. $[C_7H_7]^+$ at *m/z* = 91.1).

3.4 References

[1] J. D. Dunitz, A. Gavezzotti, *Angew. Chem. Int. Ed.* 2005, *44*, 1766-1787.

[2] Assigned set of signals of the Cp^{Bn} ligand refers to ^{1}H NMR spectra and $^{13}C\{^{1}H\}$ NMR spectra usually recorded in CD_2Cl_2 at 300 K.

4. Novel Triple Decker Complexes of Group 6 Metals

M. Schmidt, G. Balázs, F. Riedlberger and M. Scheer

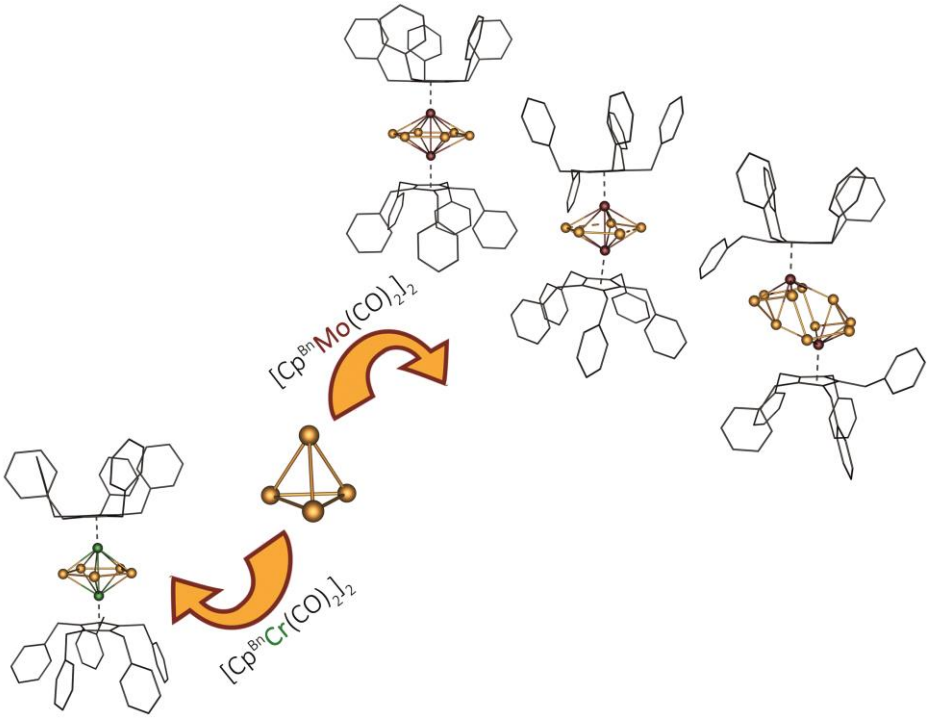

Abstract:

The co-thermolysis of $[Cp^{Bn}M(CO)_2]_2$ (M = Cr, Mo; $Cp^{Bn} = \eta^5\text{-}C_5(CH_2\{C_6H_5\})_5$) with As_4 leads to the formation of novel As_n ligand complexes bearing the Cp^{Bn} ligand. Moreover, an easy and straightforward synthesis of $[Cp^{Bn}Cr(CO)_2]_2$ (**1**) has been developed. In the case of the chromium derivative, co-thermolysis with As_4 leads to the formation of $[(Cp^{Bn}Cr)_2(\mu,\eta^{5:5}\text{-}As_5)]$ (**2**) exclusively. For molybdenum, the reaction yielded the triple decker complex $[(Cp^{Bn}Mo)_2(\mu,\eta^{6:6}\text{-}As_6)]$ (**3**). In addition, traces of $[(Cp^{Bn}Mo)_2(\mu,\eta^{5:5:1:1}\text{-}As_{10})]$ (**4**) or $[(Cp^{Bn}Mo)_2(\mu,\eta^{2}\text{-}As_2)(\mu,\eta^{3}\text{-}As_3)]$ (**5**) are obtained depending on the reaction conditions. Complex **4** possesses an unprecedented *cyclo*-As_{10} ligand, which is the largest polyarsenic cycle reported so far. Surprisingly, single crystal X-ray diffraction analysis of **3** reveals a co-crystal of $[(Cp^{TetraBn}Mo)_2(\mu,\eta^{6:6}\text{-}As_6)]$ (**3'**) ($Cp^{TetraBn} = \eta^5\text{-}C_5H(CH_2\{C_6H_5\})_4$) and **3** in a ratio of 1:1. Compounds **1**-**3** are fully characterised by single crystal X-ray structure analysis, mass spectrometry, elemental analysis and spectroscopic methods (^1H and $^{13}C\{^1H\}$ NMR spectroscopy for **1** and **3**/**3'** or EPR spectroscopy and Evans method for **2**). Furthermore, the redox chemistry of **2** and **3**/**3'** was studied by cyclic voltammetry, showing two reversible oxidations and a reversible reduction for **2**, whereas **3**/**3'** exhibit a reversible and an irreversible oxidation. The by-products **4** and **5** were mainly characterised by single crystal X-ray diffraction analysis, DFT calculations and ^1H NMR spectroscopy (**4**) or mass spectrometry (**5**).

4.1 Author contributions

- All syntheses and characterisations were performed by Monika Schmidt.
- Manuscript was written by Monika Schmidt.
- Figures were made by Monika Schmidt.
- Single crystal X-ray structure analyses and refinements were performed by Monika Schmidt.
- Cyclovoltammetric measurements of **2** and **3** were performed and interpreted by Felix Riedlberger.
- DFT computations and their description regarding **4** were performed by Dr. G. Balázs.
- Acknowledgement: The EPR spectrum of **2** was recorded by Moritz Modl.

4.2 Introduction

Since the description of the isolobal analogy in 1982, organic and inorganic chemistry became more and more connected.[1] In this context, a methine moiety can be formally exchanged by phosphorus or arsenic, offering new possibilities in the synthesis of inorganic analogues of organic molecules like the cyclopentadienyl anion $[C_5H_5]^-$ (**I**) or benzene C_6H_6 (**II**). In fact, several $(CH)_n$ units can be formally replaced by E atoms (E = P, As) in **I** or **II**. Besides the partial substitution of $(CH)_x$ units,[2] the all pnictogen analogues E_5 and E_6 (E = P, As) are of special interest. To date, both are mostly observed in metallocenes and triple decker sandwich complexes (Figure 4.1).[3] Moreover, the stabilisation in binary compounds M_4E_6 (M = K, Rb, Cs, E = P; M = Rb, Cs, E = As) has also been investigated for the *cyclo*-E_6 derivatives.[4]

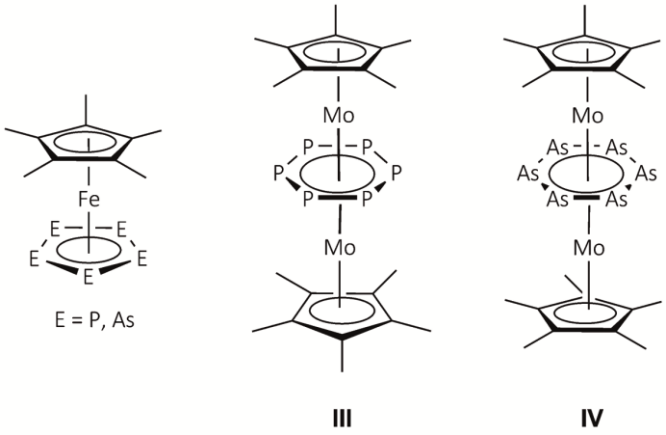

Figure 4.1 Schematic representation of common *cyclo*-E_5 and *cyclo*-E_6 ligand complexes.

The special interest in *cyclo*-E_6 ligand complexes like $[(Cp^*Mo)_2(\mu,\eta^{6:6}\text{-}E_6)]$ (E = P (**III**),[3a] As (**IV**),[3c] $Cp^* = \eta^5\text{-}C_5Me_5$) is based on the high symmetry, the planar E_6 middle deck as well as the

lone pairs at the pnictogen atoms, which are available for further coordination chemistry. These features make them excellent building blocks for supramolecular chemistry. They also act as hexagonal, trigonal or linear linkers in coordination chemistry. Moreover, bridged *cyclo*-E_6 complexes represent a supramolecular inorganic analogue of graphene. Quite recently, the coordination chemistry of **III** towards monovalent metal salts $[M]^+[X]^-$ (M = Cu, X = Br, I;[5] M = Tl, Cu, Ag, X = $[Al\{OC(CF_3)_3\}_4]$ (≡ [TEF])[6]) has been investigated, leading to the formation of coordination polymers. These contain planar two dimensional layers for the reaction with copper halides and two dimensional coordination networks for the reaction with [Tl][TEF]. Here, the network consists of alternating layers of positively and negatively charged sheets. Both can be regarded as the supramolecular inorganic analogues of graphene. In contrast, the use of M = Cu or Ag yielded the discrete coordination dimers $[M(Cp^*Mo)_2(\mu,\eta^{6:6}\text{-}P_6)\}_2]^+$.[6]

To date, the number of P_n ligand complexes of the general formula $[(Cp^RM)_2P_6]$ exceeds the number of its heavier congener $[(Cp^RM)_2As_6]$. While triple decker complexes containing a *cyclo*-P_6 ligand exist for molybdenum,[3a,7,8] tungsten,[9] vanadium,[9] niobium,[10] and titanium,[11] only two examples are accounted for arsenic in literature.[3c] Unfortunately, the reported yields for these triple decker complexes are usually lower than 10%, making further reactivity studies difficult. However, for the molybdenum complexes $[(Cp^RMo)_2(\mu,\eta^{6:6}\text{-}P_6)]$ (Cp^R = Cp* (η^5-C_5Me_5), Cp^{Bn} (η^5-$C_5\{CH_2(C_6H_5)\}_5$)) yields of 64 % (Cp*)[6] and 58 % (Cp^{Bn})[7] have been reported. Nevertheless, Cp* derivatives and especially its coordination compounds often exhibit low solubility, limiting the applicable characterisation methods. Therefore, it would be desirable to introduce the Cp^{Bn} ligand, which is known to considerably increase the solubility of the P_n ligand complexes as well as their coordination compounds. Furthermore, it was demonstrated previously that P_n ligand complexes bearing the Cp^{Bn} ligand often possess a different reactivity towards monovalent metal salts. As a result, novel soluble coordination products are obtained in comparison to the Cp* derivatives.[12]

Herein, we report on a straightforward synthesis of the precursor complex $[Cp^{Bn}Cr(CO)_2]_2$ (**1**) as well as on the subsequent reaction of $[Cp^{Bn}M(CO)_2]_2$ (M = Cr (**1**), Mo) with As_4 at high temperatures. For **1**, the reaction results in the formation of $[(Cp^{Bn}Cr)_2(\mu,\eta^{5:5}\text{-}As_5)]$ (**2**), while for M = Mo the triple decker complexes $[(Cp^{Bn}Mo)_2(\mu,\eta^{6:6}\text{-}As_6)]$ (**3**) and $[(Cp^{TetraBn}Mo)_2(\mu,\eta^{6:6}\text{-}As_6)]$ (**3'**) ($Cp^{TetraBn}$ = η^5-$C_5H(CH_2\{C_6H_5\})_4$) are the main products. Additionally, the novel arsenic rich complex $[(Cp^{Bn}Mo)_2(\mu,\eta^{5:5:1:1}\text{-}As_{10})]$ (**4**) and $[(Cp^{Bn}Mo)_2(\mu,\eta^2\text{-}As_2)(\mu,\eta^3\text{-}As_3)]$ (**5**) can be obtained as minor products depending on the reaction conditions.

4.3 Results and Discussion

Following the synthesis for $[Cp^{Bn}Mo(CO)_2]_2$,[7] **1** is easily obtained as microcrystalline powder by co-thermolysis of $Cp^{Bn}H$ and $[Cr(CO)_6]$ at high temperatures (Scheme 4.1).

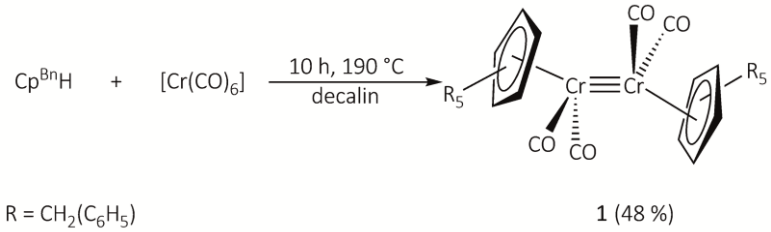

Scheme 4.1 Synthesis of **1**.

Compound **1** is soluble in CH_2Cl_2 and toluene, slightly soluble in *n*-hexane and thf and insoluble in CH_3CN. By layering a CH_2Cl_2 solution with *n*-hexane, **1** crystallises in the monoclinic space group $P2_1/c$ as dark green blocks. The molecular structure of **1** is depicted in Figure 4.2. Single crystal X-ray structure analysis of **1** reveals a dinuclear complex with *trans* conformation of the CO ligands with respect to the chromium-chromium unit and a staggered conformation of the Cp^{Bn} ligands.

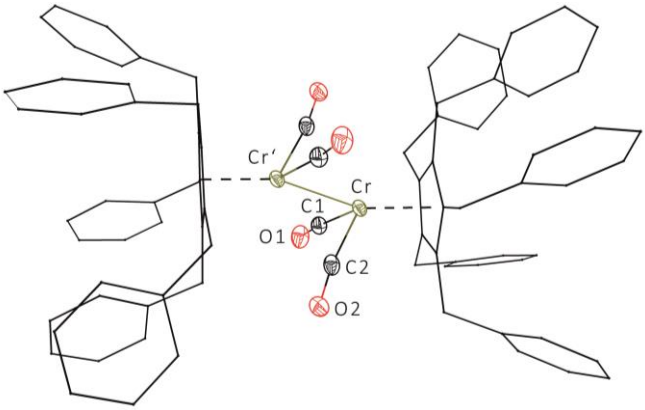

Figure 4.2 Molecular structure of **1** in the solid state. H atoms are omitted for clarity and Cp^{Bn} ligands are drawn in wire or frame model. Thermal ellipsoids are drawn at 50 % probability level. Selected bond lengths [Å] and angles [°]: Cr-Cr' 2.3024(4), Cr1-C1 1.8357(14), Cr1-C2 1.8298(14), C1-O1 1.1602(17), C2-O2 1.1673(17), Cp_{cent}-Cr-Cr' 158.942(17), Cr1-C1-O1 172.65(12), Cr1-C2-O2 171.88(11), C1-Cr-C2 89.96(6).

The expected terminal coordination mode of the carbonyl ligands is in line with the CO stretching bands of **1** in the IR spectrum (ν_{CO}(KBr) = 1817 cm^{-1}, 1848 cm^{-1}, 1879 cm^{-1}, 1897 cm^{-1}). The Cr-Cr triple bond of **1** is typically short (Cr-Cr' 2.3024(4) Å) but slightly longer than other reported Cr-Cr distances in $[Cp^RCr(CO)_2]_2$ (Cp^R = Cp (η^5-C_5H_5): Cr-Cr' 2.230(3) Å,[13] Cp*: Cr-Cr' 2.280(2) Å,[14] Cp^{3Me} (η^5-$C_5H_2Me_3$): Cr-Cr' 2.267(1) Å[15]). The ^1H and $^{13}C\{^1H\}$ NMR spectra of **1** show the corresponding signals for two chemically and magnetically equivalent Cp^{Bn} ligands as well as a

signal for the carbonyl ligands in the $^{13}C\{^{1}H\}$ NMR spectrum ($\delta[CD_2Cl_2]$ = 251.28 ppm) (see Figure S4.1-S4.2, supplementary information).

Subsequent reaction of **1** with yellow arsenic at elevated temperatures leads to the formation of **2** (Scheme 4.2). Although the thermolysis is performed overnight and with an excess of As_4, residual **1** could be found during the chromatographic workup.

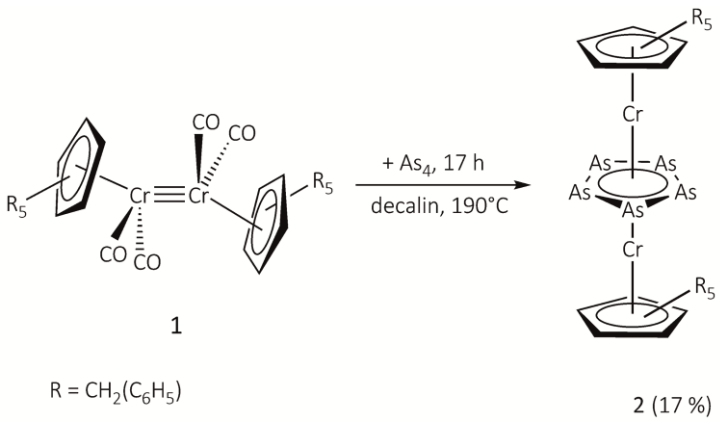

Scheme 4.2 Synthesis of **2**.

Compound **2** is soluble in CH_2Cl_2, toluene and thf and insoluble in *n*-hexane and CH_3CN. By layering a CH_2Cl_2 solution with CH_3CN, **2** crystallises in the monoclinic space group $P2_1/c$ as long brownish orange plates or needles. Single crystal X-ray structure analysis of **2** reveals a triple decker structure with a planar *cyclo*-As_5 middle deck in between two [$Cp^{Bn}Cr$] fragments (Figure 4.3). The Cp^{Bn} ligands show a staggered conformation in the solid state with respect to the *cyclo*-As_5 unit. All As-As bond lengths within the *cyclo*-As_5 middle deck are in the range of 2.4247(6) Å to 2.4402(7) Å, which is not considerably shortened compared to an As-As single bond (electron diffraction: 2.435 Å in As_4,[16] DFT calculations: 2.4372 Å in As_4[17]). The Cr1-Cr2 distance of 2.8113(7) Å is slightly elongated in comparison to reported Cr-Cr bonds in the isostructural triple decker complexes $[(Cp^RCr)_2(\mu,\eta^{5:5}\text{-}As_5)]$ (Cp^R = Cp^{Me} ($\eta^5\text{-}C_5H_4Me$): Cr-Cr 2.776(4) Å,[18] Cp' ($\eta^5\text{-}C_5EtMe_4$): Cr-Cr 2.773(2) Å[19]). Considerably longer Cr-Cr distances like in $[\{CpCr(CO)_2\}_2(\mu,\eta^2\text{-}As_2)]$ (Cr-Cr 3.026(1) Å) have been described in literature.[20]

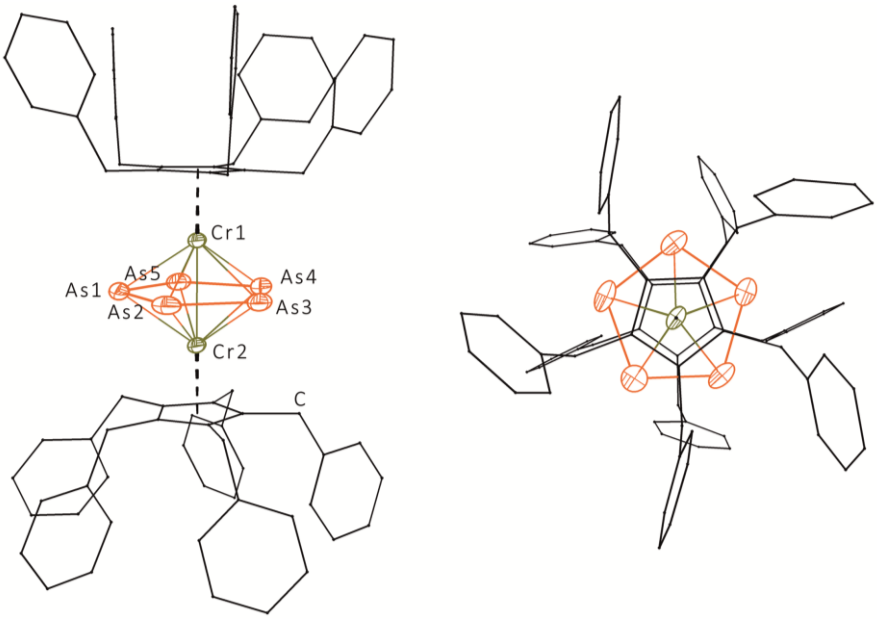

Figure 4.3 Molecular structure of **2** in the solid state (left). Top view of **2** (right). H atoms are omitted for clarity and Cp^{Bn} ligands are drawn in wire or frame model. Thermal ellipsoids are drawn at 50 % probability level. Selected bond lengths [Å] and angles [°]: Cr1-Cr2 2.8113(7), As1-As2 2.4268(7), As2-As3 2.4247(6), As3-As4 2.4326(7), As4-As5 2.4387(7), As5-As1 2.4402(7), As1-As2-As3 107.93(2), As2-As3-As4 108.30(2), As3-As4-As5 107.92(2), As4-As5-As1 107.56(2), As5-As1-As2 108.28(2).

The triple decker complex **2** is a 29 VE complex. Accordingly, **2** should exhibit paramagnetic behaviour due to the presence of at least one unpaired electron. The magnetic moment of **2** (μ_{eff} = 1.50 μ_B) was determined by Evans method, which is consistent with one unpaired electron (see Figure S4.8, supplementary information). Moreover, the EPR spectrum of **2** in CD_2Cl_2 at 77 K shows a signal without hyperfine coupling at g_{iso} = 2.011, which is in good agreement with the reported g_{iso} = 2.005 value for the isostructural complex $[(Cp'Cr)_2(\mu,\eta^{5:5}\text{-}As_5)]$[19] (see Figure S4.9, supplementary information). Thus, an average oxidation state of +1.5 (d^4/d^5 system) has been proposed for each chromium atom. The cyclic voltammogram of **2** in CH_2Cl_2 shows two reversible oxidations ($E_{1/2}$= -0.36 V; $E_{1/2}$= +0.69 V; both vs. $[Cp_2Fe]/[Cp_2Fe]^+$) and a reversible reduction ($E_{1/2}$= -1.43 V vs. $[Cp_2Fe]/[Cp_2Fe]^+$) (see Figure S4.10, supplementary Information). Unfortunately, the chemical oxidation and reduction could not be achieved during the scope of this thesis.

The co-thermolysis of $[Cp^{Bn}Mo(CO)_2]_2$ with As_4 in decalin leads to the formation of **3** and **3'** as the main products (Scheme 4.4). As the starting material $[Cp^{Bn}Mo(CO)_2]_2$ is not fully converted during these reactions even after 93 h at 190 °C, IR spectroscopic reaction control was impossible. As a consequence, the final reaction time could not be determined exactly. Hence, besides **3**/**3'**, complex **4** or **5** can be isolated in traces as by-products depending on the reaction conditions (Scheme 4.4). Unfortunately, **4** and **5** could be observed only once,[21] while **3**/**3'** seem to be the

thermodynamically favoured products and could be isolated each time. All complexes are soluble in CH_2Cl_2, toluene and thf and insoluble in CH_3CN or *n*-hexane.

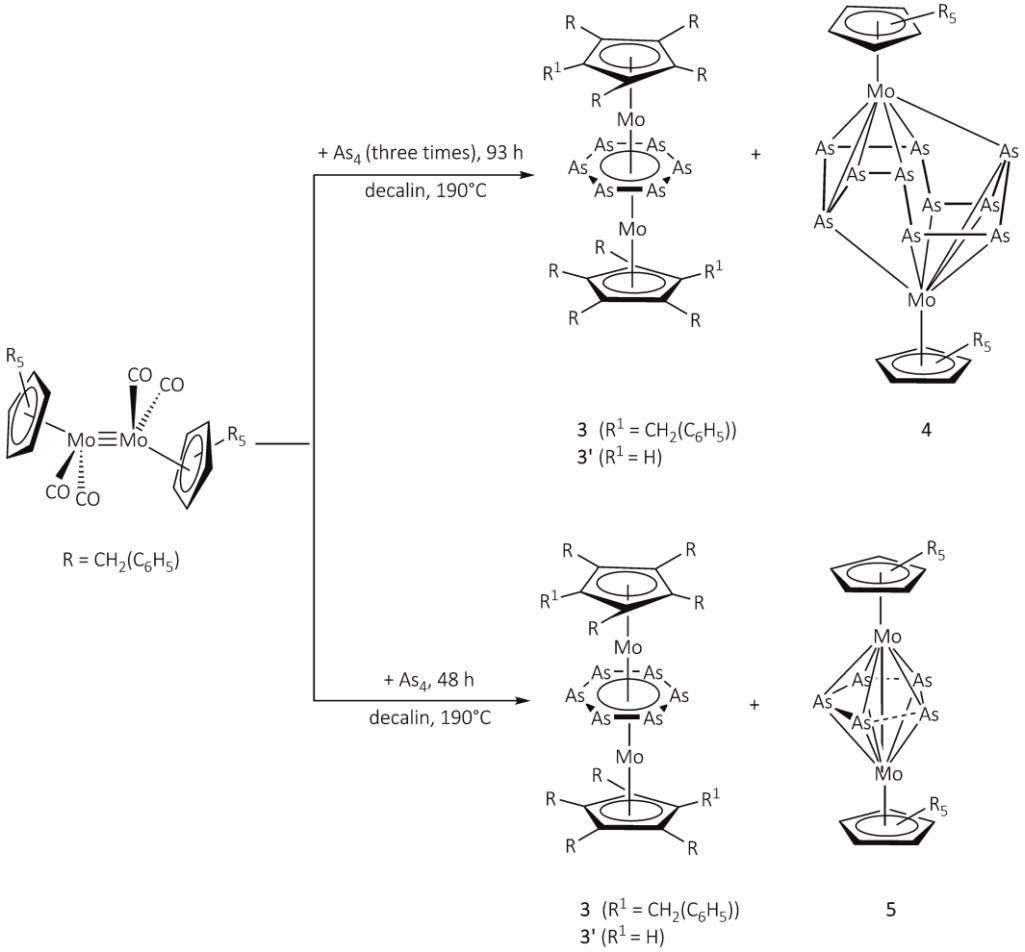

Scheme 4.4 Reactions of $[Cp^{Bn}Mo(CO)_2]_2$ with As_4.

After column chromatographic workup, **3** and **3'** can be crystallised by layering a CH_2Cl_2 solution with CH_3CN. Being very similar, these two complexes co-crystallise as brownish orange blocks in the monoclinic space group *C*2/*c*. Single crystal X-ray diffraction analysis reveals a triple decker structure with a planar *cyclo*-As_6 middle deck for **3** and **3'** stabilised by two $[Cp^RMo]$ fragments (Cp^R = Cp^{Bn} (**3**), $Cp^{TetraBn}$ (**3'**)) (Figure 4.4). Only one half of the molecule can be found in the asymmetric unit, the other half is generated by symmetry. Moreover, two sorts of triple decker complexes (**3** and **3'**) statistically take the same crystallographic position resulting in the co-crystallisation of **3** and **3'**. Therefore, the overall chemical composition of **3** and **3'** can be determined to be $C_{73}H_{64}Mo_2As_6$ indicating a ratio of **3** and **3'** of 1:1. This composition is also in line with the results found in the elemental analysis as well as the approximated integrals in the ^{1}H NMR spectra of **3** and **3'**. The presence of the $Cp^{TetraBn}$ ligand could be probably explained due to impurities of the $Cp^{Bn}H$ ligand.[22] The As-As bond lengths within the *cyclo*-As_6 units are in-

between As-As single bonds and As-As double bonds (2.354(11) Å - 2.43(5) Å) but elongated compared to the isostructural Cp' derivative [(Cp'Mo)$_2$(μ,η$^{6:6}$-As$_6$)] (2.337(3) Å - 2.365(3) Å).[3c] The Mo-Mo' distances of **3** and **3'** are consistent with the Mo-Mo bond length reported in literature (**3/3'**: 2.6638(9) Å, [(Cp'Mo)$_2$(μ,η$^{6:6}$-As$_6$)]: 2.639(1) Å[3c]).

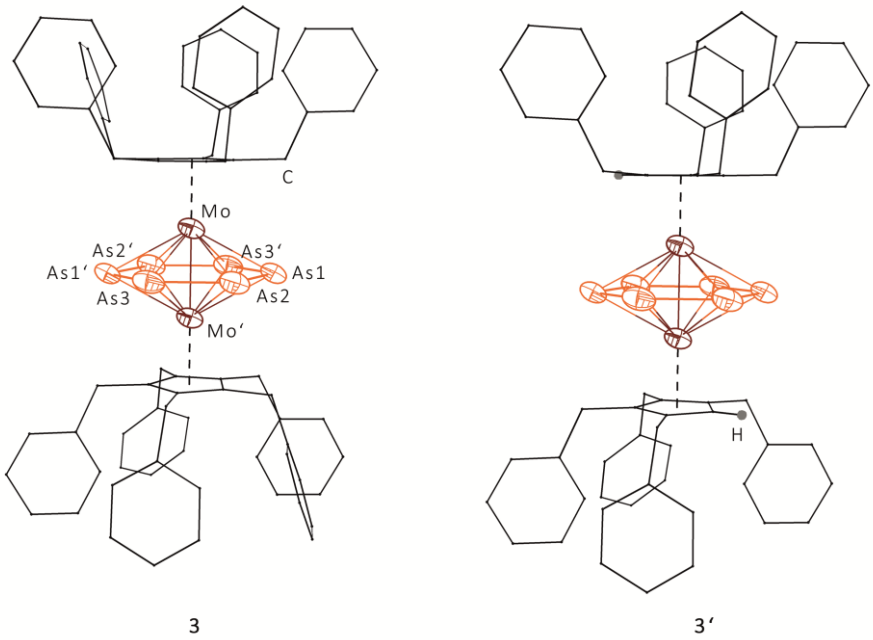

Figure 4.4 Molecular structure of **3** (left) and **3'** (right) in the solid state (main part). H atoms of the benzyl ligands are omitted for clarity and Cp^{Bn} ligands as well as the Cp^{TetraBn} ligands are drawn in wire or frame model. Due to disorder only the main part is depicted and thermal ellipsoids are drawn at 50 % probability level. **3** and **3'** crystallise on the same crystallographic position in a 1:1 ratio. Selected bond lengths [Å] and angles [°]: Mo-Mo' 2.6638(9), As1-As2 2.354(11), As2-As3 2.394(13), As3-As1' 2.43(5), As1-As2-As3 122.8(18), As2-As3-As1' 120.1(12), As3-As1'-As2' 117.1(15).

The ^{1}H and ^{13}C{^{1}H} NMR spectra of a mixture of **3** and **3'** show the corresponding set of signals for the Cp^{Bn} and Cp^{TetraBn} ligands. Therein, the chemical shifts could be exactly assigned due to ^{1}H COSY, ^{1}H ^{13}C{^{1}H} HSQC and ^{1}H ^{13}C{^{1}H} HMBC NMR spectra of **3/3'** (see Figure S4.3-S4.7, supplementary information). Moreover, the electrochemistry of **3/3'** was investigated by cyclic voltammetry. The cyclic voltammogram of **3/3'** in CH_2Cl_2 shows a reversible oxidation ($E_{1/2}$= -0.12 V vs. [Cp$_2$Fe]/[Cp$_2$Fe]$^+$) and an irreversible oxidation (E= +0.65 V vs. [Cp$_2$Fe]/[Cp$_2$Fe]$^+$) (see Figure S4.11, supplementary Information). Therefore, an oxidation of **3/3'** by [Cp$_2$Fe]$^+$ or by Ag$^+$ in CH_2Cl_2 should be possible.[23] Unfortunately, the chemical oxidation of **3/3'** could not be achieved so far.

During column chromatographic work up, only once a green fraction of **4** is obtained. By layering a CH_2Cl_2 solution with cyclohexane, **4** crystallises in the triclinic space group $P\bar{1}$ as dark green plates. Single crystal X-ray structure analysis of **4** reveals a strongly folded *cyclo*-As$_{10}$ ligand

stabilised between two [Cp^{Bn}Mo] fragments (Figure 4.5). Only one half of the molecule can be found in the asymmetric unit, the other half is generated by symmetry. The As-As distances within the *cyclo*-As_{10} unit alternate between an As-As double bond (As1-As2 2.3580(6) Å, As4-As5 2.3538(5) Å) and an As-As single bond (As2-As3 2.4224(4) Å, As3-As4 2.4223(5) Å). Therefore, the As_{10} unit can be best described as a decaarsa-2,4,7,9-tetradiene-1,6-diide stabilised by $[Cp^{Bn}Mo]^+$ fragments. Additionally to the twofold η^2-coordination mode, a η^1-coordination of the atoms As3 and As3' to molybdenum is observed. Consequently, a formal oxidation state of +2 is expected for each molybdenum atom.

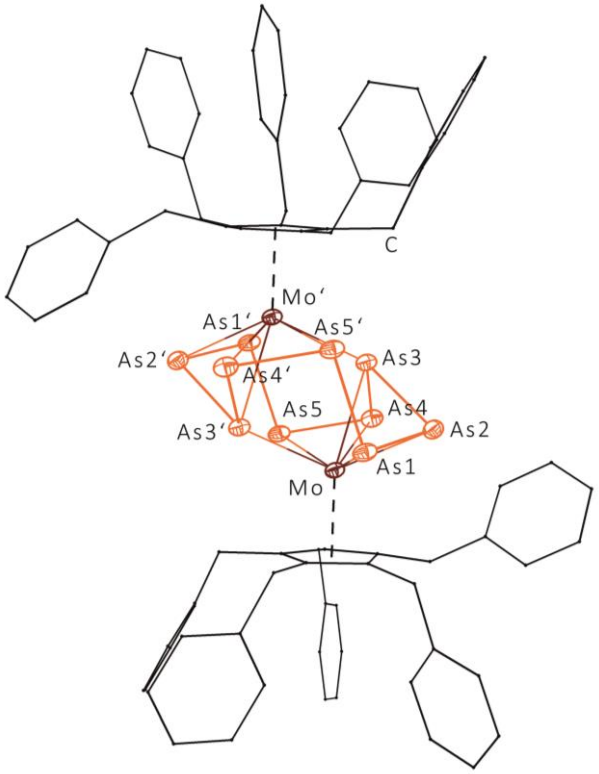

Figure 4.5 Molecular structure of **4** in the solid state. H atoms are omitted for clarity and Cp^{Bn} ligands are drawn in wire or frame model. Thermal ellipsoids are drawn at 50 % probability level. Selected bond lengths [Å] and angles [°]: As1-As2 2.3580(6), As2-As3 2.4224(4), As3-As4 2.4223(5), As4-As5 2.3538(5), As5-As1' 2.4127(5), Mo-As3' 2.6239(5), As1-As2-As3 90.333(17), As2-As3-As4 86.807(16), As3-As4-As5 90.809(18).

DFT calculations (RI-BP86/def2-TZVP) confirm the bonding situation in **4**. This is also reflected in the Wiberg Bond Indices (WBI) of the corresponding bonds. The As-As bonds with a double bond character have a bond order of 1.05, while the other As-As bonds have slightly lower bond orders (WBI of 0.83 and 0.95). Furthermore, the visualisation of the localised molecular orbitals (LMO, Figure 4.6) clearly indicates a bonding interaction between As3 and Mo (LMO 214) as well as between As3' and Mo (LMO 192). The As3'-Mo bond (LMO 192) is considerably polarised towards arsenic (~76% arsenic atomic orbital (AO) contribution), while the As3-Mo bond (LMO 214) is much less polarised (~57 % arsenic AO contribution). Furthermore, the hybridisation

of As3 is considerably different. In LMO 192 the arsenic is $sp^{0.60}$ hybridised, in LMO 214 the bonding is realised over a pure p orbital (see supplementary information, DFT part).

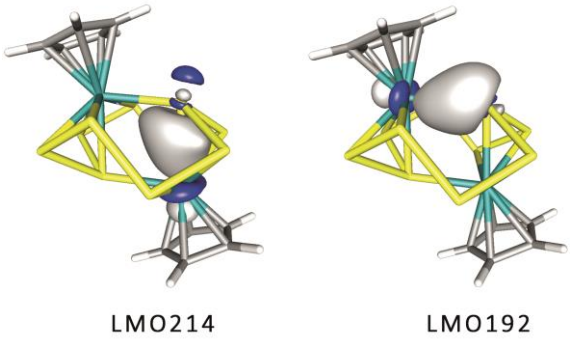

Figure 4.6 Isosurfaces of selected localised molecular orbitals in $[(CpMo)_2(\mu,\eta^{5:5:1:1}\text{-}As_{10})]$ showing the As3-Mo and As3'-Mo bonds. Calculated at the BP86/def2-TZVP level of theory.

Up to date, **4** represents the largest polyarsenic cycle known so far. Indeed, larger As_n ligand complexes up to n = 12 ($[(Cp'''Co)_3(\mu_3,\eta^{4:4:2:1}\text{-}As_{12})]$, Cp''' = η^5-1,2,4-$C_5H_2{}^tBu_3$) are reported in literature, but such complexes usually contain individually bridged arsenic subunits.[24] Accordingly, $[(Cp'''Co)_3(\mu_3,\eta^{4:4:2:1}\text{-}As_{12})]$ is built up by a norbornadiene like As_7 unit linked by an As-As bond to an envelope like As_5 unit. Besides, polyarsenic frameworks with up to 22 arsenic atoms are known for Zintl anions.[25] In addition, the isostructural P_n ligand complex $[(Cp^*Mo)_2(\mu,\eta^{5:5:1:1}\text{-}P_{10})]$ has been obtained by co-thermolysis of $[Cp^*Mo(CO)_2]_2$ with P_4, exhibiting a similar bonding situation with an alternation of the P-P bonds between a double and a single bond.[6] Therefore, $[(Cp^*Mo)_2(\mu,\eta^{5:5:1:1}\text{-}P_{10})]$ and **4** are the heavier congeners of $[C_{10}H_{10}]^{2-}$, which has been intensively studied by theoretical methods.[26]

Depending on the reaction time, **5** can be observed only once as the minor product after 48 h during column chromatographic workup. Crystals of **5** can be obtained in the dark brown oily residue after removal of the solvent. **5** crystallises as brown blocks in the monoclinic space group $P2_1/c$. Single crystal X-ray structure analysis of **5** reveals a triple decker structure with a pseudo five-membered arsenic middle deck. Here, a η^3-coordinated As_3 moiety and a η^2-coordinated As_2 unit are stabilised by two $[Cp^{Bn}Mo]$ fragments (Figure 4.7). The Cp^{Bn} ligands show an eclipsed conformation. Unfortunately, only a preliminary model of **5** can be depicted, since the arsenic unit as well as the Cp^{Bn} ligands show severe disorder over several positions. Consequently, a discussion of the As-As bond distances or bond angles is not possible to date.

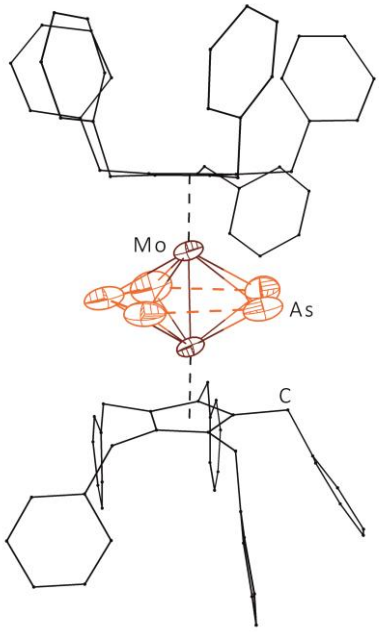

Figure 4.7 Preliminary model of the molecular structure of **5** in the solid state (main part). H atoms of the Cp^{Bn} ligands are omitted for clarity and Cp^{Bn} ligands are drawn in wire or frame model. Thermal ellipsoids are drawn at 50 % probability level.

Nevertheless, **5** shows close structural analogy to $[(CpMo)_2(\mu,\eta^2\text{-}As_2)(\mu,\eta^3\text{-}As_3)]$ and similar trends in the As-As distances as well as in the Mo-Mo bond lengths are observed.[27] Alternatively, in $[(CpMo)_2(\mu,\eta^2\text{-}As_2)(\mu,\eta^3\text{-}As_3)]$ the formal As_5 unit was proposed as a $[\eta^4\text{-}As_5]^{4-}$ ligand, exhibiting longer As-As bond lengths (2.385(3) Å - 2.752(3) Å) as expected. The latter is also expected to be paramagnetic due to formal Mo^{3+} centres. For **5**, no signal in the EPR spectra at room temperature or at 77 K was detected, suggesting an open shell system with short relaxation times. Unfortunately, the magnetic moment of **5** could not be determined by Evans method, since crystals are only obtained in traces in the oily residue. However, the peak corresponding to the molecular ion of $[\mathbf{5}]^+$ at *m/z* = 1597.9 could be detected by EI mass spectrometry.

In summary, the synthesis of the chromium precursor $[Cp^{Bn}Cr(CO)_2]_2$ (**1**) is presented. Single crystal X-ray structure analysis of **1** reveals a *trans* conformation of the CO ligands with respect to the chromium-chromium unit as well as a Cr-Cr bond in the range of a Cr-Cr triple bond. Subsequent co-thermolysis of **1** with As_4 at high temperatures leads to the selective formation of the triple decker complex $[(Cp^{Bn}Cr)_2(\mu,\eta^{5:5}\text{-}As_5)]$ (**2**), containing a *cyclo*-As_5 middle deck. The magnetic moment of **2** was determined by Evans method (μ_{eff} = 1.50 μ_B) as well as by EPR spectroscopy (g_{iso} = 2.011), which are both consistent with one unpaired electron. The cyclic voltammetric data of **2** show two reversible oxidations and a reversible reduction of the complex. Moreover, the reaction of $[Cp^{Bn}Mo(CO)_2]_2$ and As_4 has been investigated. Here, the *cyclo*-As_6 triple

decker complexes $[(Cp^{Bn}Mo)_2(\mu,\eta^{6:6}\text{-}As_6)]$ (**3**) and $[(Cp^{TetraBn}Mo)_2(\mu,\eta^{6:6}\text{-}As_6)]$ (**3'**) have been obtained. Both compounds crystallise in a 1:1 ratio at the same crystallographic position. Furthermore, the redox chemistry of **3**/**3'** has been studied by cyclic voltammetry revealing a reversible oxidation as well as a second irreversible oxidation. Additionally, the formation of the by-products $[(Cp^{Bn}Mo)_2(\mu,\eta^{5:5:1:1}\text{-}As_{10})]$ (**4**) and $[(Cp^{Bn}Mo)_2(\mu,\eta^{2}\text{-}As_2)(\mu,\eta^{3}\text{-}As_3)]$ (**5**) could be observed. While **4** contains the largest known cyclic polyarsenic ligand (As_{10} ligand) to date, for **5** only a preliminary structural model could be proposed due to severe disorder. **5** shows a triple decker structure with a distorted pseudo five-membered *cyclo*-As_5 middle deck, consisting of a η^3-As_3 moiety and a η^2-As_2 unit. Furthermore, the presence of **5** could be confirmed by EI mass spectrometry, while DFT calculations gave an insight into the bonding situation of **4**.

4.4 Experimental Part

General Remarks

All reactions were performed under an atmosphere of dry argon or nitrogen using glovebox or Schlenk techniques. Solvents were purified, degassed and dried prior to use. $[Cp^{Bn}Mo(CO_2)_2]$,[7] $Cp^{Bn}H$[28] and As_4[29] were prepared according to literature procedures. $[M(CO)_6]$ (M = Mo, Cr) was commercially available and was used without further purification.

The NMR spectra were recorded on a Bruker Avance 300, Avance III HD 400 or Avance III HD 600 spectrometer. The EI MS spectra were measured either on a ThermoQuest Finnigan MAT SSQ 710A mass spectrometer or on a Jeol AccuTOF GCX spectrometer. The LIFDI MS spectra were measured on a Finnigan MAT 95 mass spectrometer. The elemental analyses were determined with a Vario ELIII apparatus. The X-band EPR measurements of **2** and **5** were carried out with a MiniScope MS400 device with a frequency of 9.5 GHz and rectangular resonator TE102 of the company Magnettech GmbH. The IR spectrum was measured on a VARIAN FTS-800 FT-IR spectrometer.

Synthesis of $[Cp^{Bn}Cr(CO)_2]_2$ (1)

$Cp^{Bn}H$ (4.17 g, 8.07 mmol) and $[Cr(CO)]_6$ (1.78 g, 8.08 mmol) were dissolved in 150 mL decalin and the mixture was heated to reflux. The reaction progress was monitored by IR spectroscopy. After 10 h, the deep green solution was allowed to cool to room temperature. Within this time, **1** crystallises as microcrystalline powder. The mother liquor was decanted and the powder was washed with *n*-pentane and dried *in vacuo*. Crystals suitable for single crystal X-ray structure analysis were obtained by layering a CH_2Cl_2 solution of **1** with *n*-hexane.

Analytical data of **1**

Crystalline yield: 2.42 g (1.94 mmol, 48 % referred to $Cp^{Bn}H$).

^{1}H NMR (CD_2Cl_2): δ [ppm] = 3.91 (s, 20H, CH_2), 6.56 (d, 20H, C_6H_5), 6.87-6.99 (m, 30H, C_6H_5).

$^{13}C\{^1H\}$ NMR (CD_2Cl_2): δ [ppm] = 31.92 (CH_2), 105.77 (C_5), 126.28 (C_6H_5), 128.29 (C_6H_5), 129.40 (C_6H_5), 139.46 (C_6H_5), 251.28 (CO).

IR (KBr): ν_{CO} [cm^{-1}] = 1817 (vs), 1848 (vs), 1879 (vs), 1897 (vs).

EI MS (70 eV, CH_2Cl_2): *m/z* (%) = 1134.5 (20) ($[(Cp^{Bn}Cr)_2]^+$), 1082.6 (80) ($[Cp^{Bn}{}_2Cr]^+$), 516.5 (20) ($[Cp^{Bn}H]^+$), 425.4 (15) ($[Cp^{Bn}\text{-}C_7H_7]^+$), 330.3 (25) ($[Cp^{Bn}\text{-}H_2\text{-}2\ C_7H_7]^+$), 241.2 (15) ($[Cp^{Bn}\text{-}H_2\text{-}3\ C_7H_7]^+$), 181.2 (55) ($[Cp^{Bn}\text{-}H_2\text{-}4\ C_7H_7]^+$), 91.1 (100) ($[C_7H_7]^+$).

Elemental Analysis: Calculated (%) for [$C_{84}H_{70}Cr_2O_4 \cdot 0.5\ CH_2Cl_2$] (1288.39 g/mol): C 78.70, H 5.55; found C 78.68, H 5.70.

Synthesis of $[(Cp^{Bn}Cr)_2(\mu,\eta^{5:5}\text{-}As_5)]$ (2)

A freshly prepared solution of As_4 (starting from 5 g grey arsenic) in 250 mL decalin was added to a suspension of $[Cp^{Bn}Cr(CO)_2]_2$ (**1**) (780 mg, 0.63 mmol) in 50 mL decalin and refluxed for 17 h. The solvent was removed *in vacuo*. Subsequently column chromatographic work up (silica gel, *n*-hexane, 26 x 2.5 cm) with *n*-hexane/toluene (2:1) afforded a red to brownish fraction of **2**. Unreacted **1** remained mostly on the column and could be partially eluted with toluene or CH_2Cl_2. **2** can be crystallised from concentrated CH_2Cl_2 solutions layered with CH_3CN after complete diffusion as long orange brownish needles or plates.

Analytical data of **2**

Crystalline yield: 165 mg (0.11 mmol, 17 % referred to **1**).

Evans method (CD_2Cl_2): μ_{eff} = 1.50 μ_B.

X-band EPR (77 K, CD_2Cl_2): g_{iso} = 2.011.

EI MS (70 eV, toluene): *m/z* (%) = 1510.1 (7) ($[(Cp^{Bn}Cr)_2As_5]^+$), 514.3 (9) ($[Cp^{Bn}\text{-}H_2]^+$), 425.2 (100) ($[Cp^{Bn}\text{-}C_7H_7]^+$), 299.7 (59) ($[As_4]^+$), 91.1 (100) ($[C_7H_7]^+$).

Elemental Analysis: Calculated (%) for [$C_{80}H_{70}Cr_2As_5$] (1510.01 g/mol): C 63.63, H 4.67; found C 63.12, H 4.70.

Synthesis of $[(Cp^{Bn}Mo)_2(\mu,\eta^{6:6}\text{-}As_6)]$ (3), $[(Cp^{TetraBn}Mo)_2(\mu,\eta^{6:6}\text{-}As_6)]$ (3') and $[(Cp^{Bn}Mo)_2(\mu,\eta^{5:5:1:1}\text{-}As_{10})]$ (4) and $[(Cp^{Bn}Mo)_2(\mu,\eta^{2}\text{-}As_2)(\mu,\eta^{3}\text{-}As_3)]$ (5)[30]

Overall three times in a row, a freshly prepared solution of As_4 (starting from 5 g grey arsenic) in 250 mL decalin was added to a suspension of $[Cp^{Bn}Mo(CO)_2]_2$ (1.33 g, 1.00 mmol) in 50 mL decalin and refluxed for 24 h each time. Altogether the reaction mixture was refluxed for 93 h. The solvent was removed *in vacuo*. The resulting brownish residue was dissolved in *n*-hexane/toluene (2:1). Subsequently column chromatographic work up (silica gel, *n*-hexane, 16 x 3 cm) with *n*-hexane/toluene (3:2) afforded an orange to brownish fraction of **3/3'**. A solvent mixture of *n*-hexane/toluene (1:1) afforded unreacted $[Cp^{Bn}Mo(CO)_2]_2$. A final green fraction of **4** can be eluted with toluene. **2** can be crystallised from concentrated toluene solutions layered with CH_3CN after complete diffusion as long orange brownish needles or plates. Crystals of **4** suitable for single crystal X-ray structure analysis were obtained from CH_2Cl_2 solutions layered with cyclohexane after complete diffusion.

Crystalline yield of 3/3': approximately 20 mg (0.01 mmol, 1 % referred to $[Cp^{Bn}Mo(CO)_2]_2$).

Complex **3/3'** can be obtained in better yield by co-thermolysis of $[Cp^{Bn}Mo(CO)_2]_2$ (918 mg, 0.69 mmol) with As_4 (5 g grey arsenic) in decalin for 48 h with column chromatographic workup as described above. Instead of **4**, this time complex **5** can be isolated in traces as a brown fraction. Crystals of **5** for single crystal X-ray structure analysis were obtained from the oily residue after removal of the solvent.

Analytical data of **3/3'**

Crystalline yield: 96 mg (0.06 mmol, 7 % referred to $[Cp^{Bn}Mo(CO)_2]_2$).

^{1}H NMR (CD_2Cl_2): δ [ppm] = 1.66-1.71 (m, 8H, CH_2[**3'**]), 1.66-1.71(m, 8H, CH_2[**3'**]), 1.85 (s, 10H, CH_2[**3**]), 1.88 (s, 10H, CH_2[**3**]), 3.74 (s, 1H, CH[**3'**]), 3.96 (s, 1H, CH[**3'**]), 5.62 (d, C_6H_5[**3'**]), 5.64 (d, 20H, C_6H_5[**3**]), 6.23-6.26 (m, C_6H_5[**3'**]), 6.30-6.34 (m, C_6H_5[**3'**]), 6.38-6.41 (m, 20H, C_6H_5[**3**]), 6.47-6.51 (m, C_6H_5[**3'**]), 6.56-6.60 (m, 10H, C_6H_5[**3**]) 6.82-6.92 (m, C_6H_5[**3'**]) (due to strong overlap the integration of the benzyl groups of **3'** was not possible).

^{13}C{^{1}H} NMR (CD_2Cl_2): δ [ppm] = 35.11 (CH_2 [**3'**]), 36.17 (CH_2[**3'**]), 36.28 (CH_2[**3**]), 36.34 (CH_2[**3**]), 95.19 (C_5[**3'**]), 95.75 (C_5[**3'**]), 97.08 (C_5[**3**]), 97.13 (C_5[**3**]), 125.45 (C_6H_5[**3'**]), 125.64 (C_6H_5[**3'**]), 125.67 (C_6H_5[**3**]), 126.07 (C_6H_5[**3**]), 127.42 (C_6H_5[**3'**]), 127.43 (C_6H_5[**3'**]), 127.45 (C_6H_5[**3**]), 127.77 (C_6H_5[**3**]), 128.05 (C_6H_5[**3'**]), 128.08 (C_6H_5[**3'**]), 128.11 (C_6H_5[**3**]), 128.14 (C_6H_5[**3**]), 138.75 (C_6H_5[**3'**]), 139.30 (C_6H_5[**3'**]), 139.33 (C_6H_5[**3**]), 139.65 (C_6H_5[**3**]).

LIFDI MS (toluene): *m/z* (%) = 1673.3 (16) $[(Cp^{Bn}Mo)_2As_6]^+$), 1599.4 (80) $[(Cp^{Bn}Mo)_2As_5]^+$), 1582.4 (32) $[(Cp^{TetraBn}Mo)_2As_6]^+$), 1508.7 (100) $[(Cp^{TetraBn}Mo)_2As_5]^+$).

Elemental Analysis: Calculated (%) for $[C_{73}H_{64}Mo_2As_6]$ (1582.70 g/mol): C 55.40, H 4.08; found C 55.60, H 4.19.

Analytical data of **4**

Crystalline yield: few crystals.

^{1}H NMR (CD_2Cl_2): δ [ppm] = 3.89 (s, CH_2), 6.62 (d, C_6H_5), 6.95-7.05 (m, C_6H_5) (due to impurities of **3/3'** the integration of the benzyl groups of **4** was not possible).

Analytical data of **5**

Crystalline yield: few crystals.

X-band EPR (CH_2Cl_2): EPR silent.

EI MS (70 eV, CH_2Cl_2): *m/z* (%) = 1597.9 (40) ($[(Cp^{Bn}Mo)_2As_5]^+$), 1221.4 (75) ($[Cp^{Bn}{}_2Mo_2]^+$), 1128.4 (15) ($[Cp^{Bn}{}_2Mo]^+$), 514.5 (20) ($[Cp^{Bn}\text{-}H_2]^+$), 424.2 (10) ($[Cp^{Bn}\text{-}C_7H_7]^+$), 331.3 (10) ($[Cp^{Bn}\text{-}H_2\text{-}2\ C_7H_7]^+$), 241.2 (15) ($[Cp^{Bn}\text{-}H_2\text{-}3\ C_7H_7]^+$), 181.2 (50) ($[Cp^{Bn}\text{-}H_2\text{-}4\ C_7H_7]^+$), 91.1. (100) ($[C_7H_7]^+$).

4.5 Supplementary Information

NMR Investigations

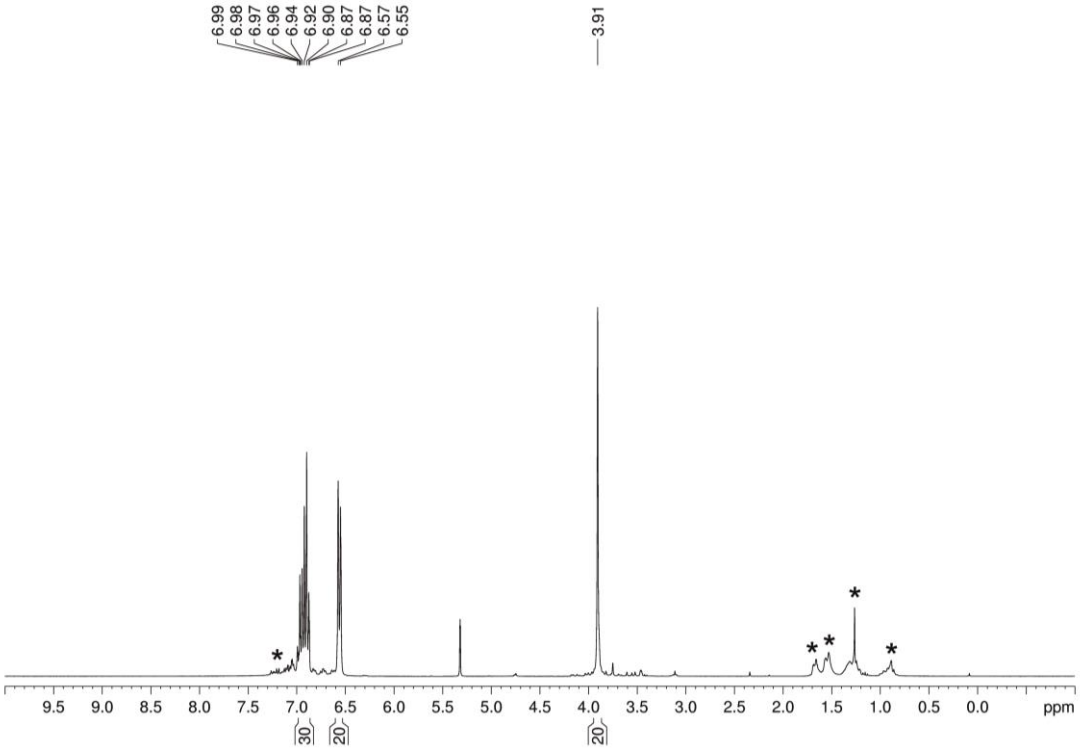

Figure S4.1 ^{1}H NMR spectrum of **1** in CD_2Cl_2 at 300 K. Signals marked with an asterisk are due to different solvents and silicon grease.

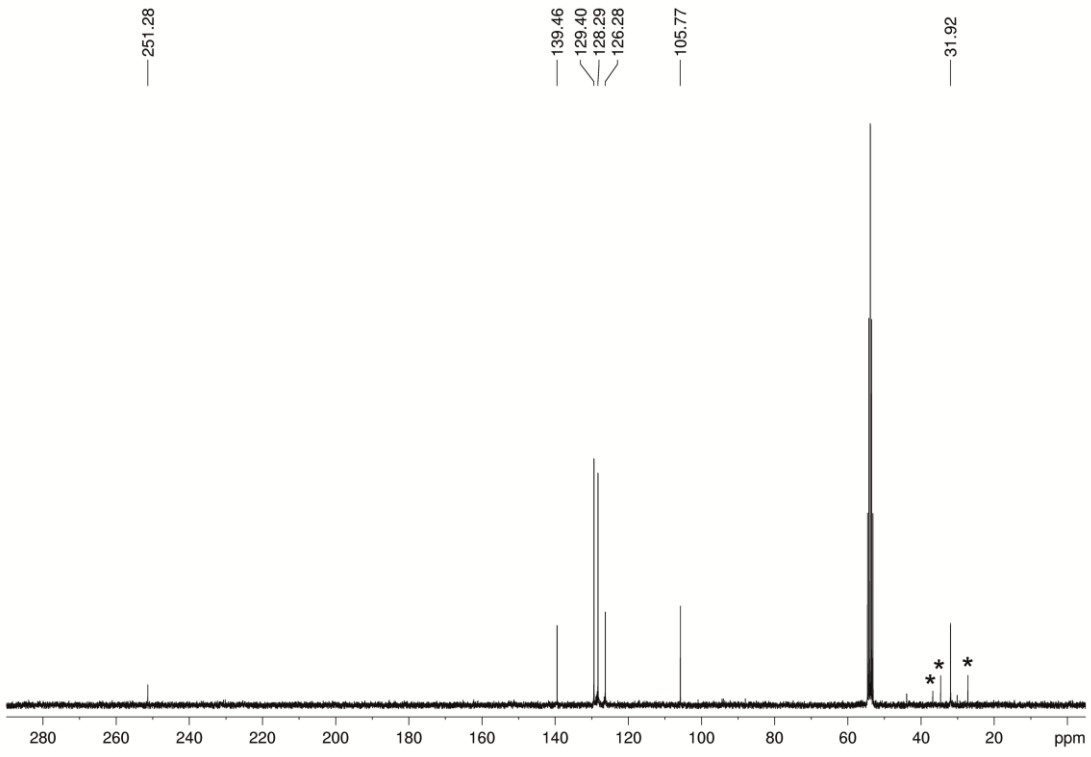

Figure S4.2 $^{13}C\{^{1}H\}$ NMR spectrum of **1** in CD_2Cl_2 at 300 K. Signals marked with an asterisk are due to different solvents and silicon grease.

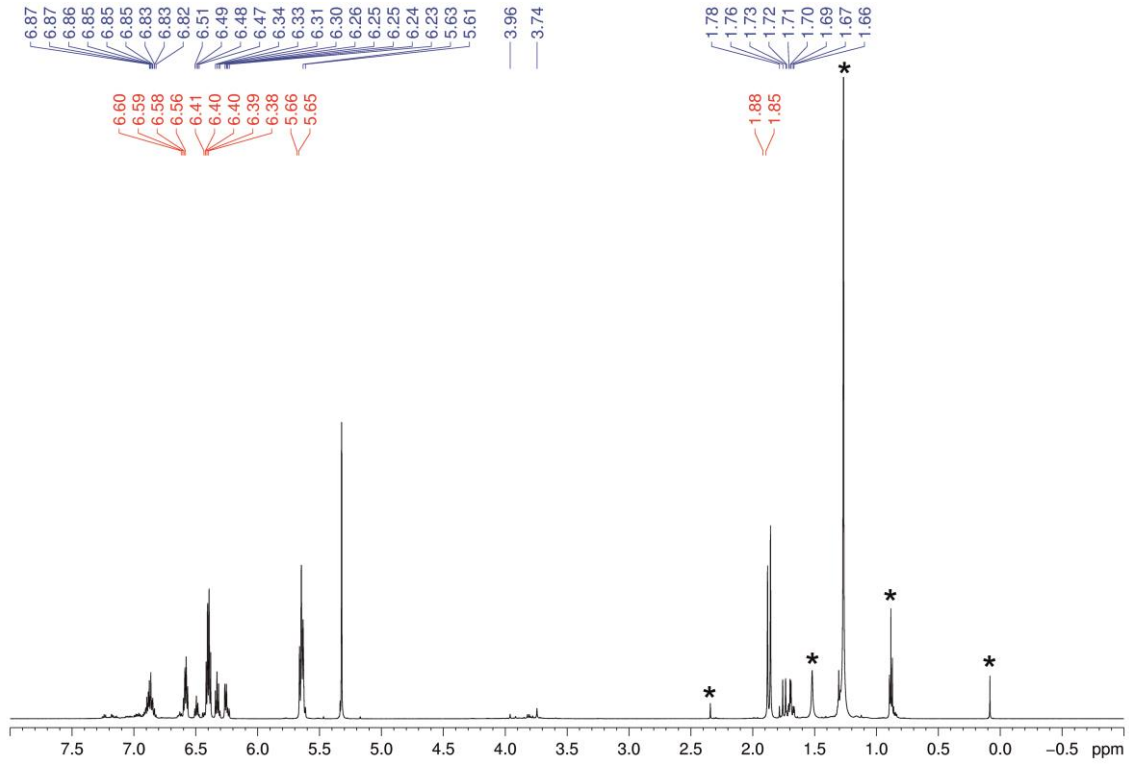

Figure S4.3 ^{1}H NMR spectrum of **3** (red)/**3'** (blue) in CD_2Cl_2 at 300 K. Signals marked with an asterisk are due to different solvents and silicon grease.

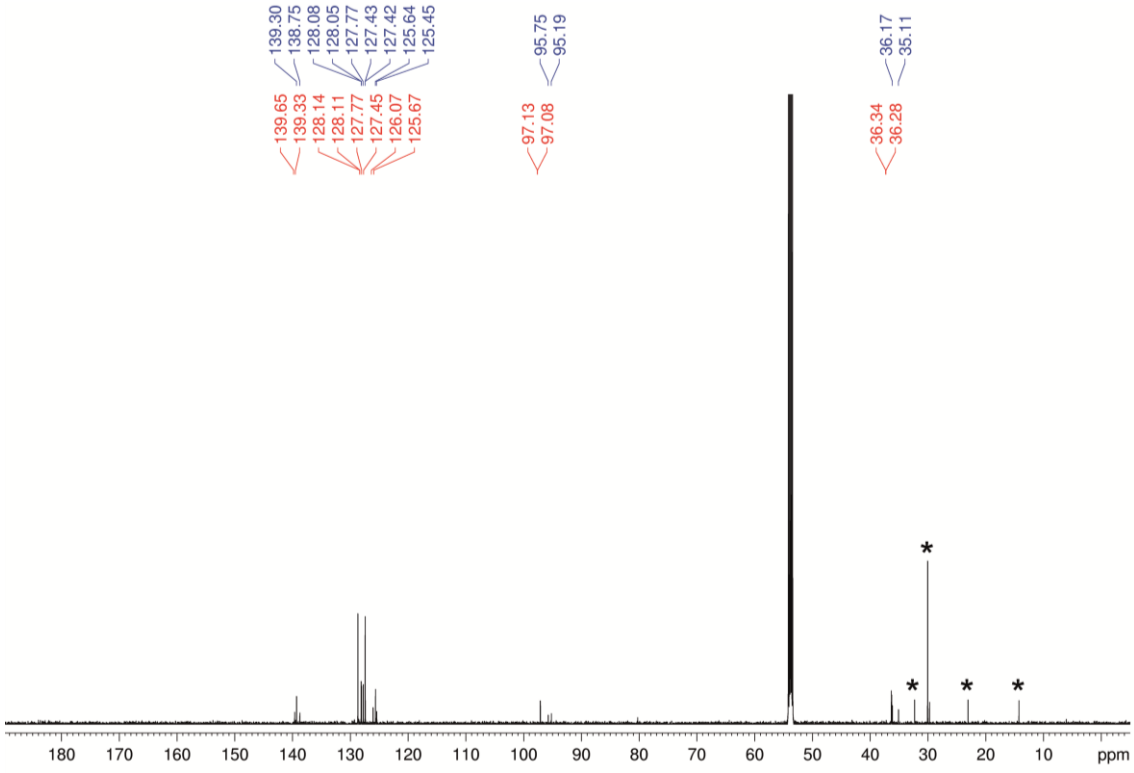

Figure S4.4 $^{13}C\{^{1}H\}$ NMR spectrum of **3** (red)/**3'** (blue) in CD_2Cl_2 at 300 K. Signals marked with an asterisk are due to different solvents and silicon grease.

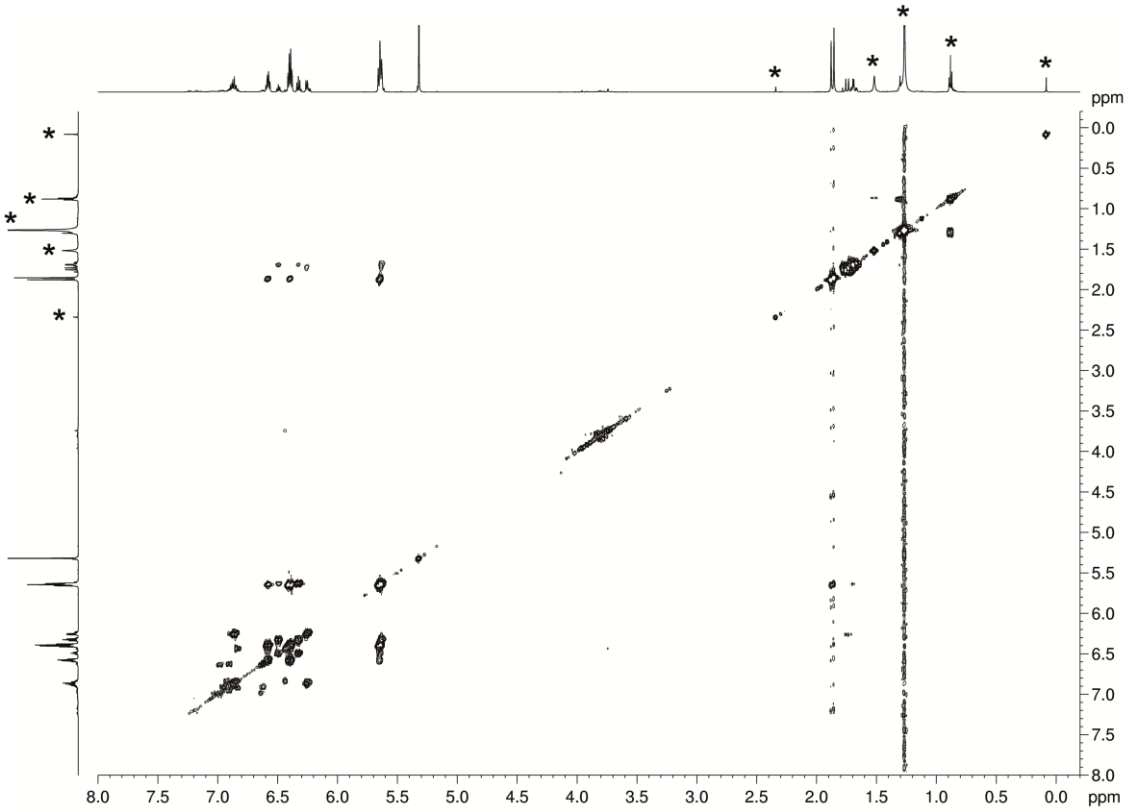

Figure S4.5 ^{1}H COSY NMR spectrum of **3/3'** in CD_2Cl_2 at 300 K. Signals marked with an asterisk are due to different solvents and silicon grease.

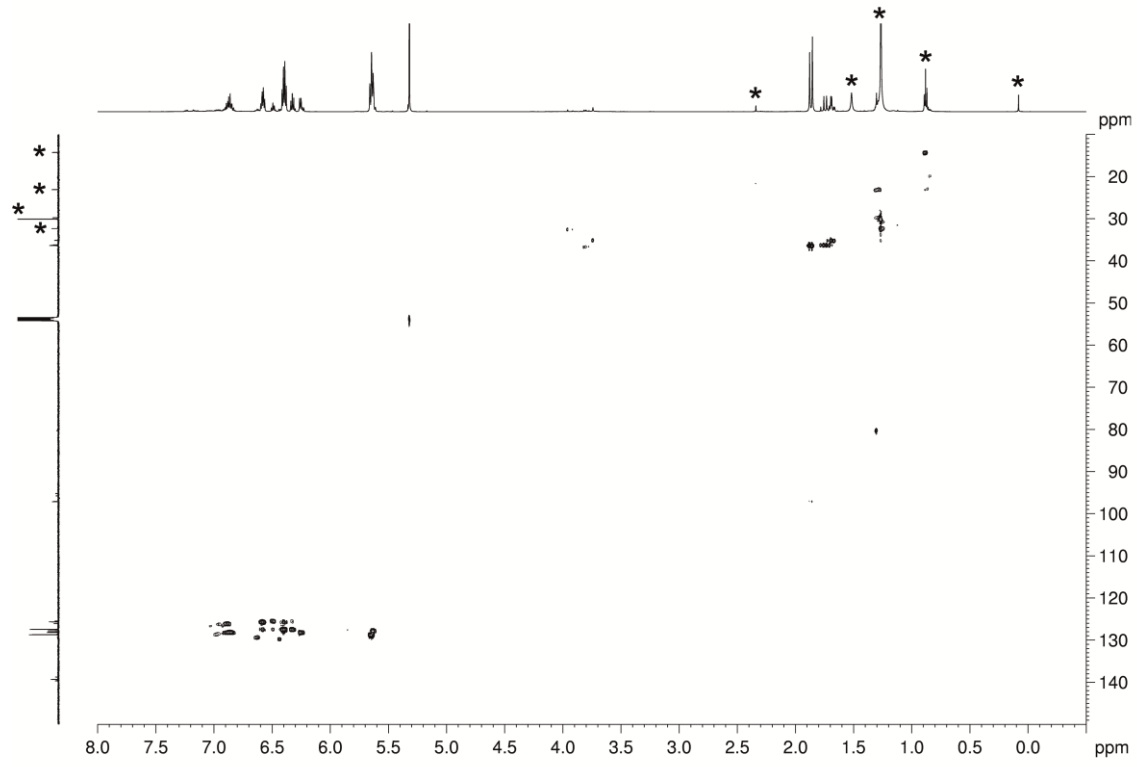

Figure S4.6 ^{1}H $^{13}C\{^{1}H\}$ HSQC NMR spectrum of **3/3'** in CD_2Cl_2 at 300 K. Signals marked with an asterisk are due to different solvents and silicon grease.

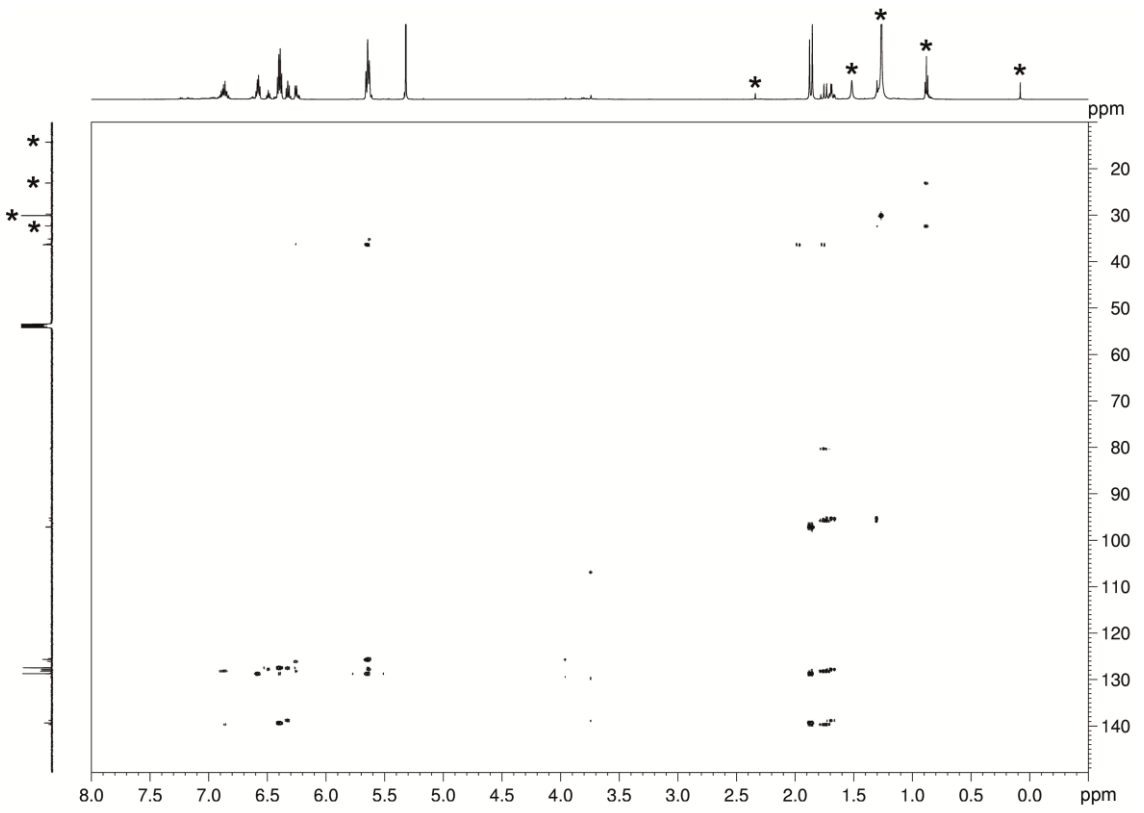

Figure S4.7 ^{1}H $^{13}C\{^{1}H\}$ HMBC NMR spectrum of **3/3'** in CD_2Cl_2 at 300 K. Signals marked with an asterisk are due to different solvents and silicon grease.

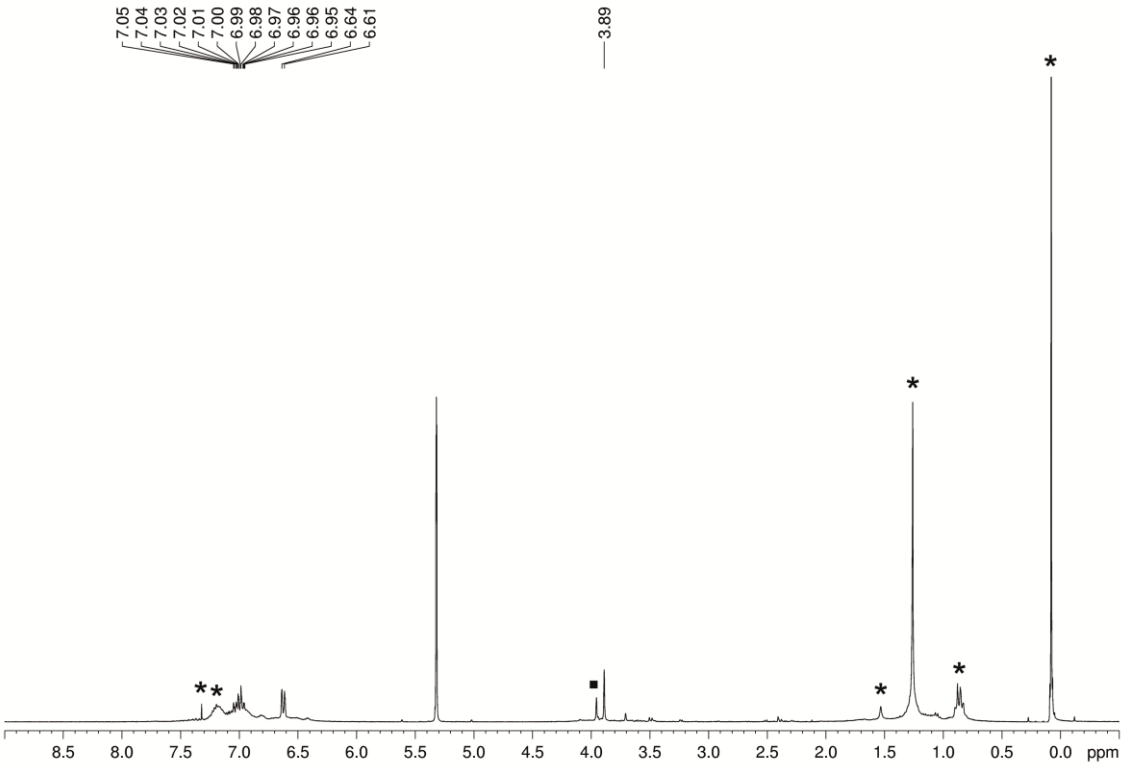

Figure S4.8 ^{1}H NMR spectrum of **4** in CD_2Cl_2 at 300 K. Signals marked with an asterisk are due to different solvents and silicon grease. Signal marked with a square is due to impurities of **3/3'**.

Determination of the magnetic moment of 2 by the Evans method

The magnetic moment μ_{eff} of **2** was determined by ^{1}H NMR spectroscopy using the Evans method.[31] The pure solvent serves as an internal reference and diamagnetic contributions are neglected according to equation (1) and (2).[32] As a result, an effective magnetic moment μ_{eff} of 1.50 μ_B is obtained, which is in good agreement with 1 unpaired electron. The ^{1}H NMR spectra were recorded on a Bruker Avance III HD 400 (^{1}H: 400.130 MHz) spectrometer at 300 K.

$$\mu_{eff} = 798\sqrt{T \cdot \chi_m} \qquad (1)$$

$$\chi_m = \frac{3 \cdot \Delta f}{1000 \cdot f \cdot c} \qquad (2)$$

χ_m = molar susceptibility of the sample in m³/mol

Δf = chemical shift difference between pure solvent and the solvent with paramagnetic compound in Hz

f = frequency of the NMR spectrometer in Hz

c = concentration of the sample in mol/L

μ_{eff} = effective magnetic moment in μ_B

T = measurement temperature in K

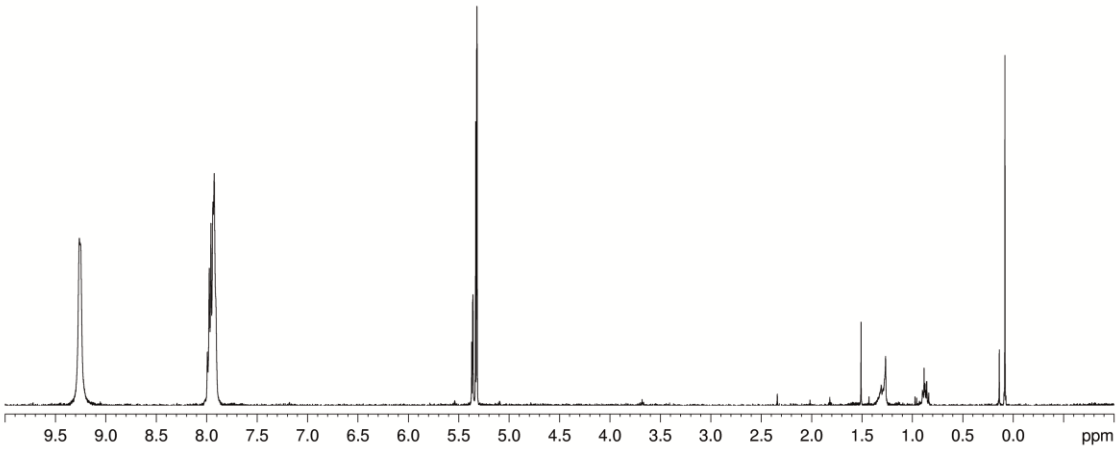

Figure S4.9 ^{1}H NMR spectrum of **2** in CD_2Cl_2 at 300 K for Evans method.

Representation of the X-Band EPR spectra of 2

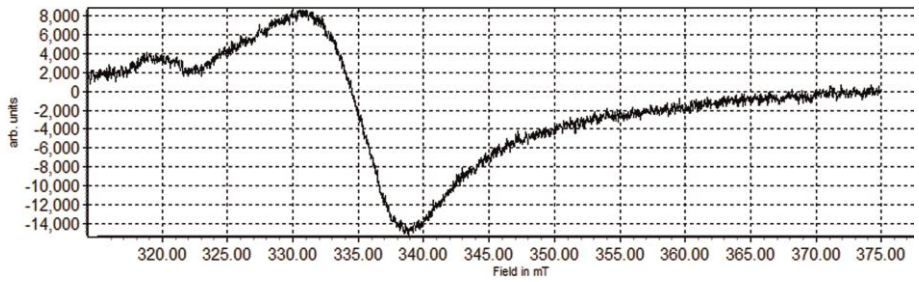

Figure S4.10 EPR spectrum of **2** in CD_2Cl_2 at 77 K.

Representation of the cyclic voltammograms of 2 and 3/3'

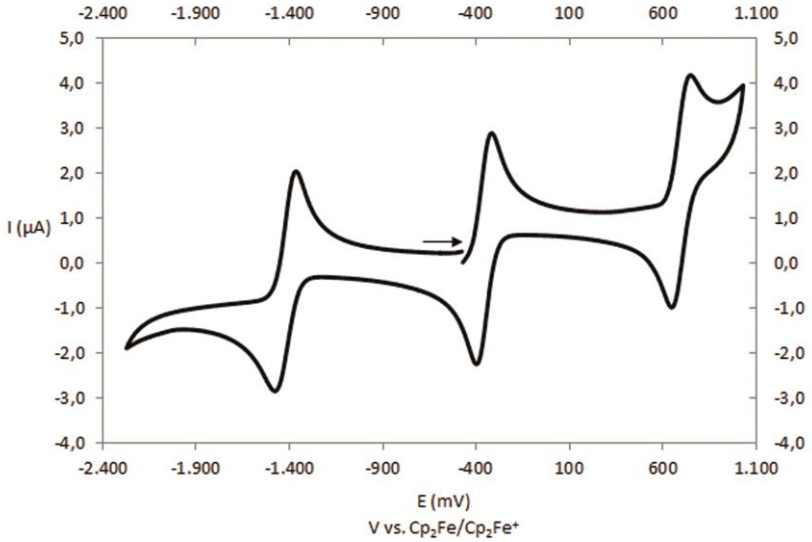

Figure S4.11 Cyclic voltammogram of **2** recorded at a platinum disc electrode in CH_2Cl_2 at 0.1 Vs^{-1} and referenced against $[Cp_2Fe]/[Cp_2Fe]^+$; supporting electrolyte $[^nBu_4N][PF_6]$ (0.1 mol/L).

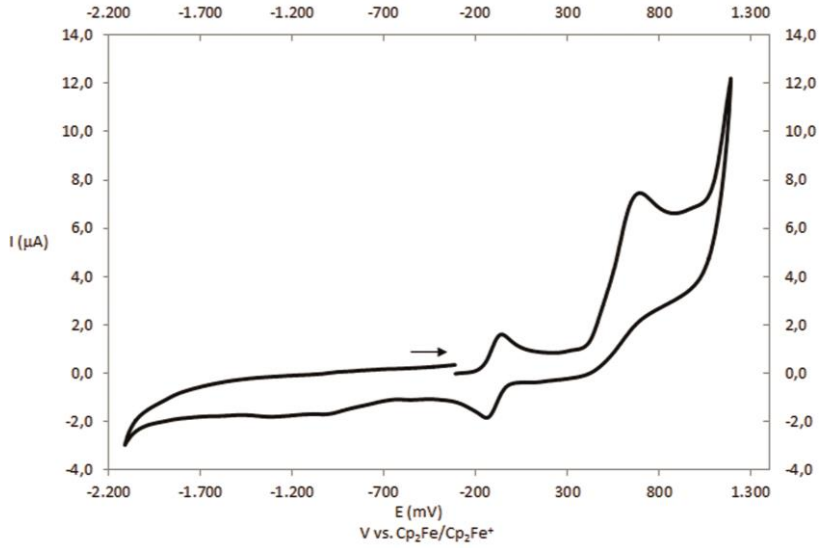

Figure S4.12 Cyclic voltammogram of **3/3'** recorded at a platinum disc electrode in CH_2Cl_2 at 0.1 Vs^{-1} and referenced against $[Cp_2Fe]/[Cp_2Fe]^+$; supporting electrolyte $[^nBu_4N][PF_6]$ (0.1 mol/L).

Details on DFT calculations

All calculations were carried out using the TURBOMOLE program package package.[33] The geometry was optimised in the C_i point group using the RI-[34]BP86[35] functional together with the def2-TZVP[36] basis set for all atoms. For the geometry optimisations the Multipole Accelerated Resolution of Identity (MARI-J)[37] approximation was used. The population analysis was performed with the corresponding modules as implemented in Turbomole.

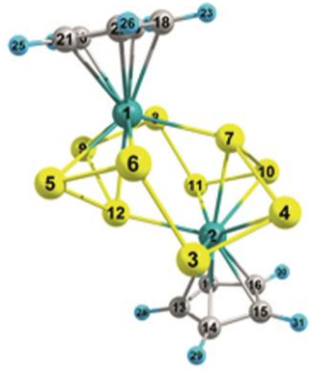

Figure S4.13 Optimised geometry of $[(CpMo)_2(\mu,\eta^{5:5:1:1}\text{-}As_{10})]$ at the BP86/def2-TZVP level of theory. Selected bond lengths (Å): As5-As6 2.389, As3-As6 2.463, As3-As4 2.388, As5-As12 2.455, Mo1-As12 2.699, Mo1-As7 2.658.

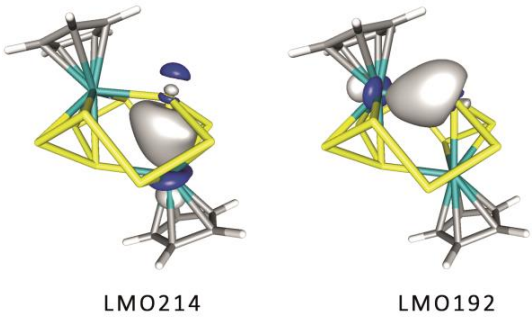

Figure S4.14 Isosurfaces of selected localised molecular orbitals in $[(CpMo)_2(\mu,\eta^{5:5:1:1}\text{-}As_{10})]$ showing the As7-Mo1 and As7-Mo2 bonds. Calculated at the BP86/def2-TZVP level of theory.

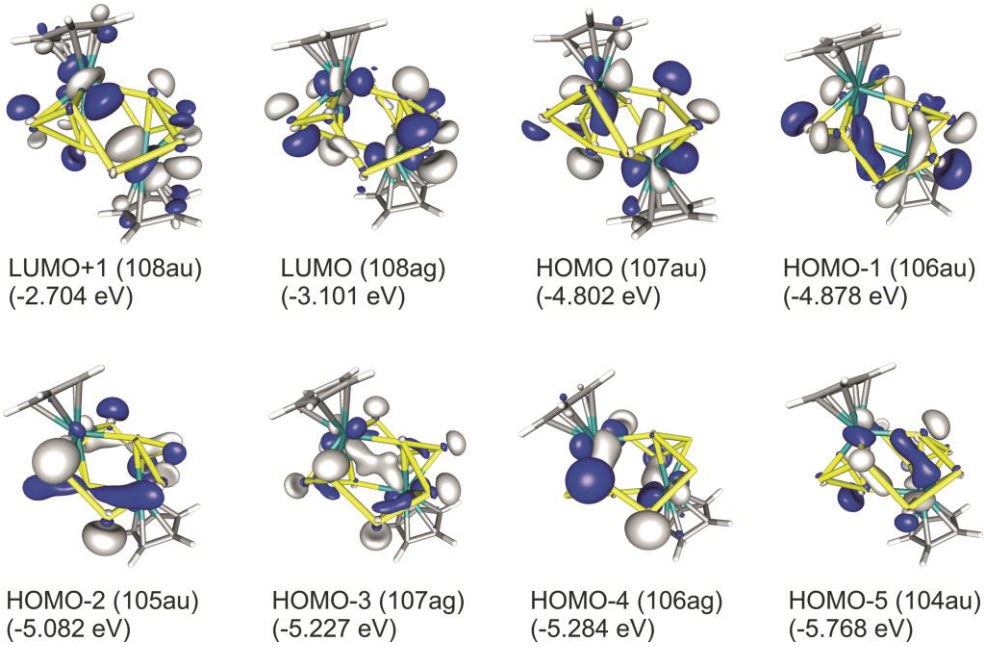

Figure S4.15 Isosurfaces of selected molecular orbitals in $[(CpMo)_2(\mu,\eta^{5:5:1:1}\text{-}As_{10})]$ at the BP86/def2-TZVP level of theory.

Table S4.1 Cartesian coordinates of the optimised geometry of $[(CpMo)_2(\mu,\eta^{5:5:1:1}\text{-}As_{10})]$ at the BP86/def2-TZVP level of theory (total energy = -22886.05552937389 a.u.).

Atom	x	y	x
Mo	1.8399803	-0.2378806	-0.6822985
Mo	-1.8399803	0.2378806	0.6822985
As	-1.4852845	-2.4568346	0.4121899
As	-2.5563945	-1.2873098	-1.3735115
As	2.0887640	-2.0282418	1.2672238
As	0.7517024	-2.7411810	-0.5792205

As	-0.5847580	0.1378483	-1.7040472
As	1.4852845	2.4568346	-0.4121899
As	2.5563945	1.2873098	1.3735115
As	-2.0887640	2.0282418	-1.2672238
As	-0.7517024	2.7411810	0.5792205
As	0.5847580	-0.1378483	1.7040472
C	-2.4143656	0.2467177	2.9802262
C	-3.1577822	-0.7942385	2.3505684
C	-4.0299523	-0.1983764	1.3848228
C	-3.8324656	1.2139102	1.4287461
C	-2.8386881	1.4878539	2.4214538
C	2.4143656	-0.2467177	-2.9802262
C	3.1577822	0.7942385	-2.3505684
C	4.0299523	0.1983764	-1.3848228
C	3.8324656	-1.2139102	-1.4287461
C	2.8386881	-1.4878539	-2.4214538
H	1.6803803	-0.1195568	-3.7695182
H	3.1013539	1.8505869	-2.5903590
H	4.3762251	-1.9505002	-0.8473229
H	2.4966147	-2.4714983	-2.7245662
H	-2.4966147	2.4714983	2.7245662
H	-1.6803803	0.1195568	3.7695182
H	-3.1013539	-1.8505869	2.5903590
H	-4.3762251	1.9505002	0.8473229
H	-4.7501525	-0.7209919	0.7645920
H	4.7501525	0.7209919	-0.7645920

Crystallographic Details

The data for **1** were collected on an Agilent Technologies Gemini R-Ultra diffractometer equipped with an Atlas^{S2} CCD detector and using an Enhanced Ultra CuK_α (λ = 1.54178 Å) sealed tube. The data for **2** were collected on an Oxford Diffraction GV50 diffractometer equipped with Titan^{S2} CCD detector and a CuK_α microfocus source. The data for **3/3'** were collected on an Agilent Technologies Gemini R-Ultra diffractometer equipped with Ruby CCD detector and an Enhanced Ultra CuK_α sealed tube. The data for **4** were collected on an Agilent Technologies diffractometer equipped with an Atlas CCD detector and a SuperNova CuK_α microfocus source. All measurements were performed at 123 K. Crystallographic data and details of the diffraction experiments are given in Table S4.2-S4.4. Using Olex2,[38] the structures were solved either with the ShelXT[39] (**1**, **2**), SIR2004[40] (**3/3'**) or SUPERFLIP[41] (**4**) structure solution program using Direct Methods and refined with the ShelXL[42] refinement package using Least Squares minimisation. Especially in case of disorder, commonly used restraints for the ShelXL program were applied (SIMU). Since **3/3'** co-crystallise on the same crystallographic position in a 1:1 ratio, the EXYZ constraint was used. Furthermore, the refinement for **5** is unstable so far, due to serious disorder. Therefore, only a preliminary model is described. Moreover, H atoms were located in idealised positions and refined isotropically according to the riding model. A semi-empirical numerical absorption correction based on gaussian[43] integration over a multifaceted crystal model (**1**-**4**) or an analytical[44] absorption correction from crystal faces (**5**) was applied. Figures were created with DIAMOND3.0.[45]

Table S4.2 Crystallographic data for **1** and **2**.

	1	**2**
Chemical formula	$C_{84}H_{70}Cr_2O_4$	$C_{80}H_{70}Cr_2As_5$
M/g·mol^{-1}	1247.40	1509.96
T/K	123	123
Crystal system	monoclinic	monoclinic
Space group	$P2_1/c$	$P2_1/c$
a/Å	11.15882(4)	24.5562(7)
b/Å	13.58072(5)	10.4172(2)
c/Å	21.32389(9)	25.9948(7)
α/°	90.00	90.00
β/°	104.0994(4)	105.696(3)
γ/°	90.00	90.00
V/Å³	3134.17(2)	6401.7(3)
Z	2	4
ρ_{cal}/g·cm^{-3}	1.322	1.567
μ/mm^{-1}	3.281	6.016
F(000)	1308.0	3052.0
Crystal size/mm^3	0.3143 × 0.1612 × 0.095	0.209 × 0.073 × 0.044
Radiation	CuK_α	CuK_α
2θ range/°	8.17 to 133.596	7.042 to 134.106
Index ranges	-13 ≤ h ≤ 13, -16 ≤ k ≤ 16, -25 ≤ l ≤ 25	-29 ≤ h ≤ 25, -8 ≤ k ≤ 12, -31 ≤ l ≤ 29
Reflections collected	85281	23335
Independent reflections	5547 [R_{int} = 0.0296, R_{sigma} = 0.0108]	11238 [R_{int} = 0.0369, R_{sigma} = 0.0419]
Data/restraints/parameters	5547/0/407	11238/0/784
Goodness-of-fit on F^2	1.060	1.035
Final R indexes [I>2σ(I)]	R_1 = 0.0263, wR_2 = 0.0743	R_1 = 0.0404, wR_2 = 0.1059
Final R indexes [All Data]	R_1 = 0.0267, wR_2 = 0.0745	R_1 = 0.0494, wR_2 = 0.1124
Largest diff. peak/hole/eA^{-3}	0.26/-0.32	0.71/-0.69

Table S4.3 Crystallographic data for **3/3'** and **4**.

	3/3'	**4**
Chemical formula	$C_{73}H_{64}Mo_2As_6$	$C_{80}H_{70}Mo_2As_{10}$
M/g·mol^{-1}	1582.64	1972.44
T/K	123	123
Crystal system	monoclinic	triclinic
Space group	*C*2/*c*	$P\bar{1}$
a/Å	23.4962(3)	9.2408(3)
b/Å	10.11463(10)	12.2615(6)
c/Å	26.3849(3)	16.6818(9)
α/°	90	78.593(4)
β/°	99.6846(11)	77.897(4)
γ/°	90	70.760(4)
V/Å³	6181.14(12)	1727.89(15)
Z	4	1
ρ_{cal}/g·cm^{-3}	1.701	1.896
μ/mm^{-1}	7.218	8.643
F(000)	3136.0	964.0
Crystal size/mm^3	0.1757 × 0.1077 × 0.0494	0.076 × 0.0205 × 0.0152
Radiation	CuK_α	CuK_α
2θ range/°	7.634 to 132.992	7.712 to 134.154
Index ranges	-27 ≤ h ≤ 27,	-10 ≤ h ≤ 10,
	-12 ≤ k ≤ 8,	-14 ≤ k ≤ 14,
	-31 ≤ l ≤ 30	19 ≤ l ≤ 18
Reflections collected	18718	10125
Independent reflections	5416	6061
	[R_{int} = 0.0253, R_{sigma} = 0.0229]	[R_{int} = 0.0282, R_{sigma} = 0.0424]
Data/restraints/parameters	5416/603/494	6061/0/415
Goodness-of-fit on F^2	1.083	0.995
Final R indexes [I>2σ(I)]	R_1 = 0.0564, wR_2 = 0.1534	R_1 = 0.0265, wR_2 = 0.0597
Final R indexes [All Data]	R_1 = 0.0592, wR_2 = 0.1561	R_1 = 0.0337, wR_2 = 0.0630
Largest diff. peak/hole/eA^{-3}	0.89/-0.77	0.89/-0.55

Table S4.4 Crystallographic data for **5**.

	5
Chemical formula	$C_{80}H_{70}Mo_2As_5$
M/g·mol^{-1}	1597.84
T/K	123
Crystal system	monoclinic
Space group	$P2_1/c$
a/Å	9.94802(12)
b/Å	32.0511(3)
c/Å	20.0606(2)
α/°	90
β/°	96.6725(11)
γ/°	90
V/Å³	6352.89(12)
Z	4
ρ_{cal}/g·cm^{-3}	1.671
μ/mm^{-1}	6.478
F(000)	3196.0
Crystal size/mm^3	0.211 × 0.145 × 0.104
Radiation	CuK_α
2θ range/°	5.222 to 134.156
Index ranges	-11 ≤ h ≤ 11,
	-38 ≤ k ≤ 38,
	-23 ≤ l ≤ 23
Reflections collected	102927
Independent reflections	11335
	[R_{int} = 0.0777, R_{sigma} = 0.0260]
Data/restraints/parameters	11335/204/832
Goodness-of-fit on F^2	2.219
Final R indexes [I>2σ(I)]	R_1 = 0.1244, wR_2 = 0.4358
Final R indexes [All Data]	R_1 = 0.1266, wR_2 = 0.4424
Largest diff. peak/hole/eA^{-3}	2.48/-6.92

4.6 References

[1] R. Hoffmann, *Angew. Chem. Int. Ed. Engl.* 1982, *21*, 711-724.

[2] selected publications: G. Märkl, *Chem. unserer Zeit* 1982, *16*, 139-148; b) C. Heindl, A. Schindler, M. Bodensteiner, E. V. Peresypkina, A. V. Virovets, M. Scheer, *Phosphorus, Sulfur Silicon Relat. Elem.* 2015, *190*, 397-403; c) C. Heindl, E. V. Peresypkina, A. V. Virovets, G. Balázs, M. Scheer, *Chem. Eur. J.* 2016, *22*, 1944-1948.

[3] selected publications: a) O. J. Scherer, H. Sitzmann, G. Wolmershäuser, *Angew. Chem. Int. Ed. Engl.* 1985, *24*, 351-353; b) O. J. Scherer, T. Brück, *Angew. Chem. Int. Ed. Engl.* 1987, *26*, 59-59; c) O. J. Scherer, H. Sitzmann, G. Wolmershäuser, *Angew. Chem. Int. Ed. Engl.* 1989, *28*, 212-213. d) O. J. Scherer, C. Blath, G. Wolmershäuser, *J. Organomet. Chem.* 1990, *387*, C21-C24.

[4] a) W. Schmettow, A. Lipka, H. G. von Schnering, *Angew. Chem. Int. Ed. Engl.* 1974, *13*, 345-345; b) H. P. Abicht, W. Hönle, H. G. von Schnering, *Z. Anorg. All. Chem.* 1984, *519*, 7-23; c) H. G. von Schnering, T. Meyer, W. Hönle, W. Schmettow, U. Hinze, W. Bauhofer, G. Kliche, *Z. Anorg. Allg. Chem.* 1987, *553*, 261-279; d) W. Hönle, G. Krogull, K. Peters, H. G. von Schnering, *Z. Kristallogr. New Cryst. Struct.* 1999, *214*, 17-18.

[5] C. Heindl, E. V. Peresypkina, D. Lüdeker, G. Brunklaus, A. V. Virovets, M. Scheer, *Chem. Eur. J.* 2016, *22*, 2599-2604.

[6] M. Fleischmann, F. Dielmann, L. J. Gregoriades, E. V. Peresypkina, A. V. Virovets, S. Huber, A. Y. Timoshkin, G. Balázs, M. Scheer, *Angew. Chem. Int. Ed.* 2015, *54*, 13110-13115.

[7] F. Dielmann, *Ph.D. thesis*, Universität Regensburg, 2011.

[8] M. Fleischmann, C. Heindl, M. Seidl, G. Balázs, A. V. Virovets, E. V. Peresypkina, M. Tsunoda, F. P. Gabbaï, M. Scheer, *Angew. Chem. Int. Ed.* 2012, *51*, 9918-9921.

[9] O. J. Scherer, J. Schwalb, H. Swarowsky, G. Wolmershäuser, W. Kaim, R. Gross, *Chem. Ber.* 1988, *121*, 443-449.

[10] O. J. Scherer, J. Vondung, G. Wolmershäuser, *Angew. Chem. Int. Ed. Engl.* 1989, *28*, 1355-1357.

[11] O. J. Scherer, H. Swarowsky, G. Wolmershäuser, W. Kaim, S. Kohlmann, *Angew. Chem. Int. Ed. Engl.* 1987, *26*, 1153-1155.

[12] a) J. Bai, A. V. Virovets, M. Scheer, *Science* 2003, *300*, 781-783. b) M. Scheer, J. Bai, B. P. Johnson, R. Merkle, A. V. Virovets, C. E. Anson, *Eur. J. Inorg. Chem.* 2005, 4023-4026. c) A. Schindler, C. Heindl, G. Balázs, C. Gröger, A. V. Virovets, E. V. Peresypkina, M. Scheer, *Chem. Eur. J.* 2012, *18*, 829-835. d) F. Dielmann, C. Heindl, F. Hastreiter, E. V. Peresypkina, A. V. Virovets, R. M. Gschwind, M. Scheer, *Angew. Chem. Int. Ed.* 2014, *53*, 13605-13608. e) F.

Dielmann, M. Fleischmann, C. Heindl, E. V. Peresypkina, A. V. Virovets, R. M. Gschwind, M. Scheer, *Chem. Eur. J.* **2015**, *21*, 6208-6214. f) C. Heindl, E. V. Peresypkina, A. V. Virovets, W. Kremer, M. Scheer, *J. Am. Chem. Soc.* **2015**, *137*, 10938-10941.

[13] M. D. Curtis, W. M. Butler, *J. Organomet. Chem.* **1978**, *155*, 131-145.

[14] J. Potenza, P. Giordano, D. Mastropaolo, A. Efraty, *Inorg. Chem.* **1974**, *13*, 2540-2544.

[15] T. K. Gasanov, I. R. Lyatifov, A. N. Shnulin, *J. Organomet. Chem.* **1989**, *361*, 173-179.

[16] Y. Morino, T. Ukaji, T. Ito, *Bull. Chem. Soc. Jpn.* **1966**, *39*, 64-71.

[17] H. A. Spinney, N. A. Piro, C. C. Cummins, *J. Am. Chem. Soc.* **2009**, *131*, 16233-16243.

[18] O. J. Scherer, W. Wiedemann, G. Wolmershäuser, *J. Organomet. Chem.* **1989**, *361*, C11-C14.

[19] O. J. Scherer, W. Wiedemann, G. Wolmershäuser, *Chem. Ber.* **1990**, *123*, 3-6.

[20] L. Y. Goh, R. C. S. Wong, W. H. Yip, T. C. W. Mak, *Organometallics* **1991**, *10,* 875-879.

[21] Although the reaction conditions (reaction time, temperature, solvent and stoichiometry of As_4) have been varied, **4** and **5** could be observed only once as a green (**4**) or brown (**5**) fraction during the column chromatographic workup.

[22] $Cp^{TetraBn}H$ is also obtained during the synthesis of $Cp^{Bn}H$. Unfortunately, the formation of $Cp^{TetraBn}H$ cannot be suppressed and separation by column chromatographic workup failed.

[23] N. G. Connelly, W. E. Geiger, *Chem. Rev.* **1996**, *96*, 877-910.

[24] C. Graßl, M. Bodensteiner, M. Zabel, M. Scheer, *Chem. Sci.* **2015**, *6*, 1379-1382.

[25] a) R. C. Haushalter, B. W. Eichhorn, A. L. Rheingold, S. J. Geib, *J. Chem. Soc., Chem. Commun.* **1988**, 1027-1028. b) M. J. Moses, J. C. Fettinger, B. W. Eichhorn, *Science* **2003**, *300*, 778-780.

[26] E.-K. Mucke, B. Schönborn, F. Köhler, R. Herges, *J. Org. Chem.* **2011**, *76*, 35-41.

[27] A. L. Rheingold, M. J. Foley, P. J. Sullivan, *J. Am. Chem. Soc.* **1982**, *104*, 4727-4279.

[28] W. M. Tsai, M. D. Rausch, *Organometallics* **1996**, *15*, 2591-2594.

[29] a) H. Erdmann, M. V. Unruh, *Z. Anorg. Chem.* **1902**, *32*, 437-452; b) O. J. Scherer, H. Sitzmann, G. Wolmershäuser, *J. Organomet. Chem.* **1986**, *309*, 77-86.

[30] Since **4** and **5** are observed only once, the corresponding synthesis is described. In contrast, **3** and **3'** can be obtained regardless of stoichiometry or reaction time. However, co-thermolysis of $[Cp^{Bn}Mo(CO)_2]_2$ with As_4 has to be lasted at least 48 h.

[31] D. F. Evans, *J. Chem. Soc.* (Resumed) **1959**, 2003-2005.

[32] G. J. P. Britovsek, V. C. Gibson, S. K. Spitzmesser, K. P. Tellmann, A. J. P. White, D. J. Williams, *J. Chem. Soc., Dalton Trans.* **2002**, 1159-1171.

[33] a) R. Ahlrichs, M. Bär, M. Häser, H. Horn, C. Kölmel, *Chem. Phys. Lett.* 1989, *162*, 165–169. b) O. Treutler, R. Ahlrichs, *J. Chem. Phys.* 1995, *102*, 346–354.

[34] a) K. Eichkorn, O. Treutler, H. Oehm, M. Häser, R. Ahlrichs, *Chem. Phys. Lett.* 1995, *242*, 652–660. b) K. Eichkorn, F. Weigend, O. Treutler, R. Ahlrichs, *Theor. Chem. Acc.* 1997, *97*, 119-124.

[35] a) P. A. M. Dirac, *Proc. Royal Soc. A* 1929, *123*, 714-733. b) J. C. Slater, *Phys. Rev.* 1951, *81*, 385-390. c) S. H. Vosko, L. Wilk, M. Nusair, *Can. J. Phys.* 1980, *58*, 1200-1211. d) J. P. Perdew, *Phys. Rev. B* 1986, *33*, 8822-8824; e) A. D. Becke, *Phys. Rev. A* 1988, *38*, 3098-3100.

[36] a) A. Schäfer, C. Huber, R. Ahlrichs, *J. Chem. Phys.* 1994, *100*, 5829-5835. b) K. Eichkorn, F. Weigend, O. Treutler, R. Ahlrichs, *Theor. Chem. Acc.* 1997, *97*, 119-124.

[37] M. Sierka, A. Hogekamp, R. Ahlrichs, *J. Chem. Phys.* 2003, *118*, 9136-9148.

[38] O. V. Dolomanov, L. J. Bourhis, R. J. Gildea, J. A. K. Howard, H. Puschmann, *J. Appl. Cryst.* 2009, *42*, 339-341.

[39] G. M. Sheldrick, *Acta Cryst.* 2015, *A71*, 3-8.

[40] M. C. Burla, R. Caliandro, M Camalli, B Carrozzini, G. L. Cascarano, L. De Caro, C. Giacovazzo, G. Polidori, D. Siliqi, R. Spagna, *J. Appl. Cryst.* 2007, *40*, 609-613.

[41] L. Palatinus, G. Chapuis, *J. Appl. Cryst.* 2007, *40*, 786-790.

[42] G. M. Sheldrick, *Acta Cryst.* 2015, *C71*, 3-8.

[43] CrysAlisPro, Version 1.171.37.33, Agilent Technologies UK Ltd, Oxford, UK.

[44] R. C. Clark, J. S. Reid, *Acta Cryst.* 1995, *A51*, 887-897.

[45] K. Brandenburg, H. Putz, Diamond3.0, Crystal and Molecular Structure Visualization, Crystal Impact GbR, Bonn, Germany, 2014.

5. Co-Thermolysis vs. Transfer Reaction: Novel As_n Ligand Complexes of Iron

M. Schmidt, F. Riedlberger, E. Mädl and M. Scheer

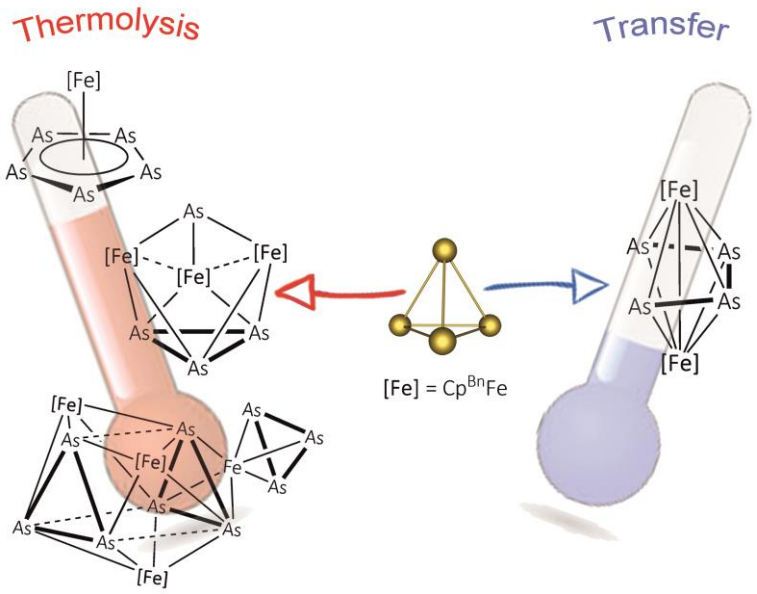

Abstract:

Different novel As_n ligand complexes of iron bearing the Cp^{Bn} ligand (Cp^{Bn} = η^5-$C_5(CH_2\{C_6H_5\})_5$) have been prepared either by co-thermolysis of $[Cp^{Bn}Fe(CO)_2]_2$ with As_4 at elevated temperatures or by transfer reaction using $[Cp''_2Zr(\eta^{1:1}\text{-}As_4)]$ (Cp'' = η^5-1,3-$C_5H_3{}^tBu_2$) as an arsenic source under mild reaction conditions. While co-thermolysis leads to the formation of $[Cp^{Bn}Fe(\eta^5\text{-}As_5)]$ (**1**), $[(Cp^{Bn}Fe)_3(\mu_3,\eta^{2:2:2}\text{-}As_3)(\mu_3\text{-}As)]$ (**2**) and $[(Cp^{Bn}Fe)_3(\mu_3,\eta^{4:4:4}\text{-}As_6)\{Fe(\eta^3\text{-}As_3)\}]$ (**3**), the reaction of *in situ* generated $[Cp^{Bn}Fe(\mu\text{-}Br)]_2$ with $[Cp''_2Zr(\eta^{1:1}\text{-}As_4)]$ yields $[(Cp^{Bn}Fe)_2(\mu,\eta^{4:4}\text{-}As_4)]$ (**4**) exclusively. Complexes **1** and **4** are fully characterised by single crystal X-ray diffraction analysis, NMR spectroscopy, mass spectrometry as well as elemental analysis. Furthermore, the redox chemistry of **1** and **4** has been investigated by cyclic voltammetry, revealing two irreversible oxidations and one irreversible reduction for **1**. For **4**, a reversible oxidation and reversible reduction is observed. Chemical oxidation of **4** with $AgBF_4$ results in an oxidative change of the structural core motif. Consequently, the *cisoid*-As_4 middle deck of **4** is extended to a *cyclo*-As_5 middle deck, stabilised in the triple decker complex $[(Cp^{Bn}Fe)_2(\mu,\eta^{5:5}\text{-}As_5)][BF_4]$ (**5**).

5.1 Author Contributions

- All syntheses and characterisations were performed by Monika Schmidt.
- Manuscript was written by Monika Schmidt.
- Figures were made by Monika Schmidt.
- Single crystal X-ray structure analyses and refinements were performed by Monika Schmidt.
- The cyclovoltammetric measurements of **1** and **4** were performed and interpreted by Dr. Eric Mädl (**1**) and Felix Riedlberger (**4**).

5.2 Introduction

Since Dahl[1] firstly reported on the synthesis of unsubstituted naked arsenic ligands, a variety of so called As_n ligand complexes has been established.[2] Beside organic arsenic derivatives,[3] $As_7(SiMe_3)_3$,[4] metallic arsenic[5] or $AsCl_3$,[6] the highly reactive As_4 has especially been used as an arsenic source in the last years.[7] In general, the As_4 tetrahedron often undergoes a successive degradation yielding smaller As_n ligand complexes. However, subsequent aggregation to larger As_n ligand complexes can also occur. Usually, the so-formed As_n units are stabilised by unsaturated transition metal fragments, which are often generated starting from cyclopentadienyl containing carbonyl transition metal complexes of the general formula $[Cp^RM(CO)_x]_y$ during co-thermolysis with As_4. A good example of the variety of realised As_n motifs are the As_n ligand complexes of iron (Scheme 5.1).

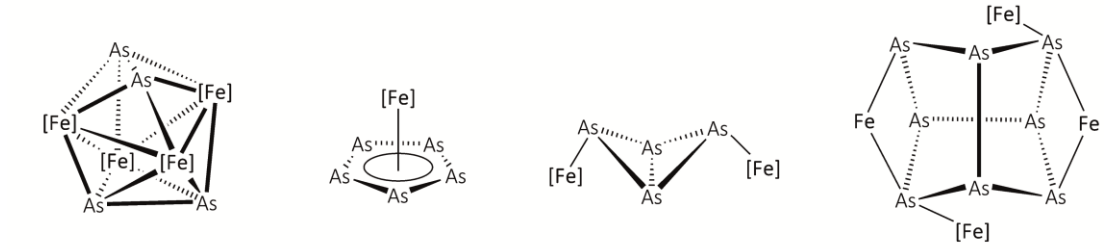

Scheme 5.1 Selected examples of As_n ligand complexes of iron.

The reaction of the parent complex $[CpFe(CO)_2]_2$ (Cp = η^5-C_5H_5) with As_4 yields $[(CpFe)_4(As_2)_2]$ (**I**), containing two As_2 units which are part of the triangulated dodecahedral $[Fe_4As_4]$ skeleton.[8] In contrast, the thermolysis of the derivatives $[Cp^RFe(CO)_2]_2$ (Cp^R = Cp* (η^5-C_5Me_5), Cp' (η^5-C_5EtMe_4)) with yellow arsenic leads to the formation of $[Cp^RFe(\eta^5\text{-}As_5)]$ (**II**), containing the *cyclo*-As_5 ligand, which is richer in arsenic.[9] Besides co-thermolysis with transition metal

precursors, As_4 can also be activated at room temperature. Recently, our group studied the reaction of As_4 with $[Cp^RFe(CO)_2]_2$ (Cp^R = Cp''' (η^5-1,2,4-$C_5H_2{}^tBu_3$),[10] Cp^{BIG} (η^5-C_5{4-^{n}BuC_6H_4}$_5$)[11]), resulting in the butterfly complexes [{$Cp^RFe(CO)_2$}$_2$(μ,$\eta^{1:1}$-As_4)] (**III**). Moreover, the formation of the butterfly like As_4 structural motif is expected to be the initial step in the degradation process of the As_4 tetrahedron. Additionally, for Cp^R = Cp''' the butterfly complex dimerises under photolytic conditions to give [{Cp'''$Fe(CO)_2$}$_2${Cp'''$Fe(CO)$}$_2$(μ_4,$\eta^{1:1:2:2}$-As_8)] (**IV**), containing a hitherto unknown As_8 realgar like unit.[10]

However, the observed structural As_n motifs certainly depend on the steric and electronic properties of the Cp^R ligand. These results prompted us to investigate the reactivity of $[Cp^{Bn}Fe(CO)_2]_2$ towards As_4 (Cp^{Bn} = η^5-$C_5(CH_2\{C_6H_5\})_5$). Since this complex shows no reactivity towards yellow arsenic at room temperature, the question arose whether As_n ligand complexes with $[Cp^{Bn}Fe]$ fragments could be obtained by co-thermolysis and alternative reactions.

Herein, we report on the co-thermolysis of $[Cp^{Bn}Fe(CO)_2]_2$ and As_4 at elevated temperatures as well as on the use of $[Cp''_2Zr(\eta^{1:1}\text{-}As_4)]$ (Cp'' = η^5-1,3-$C_5H_3{}^tBu_2$) as an arsenic transfer reagent under mild reaction conditions. While thermolysis leads to the formation of $[Cp^{Bn}Fe(\eta^5\text{-}As_5)]$ (**1**), $[(Cp^{Bn}Fe)_3(\mu_3,\eta^{2:2:2}\text{-}As_3)(\mu_3\text{-}As)]$ (**2**) and $[(Cp^{Bn}Fe)_3(\mu_3,\eta^{4:4:4}\text{-}As_6)\{Fe(\eta^3\text{-}As_3)\}]$ (**3**), the reaction of *in situ* generated $[Cp^{Bn}Fe(\mu\text{-}Br)]_2$ with $[Cp''_2Zr(\eta^{1:1}\text{-}As_4)]$ yields $[(Cp^{Bn}Fe)_2(\mu,\eta^{4:4}\text{-}As_4)$ (**4**) exclusively. Furthermore, we investigated the electrochemical redox behaviour of **1** and **4** by cyclic voltammetry. Thus, chemical oxidation of **4** results in an oxidative change of the structural core motif by a ring expansion reaction, resulting in $[(Cp^{Bn}Fe)_2(\mu,\eta^{5:5}\text{-}As_5)][BF_4]$ (**5**).

5.3 Results and Discussion

The co-thermolysis of $[Cp^{Bn}Fe(CO)_2]_2$ with As_4 in decalin leads to the formation of the complexes **1**, **2** and **3** (Scheme 5.2).

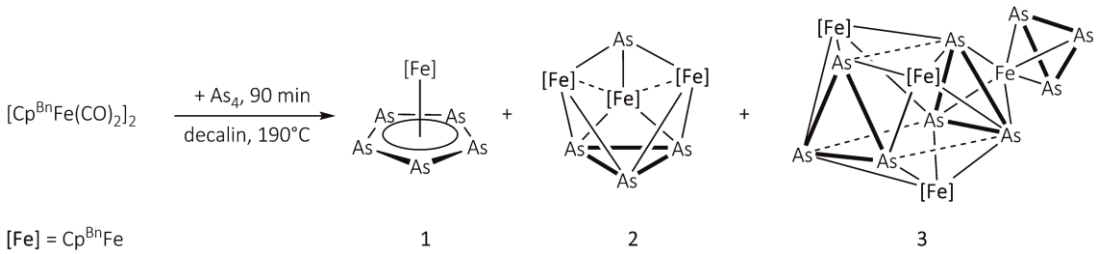

Scheme 5.2 Co-thermolysis of $[Cp^{Bn}Fe(CO)_2]_2$ with As_4.

After column chromatographic workup, **1**-**3** can be crystallised by layering a CH_2Cl_2 solution with CH_3CN. Unfortunately, **2** and **3** could not be separated from each other due to similar

retention factors R_f, identical crystal shape and colour as well as identical solubility properties. Consequently, **2** and **3** have been isolated as a co-crystallised mixture. Therefore, a doubtless assignment of the signals in the NMR spectra of both products was not possible. Complexes **1**-**3** are soluble in CH_2Cl_2 and toluene, almost insoluble in *n*-hexane and insoluble in CH_3CN.

Compound **1** crystallises as dark brown blocks in the monoclinic space group $P2_1/n$ with one molecule of **1** in the asymmetric unit. Single crystal X-ray structure analysis of **1** reveals a sandwich structure showing a η^5-coordination of the *cyclo*-As_5 ring as well as of the Cp^{Bn} ligand. Both five-membered rings are planar and parallel with respect to each other and exhibit a staggered conformation, which is also reported for the phosphorus analogue $[Cp^{Bn}Fe(\eta^5\text{-}P_5)]$[12] or the pentaarsaferrocene derivatives $[Cp^{R}Fe(\eta^5\text{-}As_5)]$ (Cp^R = Cp*,[13] Cp',[14] Cp^{BIG}[15]). In Figure 5.1, the molecular structure of **1** in the solid state is depicted. The average As-As bond length of **1** (av. 2.318 Å) is quite similar to the described As-As bond distances in the Cp* derivative (av. 2.327 Å)[13] or in the Cp' derivative (av. 2.315 Å),[14] being in-between a double (2.245(1) Å in $[\{(Me_3Si)_3CAs\}_2]$)[16] and a single bond (electron diffraction: 2.435 Å in As_4,[17] DFT calculations: 2.4372 Å in As_4[18]).

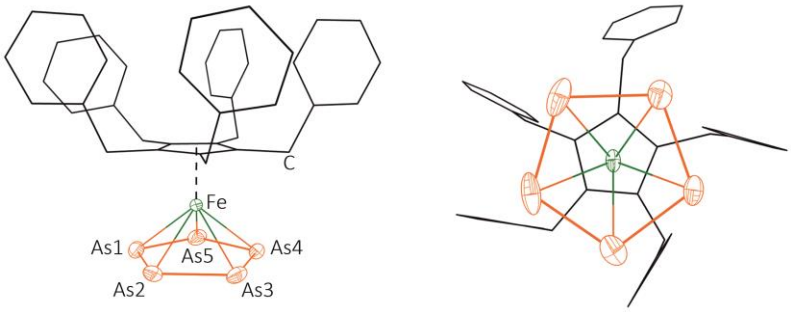

Figure 5.1 Molecular structure of **1** in the solid state (left). Top view of **1** (right). H atoms are omitted for clarity and Cp^{Bn} ligands are drawn in wire or frame model. Thermal ellipsoids are drawn at 50 % probability level. Selected bond lengths [Å] and angles [°]: As1-As2 2.3175(7), As2-As3 2.3143(5), As3-As4 2.3220(5), As4-As5 2.3173(5), As1-As5 2.3180(6), Fe-As Fe1 2.5213(5), Fe-As2 2.5112(5), Fe-As3 2.5087(5), Fe-As4 2.5223(5), Fe-As5 2.5039(6), As1-As2-As3 107.89(2), As2-As3-As4 108.23(2), As3-As4-As5 107.718(18), As1-As5-As4 108.10(2), As2-As1-As5 108.046(19).

The ^1H and $^{13}C\{^1H\}$ NMR spectra of **1** show the corresponding set of signals for the Cp^{Bn} ligand (Figure S5.1-S5.2, supplementary information). In the EI mass spectrum, the molecular ion peak for $[Cp^{Bn}Fe(\eta^5\text{-}As_5)]^+$ (*m/z* = 945.7) as well as the base peak for $[As_4]^+$ (*m/z* = 299.7) were observed. The cyclic voltammogram of **1** in CH_2Cl_2 shows an irreversible reduction at a peak potential of E = -1.99 V as well as an irreversible oxidation at E = -1.31 V (both vs. $[Cp_2Fe]/[Cp_2Fe]^+$). In addition, a further irreversible oxidation of **1** (E = +0.37 V vs. $[Cp_2Fe]/[Cp_2Fe]^+$) is obtained (see Figure S5.10, supplementary information). In this context, the first irreversible reduction and irreversible oxidation are constituted as chemically reversible couple, which has also been

reported for the lighter Cp* congener [Cp*Fe(η^5-P_5)] by the Winter group.[19] Here, [Cp*Fe(η^5-P_5)] undergoes reduction to [Cp*Fe(η^5-P_5)]$^-$, followed by dimerisation to [{Cp*Fe(P_5)}$_2$]$^{2-}$ and reoxidation to [Cp*Fe(η^5-P_5)].

Compound **2** crystallises as dark brown plates in the triclinic space group $P\bar{1}$ with one independent molecule of **2** in the asymmetric unit. The single crystal X-ray structure analysis of **2** exhibits a $\eta^{2:2:2}$-coordinating triangular *cyclo*-As_3 unit as well as a $\eta^{1:1:1}$-coordinating As atom, both stabilised by three [Cp^{Bn}Fe] fragments. Hence, the [Fe_3As_4] unit could be formally described as a threefold insertion of [Cp^{Bn}Fe] fragments into the As-As bonds of the As_4 tetrahedron. Interestingly, the obtained [Fe_3As_4] structural core motif of **2** is unknown in literature so far. Unfortunately, only a preliminary average structural model can be depicted here, as crystals of **2** show incommensurable modulation (q-vector of 0.256) (Figure 5.2). Consequently, a discussion of bond distances or bond angles is not possible.

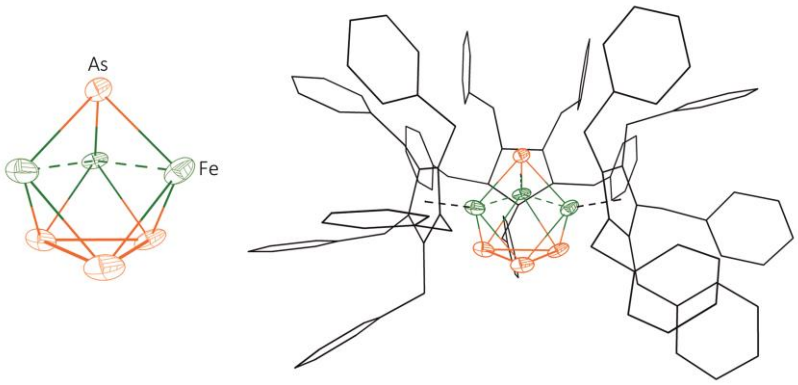

Figure 5.2 Average structural core motif of **2** (left). Average molecular structure of **2** in the solid state (right). H atoms are omitted for clarity and Cp^{Bn} ligands are drawn in wire or frame model. Thermal ellipsoids are drawn at 50 % probability level.

Complex **3** also crystallises as dark brown plates in the monoclinic space group $P2_1/m$ together with **2**. Only one half of the molecule can be found in the asymmetric unit, the other half is generated by symmetry. Unfortunately, no satisfying refinement of the single crystal X-ray structure analysis data could be performed so far, due to serious disorder of the Cp^{Bn} ligands and the [Fe_4As_9] unit. Nevertheless, the central structural core motif could be doubtlessly identified. It consists of a prismatic As_6 ligand, whose quadrangular faces are capped by [Cp^{Bn}Fe] fragments. Moreover, one of the two As_3 triangles is capped by a Fe atom, which is additionally coordinated by a *cyclo*-As_3 ligand in a η^3-fashion (Figure 5.3). The prismatic As_6 core can be found in recent reports, but the

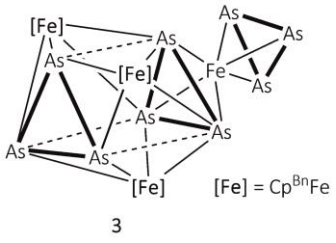

3

Figure 5. 3 Schematic representation of **3**.

complexes never showed an additional end-on coordinated *cyclo*-As_3 ligand so far.[4,15,20,21] However, the end-on coordinating *cylco*-As_3 motif is reported for $[(Cp^RFe)_3As_6\{Fe(\eta^3\text{-}As_3)\}]$ (Cp^R = Cp*, Cp'), showing an As_4 unit and an As_2 moiety stabilised by three $[Cp^RFe]$ fragments.[4]

While co-thermolysis in decalin often leads to a mixture of different products, the reaction of *in situ* generated $[Cp^{Bn}Fe(\mu\text{-}Br)]_2$[22] with the transfer reagent $[Cp''_2Zr(\eta^{1:1}\text{-}As_4)]$ leads to the formation of $[(Cp^{Bn}Fe)_2(\mu,\eta^{4:4}\text{-}As_4)]$ (**4**) in moderate yields (49 %) exclusively (Scheme 5.3).

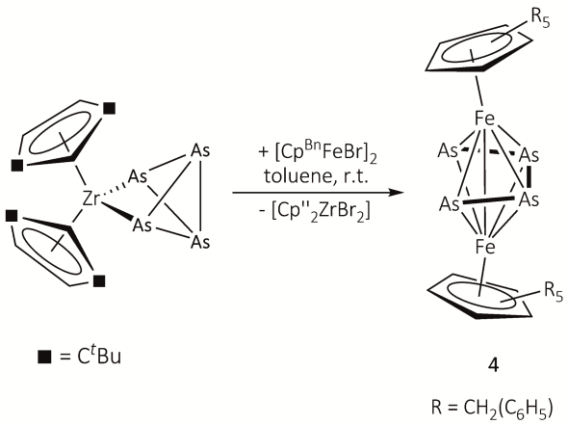

Scheme 5.3 Synthesis of **4**.

After column chromatographic workup, **4** can be crystallised by layering a CH_2Cl_2 solution with *n*-hexane. **4** crystallises as dark brown plates in the monoclinic space group $P2_1/c$ with one independent molecule of **4** in the asymmetric unit. The single crystal X-ray structure analysis of **4** reveals a *cisoid*-As_4 ligand stabilised by two $[Cp^{Bn}Fe]$ fragments. The Cp^{Bn} ligands are tilted away from the butadiene like As_4 unit and show an eclipsed conformation in the solid state (Figure 5.4). In accordance to the observed As-As bond lengths, the *cisoid*-As_4 moiety can be best described as a *cis*-tetraarsa-1,3-diene ligand. It is notable that the bond lengths of As1-As2 and As3-As4 are quite similar (av. 2.32 Å), exhibiting distinct double bond character. However, the As2-As3 bond (2.6278(5) Å) is elongated in comparison to a common As-As single bond, but similar bond lengths have also been reported for $[(Cp'''Fe)_2(\mu,\eta^{4:4}\text{-}As_4)]$ (2.3169(5) Å / 2.3336(5) Å vs. 2.6100(5) Å).[23] In contrast, the Fe-Fe distance in **4** (2.6654(5) Å) is in good agreement with reported Fe-Fe bond lengths.[23,24,25]

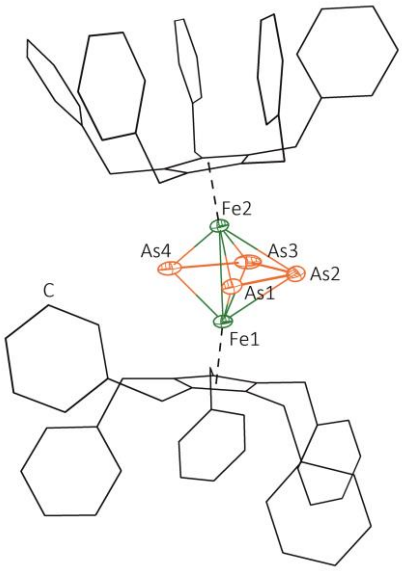

Figure 5.5 Molecular structure of **4** in the solid state. H atoms are omitted for clarity and Cp^{Bn} ligands are drawn in wire or frame model. Thermal ellipsoids are drawn at 50 % probability level. Selected bond lengths [Å] and angles [°]: Fe1–Fe2 2.6654(5), As1–As2 2.3162(4), As2–As3 2.6278(5), As3–As4 2.3231(5), As1···As4 3.6776(4), As1–As2–As3 103.190(15), As4–As3–As2 102.966(14).

Complex **4** is soluble in CH_2Cl_2 and toluene, nearly insoluble in *n*-hexane and insoluble in CH_3CN. The ^{1}H and $^{13}C\{^{1}H\}$ NMR spectra of **4** show the corresponding set of signals for the Cp^{Bn} ligands (Figure S5.3-S5.4, supplementary information) and the EI mass spectrum shows the molecular ion peak for $[Cp^{Bn}{}_2Fe_2As_4]^+$ (m/z = 1442.2) as the base peak. Moreover, the redox behaviour of **4** has been studied by cyclic voltammetry. The cyclic voltammogram of **4** in CH_2Cl_2 shows a reversible oxidation ($E_{1/2}$ = -0.69 V vs. $[Cp_2Fe]/[Cp_2Fe]^+$) and a reversible reduction ($E_{1/2}$ = -2.15 V vs. $[Cp_2Fe]/[Cp_2Fe]^+$) (see Figure S5.11, supplementary information). Therefore, a chemical oxidation of **4** with Ag^{I} salts should be possible, expecting the formation of a *cyclo*-As_4 middle deck. In contrast, the reaction of **4** with $AgBF_4$ in CH_2Cl_2 at room temperature leads to the formation of $[(Cp^{Bn}Fe)_2(\mu,\eta^{5:5}\text{-}As_5)][BF_4]$ (**5**), exhibiting a *cyclo*-As_5 ligand instead of the expected *cyclo*-As_4 unit (Scheme 5.4).

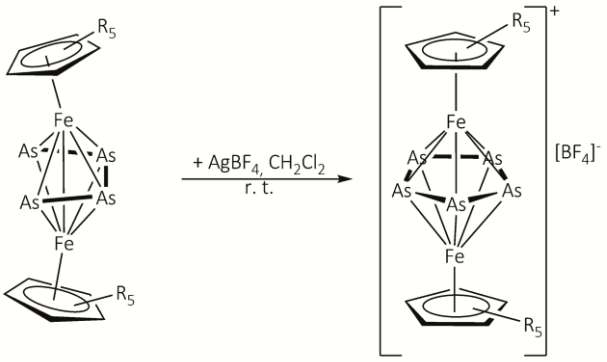

4

R = $CH_2(C_6H_5)$

5

Scheme 5.4 Oxidation of **4** with $AgBF_4$ in CH_2Cl_2 at room temperature.

Complex **5** is crystallised by layering a CH_2Cl_2 solution with *n*-hexane and crystallises as green plates in the orthorhombic space group *Pbna* with one independent molecule of **5** in the asymmetric unit. The single crystal X-ray structure analysis of **5** reveals a triple decker complex with a *cyclo*-As_5 middle deck. Although density functional theory (DFT) analysis of the hypothetic $[(CpFe)_2(\mu,\eta^{5:5}\text{-}As_5)]^+$ cation[26] predicts a potential minimum for a fully eclipsed conformation of the five-membered rings (D_{5h}), the Cp^{Bn} ligands show a staggered conformation in the solid state with respect to the *cyclo*-As_5 unit (Figure 5.6). Unfortunately, no satisfying refinement in the single crystal X-ray structure determination of **5** could be performed so far, since the benzyl groups and the BF_4^- anion are seriously disordered. However, the $[Fe_2As_5]$ core of **5** seems to be unaffected of the disorder.[27] Consequently, preliminary bond lengths of the $[Fe_2As_5]$ unit could be obtained, showing bond distances within the *cyclo*-As_5 unit between an As-As double bond and an As-As single bond. This fact is also confirmed by the DFT calculations, mentioned above.[26] In contrast, the iron atoms are no longer bonding to each other, since the Fe1···Fe2 distance can be found to be approximately 3.129(3) Å. This is considerably longer than the sum of the covalent radii of iron (2.64 Å).[28] Furthermore, in literature the triple decker complex $[CpFe(\mu,\eta^{5:5}\text{-}As_5)FeCp^*][PF_6]$ has been described, showing close similarity to the As-As bond lengths (2.319(4) Å-2.333(2) Å) and Fe···Fe distance (3.074(3) Å).[9] However, this complex shows a staggered conformation of the Cp* ring and the As_5 moiety, whereas the *cyclo*-As_5 unit and the Cp ring exhibit an eclipsed conformation.

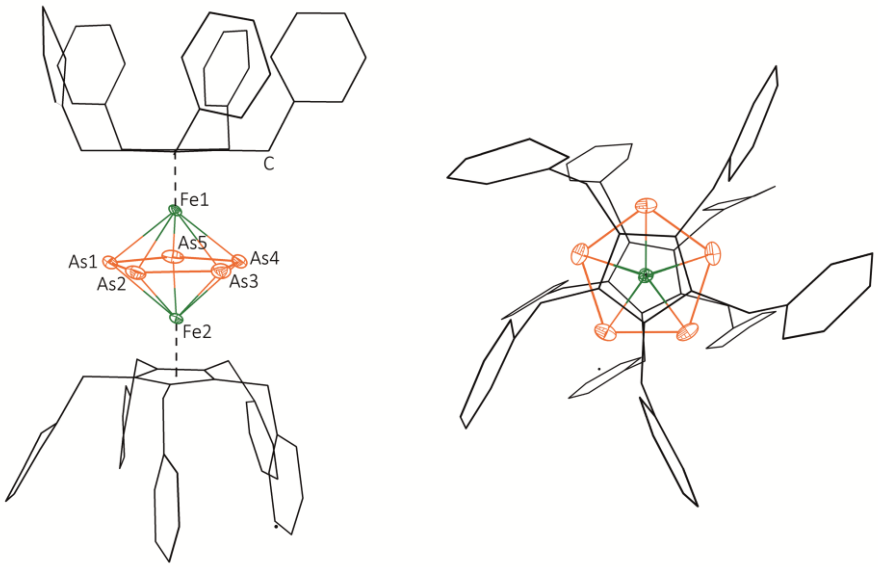

Figure 5.6 Molecular structure of **5** in the solid state (left). Top view of **5** (right). H atoms, solvent molecules and counterion are omitted for clarity. Cp^{Bn} ligands are drawn in wire or frame model. Thermal ellipsoids are drawn at 50 % probability level. Preliminary bond lengths [Å]: As1-As2 2.342(3), As2-As3 2.345(3), As3-As4 2.338(3), As4-As5 2.343(3), As5-As1 2.339(3), Fe1···Fe2 3.129(3).

5 is soluble in CH_2Cl_2 and thf and insoluble in *n*-hexane or toluene. The ^{1}H, $^{13}C\{^{1}H\}$ and $^{19}F\{^{1}H\}$ NMR spectra of **5** show the corresponding set of signals for the Cp^{Bn} ligands and the signal for the BF_4^- anion, respectively (Figure S5.5-S5.7, supplementary information), and the ESI mass spectrum shows the molecular ion peak for $[Cp^{Bn}{}_2Fe_2As_5]^+$ (*m*/*z* = 1517.5) as the base peak.

In summary, the synthesis of novel As_n ligand complexes of iron bearing the Cp^{Bn} ligand is presented. For this, two different synthetic methods have been used. Co-thermolysis of $[Cp^{Bn}Fe(CO)_2]_2$ with yellow arsenic in decalin leads to the formation of a mixture of As_n ligand complexes, consisting of $[Cp^{Bn}Fe(\eta^5\text{-}As_5)]$ (**1**), $[(Cp^{Bn}Fe)_3(\mu_3,\eta^{2:2:2}\text{-}As_3)(\mu_3\text{-}As)]$ (**2**) and $[(Cp^{Bn}Fe)_3(\mu_3,\eta^{4:4:4}\text{-}As_6)\{Fe(\eta^3\text{-}As_3)\}]$ (**3**). While **1** presents a further representative of pentaarsaferrocene derivatives of the general formula $[Cp^{R}Fe(\eta^5\text{-}As_5)]$, **2** and **3** display unprecedented iron containing arsenic clusters, which have been unknown to date. Unfortunately, **2** and **3** crystallise together and could not be separated due to similar solubility and crystallisation properties. The structural core motif of **2** could formally be explained by an insertion of three $[Cp^{Bn}Fe]$ fragments into the As-As bonds of an As_4 tetrahedron, showing a $\eta^{2:2:2}$-coordinating triangular *cyclo*-As_3 unit as well as a $\eta^{1:1:1}$-coordinating As atom. In contrast, **3** exhibits a prismatic As_6 ligand, whose quadrangular faces are capped by $[Cp^{Bn}Fe]$ fragments. In addition, one Fe atom is coordinated by one triangular As_3 face of the As_6 prism as well as by an end-on coordinated *cyclo*-As_3 ligand. Since co-thermolysis is known to yield thermodynamically favoured As_n ligand complexes, the reaction of *in situ* generated $[Cp^{Bn}Fe(\mu\text{-}Br)]_2$ with the transfer reagent $[Cp''_2Zr(\eta^{1:1}\text{-}As_4)]$ as an arsenic source at room temperature has also been studied. Here,

the triple decker complex $[(Cp^{Bn}Fe)_2(\mu,\eta^{4:4}\text{-}As_4)]$ (**4**) could be obtained, containing a *cisoid*-As_4 ligand. Besides the common characterisation methods (NMR spectroscopy, mass spectrometry, X-Ray and elemental analysis), **1** and **4** have been investigated by cyclic voltammetry. For **1**, the cyclic voltammogram reveals two irreversible oxidations and an irreversible reduction, whereby the irreversible reduction and the first irreversible oxidation can be interpreted as a chemically reversible couple. This fact has also been reported for the lighter Cp* derivative $[Cp^*Fe(\eta^5\text{-}P_5)]$. In contrast, **4** shows a reversible oxidation as well as a reversible reduction. Chemical oxidation of **4** with $AgBF_4$ leads to an expansion of the arsenic middle deck, resulting in the formation of the 30 VE triple decker complex $[(Cp^{Bn}Fe)_2(\mu,\eta^{5:5}\text{-}As_5)][BF_4]$ (**5**), possessing a *cyclo*-As_5 middle deck.

5.4 Experimental Part

All reactions were performed under an atmosphere of dry argon or nitrogen using glovebox or Schlenk techniques. Solvents were purified, degassed and dried prior to use. The synthesis of $[Cp^{Bn}Fe(CO_2)_2]$ was improved with reference to the original synthesis.[29] As_4[30] and $[Cp''_2Zr(\eta^{1:1}\text{-}As_4)]$[23] were prepared according to literature procedures. The AgX salts ($X^- = BF_4^-$, $CF_3SO_3^-$) and ^{n}BuLi (c = 1.6 mmol/L, solution in *n*-hexane) were commercially available and were used without further purification.

The NMR spectra were recorded on a Bruker Avance 300 spectrometer. The EI MS spectra were measured on a ThermoQuest Finnigan MAT SSQ 710A mass spectrometer and the ESI MS spectra were measured on a ThermoQuest Finnigan MAT TSQ 7000 mass spectrometer. The elemental analyses were determined with a Vario ELIII apparatus.

Improved Synthesis of $[Cp^{Bn}Fe(CO)_2]_2$

A mixture of $Cp^{Bn}H$ (7.50 g, 0.01 mol) and $Fe(CO)_5$ (6 mL, 0.044 mol) in toluene (100 mL) was refluxed for 5 days. During this time, 1 mL $Fe(CO)_5$ was additionally added to the reaction mixture every day. After 5 days, the deep red solution was allowed to cool to room temperature. The solvent was removed *in vacuo*, resulting in a red residue. Subsequent column chromatographic work up (silica gel, CH_2Cl_2/*n*-hexane (3:7), 21 x 6 cm) afforded first a yellow fraction of $[(\eta^4\text{-}Cp^{Bn}H)Fe(CO)_3]$ and then a red fraction of $[Cp^{Bn}Fe(CO)_2]_2$. The solvent was removed and pure $[Cp^{Bn}Fe(CO)_2]_2$ can be obtained as red powder or crystallised by layering a CH_2Cl_2 solution with *n*-hexane.

Crystalline yield: 5.45 g (4.34 mmol, 87% referred to $Cp^{Bn}H$).
All analytical data of $[Cp^{Bn}Fe(CO)_2]_2$ are included in the literature synthesis.[29]

Synthesis of $[Cp^{Bn}Fe(\eta^5\text{-}As_5)]$ (1), $[(Cp^{Bn}Fe)_3(\mu_3,\eta^{2:2:2}\text{-}As_3)(\mu_3\text{-}As)]$ (2) and $[(Cp^{Bn}Fe)_3(\mu_3,\eta^{4:4:4}\text{-}As_6)\{Fe(\eta^3\text{-}As_3)\}]$ (3)

A suspension of $[Cp^{Bn}Fe(CO)_2]_2$ (936 mg, 0.77 mmol) in 100 mL decalin was added dropwise to a freshly prepared solution of As_4 (starting from 7.5 g grey arsenic) in 250 mL decalin. The mixture was heated to reflux and the reaction progress was monitored by IR spectroscopy. After 90 min, the carbonyl bands of $[Cp^{Bn}Fe(CO)_2]_2$ disappeared and the solvent was removed *in vacuo*. Subsequent column chromatographic work up (silica gel, *n*-hexane, 20 x 2.5 cm, -30°C) with *n*-hexane/toluene (7:1) afforded at first a green fraction of **1**. Complexes **2** and **3** were eluted together as a brown zone using toluene. All complexes were crystallised by layering a toluene or CH_2Cl_2 solution with CH_3CN.

Analytical data of **1**

Crystalline yield: 227 mg (0.24 mmol, 16 % referred to $[Cp^{Bn}Fe(CO)_2]_2$).

^{1}H NMR (CD_2Cl_2): δ [ppm] = 3.64 (s, 10H, CH_2), 6.18 (d, 10H, $^3J_{HH}$ = 7.38 Hz, C_6H_5 [H^{ortho}]), 6.70 (dd, 10H, $^3J_{HH}$ = 7.38 Hz, C_6H_5 [H^{meta}]), 6.84 (t, 5H, $^3J_{HH}$ = 7.38 Hz, C_6H_5 [H^{para}]).

^{13}C{^{1}H} NMR (CD_2Cl_2): δ [ppm] = 35.00 (CH_2), 91.19 (C_5), 125.15 (C_6H_5), 126.99 (C_6H_5), 128.06 (C_6H_5), 137.83 (C_6H_5).

EI MS (70 eV, CH_2Cl_2): *m/z* (%) = 945.7 (32) ($[Cp^{Bn}FeAs_5]^+$), 795.9 (15) ($[Cp^{Bn}FeAs_3]^+$), 516.2 (9) ($[Cp^{Bn}H]^+$), 425.2 (5) ($[Cp^{Bn}\text{-}C_7H_7]^+$), 299.7 (100) ($[As_4]^+$), 224.7 (9) ($[As_3]^+$), 149.8 (19) ($[As_2]^+$), 91.1 (12) ($[C_7H_7]^+$).

Elemental Analysis: Calculated (%) for $[C_{40}H_{35}FeAs_5]$ (946.16 g/mol): C 50.78, H 3.73; found C 50.48, H 3.75.

Analytical data of **2** and **3**

Crystalline yield: 358 mg (mixture of **2** and **3**).

EI MS (70 eV, CH_2Cl_2): *m/z* (%) = 2163.1 (2) ($[(Cp^{Bn}Fe)_3As_6]^+$), 945.7 (18) ($[Cp^{Bn}FeAs_5]^+$), 796.0 (10) ($[Cp^{Bn}FeAs_3]^+$), 516.2 (100) ($[Cp^{Bn}H]^+$), 425.2 (60) ($[Cp^{Bn}\text{-}C_7H_7]^+$), 300.0 (100) ($[As_4]^+$).

Synthesis of $[(Cp^{Bn}Fe)_2(\mu,\eta^{4:4}\text{-}As_4)]$ (4)

A solution of ^{n}BuLi in *n*-hexane (0.6 mL, c = 1.6 mol/L, 0.96 mmol) was added dropwise to a solution of $Cp^{Bn}H$ (502 mg, 0.97 mmol) in thf (25 mL) at -30 °C. The solution became purple and was stirred at room temperature. After 2 h, the reaction mixture was added dropwise to a suspension of [$FeBr_2$·dme] (296 mg, 0.97 mmol) in thf (20 mL) at -30°C. The resulting green

solution was stirred for 1 h at this temperature and for 1 h at room temperature. Then, the solvent was removed under reduced pressure. The resulting brown oily residue[22] was resolved in toluene (10 mL) and was filtered into a solution of [Cp''$_2$Zr($\eta^{1:1}$-As_4)] (181 mg, 0.24 mmol) in toluene (10 mL). After stirring for 7 days at room temperature, the solvent was removed *in vacuo*. Subsequent column chromatographic workup (silica gel, *n*-hexane, 10 x 1.5 cm) afforded first a yellow fraction containing [Cp''$_2$ZrBr_2] and finally a brown fraction of **4** was eluted with toluene. Crystals of **4** suitable for single crystal X-ray diffraction analysis were obtained by layering a CH_2Cl_2 solution with *n*-hexane.

Analytical data of **4**

Crystalline yield: 170 mg (0.12 mmol, 49 % referred to [Cp''$_2$Zr($\eta^{1:1}$-As_4)]).

^{1}H NMR (CD_2Cl_2): δ [ppm] = 3.78 (s, 20H, CH_2), 6.51 (d, 20H, C_6H_5), 6.84-6.96 (m, 30H, C_6H_5).

^{13}C{^{1}H} NMR (CD_2Cl_2): δ [ppm] = 36.48 (CH_2), 96.20 (C_5), 126.18 (C_6H_5), 128.18 (C_6H_5), 129.13 (C_6H_5), 140.23 (C_6H_5).

EI MS (70 eV, toluene): *m/z* (%) = 1442.2 (100) ([$(Cp^{Bn}Fe)_2As_4$]$^+$).

Elemental Analysis: Calculated (%) for [$C_{80}H_{70}Fe_2As_4$] (1442.79 g/mol): C 66.59, H 4.89; found C 65.89, H 4.91.

Synthesis of [$(Cp^{Bn}Fe)_2(\mu,\eta^{5:5}$-$As_5)$][$BF_4$] (5)

A mixture of **4** (20 mg, 0.01 mmol) and $AgBF_4$ (4 mg, 0.02 mmol) in CH_2Cl_2 (20 mL) was stirred at room temperature. After 1 day, the solution was filtered into a thin Schlenk tube and layered with *n*-hexane. After complete diffusion, crystals of **5** were obtained. The mother liquor was decanted, the crystals were washed with *n*-pentane and dried *in vacuo*. By concentrating the decanted solution, layering with *n*-hexane and storing at -28°C, a second crop of crystals of **5** can be obtained, while the mother liquor has turned almost colourless.

Analytical data of **5**

Crystalline yield: 2.4 mg (1.50 µmol, 19 % referred to [$(Cp^{Bn}Fe)_2(\mu,\eta^{4:4}$-$As_4)$]).

^{1}H NMR (CD_2Cl_2): δ [ppm] = 3.43 (s, 20H, CH_2), 6.12 (d, 20H, C_6H_5), 6.78 (t, 20H, C_6H_5), 6.92 (t, 20H, C_6H_5).

^{13}C{^{1}H} NMR (CD_2Cl_2): δ [ppm] = 33.53 (CH_2), 89.26 (C_5), 126.75 (C_6H_5), 128.23 (C_6H_5), 129.64 (C_6H_5), 136.05 (C_6H_5).

^{19}F{^{1}H} NMR (CD_2Cl_2): δ [ppm] = -150.94 (BF_4).

Positive ion ESI MS (CH_3CN): *m/z* (%) = 1517.5 (100) ([{$Cp^{Bn}Fe$}$_2As_5$]$^+$).

Negative ion ESI MS (CH_3CN): *m/z* (%) = 86.9 (100) ($[BF_4]^-$).

Elemental Analysis: Calculated (%) for [$C_{80}H_{70}Fe_2As_5BF_4$ · 0.5 CH_2Cl_2] (1646.01 g/mol): C 58.69, H 4.35; found C 58.64, H 4.56.

$[(Cp^{Bn}Fe)_2(\mu,\eta^{5:5}\text{-}As_5)][CF_3SO_3]$ (5')[27]

A mixture of **4** (10 mg, 0.007 mmol) and $Ag(CF_3SO_3)$ (3 mg, 0.012 mmol) in CH_2Cl_2 (20 mL) was stirred at room temperature. After 1 day, the green solution was filtered into a thin Schlenk tube and layered with *n*-hexane. After complete diffusion, green plates of **5'** were obtained. The mother liquor was decanted, the crystals were washed with *n*-pentane and dried *in vacuo*. By concentrating the decanted solution, layering with *n*-hexane and storing at -28°C, a second crop of crystals of **5'** can be obtained, while the mother liquor has turned almost colourless.

Analytical data of **5'**

Crystalline yield: 0.374 mg (0.22 µmol, 4 % referred to $[(Cp^{Bn}Fe)_2(\mu,\eta^{4:4}\text{-}As_4)]$).

^{1}H NMR (CD_2Cl_2): δ [ppm] = 3.43 (s, 20H, CH_2), 6.11 (d, 20H, C_6H_5), 6.78 (t, 20H, C_6H_5), 6.92 (t, 20H, C_6H_5).

^{19}F{^{1}H} NMR (CD_2Cl_2): δ [ppm] = -78.66 (CF_3).

Elemental Analysis: Calculated (%) for [$C_{80}H_{70}Fe_2As_5SO_3CF_4$ · 0.5 CH_2Cl_2] (1709.25 g/mol): C 57.27, H 4.19, S 1.88; found C 57.50, H 4.50, S under detection limit.

5.5 Supplementary Information

NMR Investigations

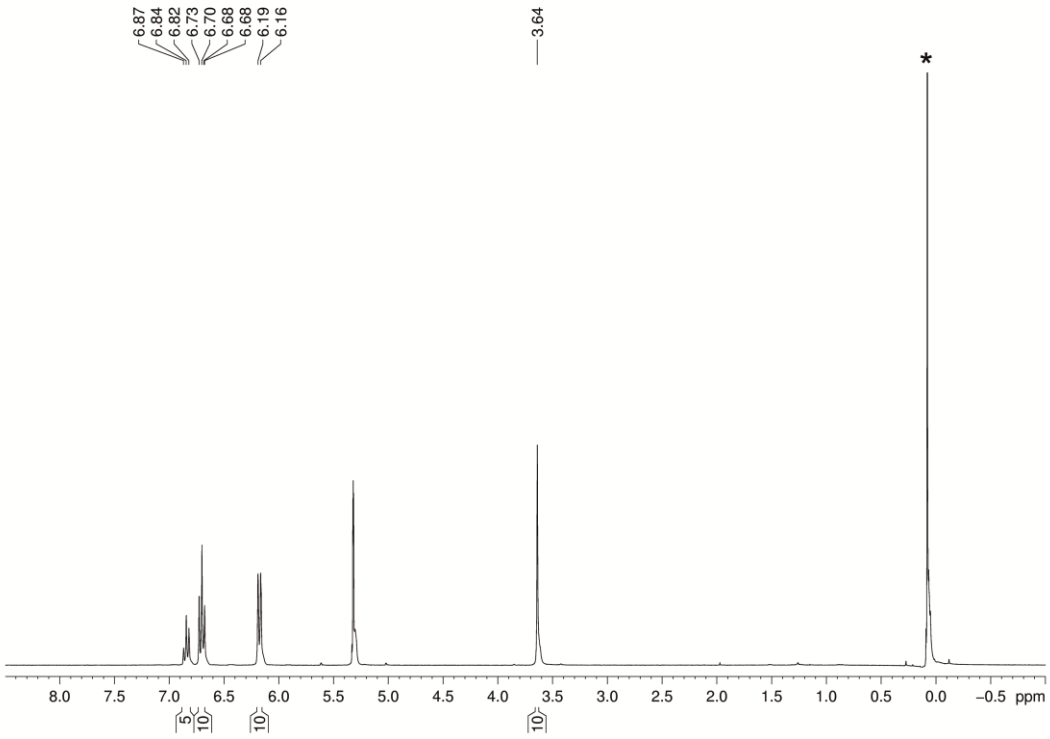

Figure S5.1 ^{1}H NMR spectrum of **1** in CD_2Cl_2 at 300 K. Signal marked with an asterisk is due to silicon grease.

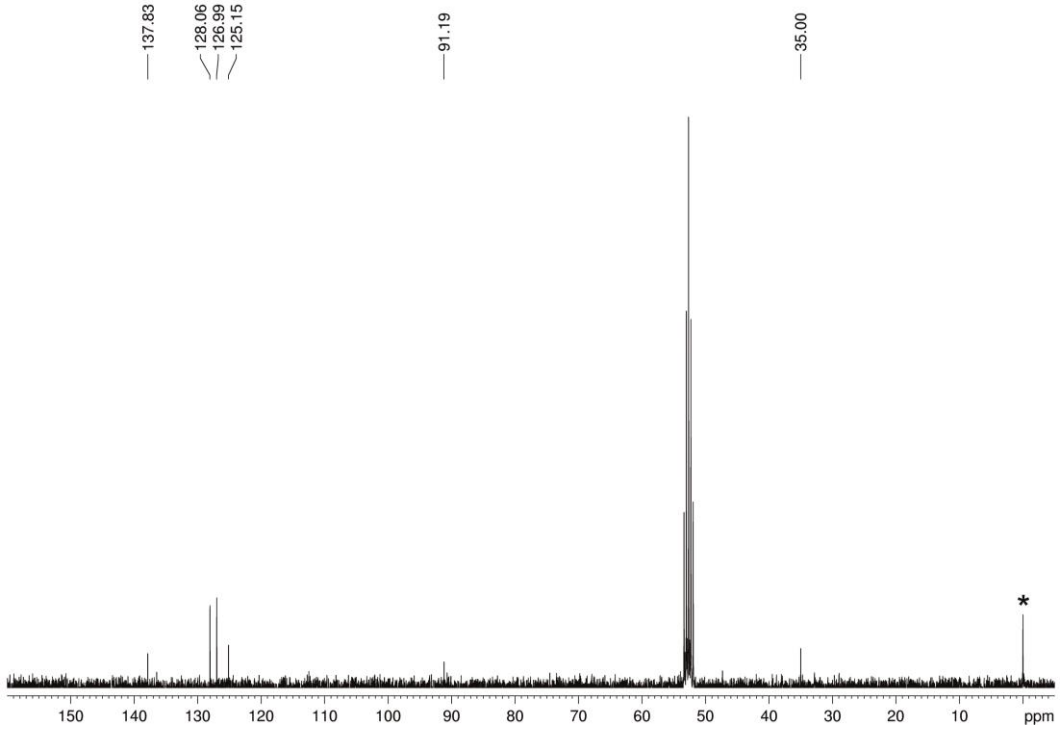

Figure S5.2 $^{13}C\{^{1}H\}$ NMR spectrum of **1** in CD_2Cl_2 at 300 K. Signal marked with an asterisk is due to silicon grease.

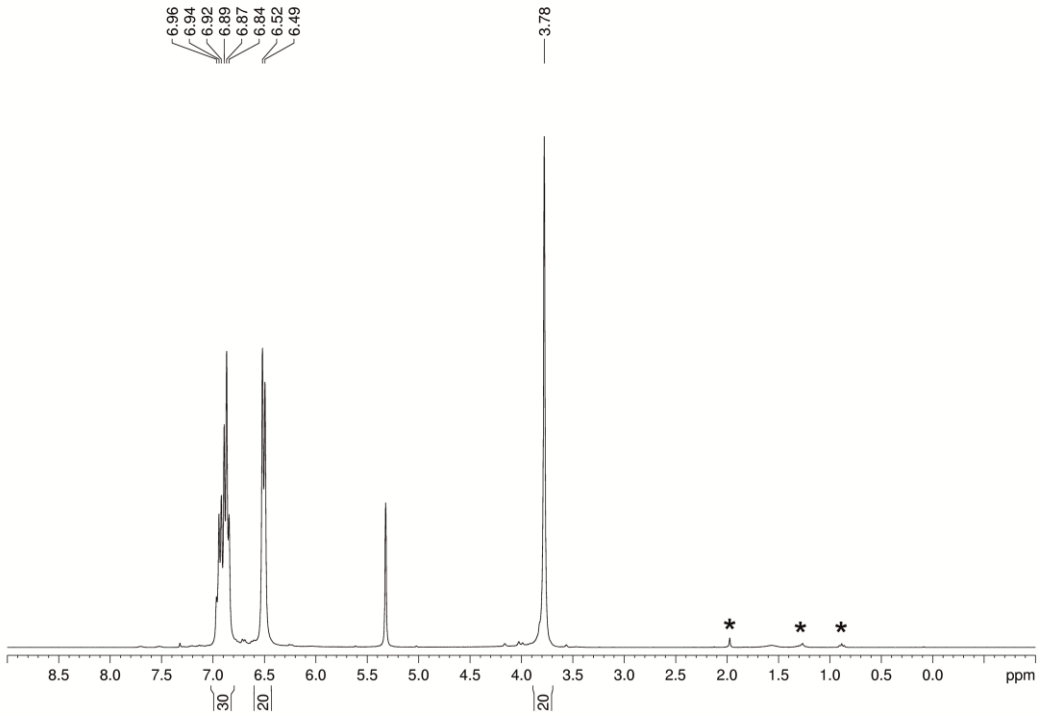

Figure S5.3 ^{1}H NMR spectrum of **4** in CD_2Cl_2 at 300 K. Signals marked with asterisk are due to different solvents.

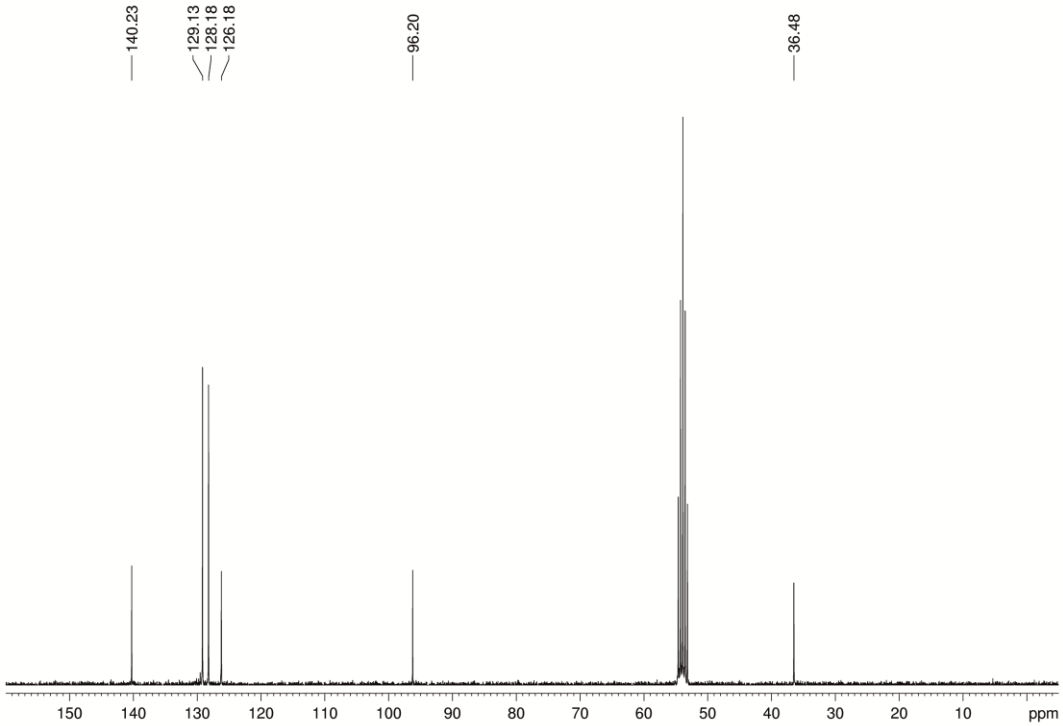

Figure S5.4 $^{13}C\{^{1}H\}$ NMR spectrum of **4** in CD_2Cl_2 at 300 K.

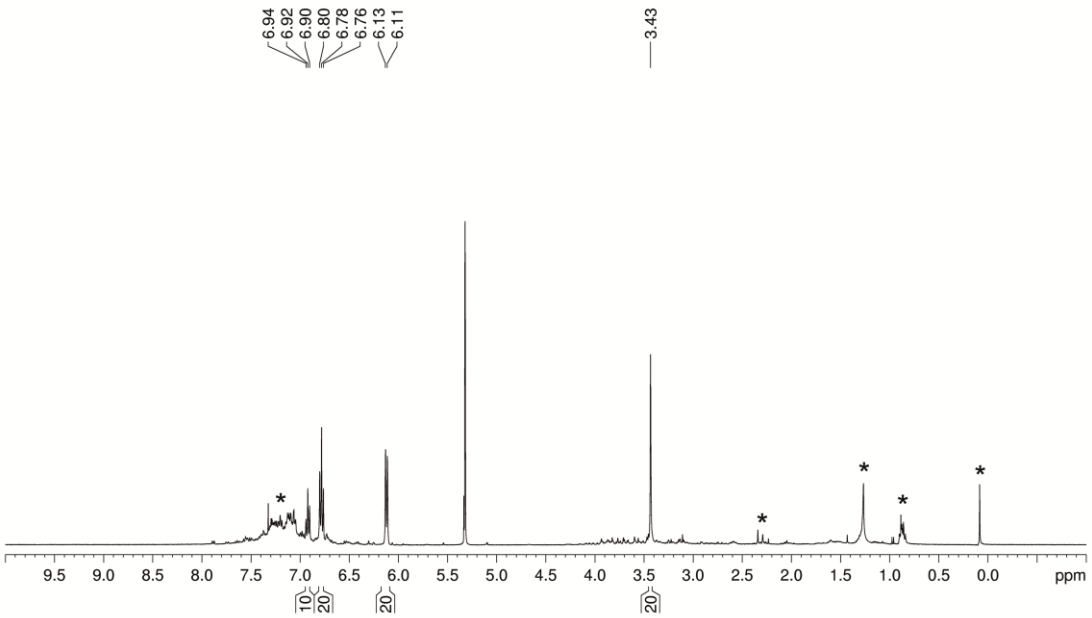

Figure S5.5 ^{1}H NMR spectrum of **5** in CD_2Cl_2 at 300 K. Signals marked with an asterisk are due to different solvents and silicon grease.

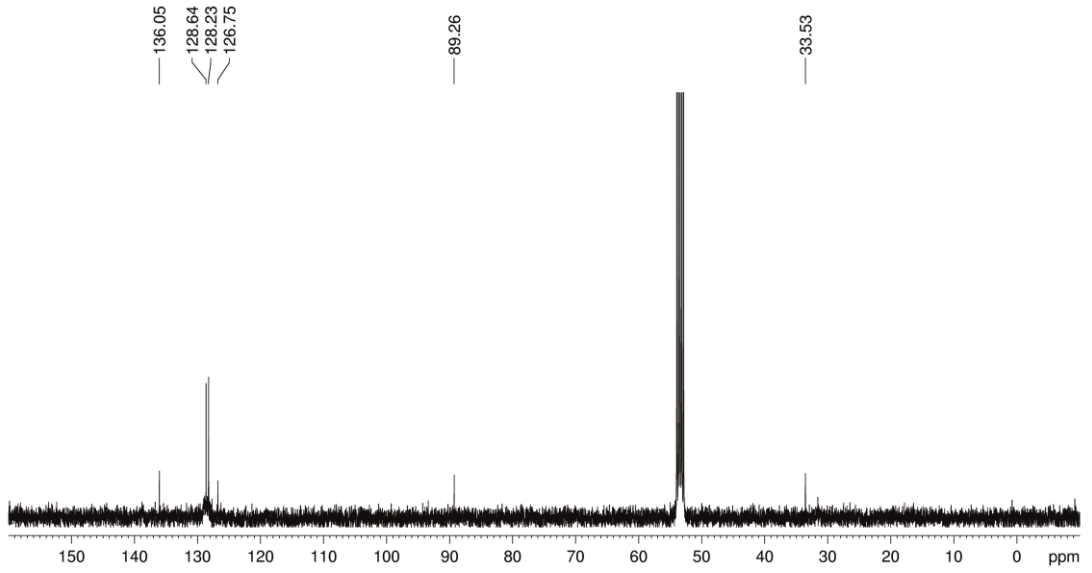

Figure S5.6 $^{13}C\{^{1}H\}$ NMR spectrum of **5** in CD_2Cl_2 at 300 K.

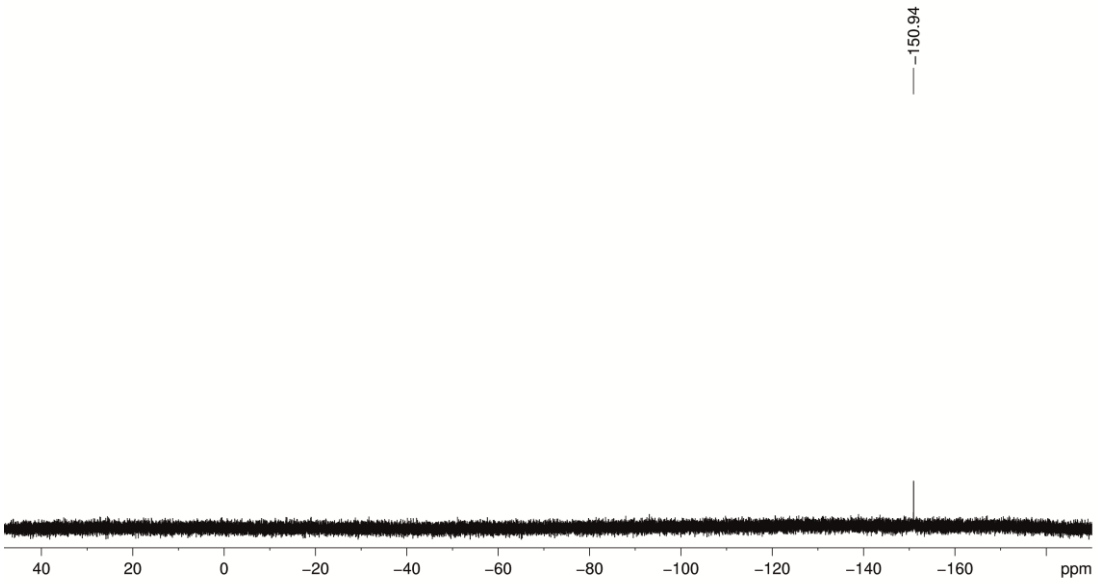

Figure S5.7 $^{19}F\{^{1}H\}$ NMR spectrum of **5** in CD_2Cl_2 at 300 K.

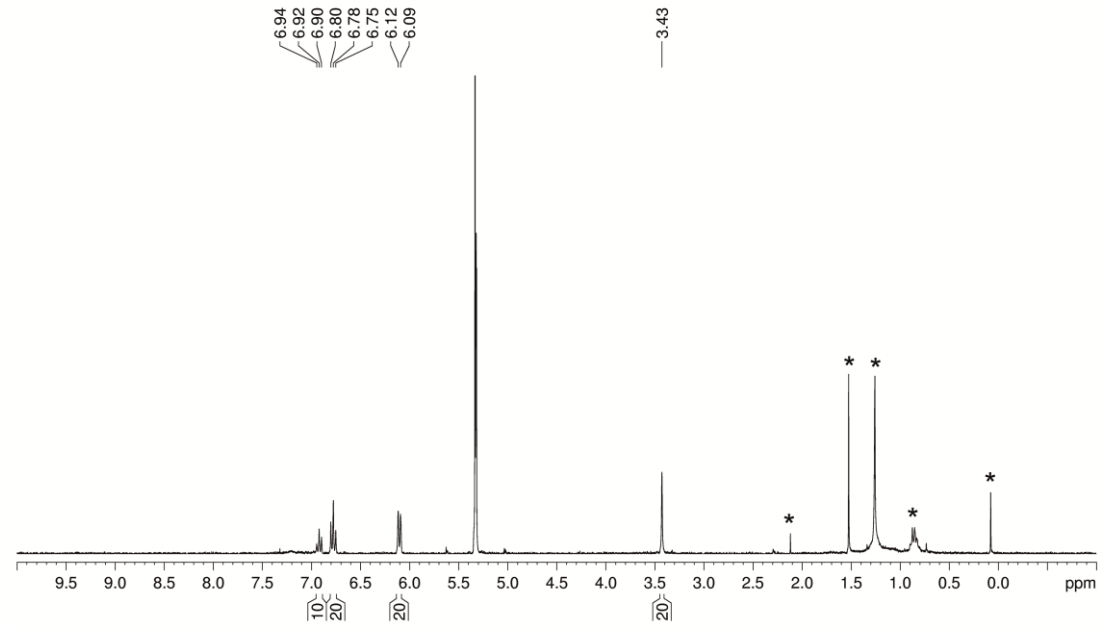

Figure S5.8 ^{1}H NMR spectrum of **5'** in CD_2Cl_2 at 300 K. Signals marked with an asterisk are due to different solvents and silicon grease.

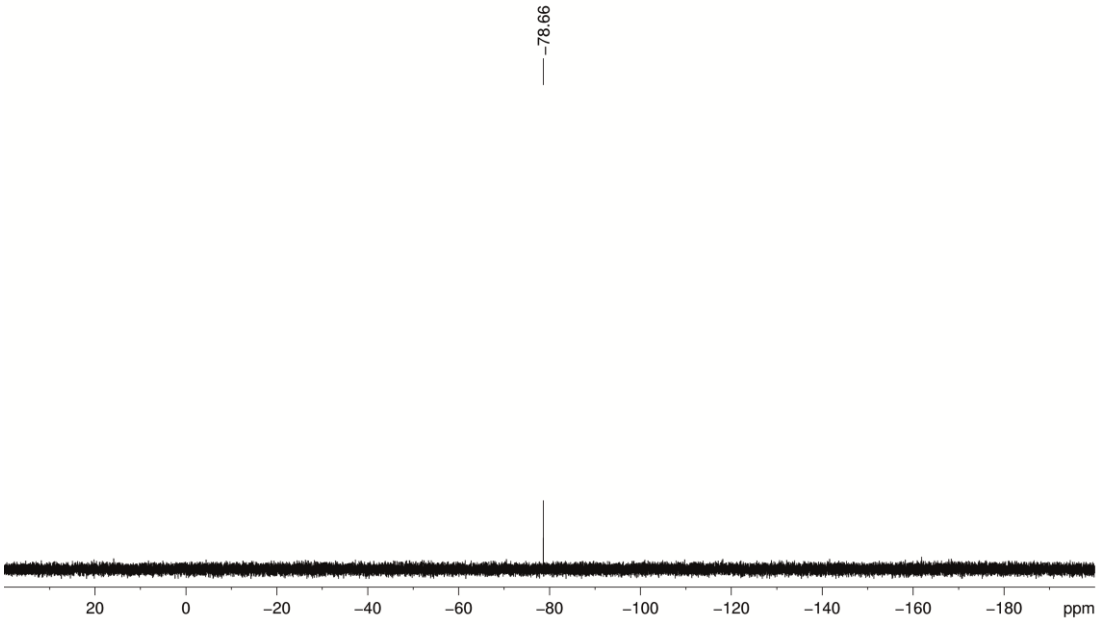

Figure S5.9 $^{19}F\{^{1}H\}$ NMR spectrum of **5'** in CD_2Cl_2 at 300 K.

Representation of the cyclic voltammograms of 1 and 4

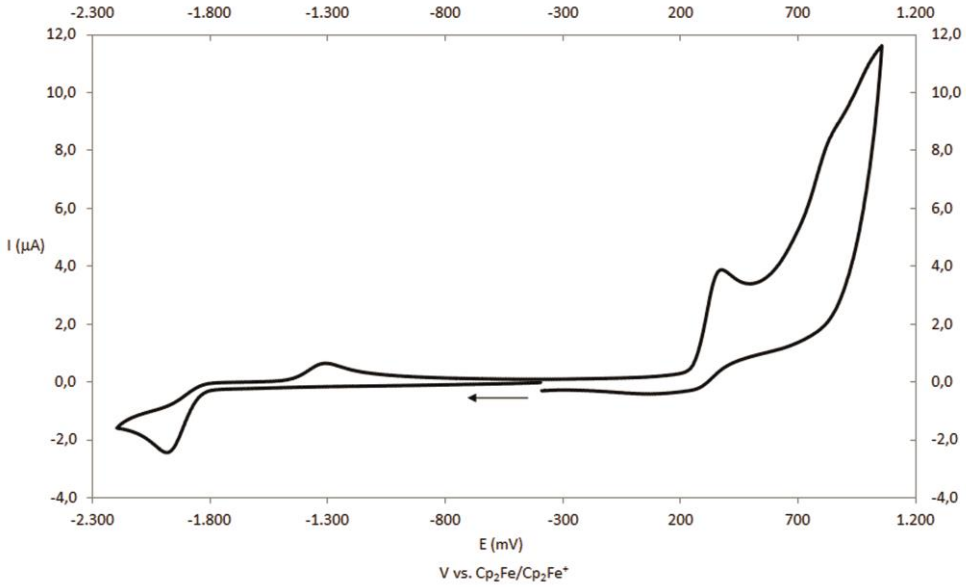

Figure S5.10 Cyclic voltammogram of **1** recorded at a platinum disc electrode in CH_2Cl_2 at 0.1 Vs^{-1} and referenced against $[Cp_2Fe]/[Cp_2Fe]^+$; supporting electrolyte $[^nBu_4N][PF_6]$ (0.1 mol/L).

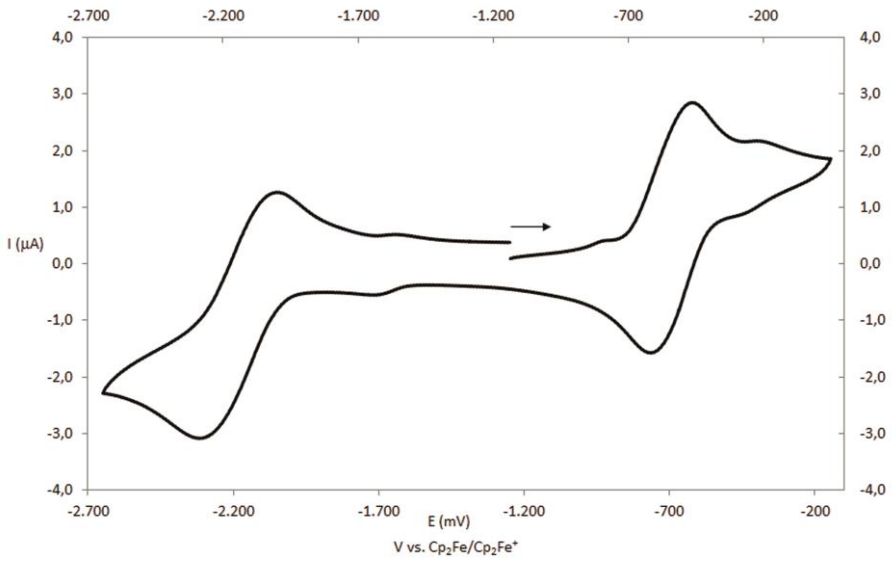

Figure S5.11 Cyclic voltammogram of **4** recorded at a platinum disc electrode in CH_2Cl_2 at 0.1 Vs^{-1} and referenced against $[Cp_2Fe]/[Cp_2Fe]^+$; supporting electrolyte $[^nBu_4N][PF_6]$ (0.1 mol/L).

Cell parameters of $[(Cp^{Bn}Fe)_2(\mu,\eta^{5:5}\text{-}As_5)][CF_3SO_3]$ (5')[27]

Table 5.1 Preliminary cell parameters of **5'**.

a/Å	b /Å	c/Å	α/°	β/°	γ/°	V/Å³
10.09	31.08	22.74	89.93	89.2	90.0	7102

Crystallographic Details

The data for **1**-**4** were collected on an Agilent Technologies diffractometer equipped with an Atlas CCD detector and a SuperNova CuK_α microfocus (λ = 1.54178 Å) source. The data for **5** were collected on an Agilent Technologies Gemini R-Ultra diffractometer equipped with an Atlas^{S2} CCD detector and using an Enhanced Ultra CuK_α sealed tube. All measurements were performed at 123 K. Crystallographic data and details of the diffraction experiments are given in Table S5.2-S5.5. Using Olex2,[31] the structures were solved either with the ShelXT[32] (**1**-**3**), SUPERFLIP[33] (**4**) or ShelXS[34] (**5**) structure solution program using Direct Methods and refined with the ShelXL[35] refinement package using Least Squares minimisation. Especially in case of disorder, commonly used restraints for the ShelXL program were applied (SIMU). Since crystals of **2** show incommensurable modulation (q-vector of 0.256), only a preliminary model could be obtained. Furthermore, the refinement of **3** and **5** is unstable so far due to serious disorder. Consequently, just the structural core motif of **2** and **3** is obtained and only the experimental data are given in Table S5.1, whereas a preliminary model is obtained for **5**. Moreover, H atoms were located in idealised positions and refined isotropically according to the riding model. A semi-empirical numerical absorption correction based on gaussian[36] integration over a multifaceted crystal model (**1** ,**2** and **5**) or an analytical[37] absorption correction from crystal faces (**4**) was applied. Figures were created with DIAMOND3.0.[38]

Table S5.2 Crystallographic data for **1** and **2**.

	1	**2**
Chemical formula	$C_{40}H_{35}FeAs_5$	$C_{120}H_{105}Fe_3As_4$
M/g·mol^{-1}	946.13	2014.26
T/K	123	123
Crystal system	monoclinic	triclinic
Space group	$P2_1/n$	$P\bar{1}$
a/Å	17.83205(15)	16.5167(3)
b/Å	10.63373(10)	18.2448(4)
c/Å	18.49105(15)	19.8400(5)
α/°	90	100.476(2)
β/°	91.1545(8)	110.474(2)
γ/°	90	112.861(2)
V/Å³	3505.58(5)	4798.7(2)
Z	4	2
ρ_{cal}/g·cm^{-3}	1.793	1.394
μ/mm^{-1}	8.908	5.502
F(000)	1864.0	2070.0
Crystal size/mm^3	0.249 × 0.185 × 0.164	0.278 × 0.059 × 0.031
Radiation	CuK_α	CuK_α
2θ range/°	6.818 to 134.142	5.654 to 127.726
Index ranges	-21 ≤ h ≤ 20, -12 ≤ k ≤ 12, -17 ≤ l ≤ 22	-18 ≤ h ≤ 17, -21 ≤ k ≤ 20, -22 ≤ l ≤ 23
Reflections collected	16081	43967
Independent reflections	6255 [R_{int} = 0.0271, R_{sigma} = 0.0237]	15249 [R_{int} = 0.0387, R_{sigma} = 0.0362]
Data/restraints/parameters	6255/0/415	-
Goodness-of-fit on F^2	1.066	-
Final R indexes [I>2σ(I)]	R_1 = 0.0321, wR_2 = 0.0818	-
Final R indexes [All Data]	R_1 = 0.0332, wR_2 = 0.0826	-
Largest diff. peak/hole/eA^{-3}	0.42/-1.01	-

Table S5.3 Crystallographic data for **3** and **4**.

	3	**4**
Chemical formula	$C_{120}H_{105}Fe_4As_9$	$C_{80}H_{70}As_4Fe_2$
M/g·mol^{-1}	2444.79	1442.74
T/K	123	123
Crystal system	monoclinic	monoclinic
Space group	$P2_1/m$	$P2_1/c$
a/Å	17.2039(10)	10.03997(19)
b/Å	20.1612(8)	31.6780(5)
c/Å	17.2182(10)	19.6456(4)
α/°	90	90
β/°	120.038(8)	94.0053(17)
γ/°	90	90
V/Å³	5170.1(6)	6232.95(19)
Z	2	4
ρ_{cal}/g·cm^{-3}	-	1.537
μ/mm^{-1}	7.922	6.443
F(000)	932.0	2936.0
Crystal size/mm^3	0.323 × 0.081 × 0.062	0.1961 × 0.1652 × 0.0678
Radiation	CuK_α	CuK_α
2θ range/°	7.374 to 123.906	7.176 to 147.118
Index ranges	-18 ≤ h ≤ 19, -21 ≤ k ≤ 22, -18 ≤ l ≤ 18	-12 ≤ h ≤ 12, -38 ≤ k ≤ 39, -23 ≤ l ≤ 23
Reflections collected	20296	49715
Independent reflections	7882 [R_{int} = 0.0288, R_{sigma} = 0.0337]	12353 [R_{int} = 0.0493, R_{sigma} = 0.0369]
Data/restraints/parameters	-	12353/0/775
Goodness-of-fit on F^2	-	1.057
Final R indexes [I>2σ(I)]	-	R_1 = 0.0351, wR_2 = 0.0961
Final R indexes [All Data]	-	R_1 = 0.0395, wR_2 = 0.0999
Largest diff. peak/hole/eA^{-3}	-	0.92/-0.53

Table S5.4 Crystallographic data for **5**.

	5 · 0.5 CH_2Cl_2
Chemical formula	$C_{80.5}H_{71}Fe_2As_5BF_4Cl$
M/g·mol^{-1}	1627.52
T/K	123
Crystal system	orthorhombic
Space group	*Pbna*
a/Å	19.62278(11)
b/Å	31.11174(17)
c/Å	22.29559(13)
α/°	90
β/°	90
γ/°	90
V/Å³	13611.43(13)
Z	8
ρ_{cal}/g·cm^{-3}	1.588
μ/mm^{-1}	6.751
F(000)	6553.0
Crystal size/mm^3	0.377 × 0.288 × 0.14
Radiation	CuK_α
2θ range/°	6.64 to 133.368
Index ranges	-23 ≤ h ≤ 23,
	-36 ≤ k ≤ 36,
	-26 ≤ l ≤ 25
Reflections collected	126412
Independent reflections	12028
	[R_{int} = 0.0346, R_{sigma} = 0.0138]
Data/restraints/parameters	12028/612/1018
Goodness-of-fit on F^2	1.205
Final R indexes [I>2σ(I)]	R_1 = 0.1476, wR_2 = 0.3316
Final R indexes [All Data]	R_1 = 0.1478, wR_2 = 0.3316
Largest diff. peak/hole/eA^{-3}	5.26/-1.65

5.6 References

[1] a) A. S. Foust, M. S. Foster, L. F. Dahl, *J. Am. Chem. Soc.* 1969, *91*, 5631-5633; b) A. S. Foust, M. S. Foster, L. F. Dahl, *J. Am. Chem. Soc.* 1969, *91*, 5633-5635.

[2] selected review articles: a) O. J. Scherer, *Angew. Chem. Int. Ed. Engl.* 1985, *24*, 924-943; b) B. Rink, O. J. Scherer, G. Heckmann, G. Wolmershäuser, *Chem. Ber.* 1992, *125*, 1011-1016; c) O. J. Scherer, *Acc. Chem. Res.* 1999, *32*, 751-762.

[3] a) A. S. Foust, M. S. Foster, L. F. Dahl, *J. Am. Chem. Soc.* 1969, *91*, 5633-5635; b) P. J. Sullivan, A. L. Rheingold, *Organometallics* 1982, *1*, 1547-1549; c) P. Mercando, A.-J. DiMaio, A. L. Rheingold, *Angew. Chem. Int. Ed. Engl.* 1987, *26*, 244-245; d) K. Mast, O. J. Scherer, G. Wolmershäuser, *Z. Anorg. Allg. Chem.* 1999, *625*, 1475-1478.

[4] a) C. v. Hänisch, D. Fenske, *Z. Anorg. Allg. Chem.* 1998, *624*, 367-369; b) C. von Hänisch, D. Fenske, F. Weigend, R. Ahlrichs, R. Ahlrichs, F. Weigend, *Chem. Eur. J.* 1997, *3*, 1494-1498.

[5] L. Y. Goh, R. C. S. Wong, W. H. Yip, T. C. W. Mak, *Organometallics* 1991, *10*, 875-879.

[6] B. Sigwarth, L. Zsolnai, H. Berke, G. Huttner, *J. Organomet. Chem.* 1982, *226*, C5-C8.

[7] selected publications: a) O. J. Scherer, H. Sitzmann, G. Wolmershäuser, *Angew. Chem. Int. Ed. Engl.* 1989, *28*, 212-213; b) O. J. Scherer, W. Wiedemann, G. Wolmershäuser, *J. Organomet. Chem.* 1989, *361*, C11-C14; c) O. J. Scherer, W. Wiedemann, G. Wolmershäuser, *Chem. Ber.* 1990, *123*, 3-6; d) C. Schwarzmaier, M. Sierka, M. Scheer, *Angew. Chem. Int. Ed.* 2013, *52*, 858-861; e) S. Heinl, M. Scheer, *Chem. Sci.* 2014, *5*, 3221-3225; f) F. Spitzer, M. Sierka, M. Latronico, P. Mastrorilli, A. V. Virovets, M. Scheer, *Angew. Chem. Int. Ed.* 2015, *54*, 4392-4396; g) C. Graßl, M. Bodensteiner, M. Zabel, M. Scheer, *Chem. Sci.* 2015, *6*, 1379-1382.

[8] O. J. Scherer, G. Kemény, G. Wolmershäuser, *Chem. Ber.* 1995, *128*, 1145-1148.

[9] O. J. Scherer, C. Blath, G. Wolmershäuser, *J. Organomet. Chem.* 1990, *387*, C21-C23

[10] C. Schwarzmaier, A. Y. Timoshkin, G. Balázs, M. Scheer, *Angew. Chem. Int. Ed.* 2014, *53*, 9077-9081.

[11] S. Heinl, M. Scheer, *Chem. Sci.* 2015, *5*, 3221-3225.

[12] F. Dielmann, R. Merkle, S. Heinl, M. Scheer, *Z. Naturforsch.* 2009, *64b*, 3-10.

[13] M. Fleischmann, S. Welsch, H. Krauss, M. Schmidt, M. Bodensteiner, E. V. Peresypkina, M. Sierka, C. Gröger, M. Scheer, *Chem. Eur. J.* 2014, *20*, 3759-3768;

[14] O. J. Scherer, C. Blath, G. Wolmershäuser, *J. Organomet. Chem.* 1990, *387*, C21-C24.

[15] S. Heinl, *Ph.D. thesis*, Universität Regensburg, 2014.

[16] A. H. Cowley, N. C. Norman, M. Pakulski, *Dalton Trans.* 1985, *1*, 383-386.

[17] Y. Morino, T. Ukaji, T. Ito, *Bull. Chem. Soc. Jpn.* 1966, *39*, 64-71.

[18] H. A. Spinney, N. A. Piro, C. C. Cummins, *J. Am. Chem. Soc.* 2009, *131*, 16233-16243.

[19] R. F. Winter, W. E. Geiger, *Organometallics* 1999, *18*, 1827-1833.

[20] H. Krauss, *Ph.D. thesis*, Universität Regensburg, 2011.

[21] G. Friedrich, O. J. Scherer, G. Wolmershäuser, *Z. Anorg. Allg. Chem.* 1996, *622*, 1478-1486.

[22] Unfortunately, $[Cp^{Bn}Fe(\mu\text{-}Br)]_2$ could not be isolated within the scope of this thesis, due to its instability in solution.

[23] M. Eckhardt, *Ph.D. thesis*, Universität Regensburg, 2014.

[24] S. Heinl, G. G. Balázs, M. Scheer, *Phosphorus, Sulfur Silicon Relat. Elem.* 2014, *189*, 1-9.

[25] L. J. Arnold, K. M. Mackay, B. K. Nicholson, *J. Organomet. Chem.* 1990, *387*, 197-207.

[26] E. J. Padma Malar, *Theor. Chem. Acc.* 2005, *114*, 213-221.

[27] Due to serious disorder of **5**, the synthesis has also been performed with $Ag(CF_3SO_3)$ (see experimental part). Thereby, the reaction of **5** with $Ag(CF_3SO_3)$ probably leads to the isostructural complex $[(Cp^{Bn}Fe)_2(\mu,\eta^{5:5}\text{-}As_5)][CF_3SO_3]$ (**5'**), since similar chemical shifts in the ^1H NMR spectra (Figure S.5. 8, supplementary information) and similar cell parameters (Table S.5.1, supplementary information) are observed. Unfortunately, only poor quality crystals have been obtained so far, so only cell parameters could be determined.

[28] B. Cordero, V. Gomez, A. E. Platero-Prats, M. Reves, J. Echeverria, E. Cremades, F. Barragan, S. Alvarez, *Dalton Trans.* 2008, 2832-2838.

[29] W. M. Tsai, M. D. Rausch, *Organometallics* 1996, *15*, 2591-2594.

[30] a) H. Erdmann, M. V. Unruh, *Z. Anorg. Chem.* 1902, *32*, 437-452; b) O. J. Scherer, H. Sitzmann, G. Wolmershäuser, *J. Organomet. Chem.* 1986, *309*, 77-86.

[31] O. V. Dolomanov, L. J. Bourhis, R. J. Gildea, J. A. K. Howard, H. Puschmann, *J. Appl. Cryst.* 2009, *42*, 339-341.

[32] G. M. Sheldrick, *Acta Cryst.* 2015, *A71*, 3-8.

[33] L. Palatinus, G. Chapuis, *J. Appl. Cryst.* 2007, *40*, 786-790.

[34] M. C. Burla, R. Caliandro, M Camalli, B Carrozzini, G. L. Cascarano, L. De Caro, C. Giacovazzo, G. Polidori, D. Siliqi, R. Spagna, *J. Appl. Cryst.* 2007, *40*, 609-613.

[35] G. M. Sheldrick, *Acta Cryst.* 2015, *C71*, 3-8.

[36] a) CrysAlisPro, Version 1.171.38.41, Agilent Technologies UK Ltd, Oxford, UK (**1** and **2**); b) CrysAlisPro, Version 1.171.37.31, Agilent Technologies UK Ltd, Oxford, UK (**4**); c) CrysAlisPro, Version 1.171.38.42b, Agilent Technologies UK Ltd, Oxford, UK (**5**).

[37] R. C. Clark, J. S. Reid, *Acta Cryst.* 1995, *A51*, 887-897.

[38] K. Brandenburg, H. Putz, Diamond3.0, Crystal and Molecular Structure Visualization, Crystal Impact GbR, Bonn, Germany, 2014.

6. A Comprehensive Study of the Coordination Behaviour of [Cp^{Bn}Fe(η^5-As$_5$)] vs. [Cp*Ru(η^5-As$_5$)] Towards Cu^I Halides

M. Schmidt and M. Scheer

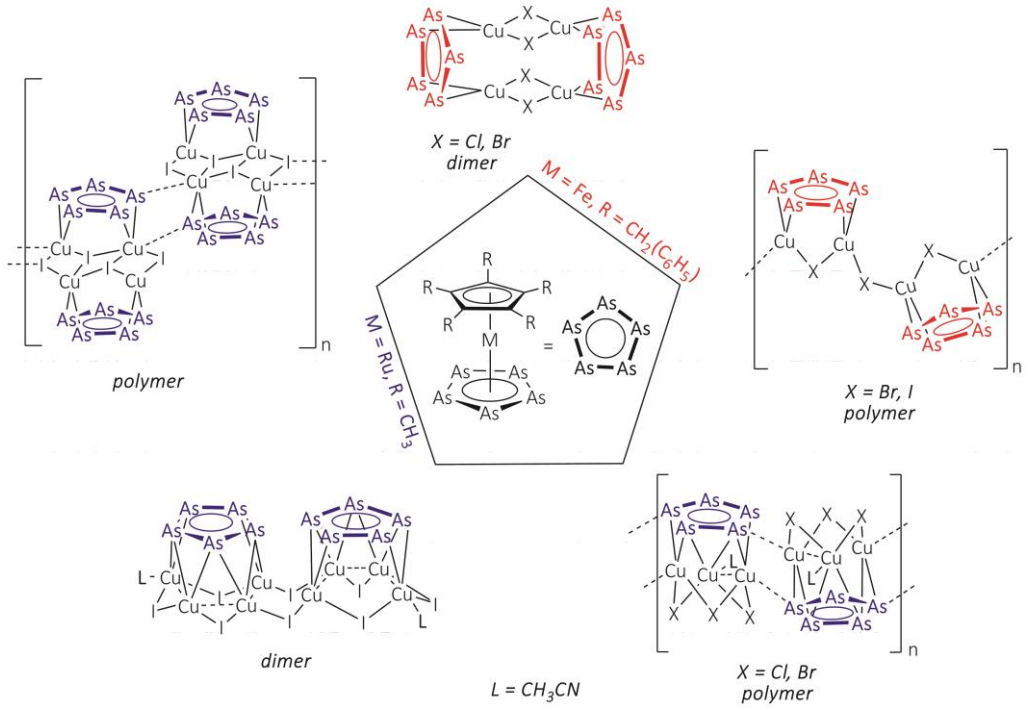

Abstract:

Because [Cp*Fe(η^5-As$_5$)] (Cp* = η^5-C$_5$Me$_5$) has only been used as building block in coordination chemistry for a short time, no related complexes have been studied concerning the influence of the Cp^R ligand or the influence of the central metal atom on the coordination behaviour. Herein, a comprehensive study on the consequences of these factors is presented. Accordingly, [Cp^{Bn}Fe(η^5-As$_5$)] (Cp^{Bn} = η^5-C$_5${CH$_2$(C$_6$H$_5$)}$_5$) and [Cp*Ru(η^5-As$_5$)] have been chosen for investigations on their reactivity towards Cu^I halides. Here, the reaction of [Cp^{Bn}Fe(η^5-As$_5$)] with CuX (X = Cl, Br, I) leads to the formation of the discrete dimer [{Cp^{Bn}Fe(η$^{5:2:2}$-As$_5$)}{Cu(μ-X)}$_2$]$_2$ (X = Cl (**1**), Br (**2**)) and polymer [{Cp^{Bn}Fe(η$^{5:2:2}$-As$_5$)}{Cu(μ-X)}$_2$]$_n$ (X = Br (**3**), I (**4**)). Using [Cp*Ru(η^5-As$_5$)] as a starting material, the reaction with CuCl and CuBr results in the formation of the one dimensional polymer [{Cp*Ru(η$^{5:2:2:2}$-As$_5$)}{Cu(μ-X)}$_3$(CH$_3$CN)]$_n$ (X = Cl (**5**), Br (**6**)). The reaction of [Cp*Fe(η^5-As$_5$)] and CuI leads to a mixture of coordination products, containing [{Cp*Ru(η$^{5:2:2}$-As$_5$)}{Cu(μ-I)}{Cu(μ$_3$-I)}]$_n$ (**7**) and [{Cp*Ru(η$^{5:2:2:2:2}$-As$_5$)}{Cu(μ-I)}$_4$(CH$_3$CN)]$_2$ (**8**). The dimeric and polymeric products have been characterised by single crystal X-ray structure analysis, elemental analysis and ESI mass spectrometry.

6.1 Author contributions

- All syntheses and characterisations were performed by Monika Schmidt.
- Manuscript was written by Monika Schmidt.
- Figures were made by Monika Schmidt.
- Single crystal X-ray structure analyses and refinements were performed by Monika Schmidt.

6.2 Introduction

Since their first synthesis in the 1970s, unsubstituted naked group 15 element ligand complexes have been of great interest. Thus, a large library of different E_n ligand complexes (E = P, As) has been developed.[1] Besides the investigations into unprecedented structural motifs, also the use of E_n ligand complexes in supramolecular chemistry is of great interest.[2] While in the past N-, O- and S- containing donor ligands have mainly been employed as building blocks in supramolecular chemistry, P_n ligand complexes recently got more and more into focus.[2,3] Here, [Cp^{R}Fe(η^5-P$_5$)] (Cp^R = Cp* (η^5-C$_5$Me$_5$), Cp^{Bn} (η^5-C$_5${CH$_2$(C$_6$H$_5$)}$_5$), Cp^{BIG} (η^5-C$_5${4-^{n}BuC$_6$H$_4$}$_5$)) are of special interest. Due to an available lone pair on each phosphorus atom, these P_n complexes show versatile reactivity patterns towards monovalent coinage metal salts. Depending on the substituents on the Cp^R ligand, the stoichiometry employed, the used metal salts and solvents, zero, one and/or two dimensional polymers are obtained.[2,4] Prominent examples are certainly the formation of fullerene like spherical aggregates[2,5,6] and nano-sized capsules[7] as well as a supramolecular complex with a lens shaped scaffold[8] or a rugby ball like compound.[9] Especially spherical aggregates are of great interest and can be found in host guest chemistry, e.g. stabilisation of labile complexes[5a] or incorporation of a reactive species like E_4 (E = P, As).[10] Thus, it appears that E_n ligand complexes (E = P, As) have a great potential for building blocks in supramolecular chemistry. Nevertheless, As_n ligand complexes have rarely been exploited for this purpose in the past. Since 2006, the Scheer group has investigated the reactivity of [Cp*Fe(η^5-As$_5$)] (**I**), [Cp*Mo(CO)$_2$(η^3-As$_3$)] and [{CpMo(CO)$_2$}$_2$(μ,η$^{2:2}$-As$_2$)] (**II**) towards monovalent metal salts.[2,4b,11,12] As a result, one dimensional polymers and discrete dimers are formed (Figure 6.1). Therein, the majority of the obtained products have a π-coordination through As-As bonds (η^2-fashion) in common, while the lighter congener phosphorus favours a σ-coordination *via* its lone pairs (η^1-fashion). Recently, we were able to observe an unexpected σ-1,3-coordination of **I** and **II** towards a preassembled linear Cu^I fragment to form a one dimensional polymer by using **I**, or a discrete dimer if **II** is used.[12a]

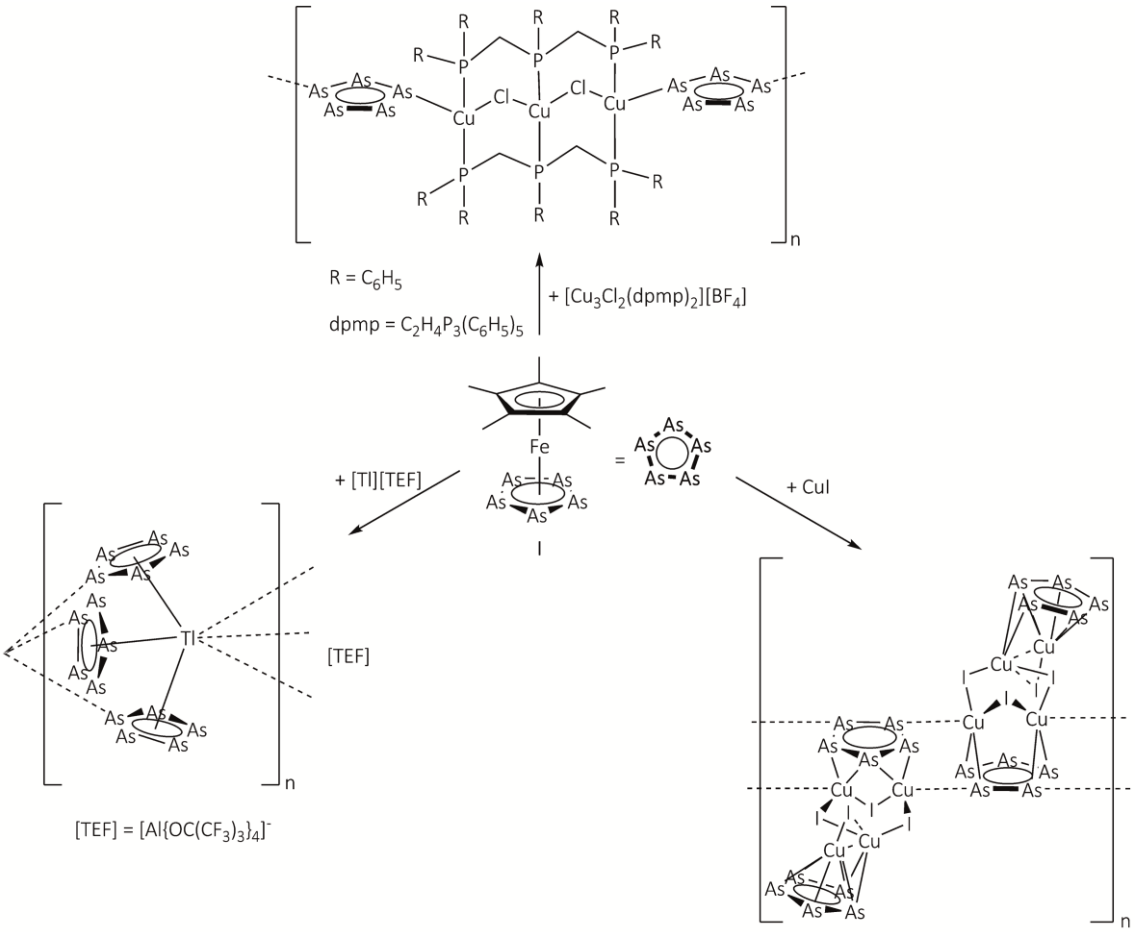

Figure 6.1 Selected reactions of **I** with a preassembled Cu^I fragment (top) and with monovalent metal salts (bottom).

Although As$_n$ ligand complexes have been incorporated in supramolecular chemistry more and more in the recent years, their potential is only poorly investigated so far. For example, the influence of the Cp^R ligand on the supramolecular chemistry of As$_n$ ligand complexes has not yet been studied. Since the reaction of [Cp^{Bn}Fe(η^5-P$_5$)] with copper(I) halides leads almost exclusively to spherical aggregates, the heavier congener [Cp^{Bn}Fe(η^5-As$_5$)] (**III**) seems to be a promising candidate to also form fullerene like supramolecular aggregates. The question arose what the effect of introducing **III** as building block in supramolecular chemistry will be with respect to the favoured coordination mode of As$_n$ ligand complexes (π-coordination) versus the formation of spherical aggregates. Moreover, the absence of studies of the coordination behaviour on As$_n$ ligand complexes of different transition metals gave rise to the question whether the reaction of [Cp*Ru(η^5-As$_5$)] (**IV**) with copper(I) halides would lead to the formation of different coordination products compared to the iron derivative **I**.

Herein, we report on the synthesis and characterisation of the first one dimensional polymers and dimers based on **III** or **IV** with Cu^I halides. The resulting products $[\{Cp^{Bn}Fe(\eta^{5:2:2}\text{-}As_5)\}\{Cu(\mu\text{-}X)\}_2]_2$ (X = Cl (**1**), Br (**2**)), $[\{Cp^{Bn}Fe(\eta^{5:2:2}\text{-}As_5)\}\{Cu(\mu\text{-}X)\}_2]_n$ (X = Br (**3**), I (**4**)), $[\{Cp^*Ru(\eta^{5:2:2:2}\text{-}As_5)\}\{Cu(\mu\text{-}X)\}_3(CH_3CN)]_n$ (X = Cl (**5**), Br (**6**)), $[\{Cp^*Ru(\eta^{5:2:2}\text{-}As_5)\}\{Cu(\mu\text{-}I)\}\{Cu(\mu_3\text{-}I)\}]_n$ (**7**) and $[\{Cp^*Ru(\eta^{5:2:2:2:2}\text{-}As_5)\}\{Cu(\mu\text{-}I)\}_4(CH_3CN)]_2$ (**8**) were characterised by single crystal X-ray diffraction analysis as well as by ESI mass spectrometry and elemental analysis.

6.3 Results and Discussion

Coordination Behaviour of III and IV Towards CuX (X = Cl, Br, I) – General Considerations

In general, all coordination compounds are obtained by diffusion reactions. Thereby, a solution of **III** in toluene, or a solution of **IV** in CH_2Cl_2, is layered with a solution of CuX (X = Cl, Br, I) in CH_3CN. After several days, crystals are growing at the phase boundary and the solutions turns to brownish orange or yellowish. After complete diffusion, the reaction of the Cp^{Bn} derivative **III** with CuCl or CuBr leads to the formation of [{Cp^{Bn}Fe(η$^{5:2:2}$-As$_5$)}{Cu(μ-X)}$_2$]$_2$ (X = Cl (**1**), Br (**2**)) (Scheme 6.1). Furthermore, in the case of CuBr and CuI the one dimensional polymer [{Cp^{Bn}Fe(η$^{5:2:2}$-As$_5$)}{Cu(μ-X)}$_2$]$_n$ (X = Br (**3**), I (**4**)) is obtained.

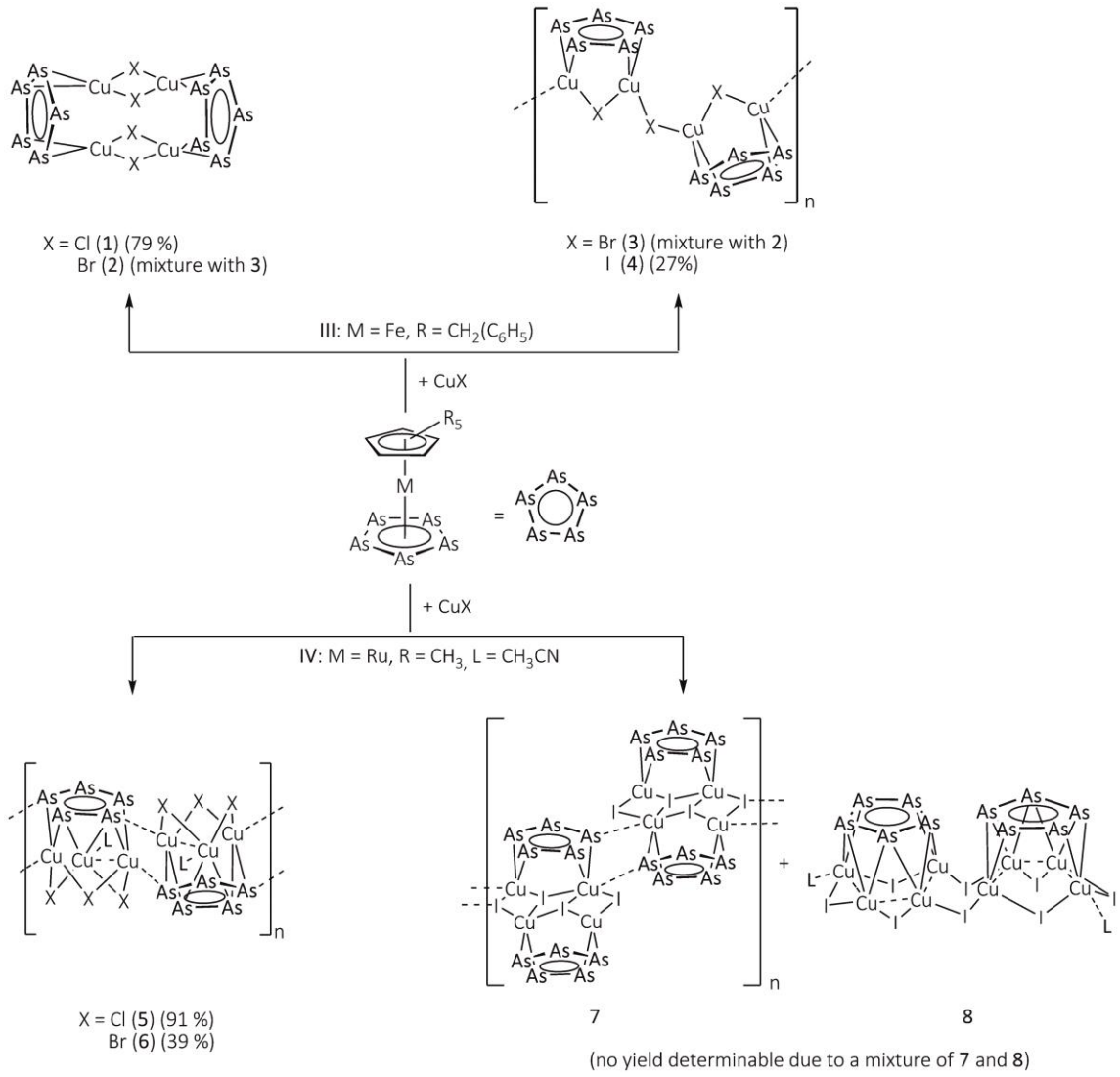

Scheme 6.1 Reactions of **III** and **IV** with CuX (X = Cl, Br, I).

Accordingly, the introduction of the Cp^{Bn} ligand results in an increase of the complexity of the coordination compounds (dimeric molecules to one dimensional polymers) going from CuCl to CuI. The formation of fullerene like aggregates as observed during the reaction of the phosphorus derivative [$Cp^{Bn}Fe(\eta^5\text{-}P_5)$] and copper(I) halides has never been observed, since **III** retains the favoured π-coordination mode of the As-As bonds.

In contrast, the reaction of the Cp* iron derivative **IV** with Cu^I halides exclusively leads to the one dimensional polymers [{$Cp^*Ru(\eta^{5:2:2:2}\text{-}As_5)$}{$Cu(\mu\text{-}X)$}$_3(CH_3CN)$]$_n$ (X = Cl (**5**), Br (**6**)) and [{$Cp^*Ru(\eta^{5:2:2}\text{-}As_5)$}{$Cu(\mu\text{-}I)$}{$Cu(\mu_3\text{-}I)$}]$_n$ (**7**), showing different CuX moieties linking monomers of **IV** (Scheme 6.1).[12b] Moreover, for CuI the formation of the dimer [{$Cp^*Ru(\eta^{5:2:2:2:2}\text{-}As_5)$}{$Cu(\mu\text{-}I)$}$_4(CH_3CN)$]$_2$ (**8**) is obtained, including a novel Cu-I connectivity pattern. Additionally, **5**-**7** are isostructural to the products of the reactions of the pentaarsaferrocene derivative **I** and CuX. However, the distribution of products seems to be independent on the nature of the pentaarsaferrocene derivative. The central metals in the Cp* pentaarsaferrocene derivatives **I** (Fe) versus **IV** (Ru) play a minor role with respect to the influence on the coordination behaviour and the found structural motifs compared to the Cp^R ligand. In contrast, the major contributions come from the preferred π-coordination of the *cyclo*-As_5 ligand as well as the halides used. For CuX, the variety of structural motifs range from well-known four-membered {CuX}$_n$ rings or a ladder like {CuX} structure as observed in **1**, **2** or **7** to scarcely reported structural core motifs like the zigzag arrangement in **3** and **4**, or the crown like substructure in **8**.

Solid State Characterisation of 1-8

In general, **1**-**8** are obtained during diffusion reactions of **III** and **IV** and CuX (X = Cl, Br, I). Here, the crystallisation can be completed by layering all mother solutions with Et_2O, leading to moderate to good crystalline yields of **1**-**8**. Furthermore, the specific outcome of the reaction can be directed by using the correct stoichiometry or a specific concentration. However, compounds **2**/**3** and **7**/**8**, respectively, crystallise simultaneously and could not be isolated separately, due to identical solubility properties as well as colour and/or crystal shape. Moreover, **1**-**8** are insoluble in all common solvents. As a result, the corresponding ESI MS spectra were recorded from the mother solution.

Cu^I Halide and III Containing Coordination Compounds 1-4

Compound **1** (X = Cl) and **2** (X = Br) are isostructural and crystallise as dark red plates in the monoclinic space group $P2_1/c$. Single crystal X-ray structure analysis reveals a dimeric structure for both compounds. Thereby, two moieties of **III** are linked *via* {Cu(μ-X)}$_2$ four-membered rings. Each Cu^I atom is side-on coordinated by the *cyclo*-As$_5$ ligand (η^2-coordination). In Figure 6.2, the molecular structure of **1** in the solid state is exemplarily depicted (for the molecular structure of **2** in the solid state see Figure S6.1, supplementary information). As a consequence of the disorder of the copper centres, two favoured orientations of the {Cu$_4$X$_4$} fragments can be realised in solid state, which can be converted into each other by a rotation of 90° (see supplementary information, Figure S6.2).

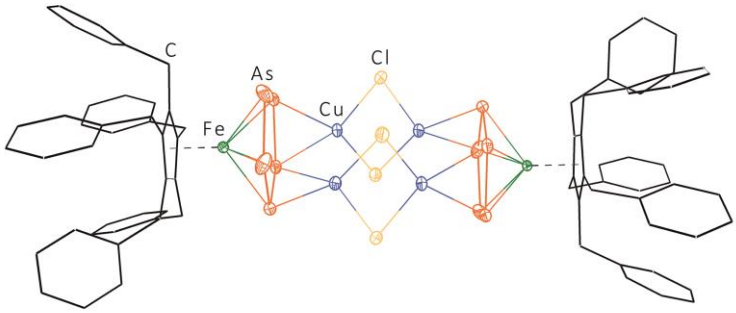

Figure 6.2 Molecular structure of **1** in the solid state. H atoms are omitted for clarity and Cp^{Bn} ligands are drawn in wire or frame model. Due to disorder only the main part is depicted. Thermal ellipsoids are drawn at 50 % probability level. **1** and **2** are isostructural dimers.

While for CuCl **1** is the only observed product, for CuBr a mixture of **2** and **3** is obtained. Polymer **3** crystallises together with **2** as red blocks in the monoclinic space group $P2_1/n$ independent of stoichiometry. In the solid state, **3** displays a one dimensional polymer built up by one molecule of **III**, which is coordinating two copper atoms in a η^2-fashion (Figure 6.3). The Cu^I centres are bridged by bromide (μ$_2$-mode). As a result of the steric demand of the Cp^{Bn} ligands, the moieties are twisted and a zigzag like arrangement is realised in the solid state. Moreover, an isostructural one dimensional polymer is received if **III** is reacted with CuI. Compound **4** crystallises in the space group $P2_1/n$ as red plates and possesses an analogue structural core motif as found for **3** (see supplementary information, Figure S6.3).

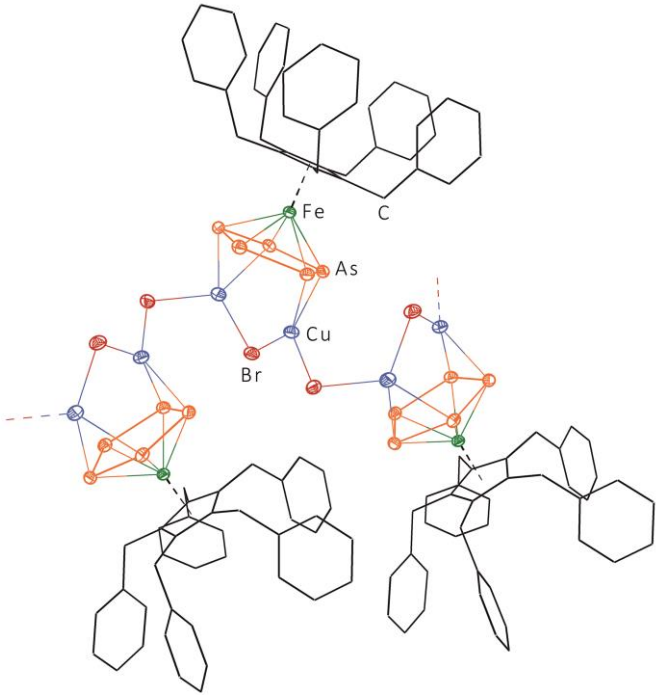

Figure 6.3 Section of the polymeric structure of **3** in the solid state. H atoms are omitted for clarity and Cp^{Bn} ligands are drawn in wire or frame model. Due to disorder only the main part is depicted. Thermal ellipsoids are drawn at 50 % probability level. **3** and **4** are isostructural polymers.

Due to the π-coordination of the *cyclo*-As$_5$ units of **III** in **1**-**4**, all As-As bond lengths within the *cyclo*-As$_5$ ligand are elongated in comparison to **III** (av. 2.32 Å) (Table 6.1).[13] However, the As-As distances are still in the range between a single As-As bond (electron diffraction: 2.435 Å in As$_4$,[14] DFT calculations: 2.4372 Å in As$_4$[15]) and a double As-As bond (2.245(1) Å in [{(Me$_3$Si)$_3$CAs}$_2$][16]). In contrast, the Cu-X and Cu-As distances in **1**-**4** are comparable to reported distances (Table 6.1).[3b,6a,11,12b,17]

Table 6.1 Selected bond lengths [Å] of **1**-**4**. Whenever more than one bond is presented in the asymmetric unit, the ranges of bond lengths are given. In case of disorder, the described bond lengths correspond to the main part.

	X	As-As	Cu-As	Cu-X
1	Cl	2.3316(7) - 2.3777(6)	2.3720(12) - 2.5496(13)	2.2193(15) - 2.3258(15)
2	Br	2.3378(6) - 2.3963(5)	2.3686(5) - 2.4881(6)	2.3773(6) / 2.4320(6)
3	Br	2.3502(14) - 2.3850(15)	2.4099(10) - 2.5251(12)	2.3859(8) - 2.4052(8)
4	I	2.3421(7) - 2.3969(6)	2.4151(7) - 2.5528(7)	2.5397(6) - 2.5619(6)

Similar structural core motifs as realised in **1** and **2** are already known for [{Cp*Mo(CO)$_2$(η$^{3:2}$-As$_3$)}{Cu(μ-X)}]$_2$ (X = Cl, Br, I)[11] as well as for coordination compounds based on P$_n$ ligand complexes[2,6a,18] or copper(I) halide aggregates.[19] Nevertheless, especially the zigzag

like arrangement is uncommon for polymeric $(CuX)_n$ (X = Br, I) networks, since four-membered $\{Cu_4X_4\}$ rings as well as cube like and ladder like structures seem to be especially preferred.[19,20]

Cu^I Halide and IV Containing Coordination Compounds 5-8

For CuCl and CuBr the isostructural one dimensional polymers **5** (X = Cl) and **6** (X = Br) are obtained. They crystallise in the monoclinic space group $P2_1/c$ as red trapezoids and red plates, respectively. Thus, polymer **5** as well as **6** are isomorphs to the iron containing polymers $[\{Cp^*Fe(\eta^{5:2:2:2}\text{-}As_5)\}\{Cu(\mu\text{-}X)\}_3(CH_3CN)]_n$ (X = Cl (**A**), Br (**B**)).[12b] The molecular structure of **6** in the solid state is exemplarily depicted in Figure 6.4 (for the molecular structure of **5** in the solid state see Figure S6.4, supplementary information).

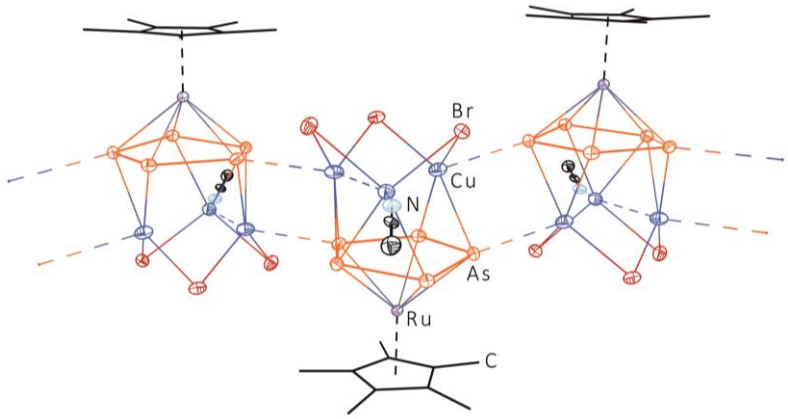

Figure 6.4 Section of the polymeric structure of **6** in the solid state. H atoms are omitted for clarity and Cp* ligands are drawn in wire or frame model. Thermal ellipsoids are drawn the 50 % probability level. **5** and **6** are isostructural one dimensional polymers.

The central structural core motif of **5** and **6** is a six-membered chair like $\{CuX\}_3$ ring, in which three Cu^I atoms are π-coordinated by the As-As bonds of the *cyclo*-As$_5$ ring. These moieties are linked *via* intermolecular Cu···As interactions to form a one dimensional polymeric strand. Theses interactions are in good agreement with the sum of the van der Waals radii of arsenic and copper (3.25 Å).[21] Besides this, Cu···Cu distances are observed (**5**: 2.6600(15) Å, **6**: 2.6594(8) Å) being also in line with the sum of the van der Waals radii (2.8 Å).[21] Accordingly, weak Cu···Cu interactions are assumed, since similar distances are known in the literature considering Cu···Cu interactions (Table 6.2).[3b,6a,22,23,24] As the structure of the ruthenium derivative **IV** in the solid state has not yet been determined, the As-As bond lengths within the *cyclo*-As$_5$ moiety cannot be compared. In contrast, the Cu-X and Cu-As distances in **5** and **6** are comparable to the iron containing isostructural compounds **A** and **B** or to other polymeric $(CuX)_n$ containing networks (Table 6.2).[3b,6a,11,12b,17]

Table 6.2 Selected bond lengths [Å] of **5** and **6**. Whenever more than one bond is presented in the asymmetric unit, the ranges of bond lengths are given.

	5 (X = Cl)	**6** (X = Br)
As-As	2.3732(12) - 2.4274(12)	2.3738(7) - 2.4258(7)
Cu-As	2.4575(14) - 2.5815(14)	2.4592(8) - 2.5847(8)
Cu-X	2.273(2) - 2.417(2)	2.3933(8) - 2.5344(7)
Cu···As	2.9170(1)	2.9271(1)
Cu···Cu	2.6600(15)	2.6594(8)

Using CuI, two different coordination compounds (**7**, **8**) were isolated. **7** and **8** crystallise simultaneously as dark red blocks or cubes in the triclinic space group $P\bar{1}$ (**7**) and the acentric orthorhombic space group $P2_12_12$ (**8**) (Flack parameter 0.135(5)), respectively. Single crystal X-ray structure determination reveals a polymeric structure for **7** (Figure 6.5). Herein, each copper atom is η^2-coordinated by an As-As bond and the unique Cu^I centres are bridged by iodine atoms (μ_2-mode and μ_3-mode). As a result, the central structural core motif of the single repeating unit resembles a {CuI}$_4$ ladder connected either *via* Cu···As (2.5329(8) Å) or Cu···I (2.8311(8) Å) interactions. Consequently, a one dimensional polymer is formed. A similar ladder like structural core motif is also known in the case of the iron derivative **I** and CuI. Thus, the linking in **7** to a polymer is only obtained *via* intermolecular Cu···I interactions, while in the isostructural Cp* iron derivative the units are connected *via* Cu···I and Cu···As interactions.[12b]

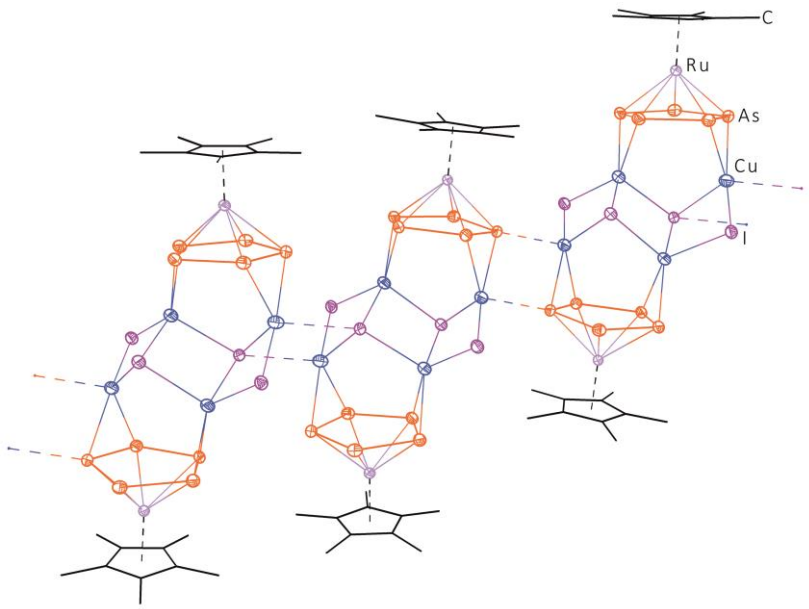

Figure 6.5 Section of the polymeric structure of **7** in the solid state. H atoms are omitted for clarity and Cp* ligands are drawn in wire or frame model. Thermal ellipsoids are drawn at 50 % probability level.

However, the {Cu_4I_4} crown like structural core motif in dimer **8** is scarcely found in literature, while the ladder like motif is widely common for polymers containing E_n ligand complexes and copper(I) halides.[20] For **8**, single crystal X-ray structure analysis reveals a modified crown like structural core motif (Figure 6.6a). Here, four Cu^I moieties are η^2-coordinated by the *cyclo*-As_5 ligand of **IV**, which in return are linked *via* Cu···Cu interactions (2.567(2) Å - 2.611(2) Å) to give a chain based arrangement. Additionally, iodine atoms bridge the copper atoms (μ_2-mode) as well as the unique crowns to achieve the dimeric structure. Nevertheless, especially in a top view, **8** resembles the hexagon structural core motif (Figure 6.6b)

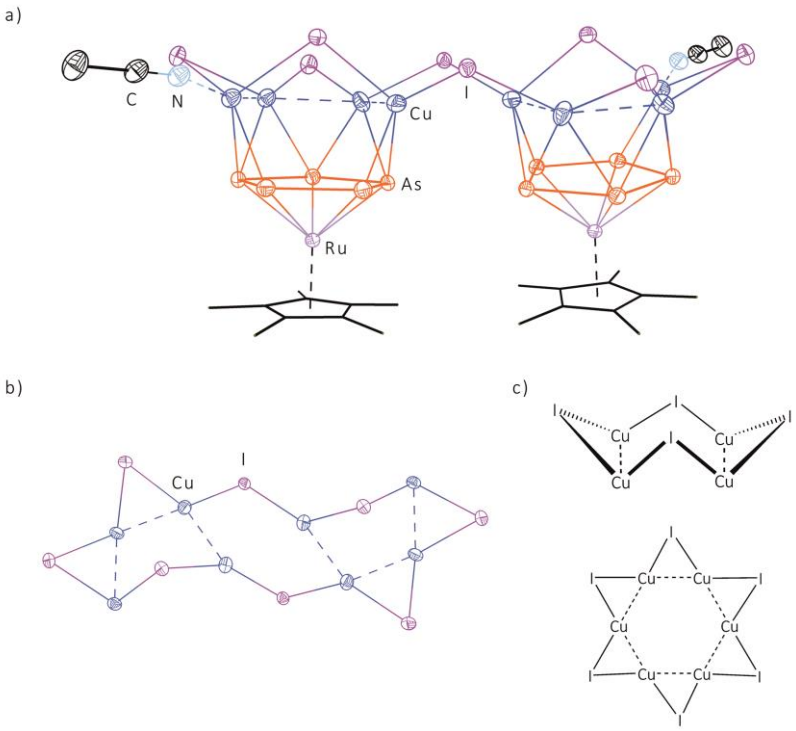

Figure 6.6 a) Dimeric structure of **8** in the solid state. H atoms are omitted for clarity and Cp* ligands are drawn in wire or frame model. In case of disorder only the main part is depicted. Thermal ellipsoids are drawn at 50 % probability level. b) Top view of the core structure of **8**. [Cp*Ru(η^5-As_5)] fragments as well as coordinated CH_3CN molecules are omitted for clarity. c) Schematic illustration of the crown structural motif (above) and the hexagon structural motif (below).

As it can be seen in Table 6.3, all Cu-E (E = As, I) bond lengths of **7** and **8** show a similar trend as discussed before. Nevertheless, **8** displays some conspicuity in regard of the As-As distances. While in **7** all As-As bond lengths are still in the range between a double and a single bond, in **8** an obvious elongation is observed. As a result of the fourfold coordination mode of the Cu^I atoms by **IV**, the distances within the *cyclo*-As_5 ligands are partially longer than a common As-As single bond. In contrast, the Cu···Cu distances are shortened, assuming homometallic d^{10}-d^{10} interactions between the copper centres.[24]

Table 6.3 Selected bond lengths [Å] of **7** and **8**. Whenever more than one bond is presented in the asymmetric unit, the ranges of bond lengths are given.

	7	**8**
As-As	2.3421(7) - 2.4103(9)	2.3728(15) - 2.4886(16)
Cu-As	2.48992(9) - 2.5596(8)	2.4958(18) - 2.5888(19)
Cu-I	2.6116(7) - 2.7880(8)	2.5967(17) - 2.7111(17)
Cu···Cu	-	2.567(2) - 2.611(2)
Cu···I	2.8311(8)	-
Cu···As	2.5329(8)	-

In summary, a comprehensive study of the coordination behaviour of **III** bearing the Cp^{Bn} ligand and the Cp* ruthenium derivative **IV** towards copper(I) halides is presented. The reaction of **III** and **IV** with CuX (X = Cl, Br, I) leads to the formation of dimeric compounds (**1**, **2** and **8**) as well as one dimensional polymers (**3**, **4**, **5**, **6** and **7**). While in the case of **III** and CuX in general an increase of complexity of the coordination compounds (dimeric to polymeric) by going from CuCl to CuBr to CuI is observed, for **IV** and CuX one dimensional polymers are mainly obtained. Besides common structural {CuX}$_n$ motifs like in **1**, **2** and **7**, respectively, also scarcely realised structural core motifs like a crown like (**8**) and zigzag like arrangement (**3** and **4**) are observed. Moreover, **5** and **6** are isomorphs to the Cp* iron derivatives **A** and **B**. Additionally, all compounds have one feature in common: the Cu^I atoms are always η^2-coordinated by an As-As bond of the *cyclo*-As$_5$ ligand of **III** or **IV**. This demonstrates the preference of the As$_n$ ligand complexes for π-coordination, while σ-coordination plays a minor role (weak Cu···As interactions in one dimensional polymers). Whereas starting from the *cyclo*-As$_5$ ligand complexes **III** and **IV** the coordination mode in the obtained products is independent on the metal atom or Cp^R ligand, a strong dependency is observed on the copper(I) halide used. Nevertheless, these results demonstrate the versatility of As$_n$ ligand complexes in coordination chemistry.

6.4 Experimental Part

General Remarks

All reactions were performed under an atmosphere of dry argon or nitrogen using glovebox or Schlenk techniques. Solvents were purified, degassed and dried prior to use. [Cp*Ru(η^5-As$_5$)] was prepared according to literature procedure.[25] The Cu^I halides are commercially available and were used without further purification.

The ESI MS spectra of the mother solutions were measured on a ThermoQuest Finnigan MAT TSQ 7000 mass spectrometer. The elemental analyses were determined with a Vario ELIII apparatus.

Synthesis of [{Cp^{Bn}Fe(η$^{5:2:2}$-As$_5$)}{Cu(μ-Cl)}$_2$]$_2$ (1)

In a thin Schlenk tube, a green solution of [Cp^{Bn}Fe(η^5-As$_5$)] (10 mg, 0.01 mmol) in toluene was layered with a solution of CuCl (20 mg, 0.20 mmol) in CH_3CN. After several days, dark red crystals of **1** are showing up at the phase boundary and the mother solution turns yellowish orange. Sometimes, the formation of a metallic mirror and/or brown powder is observed. After complete diffusion, the mother liquor is decanted, the crystals are washed with a small amount of CH_3CN, CH_2Cl_2 and *n*-pentane and are dried *in vacuo*. By concentrating the decanted solution, layering with Et_2O and storing at -28°C, a second crop of crystals of **1** can be obtained, while the mother liquor has turned almost colourless.

Analytical data of **1**

Crystalline yield: 10 mg (4.73 μmol, 79 % referred to [Cp^{Bn}Fe(η^5-As$_5$)]).

Positive ion ESI MS (mother liquor, toluene/CH_3CN): *m/z* (%) = 2152.3 (12) ([{Cp^{Bn}FeAs$_5$}$_2$Cu$_3$Cl$_2$]$^+$), 2053.9 (38) ([{Cp^{Bn}FeAs$_5$}$_2$Cu$_2$Cl]$^+$), 1955.6 (100) ([{Cp^{Bn}FeAs$_5$}$_2$Cu]$^+$), 1517.1 (14) ([Cp$^{Bn}{}_2$Fe$_2$As$_5$]$^+$), 1049.7 (86) ([{Cp^{Bn}FeAs$_5$}Cu(CH$_3$CN)]$^+$), 1008.7 (16) ([{Cp^{Bn}FeAs$_5$}Cu]$^+$).

Negative ion ESI MS (mother liquor, toluene/CH_3CN): *m/z* (%) = 892.0 (100) ([Cu$_7$Cl$_8$(H$_2$0)$_9$]$^-$), 521.6 (15) ([Cu$_4$Cl$_5$(H$_2$0)$_5$]$^-$).

Elemental Analysis: Calculated (%) for [C$_{80}$H$_{70}$Fe$_2$As$_{10}$Cu$_4$Cl$_4$] (2288.31 g/mol): C 41.99, H 3.08; found C 42.28, H 3.22.

Synthesis of [{Cp^{Bn}Fe(η$^{5:2:2}$-As$_5$)}{Cu(μ-Br)}$_2$]$_2$ (2) and [{Cp^{Bn}Fe(η$^{5:2:2}$-As$_5$)}{Cu(μ-Br)}$_2$]$_n$ (3)

In a thin Schlenk tube, a green solution of [Cp^{Bn}Fe(η^5-As$_5$)] (47 mg, 0.05 mmol) in toluene was layered with a solution of CuBr (36 mg, 0.25 mmol) in CH_3CN. After several days, dark red crystals of **2** and **3** are forming at the phase boundary and the mother solution turns yellowish orange to brownish. Sometimes, the formation of a metallic mirror and/or brown powder is observed. After complete diffusion, the mother liquor is decanted, the crystals are washed with a small amount of CH_3CN, CH_2Cl_2 and *n*-pentane and are dried *in vacuo*. By concentrating the decanted solution, layering with Et_2O and storing at -28°C, a second crop of crystals of **2** and **3** can be obtained, while the mother liquor has turned almost colourless.

Analytical data of **2** and **3**

Crystalline yield: 34 mg (mixture of **2** and **3**).

Positive ion ESI MS (mother liquor, toluene/CH_3CN): *m/z* (%) = 1517.4 (16) ($[Cp^{Bn}{}_2Fe_2As_5]^+$), 1337.8 (24) ($[\{Cp^{Bn}FeAs_5\}Cu_2Br_3(CH_3CN)]^+$), 1296.7 (26) ($[\{Cp^{Bn}FeAs_5\}Cu_2Br_3]^+$), 1193.6 (34) ($[\{Cp^{Bn}FeAs_5\}Cu_2Br(CH_3CN)]^+$), 1049.9 (100) ($[\{Cp^{Bn}FeAs_5\}Cu(CH_3CN)]^+$).

Negative ion ESI MS (mother liquor, toluene/CH_3CN): *m/z* (%) = 798.2 (9) ($[Cu_5Br_6]^-$), 654.3 (15) ($[Cu_4Br_5]^-$), 510.4 (35) ($[Cu_3Br_4]^-$), 366.4 (100) ($[Cu_2Br_3]^-$), 222.6 (28) ($[CuBr_2]^-$).

Elemental Analysis: Calculated (%) for $[C_{80}H_{70}Fe_2As_{10}Cu_4Br_4]$ (2466.12 g/mol) and $[C_{40}H_{35}FeAs_5Cu_2Br_2]_n$ (1233. 06 g/mol): C 38.96, H 2.86; found C 39.16, H 2.93.

Synthesis of $[\{Cp^{Bn}Fe(\eta^{5:2:2}\text{-}As_5)\}\{Cu(\mu\text{-}I)\}_2]_n$ (4)

In a thin Schlenk tube, a green solution of $[Cp^{Bn}Fe(\eta^5\text{-}As_5)]$ (10 mg, 0.01 mmol) in toluene was layered with a solution of CuI (19 mg, 0.10 mmol) in CH_3CN. After several days, dark red crystals of **4** are showing up at the phase boundary and the mother solution turns yellowish to brownish. Sometimes, the formation of a metallic mirror and/or brown powder is observed. After complete diffusion, the mother liquor is decanted, the crystals are washed with a small amount of CH_3CN, CH_2Cl_2 and *n*-pentane and are dried *in vacuo*. By concentrating the decanted solution, layering with Et_2O and storing at -28°C, a second crop of crystals of **4** can be obtained, while the mother liquor has turned almost colourless.

Analytical data of **4**

Crystalline yield: 4 mg (3.01 µmol, 27 % referred to $[Cp^{Bn}Fe(\eta^5\text{-}As_5)]$).

Positive ion ESI MS (mother liquor, toluene/CH_3CN): *m/z* (%) = 2147.3 (10) ($[\{Cp^{Bn}FeAs_5\}_2Cu_2I]^+$), 1955.4 (14) ($[\{Cp^{Bn}FeAs_5\}_2Cu]^+$), 1670.0 (10) ($[Cu_9I_8(CH_3CN)_2]^+$), 1626.9 (12) ($[Cu_9I_8(CH_3CN)]^+$), 1587.7 (18) ($[Cu_9I_8]^+$), 1517.4 (74) ($[Cp^{Bn}{}_2Fe_2As_5]^+$), 1290.0 (14) ($[Cu_7I_6(CH_3CN)_2]^+$), 1087.9 (58) ($[\{Cp^{Bn}\}_2Fe]^+$), 1049.8 (100) ($[\{Cp^{Bn}FeAs_5\}Cu(CH_3CN)]^+$).

Negative ion ESI MS (mother liquor, toluene/CH_3CN): *m/z* (%) = 1650.0 (2) ($[Cu_8I_9]^-$), 1460.1 (2) ($[Cu_7I_8]^-$), 12701.2 (8) ($[Cu_6I_7]^-$), 1078.3 (16) ($[Cu_5I_4]^-$), 888.3 (20) ($[Cu_4I_5]^-$), 698.3 (60) ($[Cu_3I_4]^-$), 507.5 (84) ($[Cu_2I_3]^-$), 316.6 (100) ($[CuI_2]^-$), 126.8 (2) ($[I]^-$).

Elemental Analysis: Calculated (%) for $[C_{40}H_{35}FeAs_5Cu_2I_2 \cdot 0.5\ C_5H_{12}]$ (1363.13 g/mol): C 37.44, H 3.03; found C 37.76, H 2.97.

Synthesis of [{Cp*Ru(η$^{5:2:2:2}$-As$_5$)}{Cu(μ-Cl)}$_3$(CH$_3$CN)]$_n$ (5)

In a thin Schlenk tube, an orange solution of [Cp*Ru(η^5-As$_5$)] (20 mg, 0.03 mmol) in CH_2Cl_2 was layered with a solution of CuCl (10mg, 0.10 mmol) in CH_3CN. After several days, dark red crystals of **5** are showing up at the phase boundary and the mother solution turns light yellowish. After complete diffusion, the mother liquor is decanted, the crystals are washed with a small amount of CH_3CN and *n*-pentane and are dried *in vacuo*.

Analytical data of **5**

Crystalline yield: 28 mg (0.03 mmol, 91 % referred to [Cp*Ru(η^5-As$_5$)]).

Positive ion ESI MS (mother liquor, CH_2Cl_2/CH_3CN): *m/z* (%) = 715.7 (3) ([{Cp*RuAs$_5$}Cu(CH$_3$CN)]$^+$), 674.6 (3) ([{Cp*RuAs$_5$}Cu]$^+$), 371.1 (100) ([Cp*$_2$Ru]$^+$).

Negative ion ESI MS (mother liquor, CH_2Cl_2/CH_3CN): *m/z* (%) = 628.5 (2) ([Cu$_6$Cl$_7$]$^-$), 530.5 (4) ([Cu$_5$Cl$_6$]$^-$), 332.7 (7) ([Cu$_3$Cl$_4$]$^-$), 232.9 (36) ([Cu$_2$Cl$_3$]$^-$), 135.0 (17) ([CuCl$_2$]$^-$).

Elemental Analysis: Calculated (%) for [$C_{10}H_{15}RuAs_5Cu_3Cl_3 \cdot CH_3CN$] (948.95 g/mol): C 15.19, H 1.91, N 1.48; found C 15.14, H 1.94, N 1.37.

Synthesis of [{Cp*Ru(η$^{5:2:2:2}$-As$_5$)}{Cu(μ-Br)}$_3$(CH$_3$CN)]$_n$ (6)

In a thin Schlenk tube, an orange solution of [Cp*Ru(η^5-As$_5$)] (20 mg, 0.03 mmol) in CH_2Cl_2 was layered with a solution of CuBr (10 mg, 0.10 mmol) in CH_3CN. After several days, dark red crystals of **6** are showing up at the phase boundary and the mother solution turns yellowish. After complete diffusion, the mother liquor is decanted, the crystals are washed with a small amount of CH_3CN and *n*-pentane and are dried *in vacuo*. By concentrating the decanted solution, layering with Et_2O and storing at -28°C, a second crop of crystals of **6** can be obtained, while the mother liquor has turned almost colourless.

Analytical data of **6**

Crystalline yield: 14 mg (0.013 mmol, 39 % referred to [Cp*Ru(η^5-As$_5$)]).

Positive ion ESI MS (mother liquor, CH_2Cl_2/CH_3CN): *m/z* (%) = 1574.2 (7) ([{Cp*RuAs$_5$}$_2$Cu$_3$Br$_2$]$^+$), 1430.2 (17) ([{Cp*RuAs$_5$}$_2$Cu$_2$Br]$^+$), 1285.4 (13) ([{Cp*RuAs$_5$}$_2$Cu]$^+$), 1003.4 (10) ([{Cp*RuAs$_5$}Cu$_3$Br$_2$(CH$_3$CN)]$^+$), 962.4 (6) ([{Cp*RuAs$_5$}Cu$_3$Br$_2$]$^+$), 848.8 (46) ([Cp*$_2$Ru$_2$As$_5$]$^+$), 715.6 (100) ([{Cp*RuAs$_5$}Cu(CH$_3$CN)]$^+$), 674.6 (16) ([{Cp*RuAs$_5$}Cu]$^+$).

Negative ion ESI MS (mother liquor, CH_2Cl_2/CH_3CN): *m/z* (%) = 796.1 (7) ([Cu$_6$Br$_7$]$^-$), 654.4 (8) ([Cu$_4$Br$_5$]$^-$), 510.5 (18) ([Cu$_3$Br$_4$]$^-$), 366.5 (41) ([Cu$_2$Br$_3$]$^-$), 222.7 (100) ([CuBr$_2$]$^-$).

Elemental Analysis Calculated (%) for [$C_{10}H_{15}RuAs_5Cu_3Br_3 \cdot CH_3CN$] (1082.31 g/mol): C 13.32, H 1.68, N 1.29; found C 13.42, H 1.75, N 1.16.

Synthesis of [{Cp*Ru($\eta^{5:2:2}$-As$_5$)}{Cu(μ-I)}{Cu(μ_3-I)}]$_n$ (7) and [{Cp*Ru($\eta^{5:2:2:2:2}$-As$_5$)}{Cu(μ-I)}$_4$(CH$_3$CN)]$_2$ (8)

In a thin Schlenk tube, an orange solution of [Cp*Ru(η^5-As$_5$)] (20 mg, 0.03 mmol) in CH_2Cl_2 was layered with a solution of CuI (19 mg, 0.10 mmol) in CH_3CN. After complete diffusion, the reaction mixture is concentrated, layered with Et_2O and stored at -28 °C. After several days dark red crystals of **7** and **8** are obtained and the mother solution turns colourless. The mother liquor is decanted and the crystals are washed with a small amount of CH_3CN and *n*-pentane and are dried *in vacuo*.

Analytical data of **7** and **8**

Crystalline yield: 32 mg (mixture of **7** and **8**).

Positive ion ESI MS (mother liquor, CH_2Cl_2/CH_3CN): *m/z* (%) = 1668.2 (3) ([{Cp*RuAs$_5$}$_2$Cu$_3$I$_2$]$^+$), 1476.3 (11) ([{Cp*RuAs$_5$}$_2$Cu$_2$I]$^+$), 1286.6 (13) ([{Cp*RuAs$_5$}$_2$Cu]$^+$), 1097.5 (4) ([{Cp*RuAs$_5$}Cu$_3$I$_2$(CH$_3$CN)]$^+$), 1058.4 (3) ([{Cp*RuAs$_5$}Cu$_3$I$_2$]$^+$), 907.6 (14) ([{Cp*RuAs$_5$}Cu$_2$I(CH$_3$CN)]$^+$), 848.9 (98) ([Cp*$_2$Ru$_2$As$_5$]$^+$), 715.7 (100) ([{Cp*RuAs$_5$}Cu(CH$_3$CN)]$^+$), 674.6 (22) ([{Cp*RuAs$_5$}Cu]$^+$).

Negative ion ESI MS (mother liquor, CH_2Cl_2/CH_3CN): *m/z* (%) = 1078.3 (4) ([Cu$_5$I$_6$]$^-$), 888.4 (8) ([Cu$_4$I$_5$]$^-$), 698.5 (29) ([Cu$_3$I$_4$]$^-$), 506.6 (48) ([Cu$_2$I$_3$]$^-$), 316.6 (100) ([CuBr$_2$]$^-$), 126.7 (1) ([I]$^-$).

6.5 Supplementary Information

Crystallographic Details

The data for **1**, **2** and **7** were collected on an Agilent Technologies diffractometer equipped with an Atlas CCD detector and a SuperNova CuK$_\alpha$ microfocus (λ = 1.54178 Å) source. The data for **3**, **4**, **5**, **6** and **8** were collected on an Agilent Technologies Gemini R-Ultra diffractometer equipped with Ruby CCD detector and using either an Enhanced Ultra CuK$_\alpha$ sealed tube (**3**, **4** and **8**) or an Enhanced Ultra MoK$_\alpha$ (λ = 0.71073 Å) sealed tube (**5** and **6**). All measurements were performed at 123 K. Crystallographic data and details of the diffraction experiments are given in Table S6.1-S6.4. Using Olex2,[26] the structures were solved either with the ShelXT[27] (**1**-**4**, **6**-**8**) or SIR2004[28] (**5**) structure solution program using Direct Methods and refined with the ShelXL[29] refinement package using Least Squares minimisation. Especially in case of disorder, commonly used restraints for the ShelXL program were applied (SIMU). Since the refinement has been unstable for **5** and the isostructural coordination compound [{Cp*Fe(η$^{5:2:2:2}$-As$_5$)}{Cu(μ-Cl)}$_3$(CH$_3$CN)]$_n$ (**A**) shows pseudo-merohedral twinning, the same situation has been assumed for **5**. Consequently, with the aid of PLATON and employing the twin law (1 0 0/0 -1 0/0 0 -1) the batch scale factor can be refined to 0.3498(13). For **8**, pseudo-merohedral twinning is observed and the analogue approach leads to the batch scale factor of 0.135(5). Moreover, H atoms were located in idealised positions and refined isotropically according to the riding model. A semi-empirical numerical absorption correction based on gaussian[30] integration over a multifaceted crystal model (**1**, **2**, **5** and **7**) or an analytical[31] absorption correction from crystal faces (**3**, **4**, **6** and **8**) was applied. Figures were created with DIAMOND3.0.[32]

Table S6.1 Crystallographic data for **1** and **2**.

	1	**2**
Chemical formula	$C_{80}H_{70}Fe_2As_{10}Cu_4Cl_4$	$C_{80}H_{70}Fe_2As_{10}Cu_4Br_4$
M/g·mol^{-1}	2288.22	2466.06
T/K	123	123
Crystal system	monoclinic	monoclinic
Space group	$P2_1/c$	$P2_1/c$
a/Å	25.2235(2)	12.70527(15)
b/Å	10.25350(10)	10.17455(11)
c/Å	29.1237(3)	29.4113(4)
α/°	90.00	90.00
β/°	94.0612(8)	94.5379(12)
γ/°	90.00	90.00
V/Å³	7513.33(12)	3790.10(8)
Z	4	2
ρ_{cal}/g·cm^{-3}	2.023	2.161
μ/mm^{-1}	10.806	11.885
F(000)	4464.0	2376.0
Crystal size/mm^3	0.254 x 0.170 x 0.152	0.096 x 0.047 × 0.037
Radiation	CuK_α	CuK_α
2θ range/°	6.084 to 134.158	6.98 to 134.128
Index ranges	-30 ≤ h ≤ 28,	-15 ≤ h ≤ 14,
	-12 ≤ k ≤ 8,	-12 ≤ k ≤ 12,
	-34 ≤ l ≤ 33	-34 ≤ l ≤ 35
Reflections collected	32807	19795
Independent reflections	13343	6727
	[R_{int} = 0.0267, R_{sigma} = 0.0288]	[R_{int} = 0.0218, R_{sigma} = 0.0207]
Data/restraints/parameters	13343/12/937	6727/0/459
Goodness-of-fit on F^2	1.108	1.030
Final R indexes [I>2σ(I)]	R_1 = 0.0326, wR_2 = 0.0885	R_1 = 0.0239, wR_2 = 0.0548
Final R indexes [All Data]	R_1 = 0.0394, wR_2 = 0.0993	R_1 = 0.0268, wR_2 = 0.0562
Largest diff. peak/hole/eA^{-3}	0.85/-0.97	1.10/-1.09

Table S6.2 Crystallographic data for **3** and **4**.

	3	**4**
Chemical formula	$C_{40}H_{35}FeAs_5Cu_2Br_2$	$C_{40}H_{35}FeAs_5Cu_2I_2$
M/g·mol^{-1}	1233.03	1327.01
T/K	123	123
Crystal system	monoclinic	monoclinic
Space group	*P*2$_1$/*n*	*P*2$_1$/n
a/Å	18.13262(13)	18.34919(16)
b/Å	10.12407(8)	10.19511(12)
c/Å	20.89695(15)	21.2139(2)
α/°	90.00	90.00
β/°	99.0810(6)	98.8118(10)
γ/°	90.00	90.00
V/Å³	3788.10(5)	3921.69(7)
Z	4	4
ρ_{cal}/g·cm^{-3}	2.162	2.248
μ/mm^{-1}	11.891	21.461
F(000)	2376.0	2520.0
Crystal size/mm^3	0.115 × 0.078 × 0.041	0.196 × 0.051 × 0.025
Radiation	CuK_α	CuK_α
2θ range/°	6.002 to 134.14	6.916 to 133.092
Index ranges	-21 ≤ h ≤ 21, -11 ≤ k ≤ 8, -23 ≤ l ≤ 24	-21 ≤ h ≤ 18, -12 ≤ k ≤ 11, -25 ≤ l ≤ 20
Reflections collected	16476	16511
Independent reflections	6670 [R_{int} = 0.0284, R_{sigma} = 0.0318]	6801 [R_{int} = 0.0337, R_{sigma} = 0.0404]
Data/restraints/parameters	6670/0/471	6801/0/451
Goodness-of-fit on F^2	1.125	1.029
Final R indexes [I>2σ(I)]	R_1 = 0.0313, wR_2 = 0.0926	R_1 = 0.0281, wR_2 = 0.0679
Final R indexes [All Data]	R_1 = 0.0352, wR_2 = 0.1032	R_1 = 0.0315, wR_2 = 0.0700
Largest diff. peak/hole/eA^{-3}	1.59/-0.91	1.05/-0.82

Table S6.3 Crystallographic data for **5** and **6**.

	5	**6**
Chemical formula	$C_{12}H_{18}RuAs_5Cu_3Cl_3N$	$C_{12}H_{18}RuAs_5Cu_3Br_3N$
M/g·mol^{-1}	948.91	1082.29
T/K	123	123
Crystal system	monoclinic	monoclinic
Space group	*P*2$_1$/*c*	*P*2$_1$/c
a/Å	11.6981(5)	11.8441(4)
b/Å	22.0062(13)	22.1513(7)
c/Å	8.5377(4)	8.6847(3)
α/°	90.00	90.00
β/°	90.299(4)	90.518(3)
γ/°	90.00	90.00
V/Å³	2197.9(2)	2278.45(13)
Z	4	4
ρ_{cal}/g·cm^{-3}	2.868	3.155
μ/mm^{-1}	11.372	15.879
F(000)	1776.0	1992.0
Crystal size/mm^3	0.285 × 0.225 × 0.084	0.413 × 0.264 × 0.106
Radiation	MoK$_\alpha$	MoK$_\alpha$
2θ range/°	5.892 to 50.242	6.126 to 50.264
Index ranges	-13 ≤ h ≤ 13,	-14 ≤ h ≤ 14,
	-26 ≤ k ≤ 26,	-26 ≤ k ≤ 26,
	-10 ≤ l ≤ 7	-7 ≤ l ≤ 10
Reflections collected	13324	9098
Independent reflections	3916	4060
	[R_{int} = 0.0501, R_{sigma} = 0.0466]	[R_{int} = 0.0319, R_{sigma} = 0.0450]
Data/restraints/parameters	3916/0/233	4060/0/232
Goodness-of-fit on F^2	1.044	1.059
Final R indexes [I>2σ(I)]	R_1 = 0.0391, wR_2 = 0.0987	R_1 = 0.0267, wR_2 = 0.0502
Final R indexes [All Data]	R_1 = 0.0404, wR_2 = 0.1005	R_1 = 0.0318, wR_2 = 0.0521
Largest diff. peak/hole/eA^{-3}	1.16/-1.26	0.88/-0.79

Table S6.4 Crystallographic data for **7** and **8**.

	7	**8**
Chemical formula	$C_{20}H_{30}Ru_2As_{10}Cu_4I_4$	$C_{24}H_{36}Ru_2As_{10}Cu_8I_8N_2$
M/g·mol^{-1}	1983.54	2827.41
T/K	123	123
Crystal system	triclinic	orthorhombic
Space group	$P\bar{1}$	$P2_12_12$
a/Å	11.4410(2)	17.5428(2)
b/Å	11.9552(2)	14.42237(18)
c/Å	15.4574(3)	10.59373(13)
α/°	107.0359(17)	90.00
β/°	94.2255(16)	90.00
γ/°	101.8642(17)	90.00
V/Å³	1957.94(7)	2680.31(6)
Z	2	2
ρ_{cal}/g·cm^{-3}	3.365	3.503
μ/mm^{-1}	42.739	51.023
F(000)	1792.0	2536.0
Crystal size/mm^3	0.083 × 0.061 × 0.053	0.119 × 0.074 × 0.061
Radiation	CuK_α	CuK_α
2θ range/°	6.042 to 134.13	7.936 to 134.132
Index ranges	-13 ≤ h ≤ 13, -14 ≤ k ≤ 14, -18 ≤ l ≤ 18	-20 ≤ h ≤ 17, -12 ≤ k ≤ 17, -12 ≤ l ≤ 12
Reflections collected	72680	9885
Independent reflections	6987 [R_{int} = 0.0704, R_{sigma} = 0.0269]	4480 [R_{int} = 0.0397, R_{sigma} = 0.0442]
Data/restraints/parameters	6987/0/372	4480/280/296
Goodness-of-fit on F^2	1.023	1.056
Final R indexes [I>2σ(I)]	R_1 = 0.0220, wR_2 = 0.0482	R_1 = 0.0266, wR_2 = 0.0672
Final R indexes [All Data]	R_1 = 0.0266, wR_2 = 0.0499	R_1 = 0.0269, wR_2 = 0.0674
Largest diff. peak/hole/eA^{-3}	1.00/-0.97	1.05/-0.95
Flack parameter	-	0.135(5)

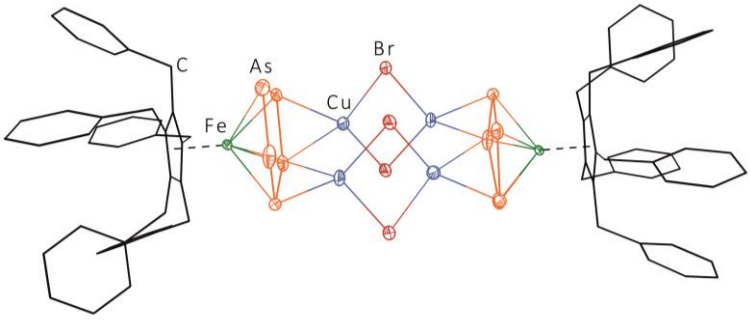

Figure S6.1 Molecular structure of **2** in the solid state. H atoms are omitted for clarity and Cp^{Bn} ligands are drawn in wire or frame model. Due to disorder only the main part is depicted. Thermal ellipsoids are drawn at the 50 % probability level. **1** and **2** are isostructural dimers.

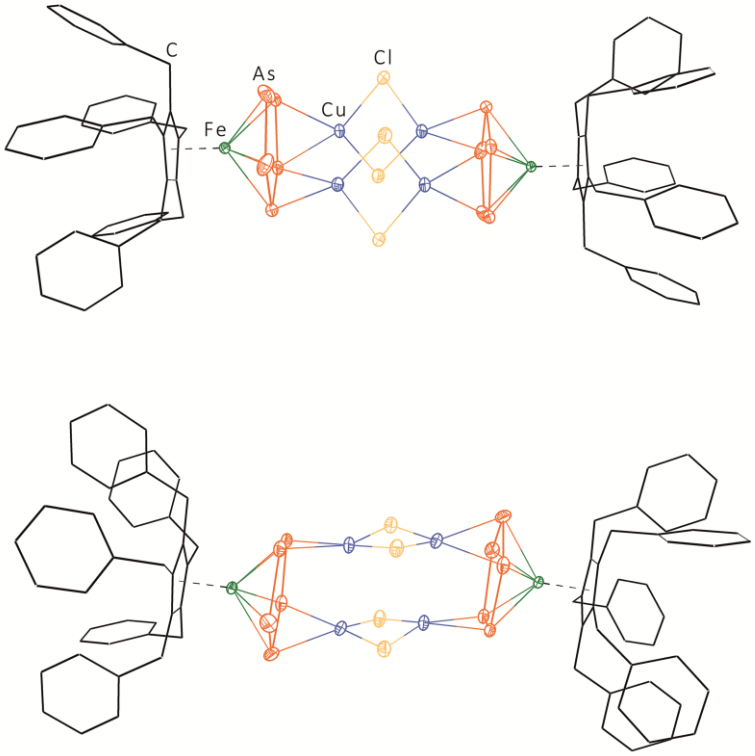

Figure S6.2 Molecular structure of **1** in the solid state. Due to the disorder of the Cu^I centres two favoured orientations are possible. H atoms are omitted for clarity and Cp^{Bn} ligands are drawn in wire or frame model. Thermal ellipsoids are drawn at 50 % probability level. **1** and **2** are isostructural dimers.

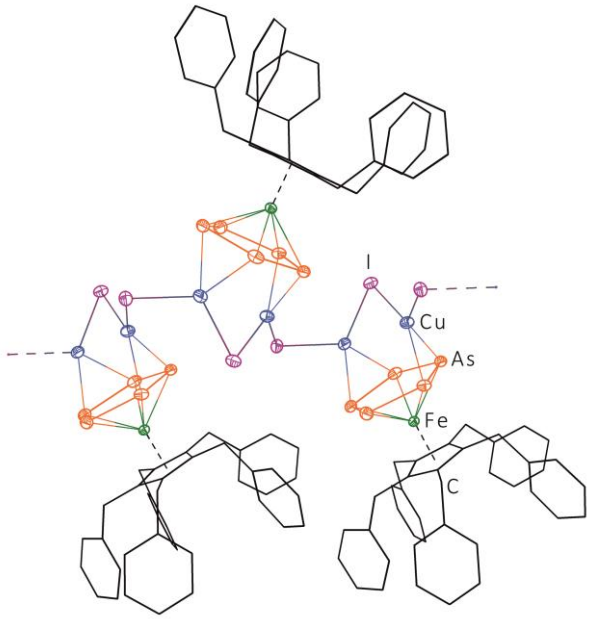

Figure S6.3 Section of the polymeric structure of **4** in the solid state. H atoms are omitted for clarity and Cp^{Bn} ligands are drawn in wire or frame model. Thermal ellipsoids are drawn at 50 % probability level. **3** and **4** are isostructural one dimensional polymers.

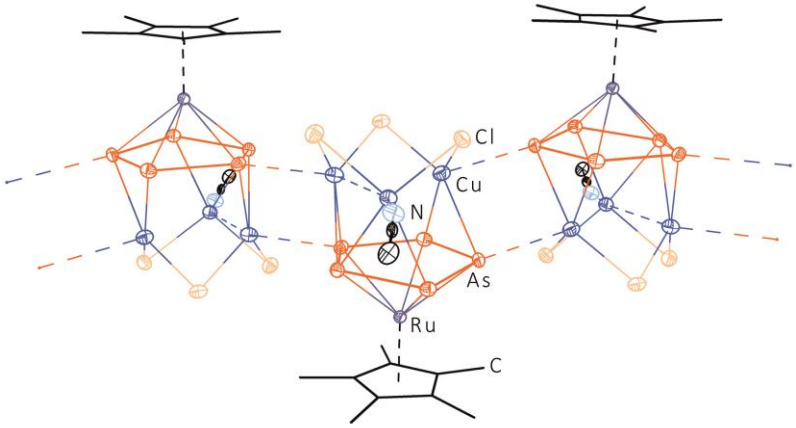

Figure S6.4 Section of the polymeric structure of **5** in the solid state. H atoms are omitted for clarity and Cp* ligands are drawn in wire or frame model. Thermal ellipsoids are drawn at 50 % probability level. **5** and **6** are isostructural one dimensional polymers.

6.6 References

[1] a) O. J. Scherer, *Angew. Chem. Int. Ed. Engl.* 1985, *24*, 924-943; b) O. J. Scherer, *Acc. Chem. Res.* 1999, *32*, 751-762; c) B. M. Crossairt, N. A. Piro, C. C. Cummins, *Chem. Rev.* 2010, *110*, 4164-4177; d) M. Caporali, L. Gonsalvi, A. Rossin, M. Peruzzini, *Chem. Rev.* 2010, *110*, 4178-4235; e) M. Scheer, G. Balázs, A. Seitz, *Chem. Rev.* 2010, *110*, 4236-4256; c) N. A. Giffin, J. D. Masuda, *Coord. Chem. Rev.* 2011, *255*, 1342-1359.

[2] M. Scheer, *Dalton Trans.* 2008, *33*, 4321-4524.

[3] a) C. Heindl, A. Kuntz, E. V. Peresypkina, A. V. Virovets, M. Zabel, D. Ludeker, G. Brunklaus, M. Scheer, *Dalton Trans.* 2015, *44*, 6502-6509; b) M. Fleischmann, S. Welsch, E. V. Peresypkina, A. V. Virovets, M. Scheer, *Chem. Eur. J.* 2015, *21*, 14332-14336; c) M. Fleischmann, F. Dielmann, L. J. Gregoriades, E. V. Peresypkina, A. V. Virovets, S. Huber, A. Y. Timoshkin, G. Balázs, M. Scheer, *Angew. Chem. Int. Ed.* 2015, *54*, 13110-13115; d) B. Attenberger, E. V. Peresypkina, M. Scheer, *Inorg. Chem.* 2015, *54*, 7021-7029; e) C. Heindl, E. V. Peresypkina, D. Lüdeker, G. Brunklaus, A. V. Virovets, M. Scheer, *Chem. Eur. J.* 2016, *22*, 2599-2604;

[4] a) F. Dielmann, A. Schindler, S. Scheuermayer, J. Bai, R. Merkle, M. Zabel, A. V. Virovets, E. V. Peresypkina, G. Brunklaus, H. Eckert, M. Scheer, *Chem. Eur. J.* 2012, *18*, 1168-1179; b) M. Fleischmann, S. Welsch, H. Krauss, M. Schmidt, M. Bodensteiner, E. V. Peresypkina, M. Sierka, C. Gröger, M. Scheer, *Chem. Eur. J.* 2014, *20*, 3759-3768.

[5] a) A. Schindler, C. Heindl, G. Balázs, C. Gröger, A. V. Virovets, E. V. Peresypkina, M. Scheer, *Chem. Eur. J.* 2012, *18*, 829-835; b) F. Dielmann, C. Heindl, F. Hastreiter, E. V. Peresypkina, A. V. Virovets, R. M. Gschwind, M. Scheer, *Angew. Chem. Int. Ed.* 2014, *53*, 13605-13608; c) S. Heinl, E. Peresypkina, J. Sutter, M. Scheer, *Angew. Chem. Int. Ed.* 2015, *54*, 13431-13435; d) F. Dielmann, M. Fleischmann, C. Heindl, E. V. Peresypkina, A. V. Virovets, R. M. Gschwind, M. Scheer, *Chem. Eur. J.* 2015, *21*, 6208-6214.

[6] a) C. Heindl, *Ph.D. thesis*, Universität Regensburg, 2015; b) B. Krämer, *master thesis*, Universität Regensburg, 2014.

[7] S. Welsch, C. Gröger, M. Sierka, M. Scheer, *Angew. Chem. Int. Ed.* 2011, *50*, 1435-1438.

[8] S. Heinl, *Ph.D. thesis*, Universität Regensburg, 2014.

[9] C. Heindl, E. V. Peresypkina, A. V. Virovets, W. Kremer, M. Scheer, *J. Am. Chem. Soc.* 2015, *137*, 10938-10941.

[10] C. Schwarzmaier, A. Schindler, C. Heindl, S. Scheuermayer, E. V. Peresypkina, A. V. Virovets, M. Neumeier, R. Gschwind, M. Scheer, *Angew. Chem. Int. Ed.* 2013, *52*, 10896-10899.

[11] L. J. Gregoriades, H. Krauss, J. Wachter, A. V. Virovets, M. Sierka, M. Scheer, *Angew. Chem. Int. Ed.* 2006, *45*, 4189-4192.

[12] a) M. Fleischmann, L. Dütsch, M. E. Moussa, A. Schindler, G. Balazs, C. Lescop, M. Scheer, *Chem. Commun.* 2015, *51*, 2893-2895; b) H. Krauss, G. Balázs, M. Bodensteiner, M. Scheer, *Chem. Sci.* 2010, *1*, 337-342.

[13] Refers to [$Cp^{Bn}Fe(\eta^5\text{-}As_5)$] in this thesis (chapter 5).

[14] Y. Morino, T. Ukaji, T. Ito, *Bull. Chem. Soc. Jpn.* 1966, *39*, 64-71.

[15] H. A. Spinney, N. A. Piro, C. C. Cummins, *J. Am. Chem. Soc.* 2009, *131*, 16233-16243.

[16] A. H. Cowley, N. C. Norman, M. Pakulski, *Dalton Trans.* 1985, *1*, 383-386.

[17] H. Maelger, F. Oblrich, J. Kopf, D. Abeln, E. Weiss, *Z. Naturforsch. 1992*, *47b*, 1276-1280.

[18] a) J. Bai, A. V. Virovets, M. Scheer, *Angew. Chem. Int. Ed.* 2002, *41*, 1737-1739; b) M. Scheer, L. J. Gregoriades, J. Bai, M. Sierka, G. Brunklaus, H. Eckert, *Chem. Eur. J.* 2005, *11*, 2163-2169; c) A. Schindler, M. Zabel, J. F. Nixon, M. Scheer, *Z. Naturforsch.* 2009, *64b*, 1429-1437.

[19] R. Peng, M. Li, D. Li, *Coord. Chem. Rev.* 2010, *254*, 1-18.

[20] Refers to entries in WebCSD data base (http://webcsd.ccdc.cam.ac.uk/index.php) found in June 2016.

[21] A. Bondi, *J. Phys. Chem.* 1964, *68*, 441-451.

[22] W. F. Fu, X. Gan, C. M. Che, Q. Y. Cao, Z. Y. Zhou, N. N. Y. Zhu, *Chem. Eur. J.* 2004, *10*, 2228-2236.

[23] K. Chen, J. Shearer, V. J. Catalano, *Inorg. Chem.* 2015, *54*, 6245-6256.

[24] S. Sculfort, P. Braunstein, *Chem. Soc. Rev.* 2011, *40*, 2741-2760.

[25] O. J. Scherer, C. Blath, G. Heckmann, G. Wolmershäuser, *J. Organomet. Chem.* 1991, *409*, C15-C18.

[26] O. V. Dolomanov, L. J. Bourhis, R. J. Gildea, J. A. K. Howard, H. Puschmann, *J. Appl. Cryst.* 2009, *42*, 339-341.

[27] G. M. Sheldrick, *Acta Cryst.* 2015, *A71*, 3-8.

[28] M. C. Burla, R. Caliandro, M Camalli, B Carrozzini, G. L. Cascarano, L. De Caro, C. Giacovazzo, G. Polidori, D. Siliqi, R. Spagna, *J. Appl. Cryst.* 2007, *40*, 609-613.

[29] G. M. Sheldrick, *Acta Cryst.* 2015, *C71*, 3-8.

[30] CrysAlisPro, Version 1.171.38.41, Agilent Technologies UK Ltd, Oxford, UK.

[31] R. C. Clark, J. S. Reid, *Acta Cryst.* 1995, *A51*, 887-897.

[32] K. Brandenburg, H. Putz, Diamond3.0, Crystal and Molecular Structure Visualization, Crystal Impact GbR, Bonn, Germany, 2014.

7. Novel Coordination Compounds of [Cp*Fe(η^5-As$_5$)] and Monovalent Metal Salts

M. Schmidt and M. Scheer

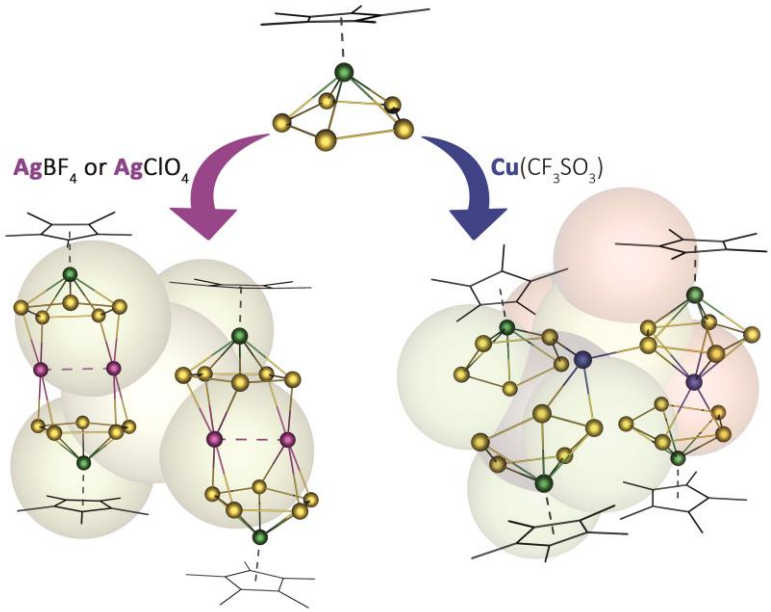

Abstract:

The coordination behaviour of [Cp*Fe(η^5-As$_5$)] towards silver salts AgX (X$^-$ = BF_4^-, ClO_4^-) with a coordinating anion is presented. By diffusion reactions, the discrete dimers [Ag{Cp*Fe(η$^{5:2:2}$-As$_5$)X]$_2$ (X = BF_4^- (**1a**), ClO_4^- (**2a**)) and [Ag{Cp*Fe(η$^{5:3:2}$-As$_5$)}X]$_2$ (X$^-$ = BF_4^- (**1b**), ClO_4^- (**2b**)) are obtained, which crystallise as co-crystals in the solid state. Besides the coordination behaviour of [Cp*Fe(η^5-As$_5$)] towards Ag^I salts, the reactivity of the latter towards Cu(CF$_3$SO$_3$) · 0.5 C$_7$H$_8$ has also been studied, yielding the discrete, soluble dimer [Cu$_2${Cp*Fe(η$^{5:5:1}$-As$_5$)}{Cp*Fe(η$^{5:2}$-As$_5$)}$_2${Cp*Fe(η$^{5:1}$-As$_5$)}{CF$_3$SO$_3$}$_2$] (**3**) exclusively. Moreover, the subsequent reaction of **1a** and **1b** with [Cp'''Co(μ-Cl)]$_2$ (Cp''' = η^5-1,2,4-C$_5$H$_2$^{t}Bu$_3$) has been investigated. Surprisingly, the former *cyclo*-As$_5$ ligand has been degraded and rearranged to afford [(Cp'''Co)$_3$(μ$_3$,η$^{4:4:4}$-As$_6$)][BF$_4$]$_2$ (**4**) as well as the by-product [(Cp'''Co)$_2$(μ-Cl)$_3$][BF$_4$] (**5**).

7.1 Author contributions

- All syntheses and characterisations were performed by Monika Schmidt.
- Manuscript was written by Monika Schmidt.
- Figures were made by Monika Schmidt.
- Single crystal X-ray structure analyses and refinements were performed by Monika Schmidt.
- Acknowledgement: The EPR spectra of **4** and **5** were recorded by Moritz Modl.

7.2 Introduction

In 2010, which marks the 20th anniversary of the synthesis of [Cp*Fe(η^5-As$_5$)] (**I**) (Cp* = η^5-C$_5$Me$_5$), **I** has first been used as building block in coordination chemistry by studying the reactivity towards Cu^I halides.[1] In addition, computational studies gave insight into the bonding situation of **I** in comparison to [Cp*Fe(η^5-P$_5$)] (**II**), revealing a reversed order of the unoccupied orbitals (LUMO, LUMO+1). However, the HOMO is localised at the *cyclo*-E$_5$ ring in both cases. Experimentally, a sharp contrast in the coordination behaviour of **I** and **II** towards monovalent metal salts like CuX (X = Cl, Br, I) is observed. While **I** tends to form π-coordination through As-As bonds (η^2-fashion), its lighter congener **II** favours a σ-coordination *via* the lone pairs (η^1-fashion), opening an access to fullerene like spherical aggregates and/or to one or two dimensional polymers.[1,2] However, the reaction of **I** with CuX leads to the formation of one dimensional polymers connected *via* weak Cu···As and/or Cu···X interactions exclusively (Scheme 7.1). Although coordination *via* the lone pairs of the *cyclo*-As$_5$ ring plays a minor role, we were able to observe isostructural polymers for **I** and **II** displaying an unexpected σ-1,3-coordination towards the preassembled linear Cu^I fragment [Cu$_3$(μ-Cl)$_2$(dpmp)$_2$][BF$_4$] (dpmp = bis(diphenylphosphino-methyl)phenylphosphine).[3] Changing from copper(I) halides to the monovalent metal salts bearing a weakly coordinating anion, a η^5-coordination of **I** by [M][TEF] (M = In$^+$, Tl$^+$; [TEF]$^-$ = [Al{OC(CF$_3$)$_3$}$_4$]$^-$) or the formation of dimers and paddle wheel trimers in combination with [Ag][FAL] ([FAL]$^-$ = [FAl{OC$_6$F$_{10}$(C$_6$F$_5$)}$_3$]$^-$) is found (Scheme 7.1).[4]

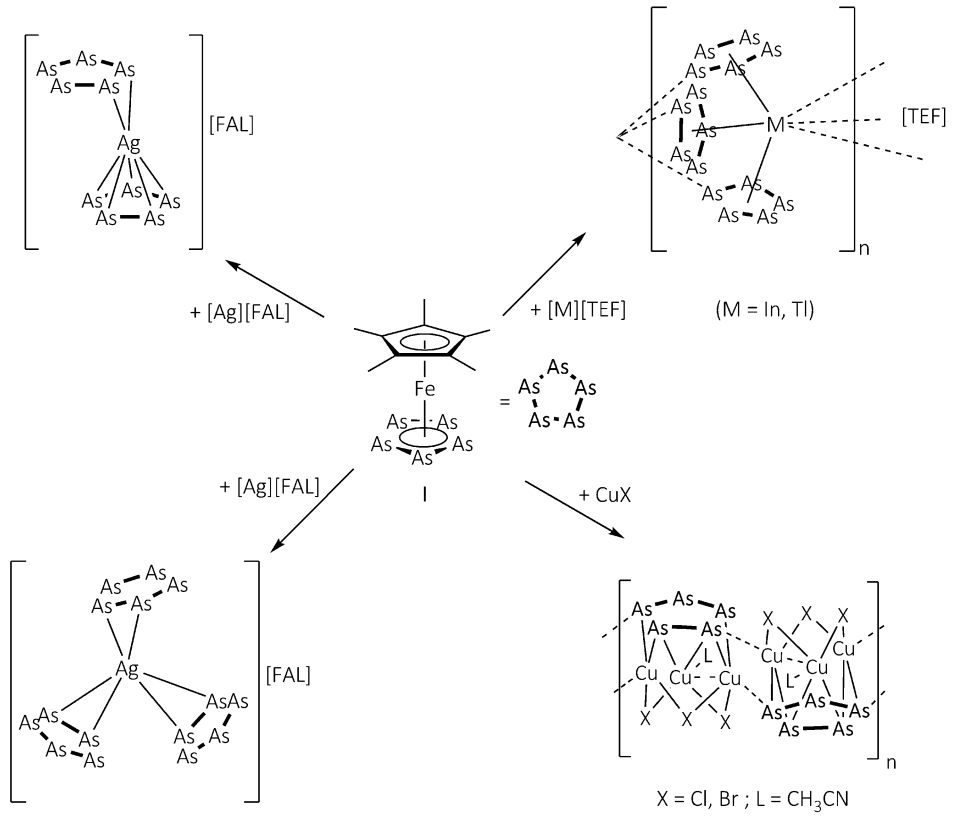

Scheme 7.1 Schematic illustration of coordination compounds originating from **I** and monovalent metal salts.

Despite the reported studies, the potential of **I** as a building block in supramolecular chemistry has only been marginally exploited. Hence, we were especially interested in the reactivity of **I** towards AgX (X^- = BF_4^-, ClO_4^-). Thereby, in this case the anions BF_4^- and ClO_4^- are considered as coordinating anions in comparison to the weakly coordinating anions $[TEF]^-$ and $[FAL]^-$. Furthermore, the use of copper(I) salts was exclusively limited to Cu^I halides. Other copper sources like $Cu(CF_3SO_3) \cdot 0.5\ C_7H_8$ have not been used in reactivity studies with the *cyclo*-As_5 ligand complex **I** so far. Consequently, the question arose which coordination behaviour exhibits **I** towards [M][X] (M = Ag^+, X^- = BF_4^-, ClO_4^-; M = Cu^+, X^- = $CF_3SO_3^-$).

Herein we report on the synthesis of the novel dimeric coordination compounds $[Ag\{Cp^*Fe(\eta^{5:2:2}\text{-}As_5)\}X]_2$ (X^- = BF_4^- (**1a**), ClO_4^- (**2a**)), $[Ag\{Cp^*Fe(\eta^{5:3:2}\text{-}As_5)\}X]_2$ (X^- = BF_4^- (**1b**), ClO_4^- (**2b**)) and $[Cu_2\{Cp^*Fe(\eta^{5:5:1}\text{-}As_5)\}\{Cp^*Fe(\eta^{5:2}\text{-}As_5)\}_2\{Cp^*Fe(\eta^{5:1}\text{-}As_5)\}\{CF_3SO_3\}_2]$ (**3**). Moreover, the subsequent reaction of *in situ* generated **1a** and **1b** with $[Cp'''Co(\mu\text{-}Cl)]_2$ ($Cp''' = \eta^5\text{-}1,2,4\text{-}C_5H_2{}^tBu_3$) is presented, leading to the formation of the prismatic complex $[(Cp'''Co)_3(\mu_3,\eta^{4:4:4}\text{-}As_6)][BF_4]_2$ (**4**) as well as the by-product $[(Cp'''Co)_2(\mu\text{-}Cl)_3][BF_4]$ (**5**).

7.3 Results and Discussion

Coordination Behaviour of [Cp*Fe(η^5-As$_5$)] (I) Towards AgX (X$^-$ = BF_4^-, ClO_4^-) and Cu(CF$_3$SO$_3$) · 0.5 C$_7$H$_8$

All coordination compounds containing AgX (X$^-$ = BF_4^-, ClO_4^-) are obtained by diffusion reactions. Thereby, a solution of **I** in toluene or thf is layered with a solution of AgX in CH_3CN. An immediate colour change to brown is obtained at the phase boundary. During the diffusion process, a black to brownish powder precipitates and a metallic mirror as well as small crystals of the dimers [Ag{Cp*Fe(η$^{5:2:2}$-As$_5$)}X]$_2$ (X$^-$ = BF_4^- (**1a**), ClO_4^- (**2a**)) and [Ag{Cp*Fe(η$^{5:3:2}$-As$_5$)}X]$_2$ (X$^-$ = BF_4^- (**1b**), ClO_4^- (**2b**)) are formed. Unfortunately, the obtained yields are low (**1**: 8 %), since compounds **1** and **2** exhibit high sensitivity to air and moisture and redox chemistry occurs during the diffusion process (metallic mirror and unidentified powder).[5] Furthermore, the yield of **2** cannot be determined due to explosion hazard, which is attributed to the ClO_4^- counterions. In contrast, the reaction of **I** with Cu(CF$_3$SO$_3$) · 0.5 C$_7$H$_8$ in CH_2Cl_2 leads to the formation of the discrete dimer [Cu$_2${Cp*Fe(η$^{5:5:1}$-As$_5$)}{Cp*Fe(η$^{5:2}$-As$_5$)}$_2${Cp*Fe(η$^{5:1}$-As$_5$)}{CF$_3$SO$_3$}$_2$] (**3**) in moderate yields (47 %) exclusively (Scheme 7.2).

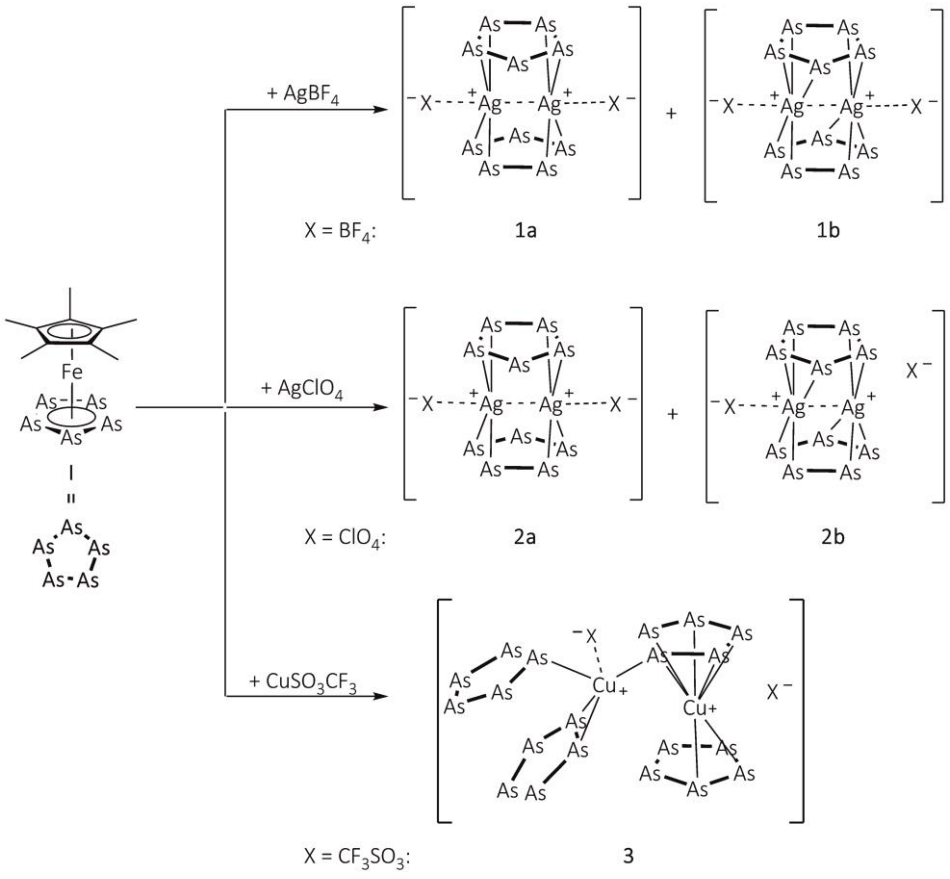

Scheme 7.2 Reactions of **I** with AgX (X$^-$ = BF_4^-, ClO_4^-) or Cu(CF$_3$SO$_3$) · 0.5 C$_7$H$_8$.

Crystals of **3** are obtained by layering the reaction mixture with Et_2O after complete diffusion. In addition, the crystallisation of **1**-**3** can be completed by concentrating the mother solution and subsequent layering with Et_2O (-30°C). However, compounds **1a** and **1b** as well as **2a** and **2b** crystallise together as co-crystals in the solid state.

Characterisation of the Coordination Compounds 1, 2 and 3

Compounds **1a** and **1b** co-crystallise in the solid state as dark red needles in the monoclinic space group $P2_1/n$. The dimers **2a** and **2b** co-crystallise as dark brown needles in the triclinic space group $P\bar{1}$. Single crystal X-ray structure analysis reveals a dimeric structure for **1** and **2** taking in account that the central structural core motifs of **1a** and **2a** as well as **1b** and **2b** are isostructural to each other besides of a different counterion. Thereby, two moieties of **I** are connected by Ag^+ cations coordinated in a $\eta^{2:2}$-fashion (**1a**/**2a**) or an unexpected $\eta^{3:2}$-mode (**1b**/**2b**) by the As-As bonds of the *cyclo*-As_5 ring of **I**. The asymmetric units of **1** and **2** contain one molecule of $[Ag\{Cp^*Fe(\eta^{5:2:2}\text{-}As_5)\}]_2^{2+}$ and one molecule of $[Ag\{Cp^*Fe(\eta^{5:3:2}\text{-}As_5)\}]_2^{2+}$ and four BF_4^- or ClO_4^- anions, respectively. They are either interacting with the Ag^+ cations or are separated in the case of one ClO_4^- anion in **2b**. If one ignores the Ag···Ag and Ag···Z (Z = F, O) interactions in **1** and **2**, respectively, each Ag^+ cation has either a strongly distorted tetrahedral geometry (**1a**/**2a**) or a distorted trigonal bipyramidal geometry (**1b**/**2b**). In Figure 7.1, the molecular structure of the co-crystals **1a** and **1b** in the solid state is exemplarily depicted (for the molecular structure of **2a** and **2b** in the solid state see Figure S7.7, supplementary information).

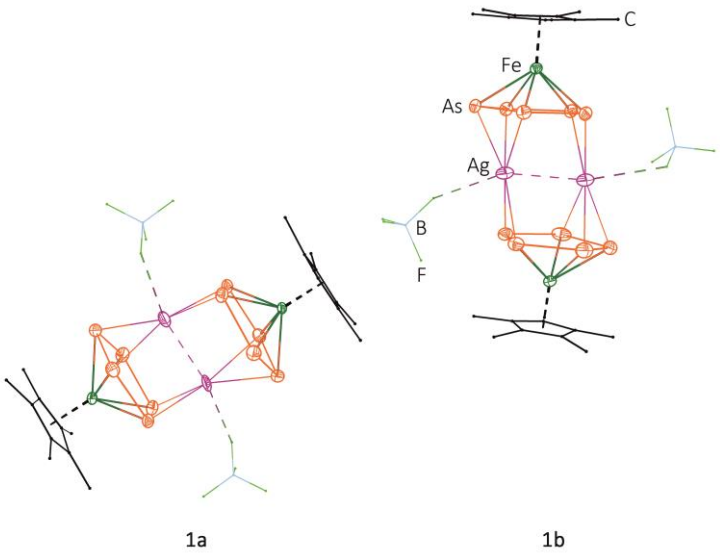

Figure 7.1 Molecular structures of the co-crystals **1a** and **1b** in the solid state (in the asymmetric unit). H atoms and solvent molecules are omitted for clarity. Cp* ligands and BF_4^- anions are drawn in wire or frame model. Due to the disorder of the Ag^+ centre in **1a** only one part is depicted. Thermal ellipsoids are drawn at 50 % probability level. **1a**/**2a** and **1b**/**2b** are isostructural dimers.

The two as well as the three folded π-coordination leads to an elongation of the As-As distances of **1a**/**2a** (**1a**: 2.3415(9) Å - 2.4094(9) Å; **2a**: 2.3489(11) Å - 2.4132(12) Å) and **1b**/**2b** (**1b**: 2.3488(10) Å - 2.4098(9) Å; **2b**: 2.3477(13) Å - 2.4153(12) Å) within the *cyclo*-As$_5$ unit in comparison to the As$_5$ ligand in the pentaarsaferrocene derivative **I** (2.317(1) Å - 2.330(1) Å)[4a] (Table 7.1). The Ag$^+$ cations in **1a**, **2a** and **2b** are equally disordered over two positions. Therefore, the Ag···Ag distances between two adjacent Ag$^+$ cations in **1a** reach from 2.885(15) Å to 2.946(15) Å, whereas in **2a**/**2b** Ag···Ag distances of 2.794(19) Å to 3.134(18) Å can be found. Thus, the Ag···Ag distances of **1a**, **2a** and **2b** are shorter than the sum of the van der Waals radii of two Ag atoms (3.44 Å)[6] and even partially shorter than the sum of the covalent radii of silver (2.90 Å).[7] Therefore, argentophilic interactions can be expected at least for the silver dimers **1a**, **2a** and **2b**. In contrast, the Ag···Ag distance in **1b** (2.8973(8) Å) is close to a covalent bond for silver (2.90 Å).[7] Comparable Ag-Ag bond lengths or Ag···Ag interactions have been reported in the literature.[8,9] In addition, the counterions are associated with the Ag$^+$ centres *via* weak Ag···Z interactions (Z = F (**1a**/**1b**): 2.68256(3) Å – 2.844(4) Å, Z = O (**2a**/**2b**): 2.561(10) Å – 2.855(10) Å), being shorter than the sum of the van der Waals radii of silver and Z (Z = F: 3.19 Å; Z = O: 3.24 Å).[6] These Ag···Z distances are in good agreement with reported Ag-F or Ag-O distances.[10] Moreover, the Ag-As bond lengths are in the range of Ag-As distances as reported in the arsinidene-bridged cluster [Ag$_{14}$(AsPh)$_6$Cl$_2$(PR$_3$)$_8$] (PR$_3$ = PEt$_3$, PMe^{n}Pr$_2$, P^{n}Pr$_3$) or [Ag$_4$(As$_4$Ph$_4$)$_2$(PR$_3$)$_4$] (PR$_3$ = PEt$_3$, P^{n}Pr$_3$).[8a] In Table 7.1, selected bond lengths of **1**-**2** are summarised.

Table 7.1 Selected bond lengths [Å] of **1a**/**1b** (Z = F) and **2a**/**2b** (Z = O). Whenever more than one bond is presented in the asymmetric unit (especially due to the disorder of the Ag cations), the ranges of bond lengths are given.

	1a	**1b**	**2a**	**2b**
As-As	2.3415(9) - 2.4094(9)	2.3488(10) - 2.4098(9)	2.3489(11) - 2.4132(12)	2.3477(13) - 2.4153(12)
Ag-As	2.551(10) - 2.798(10)	2.6127(8) - 2.9857(9)	2.586(9) - 3.047(9)	2.572(9) - 3.067(7)
Ag···Ag	2.885(15) / 2.946(15)	2.8973(8)	2.794(19) - 3.134(18)	2.743(11) / 3.124(11)
Ag···Z	2.683(5) – 2.834(10)	2.68256(3) / 2.844(4)	2.583(12) – 2796(11).	2.561(10) / 2.855(10)

Besides the dimer and trimer derived from the pentaarsaferrocene derivative **I** and [Ag][FAL] mentioned above,[4b] **1** and **2** represent the first examples for coordination compounds containing silver salts with a coordinating anion and **I**. Complexes **1a** and **2a** demonstrate the preference of As$_n$ ligand complexes for π-coordination. Surprisingly, short Ag···Ag distances are obtained for all dimers, suggesting argentophilic interactions. Further spectroscopic investigations concerning these short bond distances will be part of further studies. In contrast, **1b** and **2b** reveal an

unexpected $\eta^{3:2}$-coordination mode of the *cyclo*-As_5 units of **1b** and **2b**, respectively. Moreover, the Ag^+ cations show the expected weak interactions towards the X^- anions (X^- = BF_4^- or ClO_4^-), whereas the reported dimer and paddle wheel trimer of **I** and [Ag][FAL] exhibit charge separated ion pairs.[4b]

Compounds **1** and **2** are insoluble in all common solvents. As a result, the corresponding ESI MS spectra were recorded from the mother solution displaying several fragments of **1** and **2**. Here, even larger fragments were detected and could be assigned to $[\{Cp^*FeAs_5\}_2Ag_2\{BF\}_4]^+$ (*m*/*z* = 1434.2, **1**) and $[\{Cp^*FeAs_5\}_2Ag]^+$ (*m*/*z* = 1238.4, **2**), respectively. The composition for **1** is in line with results from the elemental analysis, while crystals of **2** could not be isolated in larger amounts due to explosion by shock, friction and loss of solvent.

Compound **3** crystallises as dark brown plates in the monoclinic space group *I*2/*m* with half a molecule of **3** in the asymmetric unit, whereas the other half is generated by symmetry. Single crystal X-ray structure analysis reveals a dimeric composition of **3**. Here, the Cu1 atom is coordinated in an unprecedented η^5-fashion by the *cyclo*-As_5 ligand of **I** as well as through an As-As bond (η^2-mode) of an adjacent moiety of **I** (Figure 7.2).

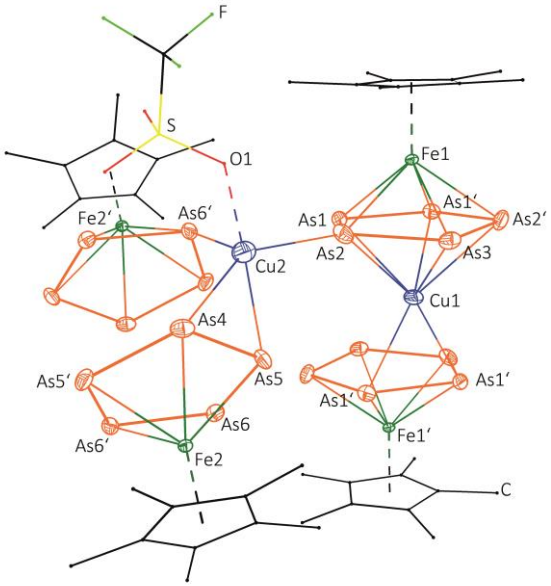

Figure 7.2 Molecular structure of **3** in the solid state. One of the four possible orientations in the asymmetric unit is depicted. H atoms, counterion and solvent molecules are omitted for clarity. Only the coordinating triflate anion is shown. Cp* ligands and triflate anion are drawn in wire or frame model. Thermal ellipsoids are drawn at 50% probability level. Selected bond lengths [Å] and angles [°]: Cu1-As1 2.636(3), Cu1-As1' 2.483(3), Cu1-As2 2.653(3), Cu1-As3 2.611(4), Cu2-As2 2.457(6), Cu2-As4 2.519(6), Cu2-As5 2.303(5), Cu2-As6' 2.840(6), Cu2-O1 2.108(8), As1-As1' 2.3750(19), As1-As2 2.3643(13), As2-As3 2.3660(13), As4-As5 2.3579(12), As5-As6 2.3616(13), As6-As6' 2.3697(19), As2-Cu2-As5 90.08(2), As4-Cu2-As6' 116.5(2), As1'-Cu1-As1' 57.14(9), As2-Cu2-O1 104.2(3), O1-Cu2-As6' 102.5(2).

In addition, Cu2 is σ-coordinated by As2 and As6' as well as through an As-As bond (η^2-coordination), resulting in a distorted tetrahedral environment for Cu2. The distortion is also noticeable in the bond angles ranging from 90.08(2)° to 116.5(3)°, which is typical for copper in the oxidation state +1.[11] Furthermore, one of the oxygen atoms of one triflate anion interacts with Cu2. The second triflate anion appears separated in the asymmetric unit. In addition, four orientations of the cooper centres can be realised due to disorder and symmetry generation. Consequently, the individual conformations can be converted into each other by rotation.

The As-As bond lengths within the *cyclo*-As_5 ligand of **3** are very uniform, but slightly elongated (2.3579(12) Å - 2.3750(19) Å) in comparison to those in **I** (2.137(1) Å – 2.330(1) Å). In contrast, the Cu-As distances of **3** range from 2.303(5) Å to 2.840(6) Å, being partially severely elongated in comparison to reported Cu-As distances. In the literature, average Cu-As distances of 2.34 Å-2.42 Å are common,[12] however, in coordination compounds even longer Cu-As distance up to 2.97 Å and 2.83 Å are known as well.[1,13] Therefore, Cu···As interactions can be discussed, since the observed Cu-As distances in **3** are shorter than the sum of the van der Waals radii of copper and arsenic (3.25 Å).[6] Additionally, the elongated As-As bond lengths within the *cyclo*-As_5 ligands of **3** suggest a coordination of the Cu^+ cations. Furthermore, the Cu2···O1 distance can be determined to be 2.108(8) Å, which is in good agreement with the reported Cu^I-O distance in $Cu(CF_3SO_3) \cdot C_7H_8$ (2.048(5) Å and 2.043(6) Å).[14] This distance is also remarkably shorter than the sum of the van der Waals radii of copper and oxygen (2.92 Å).[6] However, coordination compounds deriving from As_n ligand complexes and $Cu(CF_3SO_3)$ are unknown to date. Hence, **3** displays the first coordination compound containing $Cu(CF_3SO_3)$ and **I**, exhibiting an uncommon σ-coordination to copper as well as a η^5-coordination and η^2-coordination of the *cyclo*-As_5 unit of **3** to a single copper centre.

Compound **3** is moderately soluble in CH_2Cl_2, Et_2O and CH_3CN and insoluble in *n*-hexane or toluene. The ^1H NMR spectrum of **3** in CD_2Cl_2 shows a singlet at δ = 1.36 ppm for the Cp* ligands, which is lowfield shifted in comparison to the observed signal of the pentaarsaferrocene derivative **I** (δ = 1.08 ppm), indicating a coordination of **I** to the copper atom(s). In the $^{13}C\{^1H\}$ NMR spectrum, the corresponding signal for the CH_3 groups could be found at δ = 11.65 ppm. Unfortunately, due to the poor solubility no signal for the Cp ring could be detected in the $^{13}C\{^1H\}$ NMR spectrum. Moreover, the $^{19}F\{^1H\}$ NMR spectrum shows the corresponding signal for the triflate anion (δ = -77.71 ppm). As mentioned, the Cu^+ cations are expected to be weakly coordinated by the *cyclo*-As_5 ligand of **3**. Therefore, in the ESI mass spectrum the fragment $[(Cp^*FeAs_5)_2Cu]^+$ (*m/z* = 1194.6) could be assigned.

Rearrangement of 1 to 4

Since salt metathesis is often the essential force in many reactions, the question arose whether the silver containing dimers **1**-**2** are suitable precursors for the formation of triple decker complexes of the general formula [Cp*FeAs$_5$MCp^R] (M = transition metal, Cp^R = any cyclopentadienyl ligand). Unfortunately, **1**-**2** are not soluble and **2** explode by shock or friction due to the unfavourable perchlorate anions. Consequently, we decided to react *in situ* generated **1** in a mixture of toluene/CH$_3$CN with [Cp'''Co(μ-Cl)]$_2$ in thf yielding [(Cp'''Co)$_3$(μ$_3$,η$^{4:4:4}$-As$_6$)][BF$_4$]$_2$ (**4**), [(Cp'''Co)$_2$(μ-Cl)$_3$][BF$_4$] (**5**) as well as an unidentified green brownish powder (probably a mixture of AgCl and different polyarsenides of iron) (Scheme 7.3). Thereby, the *cyclo*-As$_5$ ligand of **1** is completely degraded and rearranged to give **4**.[15] Furthermore, the fragmentation products do not contain the [Cp*Fe]$^+$ fragment anymore. Hence, it must be probably split off to form the known intermediate [Cp*Fe(μ-Cl)]$_2$, which can only be isolated by using Cp^R ligands with high steric demand.[16] Similar fragmentation reactions have been observed by reacting [Cp*Fe(η^5-{1,2,4-P$_3$C$_2$mes$_2$})](mes = 2,4,6-trimethylphenyl) with CuX (X = Cl, Br, I) to form different coordination products.[17] Unfortunately, no fragmentation products containing the [Cp*Fe]$^+$ fragment could be isolated so far.[18]

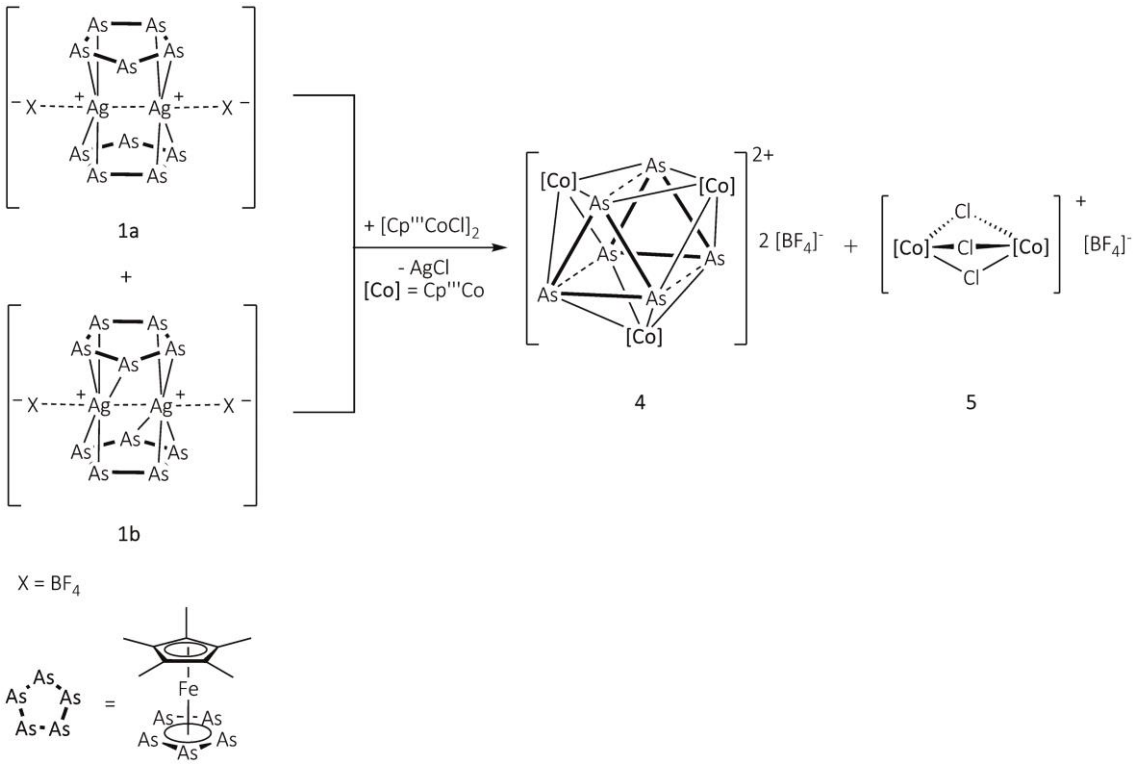

Scheme 7.3 Reaction of **1** with [Cp'''Co(μ-Cl)]$_2$.

Crystals of **4** are obtained by layering a concentrated solution (toluene/CH_3CN/thf) of **4** with *n*-pentane or *n*-hexane. Compound **4** crystallises as dark black plates in the triclinic space group $P\bar{1}$. Additionally, few dark blue plates of **5** are obtained (see supplementary information, Figure S7.8). Single crystal X-ray structure analysis of **4** reveals an As_6 prism as the central structural core motif. Here, the quadrangular faces are capped by [Cp'''Co] fragments (Figure 7.3). The As_6 prism in **4** consists of two As_3 triangles, exhibiting an average As-As bond length of 2.562 Å. Additionally, the As_3 units are connected through As-As single bonds (av. 2.791 Å). All As-As distances are longer than an usual As-As single bond (electron diffraction: 2.435 Å in As_4,[19] DFT calculations: 2.4372 Å in As_4[20]). Nevertheless, the observed bond lengths in the As_6 unit are still shorter than the sum of the van der Waals radii of arsenic (3.7 Å).[6] Furthermore, the isostructural clusters $[Cp^RCoAs_6]^{2+}$ (Cp^R = Cp*, Cp^{tBu} (η^5-$C_5Me_4{}^tBu$)) were reported in literature, showing similar trends in the As-As bond lengths (Cp^R = Cp*: 2.564 Å / 2.854 Å; Cp^R = Cp^{tBu}: 2.564 Å / 2.834 Å).[21] Applying the Wade concept,[22] **4** can be best described as a *nido* type cluster with 22 valence electrons.[23] Moreover, other Wade clusters with the general formula $[(Cp^RM)_3As_6]$ are known in literature, showing close structural analogy to **4** as well as elongated As-As bond lengths within the As_6 prism.[24]

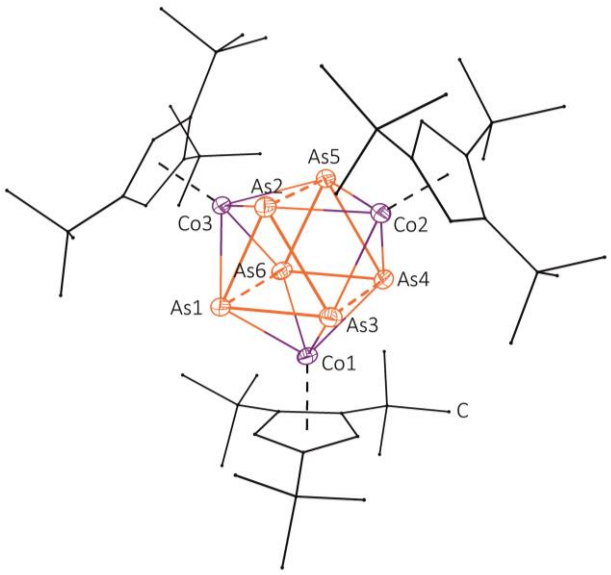

Figure 7.3 Molecular structure of **4** in the solid state. H atoms and counterions are omitted for clarity. Cp''' ligands are drawn in wire or frame model. Thermal ellipsoids are drawn at 50% probability level. Selected bond lengths [Å] and angles [°]: Co1-As1 2.3620(13), Co1-As3 2.4057(13), Co1-As4 2.3878(13), Co1-As6 2.3860(13), Co2-As2 2.3835(13), Co2-As3 2.3831(13), Co2-As4 2.3782(13), Co2-As5 2.3776(13), Co3-As1 2.3898(13), Co3-As2 2.3777(14), Co3-As5 2.3803(13), Co3-As6 2.3975(13), As1-As2 2.5530(10), As1-As3 2.5643(10), As1-As6 2.7906(11), As2-As3 2.5632(10), As2-As5 2.8138(11), As3-As4 2.7671(10), As4-As5 2.5707(10), As4-As6 2.5642(10), As5-As6 2.5546(10), As1-As2-As3 60.16(3), As1-As2-As5 89.55(3), As1-As3-As2 59.72(3), As1-As3-As4 89.65(3), As1-As6-As4 89.14(3), As1-As6-As5 90.04(3), As2-As1-As3 60.12(3), As2-As3-As4 90.44(3), As2-As1-As6 90.48(3), As2-As5-As4 89.25(3), As2-As5-As6 89.93(3), As3-As1-As6 90.34(3), As3-As2-As5 89.71(3), As3-As4-As5 90.60(3), As3-As4-As6 90.87(3), As4-As5-As6 60.04(3), As4-As6-As5 60.29(3), As5-As4-As6 59.67(3).

Compound **4** is soluble in CH_2Cl_2, CH_3CN and thf and insoluble in *n*-hexane or toluene. The ^{1}H NMR spectrum of **4** in CD_3CN shows the corresponding set of signals for the Cp''' ligands, which are slightly broadened. EPR spectroscopy has been performed, to get an insight in the electronic structure of **4**. Unfortunately, no signal in the EPR spectra at room temperature or at 77 K is detected, suggesting diamagnetisms (22 VE) or an open shell system with short relaxation times. Moreover, a broadening of the signals in the NMR spectra due to paramagnetic impurities could also be a possible explanation. However, the molecular ion peak for $[\mathbf{4}]^{2+}$ at *m/z* = 663.1 could be detected as the base peak by ESI mass spectrometry.

In summary, we could isolate the first coordination compounds containing **I** and monovalent metal salts with a coordinating anion [M][X] (M = Ag^+, X^- = BF_4^-, ClO_4^-; M = Cu^+, X^- = $CF_3SO_3^-$). First, the reaction of **I** with AgX yields the discrete and isostructural dimers $[Ag\{Cp^*Fe(\eta^{5:2:2}\text{-}As_5)X]_2$ (X = BF_4^- (**1a**), ClO_4^- (**2a**)) and $[Ag\{Cp^*Fe(\eta^{5:3:2}\text{-}As_5)\}X]_2$ (X^- = BF_4^- (**1b**), ClO_4^- (**2b**)), crystallising as co-crystals in the solid state. For **1a** and **2a**, only π-coordination by As-As bonds of the *cyclo*-As_5 unit ($\eta^{2:2}$-coordination) is observed, whereas **1b** and **2b** show an unexpected $\eta^{3:2}$-coordination mode. In addition, the BF_4^- or ClO_4^- anions interact mainly with the Ag^+ centre, confirming the coordinating nature of these counterions. Surprisingly, short Ag···Ag distances are observed in all dimers, being sometimes even shorter than the sum of the covalent radii of silver. Unfortunately, spectroscopic studies could not be conducted within the scope of this thesis and will be part of further studies. In contrast, the reaction of **I** with $Cu(CF_3SO_3) \cdot 0.5\ C_7H_8$ leads to the formation of the discrete dimer $[Cu_2\{Cp^*Fe(\eta^{5:5:1}\text{-}As_5)\}\{Cp^*Fe(\eta^{5:2}\text{-}As_5)\}_2\{Cp^*Fe(\eta^{5:1}\text{-}As_5)\}\{CF_3SO_3\}_2]$ (**3**) exclusively. Besides the mentioned coordination *via* As-As bonds of the *cyclo*-As_5 ligand (η^2-coordination), an uncommon η^5-coordination as well as a σ-coordination of **I** to Cu^+ is observed. Here, one triflate anion interacts with a Cu^+ cation, while the other triflate anion is separated in the asymmetric unit. Subsequent reaction of *in situ* generated **1a** and **1b** with $[Cp'''Co(\mu\text{-}Cl)]_2$ leads to the degradation and rearrangement of the former *cyclo*-As_5 unit of **I** to yield $[(Cp'''Co)_3(\mu_3,\eta^{4:4:4}\text{-}As_6)][BF_4]_2$ (**4**). Complex **4** displays a prismatic As_6 unit as the central structural motif, in which the quadrangular faces are capped by [Cp'''Co] fragments. In accordance to the wade concept, **4** can be best described as a *nido* cluster with 22 valence electrons. Furthermore the by-product $[(Cp'''Co)_2(\mu\text{-}Cl)_3][BF_4]$ (**5**) has been obtained.

7.4 Experimental Part

All reactions were performed under an atmosphere of dry argon or nitrogen using glovebox or Schlenk techniques. Solvents were purified, degassed and dried prior to use. $[Cp^*Fe(\eta^5\text{-}As_5)]$[25] and $[Cp'''Co(\mu\text{-}Cl)]_2$[26] were prepared according to literature procedures. The AgX salts (X^- = BF_4^-,

ClO_4^-) and $Cu(CF_3SO_3) \cdot 0.5\ C_7H_8$ are commercially available and were used without further purification.

The NMR spectra were recorded on a Bruker Avance 300 or Avance III HD 400 spectrometer. The ESI MS spectra of the mother solutions were measured on a ThermoQuest Finnigan MAT TSQ 7000 mass spectrometer. The elemental analyses were determined with a Vario ELIII apparatus. The X-band EPR measurements of **4** and **5** were carried out with a MiniScope MS400 device with a frequency of 9.5 GHz and rectangular resonator TE102 of the company Magnettech GmbH.

Synthesis of [Ag{Cp*Fe(η$^{5:2:2}$-As$_5$)}X]$_2$ (X$^-$ = BF_4^- (1a), ClO_4^- (2a)) and [Ag{Cp*Fe(η$^{5:3:2}$-As$_5$)}X]$_2$ (X$^-$ = BF_4^- (1b), ClO_4^- (2b))

In a thin Schlenk tube, a green solution of [Cp*Fe(η^5-As$_5$)] (**1**: 20 mg, 0.04 mmol, **2**: 42 mg, 0.07 mmol) in toluene or thf was layered with a solution of AgX (X$^-$ = BF_4^- : 14 mg, 0.07 mmol, ClO_4^-: 22 mg, 0.11 mmol) in CH_3CN. At the phase boundary a colour change to brown can be observed immediately. Furthermore, the formation of dark red needles of **1** and dark brown plates of **2**, a metallic mirror as well as brown powder can be observed during the diffusion. After complete diffusion, the mother liquor of **1** is decanted and the crystals were washed with a small amount of *n*-pentane and dried *in vacuo*. Crystals of **2** could not be isolated in a sizeable amount due to explosion hazard. By concentrating the decanted solution and layering with Et_2O a second crop of **1** or **2** can be obtained, while the mother liquor has turned almost colourless.

Analytical data of **1**

Crystalline yield: 2.4 mg (1.5 µmol, 8 % referred to [Cp*Fe(η^5-As$_5$)]).

Positive ion ESI MS (mother liquor, toluene/CH_3CN): *m/z* (%) = 1434.2 (3) ([{Cp*FeAs$_5$}$_2$Ag$_2${BF$_4$}]$^+$), 1238.4 (40) ([{Cp*FeAs$_5$}$_2$Ag]$^+$), 713.7 (84) ([{Cp*FeAs$_5$}Ag(CH_3CN)]$^+$), 672.6 (8) ([{Cp*FeAs$_5$}Ag]$^+$), 326.1 (100) ([Cp*$_2$Fe]$^+$).

Negative ion ESI MS (mother liquor, toluene/CH_3CN): *m/z* (%) = 86.8 (100) ([BF_4]$^-$).

Elemental Analysis: Calculated (%) for [$C_{20}H_{30}Fe_2As_{10}Ag_2B_2F_8 \cdot CH_3CN$] (1561.76 g/mol): C 16.92, H 2.13, N 0.90; found C 17.07, H 2.25, N 0.97.

Analytical data of **2**

Crystalline yield: The yield of **2** could not be determined due to explosion of **2** by shock, friction or loss of solvent.

Positive ion ESI MS (mother liquor, toluene/CH_3CN/Et_2O): *m/z* (%) = 1238.4 (60) ([{Cp*FeAs$_5$}$_2$Ag]$^+$), 565.7 (8) ([Cp*FeAs$_5$]$^+$), 326.1 (100) ([Cp*$_2$Fe]$^+$).

Negative ion ESI MS (mother liquor, toluene/CH_3CN/Et_2O): *m/z* (%) = 352.6 (20) ([Fe(ClO$_4$)$_3$]$^-$), 306.6 (5) ([Ag(ClO$_4$)$_2$]$^-$), 98.8 (20) ([ClO$_4$]$^-$).

Synthesis of [Cu$_2${Cp*Fe(η$^{5:5:1}$-As$_5$)}{Cp*Fe(η$^{5:2}$-As$_5$)}$_2${Cp*Fe(η$^{5:1}$-As$_5$)}{CF$_3$SO$_3$}$_2$] (3)

To a solution of Cu(CF_3SO_3) · 0.5 C_7H_8 (18 mg, 0.07 mmol) in CH_2Cl_2 a solution of [Cp*Fe(η^5-As$_5$)] (20 mg, 0.04 mmol) in CH_2Cl_2 is added and stirred for 10 minutes resulting in a red brownish solution. Then, the reaction mixture is concentrated, transferred into a thin Schlenk tube and layered with *n*-hexane or Et_2O. After complete diffusion, small dark brown plates and needles of **3** are obtained. The crystals were washed with a small amount of *n*-pentane and dried *in vacuo*.

Analytical data of **3**

Crystalline yield: 6.4 mg (4.1 µmol, 47 % referred to [Cp*Fe(η^5-As$_5$)]).

^{1}H NMR (CD_2Cl_2): δ [ppm] = 1.36 (s, CH_3).

^{13}C{^{1}H} NMR (CD_2Cl_2): δ [ppm] = 11.65 (CH_3), Cp signal is not observed.

^{19}F{^{1}H} NMR (CD_2Cl_2): δ [ppm] = -77.71 (CF_3).

Positive ion ESI MS (CH_3CN): *m/z* (%) = 1194.6 (35) [{Cp*FeAs$_5$}$_2$Cu]$^+$), 326.0 (100) ([Cp*$_2$Fe]$^+$).

Negative ion ESI MS (CH_3CN): *m/z* (%) = 360.7 (10) ([Cu{CF_3SO_3}$_2$]$^-$), 148.9 (100) ([CF_3SO_3]$^-$).

Elemental Analysis: Calculated (%) for [$C_{22}H_{33}Fe_2As_{10}Cu_2S_2O_6F_3$] (1556.59 g/mol): C 16.98, H 1.94, S 4.11; found C 16.53, H 1.84, S 4.67.

Synthesis of [(Cp'''Co)$_3$(µ$_3$,η$^{4:4:4}$-As$_6$)][BF$_4$]$_2$ (4) and [(Cp'''Co)$_2$(µ-Cl)$_3$][BF$_4$] (5)

In a thin Schlenk tube, a green solution of [Cp*Fe(η^5-As$_5$)] (20 mg, 0.04 mmol) in toluene was layered with a solution of $AgBF_4$ (14 mg, 0.07 mmol) in CH_3CN. At the phase boundary, a colour change to brown can be observed. During diffusion, the formation of dark red needles of **1** (2.4 mg, 8 % referred to [Cp*Fe(η^5-As$_5$)]) and a metallic mirror as well as brown powder can be observed. After complete diffusion, the mother liquor is decanted and concentrated. Then, the brown solution of **1** was added to [Cp'''Co(µ-Cl)]$_2$ (56 mg, 0.07 mmol) in thf and stirred at room temperature. After 2 hours, the solvent was concentrated *in vacuo*. The brown solution is filtered into a thin Schlenk tube and layered with *n*-pentane. After complete diffusion, black plates of **4** and dark blue plates of **5** can be obtained next to each other and cannot be separated from each other.

Analytical data of **4**

Crystalline yield: few crystals.

^{1}H NMR (CD_2Cl_2): δ [ppm] = 1.37 (s, 27H, ^{t}Bu$_3$), 1.56 (s, 54H, ^{t}Bu$_3$), 6.25 (s, 6H, CH).

^{13}C{^{1}H} NMR (CD_2Cl_2): δ [ppm] = 31.13 (^{t}Bu$_3$), 34.49 (^{t}Bu$_3$), 36.20 (^{t}Bu$_3$), 88.33 (C_5) (due to broadening of the signals no further assignment possible).

Positive ion ESI MS (CH_3CN): *m/z* (%) = 1345.2 ([{(Cp'''Co)$_3$As$_6$}F]$^+$) (8), 1326.2 ([{(Cp'''Co)$_3$As$_6$}]$^+$) (2), 663.1 ([{(Cp'''Co)$_3$As$_6$}]$^{2+}$) (100).

X-band EPR (CH_2Cl_2): EPR silent.

Analytical data of **5**

Crystalline yield: few crystals.

X-band EPR (77 K, CD_2Cl_2): g_{iso} = 2.004.

7.5 Supplementary Information

NMR Investigations

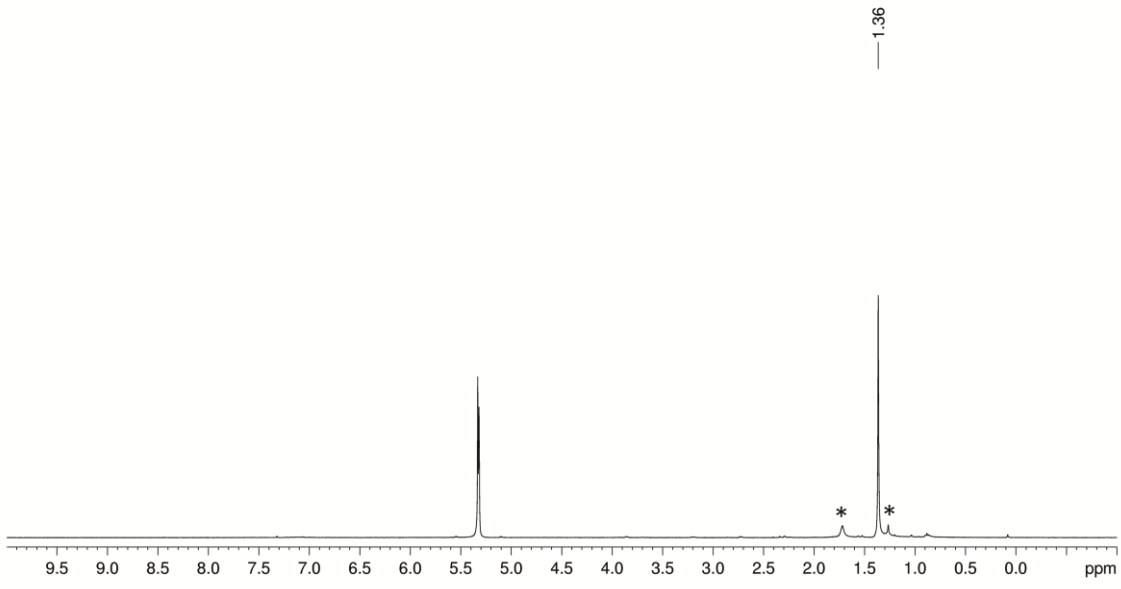

Figure S7.1 ^{1}H NMR spectrum of **3** in CD_2Cl_2 at 300 K. Signals marked with an asterisk are due to different solvents.

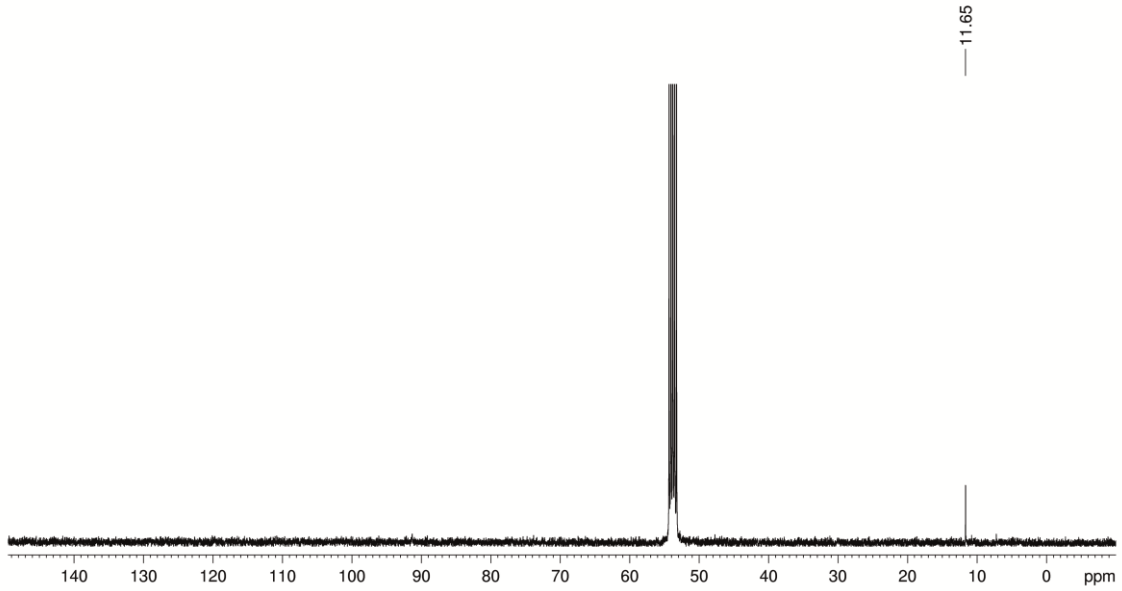

Figure S7.2 $^{13}C\{^1H\}$ NMR spectrum of **3** in CD_2Cl_2 at 300 K.

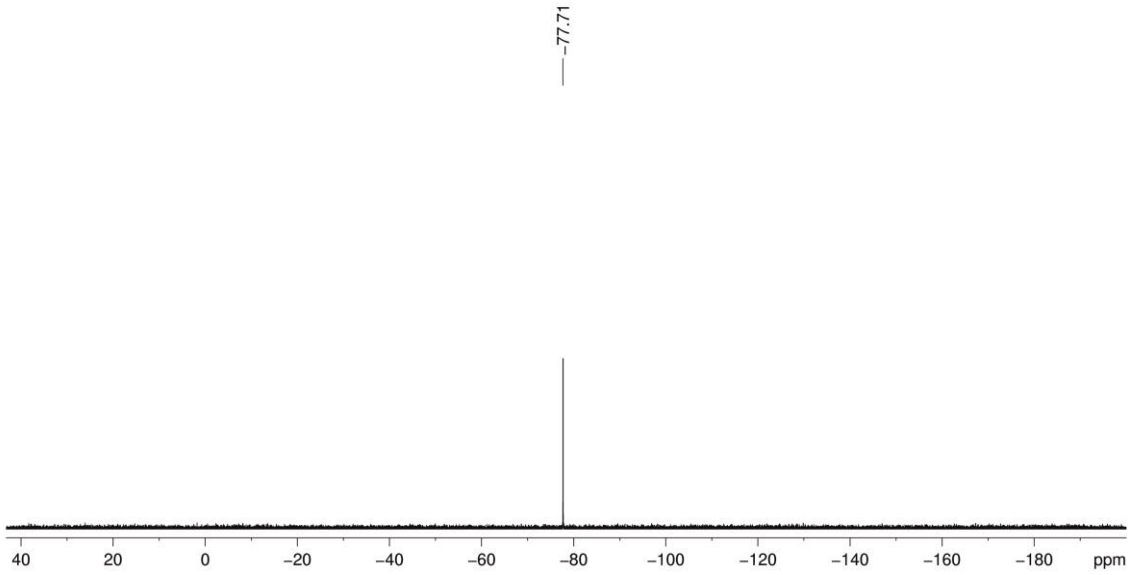

Figure S7.3 $^{19}F\{^1H\}$ NMR spectrum of **3** in CD_2Cl_2 at 300 K.

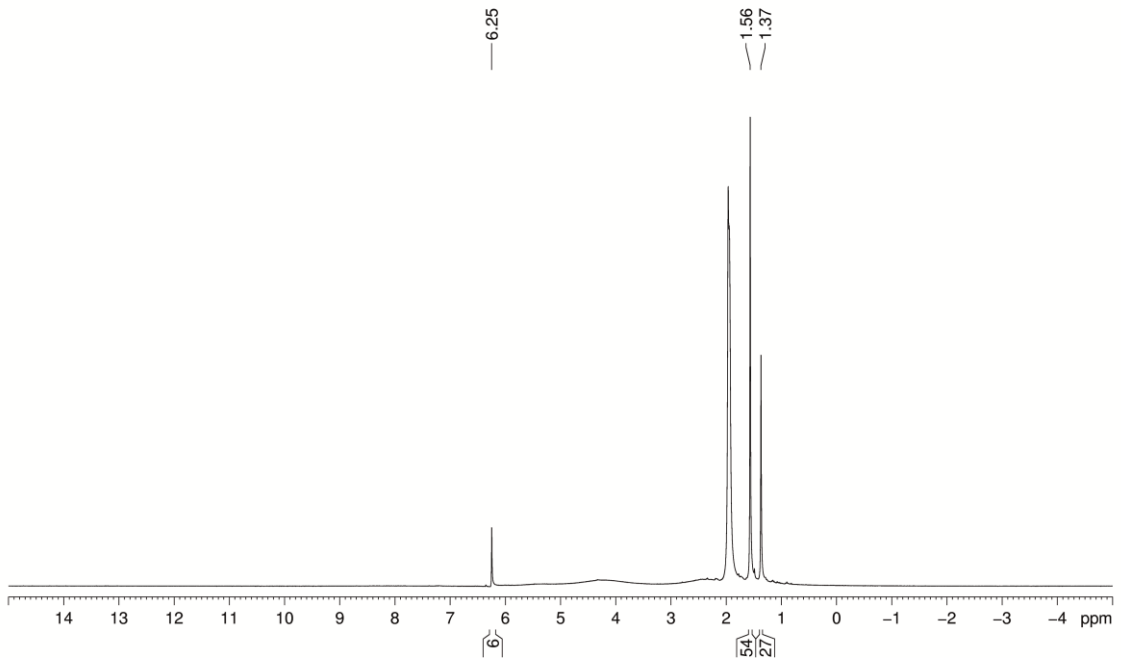

Figure S7.4 ^{1}H NMR spectrum of **4** in CD_3CN at 300 K.

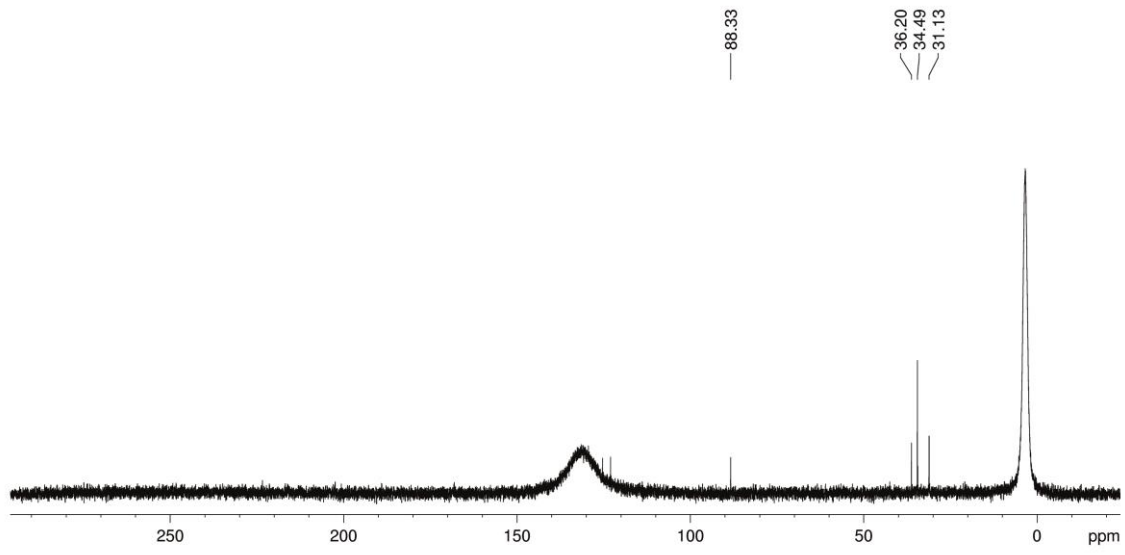

Figure S7.5 $^{13}C\{^{1}H\}$ NMR spectrum of **4** in CD_3CN at 300 K.

Representation of the X-Band EPR spectra of 5

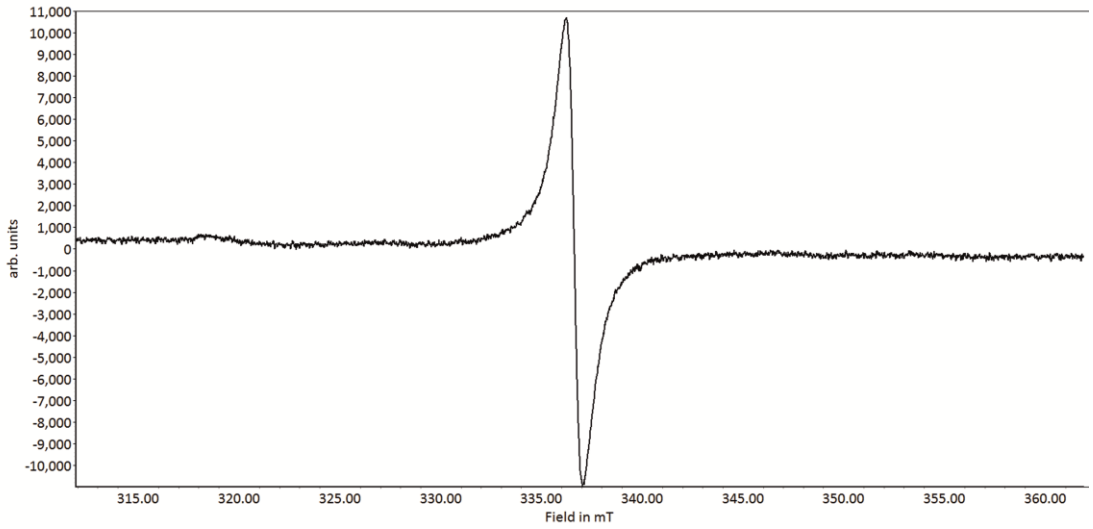

Figure S7.6 EPR spectrum of **5** in CH_2Cl_2 at 77 K.

Crystallographic Details

The data for **1a**, **1b**, **2a** and **2b** were collected on an Agilent Technologies Gemini R-Ultra diffractometer equipped with Ruby CCD detector and using an Enhanced Ultra CuK_α sealed tube (λ = 1.54178 Å). The data for **3**, **4** and **5** were collected on an Oxford Diffraction GV50 diffractometer equipped with Titan^{S2} CCD detector and a CuK_α microfocus source. All measurements were performed at 123 K. Crystallographic data and details of the diffraction experiments are given in Table S7.1-S7.3. Using Olex2,[27] the structures were solved either with the ShelXT[28] (**1a**, **1b**, **3**, **4**, **5**) or ShelXS[29] (**2a** and **2b**) structure solution program using Direct Methods and refined with the ShelXL[30] refinement package using Least Squares minimisation. Especially in case of disorder, commonly used restraints for the ShelXL program were applied (SIMU). Moreover, H atoms were located in idealised positions and refined isotropically according to the riding model. A semi-empirical numerical absorption correction based on gaussian[31] integration over a multifaceted crystal model (**3**, **4** and **5**) or an analytical[32] absorption correction from crystal faces (**1a** and **1b**) was applied. For **2a** and **2b**, a semi-empirical numerical absorption correction (multiscan) was applied.[33] Figures were created with DIAMOND3.0.[34]

Table S7.1 Crystallographic data for **1a**/**1b** and **2a**/**2b**.

	1a/**1b** · CH_3CN	**2a**/**2b** · 2 CH_3CN
Chemical formula	$C_{22}H_{33}Fe_2As_{10}Ag_2B_2F_8N$	$C_{44}H_{66}Fe_4As_{20}Ag_4Cl_4O_{16}N_2$
M/g·mol^{-1}	1561.75	3174.06
T/K	123	123
Crystal system	monoclinic	triclinic
Space group	$P2_1/n$	$P\bar{1}$
a/Å	12.08320(15)	12.2404(4)
b/Å	24.3361(3)	15.6069(5)
c/Å	26.0164(3)	22.7037(5)
α/°	90.00	93.535(2)
β/°	90.9136(11)	102.897(2)
γ/°	90.00	111.657(3)
V/Å³	7649.36(15)	3879.4(2)
Z	8	2
ρ_{cal}/g·cm^{-3}	2.712	2.717
μ/mm^{-1}	24.215	24.992
F(000)	5840.0	2984.0
Crystal size/mm^3	0.1909 × 0.1211 × 0.0784	0.2932 × 0.039 × 0.0214
Radiation	CuK_α	CuK_α
2θ range/°	7.264 to 134.154	7.9 to 134.21
Index ranges	-14 ≤ h ≤ 10, -20 ≤ k ≤ 28, -27 ≤ l ≤ 31	-12 ≤ h ≤ 14, -18 ≤ k ≤ 18, -26 ≤ l ≤ 27
Reflections collected	38244	32302
Independent reflections	13434 [R_{int} = 0.0422, R_{sigma} = 0.0435]	13591 [R_{int} = 0.0535, R_{sigma} = 0.0633]
Data/restraints/parameters	13434/0/887	13591/96/925
Goodness-of-fit on F^2	1.070	0.991
Final R indexes [I>2σ(I)]	R_1 = 0.0407, wR_2 = 0.1040	R_1 = 0.0454, wR_2 = 0.1076
Final R indexes [All Data]	R_1 = 0.0504, wR_2 = 0.1123	R_1 = 0.0691, wR_2 = 0.1214
Largest diff. peak/hole/eA^{-3}	1.40/-1.36	1.40/-1.40

Table S7.2 Crystallographic data for **3** and **4**.

	3 · CH_2Cl_2	**4**
Chemical formula	$C_{23}H_{32}Fe_2As_{10}Cu_2S_2O_6F_6Cl_2$	$C_{51}H_{87}Co_3As_6B_2F_8$
M/g·mol^{-1}	1641.48	1500.13
T/K	123	123
Crystal system	monoclinic	triclinic
Space group	*I*2/*m*	$P\bar{1}$
a/Å	13.7212(2)	10.3137(2)
b/Å	12.04356(19)	14.0207(5)
c/Å	25.2510(3)	22.8866(5)
α/°	90.00	91.922(2)
β/°	96.0032(12)	98.6557(19)
γ/°	90.00	90.119(2)
V/Å³	4149.89(10)	3269.89(16)
Z	4	2
ρ_{cal}/g·cm^{-3}	2.627	1.524
μ/mm^{-1}	18.233	9.704
F(000)	3112.0	1508.0
Crystal size/mm^3	0.378 × 0.047 × 0.037	0.162 × 0.109 × 0.048
Radiation	CuK_α	CuK_α
2θ range/°	7.04 to 134.15	6.308 to 134.132
Index ranges	-15 ≤ h ≤ 16, -14 ≤ k ≤ 13, -30 ≤ l ≤ 30	-12 ≤ h ≤ 7, -16 ≤ k ≤ 16, -27 ≤ l ≤ 27
Reflections collected	18292	20424
Independent reflections	3894 [R_{int} = 0.0326, R_{sigma} = 0.0200]	11579 [R_{int} = 0.0292, R_{sigma} = 0.0360]
Data/restraints/parameters	3894/0/285	11579/156/748
Goodness-of-fit on F^2	1.333	1.049
Final R indexes [I>2σ(I)]	R_1 = 0.0483, wR_2 = 0.1212	R_1 = 0.0707, wR_2 = 0.2234
Final R indexes [All Data]	R_1 = 0.0486, wR_2 = 0.1213	R_1 = 0.0757, wR_2 = 0.2305
Largest diff. peak/hole/eA^{-3}	0.72/-1.13	4.72/-1.05

Table S7.3 Crystallographic data for **5**.

	5
Chemical formula	$C_{34}H_{58}Co_2Cl_3BF_4$
M/g·mol^{-1}	777.82
T/K	123
Crystal system	triclinic
Space group	$P\bar{1}$
a/Å	10.2551(6)
b/Å	13.2032(10)
c/Å	15.3820(9)
α/°	66.205(7)
β/°	87.160(5)
γ/°	79.511(6)
V/Å³	1873.2(2)
Z	2
ρ_{cal}/g·cm^{-3}	1.379
μ/mm^{-1}	9.251
F(000)	816.0
Crystal size/mm^3	0.677 × 0.107 × 0.049
Radiation	CuK_α
2θ range/°	6.282 to 134.158
Index ranges	-11 ≤ h ≤ 12, -15 ≤ k ≤ 15, -18 ≤ l ≤ 15
Reflections collected	11136
Independent reflections	6637 [R_{int} = 0.0673, R_{sigma} = 0.0863]
Data/restraints/parameters	6637/60/460
Goodness-of-fit on F^2	1.041
Final R indexes [I>2σ(I)]	R_1 = 0.0739, wR_2 = 0.1889
Final R indexes [All Data]	R_1 = 0.0838, wR_2 = 0.2017
Largest diff. peak/hole/eA^{-3}	1.50/-0.93

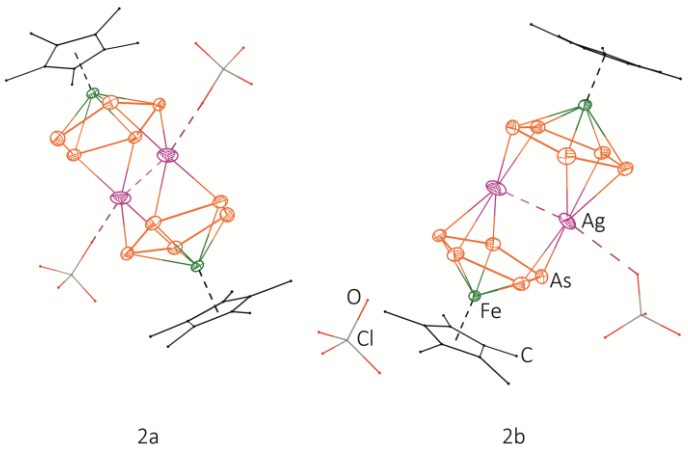

Figure S7.7 Molecular structure of **2a** and **2b** in the solid state. H atoms and solvent molecules are omitted for clarity. Cp* ligands and ClO_4^- anions are drawn in wire or frame model. Due to the disorder of the silver cations in **2a** and **2b** only one part is depicted. Thermal ellipsoids are drawn at 50 % probability level. **1a**/**2a** and **1b**/**2b** are isostructural dimers.

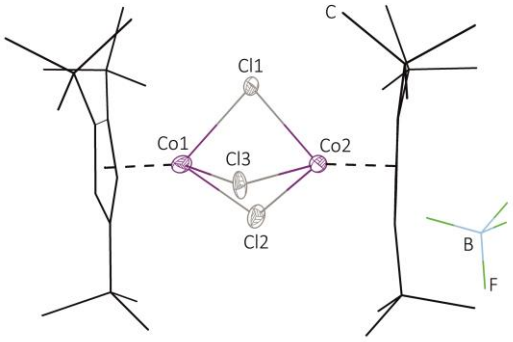

Figure S7.8 Molecular structure of **4** in the solid state. H atoms are omitted for clarity. Cp''' ligands and BF_4^- are drawn in wire or frame model. Thermal ellipsoids are drawn at 50% probability level. Selected bond lengths [Å] and angles [°]: Co1···Co2 2.9479(10), Co1-Cl1 2.3000(12), Co1-Cl2 2.3112(15), Co1-Cl3 2.3087(13), Co2-Cl1 2.3211(12), Co2-Cl2 2.3102(14), Co2-Cl3 2.3029(13), Cl1-Co1-Cl2 81.87(5), Cl2-Co1-Cl2 85.71(5), Cl1-Co1-Cl3 83.47(5), Cl1-Co2-Cl2 81.44(5), Cl1-Co2-Cl3 83.13(5), Cl2-Co2-Cl3 85.87(5), Cl1-Co1-Co2 50.68(3), Cl2-Co1-Co2 50.35(4), Cl3-Co1-Co2 50.18(3), Cl1-Co2-Co1 50.05(3), Cl2-Co2-Co1 50.38(4), Cl3-Co2-Co1 50.35(3).

7.6 References

[1] H. Krauss, G. Balázs, M. Bodensteiner, M. Scheer, *Chem. Sci.* 2010, *1*, 337-342.

[2] a) J. Bai, A. V. Virovets, M. Scheer, *Angew. Chem. Int. Ed.* 2002, *41*, 1737-1740; b) M. Scheer, J. Bai, B. P. Johnson, R. Merkle, A. V. Virovets, C. E. Anson, *Eur. J. Inorg. Chem.* 2005, 4023-4026; c) M. Scheer, *Dalton Trans.* 2008, *33*, 4321-4524; d) M. Scheer, A. Schindler, C. Gröger, A. V. Virovets, E. V. Peresypkina, *Angew. Chem.* 2009, *121*, 5148-5151.

[3] M. Fleischmann, L. Dütsch, M. E. Moussa, A. Schindler, G. Balazs, C. Lescop, M. Scheer, *Chem. Commun.* 2015, *51*, 2893-2895.

[4] a) M. Fleischmann, S. Welsch, H. Krauss, M. Schmidt, M. Bodensteiner, E. V. Peresypkina, M. Sierka, C. Gröger, M. Scheer, *Chem. Eur. J.* 2014, *20*, 3759-3768; b) M. Fleischmann, *Ph.D. thesis*, Universität Regensburg, 2015.

[5] In contrast, the mentioned reaction of [Cp*Fe(η^5-As_5)] (**I**) with [Ag][FAL] ([FAL]$^-$ = [FAl{$OC_6F_{10}(C_6F_5)$}$_3$]$^-$) (see introductory chapter 7.2) leads to the formation of [Ag{Cp*Fe($\eta^{5:5:2}$-As_5)}$_2$][FAL] (62 %) and [Ag{Cp*Fe($\eta^{5:2:2.:2}$-As_5)}$_3$][FAL] (44 %) in moderate yields. Furthermore, both coordination compounds were not obtained during diffusion reaction, but by reacting **I** with the Ag^I salt by stirring at room temperature. Therefore, redox chemistry could probably be suppressed.

[6] A. Bondi, *J. Phys. Chem.* 1964, *68*, 441-451.

[7] B. Cordero, V. Gomez, A. E. Platero-Prats, M. Reves, J. Echeverria, E. Cremades, F. Barragan, S. Alvarez, *Dalton Trans.* 2008, 2832-2838.

[8] a) D. Fenske, F. Simon, *Z. Anorg. Allg. Chem.* 1996, *622*, 45-52; b) V. McKee, J. Nelson, D. J. Speed, R. M. Town, *J. Chem. So., Dalton Tran.* 2001, 3641-3646; c) Y. A. Wanniarachchi, M. A. Khan, L. M. Slaughter, *Organometallics* 2004, *23*, 5881-5884; d) É. Fournier, A. Decken, Pierre D. Harvey, *Eur. J. Inorg. Chem.* 2004, *2004*, 4420-4429; e) F. Hung-Low, A. Renz, K. K. Klausmeyer, *J. Chem. Crystallogr.* 2011, *41*, 1174-1179; f) J. Huang, Z.-P. Deng, Y.-H. Xiao, L.-H. Huo, S.-N. Zhao, F.-Y. Ge, S. Gao, *Dalton Trans.* 2015, *44*, 5837-5847.

[9] S. Sculfort, P. Braunstein, *Chem. Soc. Rev.* 2011, *40*, 2741-2760.

[10] a) M. Camalli, F. Caruso, *Inorg. Chim. Acta* 1987, *127*, 209-213; b) G. Huang, C.-K. Tsang, Z. Xu, K. Li, M. Zeller, A. D. Hunter, S. S.-Y. Chui, C.-M. Che, *Crys. Growth Des.* 2009, *9*, 1444-1451; c) H. Fenton, I. S. Tidmarsh, M. D. Ward, *Dalton Trans.* 2010, *39*, 3805-3815; d) V. Rosa, C. Fliedel, A. Ghisolfi, R. Pattacini, T. Aviles, P. Braunstein, *Dalton Trans.* 2013, *42*, 12109-12119; e) P. Yang, F. Cui, X.-J. Yang, B. Wu, *Crys. Growth Des.* 2013, *13*, 186-194.

[11] R. Peng, M. Li, D. Li, *Coord. Chem. Rev.* 2010, *254*, 1-18.

[12] Refers to entries in WebCSD data base searching Cu-As distances on 1.08.2016 (http://webcsd.ccdc.cam.ac.uk/index.php).

[13] J. Besinger, D. Fenske, *Z. Anorg. Allg. Chem.* 2001, *627*, 1487-1494.

[14] P. J. J. A. Timmermans, A. Mackor, A. L. Spek, B. Kojić-Prodić, *J. Organomet. Chem.* 1984, *276*, 287-295.

[15] Since **4** crystallises together with **5**, the yield could not be determined.

[16] a) H. Sitzmann, T. Dezember, W. Kaim, F. Baumann, D. Stalke, J. Kärcher, E. Dormann, H. Winter, C. Wachter, *Angew. Chem. Int. Ed.* 1996, *35*, 2872-2874; b) M. Wallasch, G. Wolmershäuser, H. Sitzmann, *Angew. Chem. Int. Ed.* 2005, *43*, 2597-2599; c) M. D. Walter, J. Grunenberg, P. S. White, *Chem. Sci.* 2011, *2*, 2120-2130.

[17] C. Heindl, A. Kuntz, E. V. Peresypkina, A. V. Virovets, M. Zabel, D. Ludeker, G. Brunklaus, M. Scheer, *Dalton Trans.*2015, *44*, 6502-6509.

[18] According to the proposed dissociation of [Cp*Fe(μ-Br)]$_2$ to [Cp*$_2$Fe] and FeBr$_2$ (reference [16]), characterisation of the reaction mixture of **1** and [Cp'''Co(μ-Cl)]$_2$ by ^{1}H NMR spectroscopy should offer an opportunity to give an insight in the reaction process.

[19] Y. Morino, T. Ukaji, T. Ito, *Bull. Chem. Soc. Jpn.* 1966, *39*, 64-71.

[20] H. A. Spinney, N. A. Piro, C. C. Cummins, *J. Am. Chem. Soc.* 2009, *131*, 16233-16243.

[21] C. von Hänisch, D. Fenske, F. Weigend, R. Ahlrichs, R. Ahlrichs, F. Weigend, *Chem. Eur. J.* 1997, *3*, 1494-1498.

[22] K. Wade, *Adv. Inorg. Chem. Radiochem.* 1976, 18, 1-66.

[23] D. M. P. Mingos, *Acc. Chem. Res.* 1984, *17*, 311-319.

[24] a) O. J. Scherer, K. Pfeiffer, G. Heckmann, G. Wolmershäuser, *J. Organomet. Chem.* 1992, *425*, 141-149; b) M. Detzel, K.Pfeiffer, O. J. Scherer, G. Wolmershäuser, *Angew. Chem. Int. Ed. Engl.* 1993, *32*, 914-916; c) G. Friedrich, O. J. Scherer, G. Wolmershäuser, *Z. Anorg. Allg. Chem.* 1996, *622*, 1478-1486; d) C. v. Hänisch, D. Fenske, *Z. Anorg. Allg. Chem.* 1998, *624*, 367-369; e) H. Krauss, *Ph.D. thesis*, Universität Regensburg, 2011; f) S. Heinl, *Ph.D. thesis*, Universität Regensburg, 2014.

[25] O. J. Scherer, C. Blath, G. Wolmershäuser, *J. Organomet. Chem.* 1990, *387*, C21-C24.

[26] F. Baumann, E. Dormann, Y. Ehleiter, W. Kaim, J. Kärcher, M. Kelemen, R. Krammer, D. Saurenz, D. Stalke, C. Wachter, G. Wolmershäuser, H. Sitzmann, *J. Organomet. Chem.* 1999, *587*, 267-283.

[27] O. V. Dolomanov, L. J. Bourhis, R. J. Gildea, J. A. K. Howard, H. Puschmann, *J. Appl. Cryst.* 2009, *42*, 339-341.

[28] G. M. Sheldrick, *Acta Cryst.* 2015, *A71*, 3-8.

[29] M. C. Burla, R. Caliandro, M Camalli, B Carrozzini, G. L. Cascarano, L. De Caro, C. Giacovazzo, G. Polidori, D. Siliqi, R. Spagna, *J. Appl. Cryst.* 2007, *40*, 609-613.

[30] G. M. Sheldrick, *Acta Cryst.* 2015, *C71*, 3-8.

[31] CrysAlisPro, Version 1.171.38.42b, Agilent Technologies UK Ltd, Oxford, UK.

[32] R. C. Clark, J. S. Reid, *Acta Cryst.* 1995, *A51*, 887-897.

[33] CrysAlisPro, Version 1.171.37.33, Agilent Technologies UK Ltd, Oxford, UK.

[34] K. Brandenburg, H. Putz, Diamond3.0, Crystal and Molecular Structure Visualization, Crystal Impact GbR, Bonn, Germany, 2014.

8. A Breakthrough in Redox Chemistry: The Chemical Reduction of [Cp*Fe(η^5-As$_5$)]

M. Schmidt, D. Konieczny, E. V. Peresypkina, A. V. Virovets, M. Bodensteiner, G. Balázs, F. Riedlberger, H. Krauss and M. Scheer

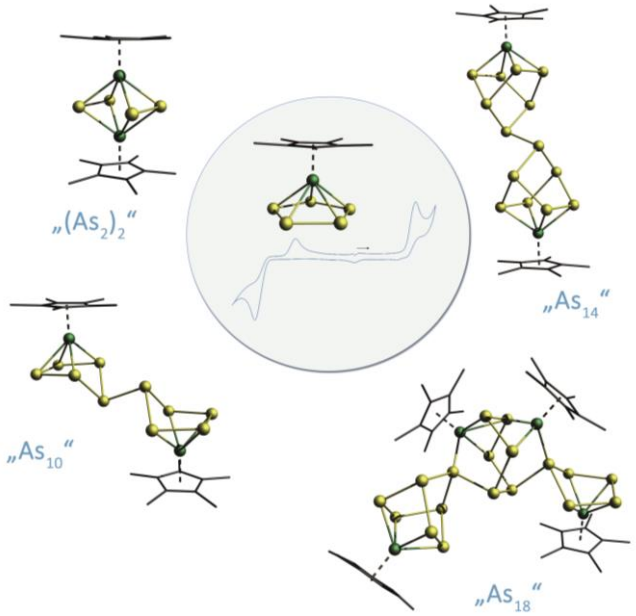

Abstract:

The redox chemistry of [Cp*Fe(η^5-As$_5$)] (Cp* = η^5-C$_5$Me$_5$) has been investigated by cyclic voltammetry. It shows two irreversible oxidations as well as an irreversible reduction. Subsequent chemical reduction of [Cp*Fe(η^5-As$_5$)] with KH has been performed, resulting in the formation of a mixture of diverse anionic polyarsenide complexes. Besides the dianion [(Cp*Fe)$_2$(μ,η$^{4:4}$-As$_{10}$)]$^{2-}$ ([**1**]$^{2-}$) and the triple decker complex [{Cp*Fe(μ,η$^{2:2}$-As$_2$)}$_2$]$^-$ ([**2**]$^-$), even larger polyarsenide As$_n$ frameworks - up to n = 14 and n = 18 – stabilised by [Cp*Fe] fragments could be obtained. This includes [(Cp*Fe)$_2$(μ,η$^{4:4}$-As$_{14}$)]$^{2-}$ ([**3**]$^{2-}$) as well as [(Cp*Fe)$_4${μ$_4$,η$^{4:4:4:4}$-As$_{18}$}]$^{2-}$ ([**4**]$^{2-}$). Along with compound [**3**]$^{2-}$, the dianion [**4**]$^{2-}$ represents the largest anionic As$_n$ ligand complex reported so far. Moreover, [**2**]$^-$ can also be obtained by treatment of [Cp*Fe(η^5-As$_5$)] with elemental potassium. All complexes were characterised by single crystal X-ray diffraction analysis as well as ^{1}H NMR spectroscopy. In addition, to get an insight in the electronic structure of [**1**]$^{2-}$, DFT calculations have been performed, showing a fast dimerisation of the presumably formed intermediate [Cp*Fe(η^5-As$_5$)]$^-$ to [**1**]$^{2-}$. Since [**2**]$^-$ is paramagnetic, it was characterised by EPR spectroscopy, revealing that the unpaired electron is localised at the [Fe$_2$As$_4$] core.

8.1 Author contributions

- All syntheses were first performed by David Konieczny during his master thesis and were additionally investigated in detail by Monika Schmidt.
- The thorough characterisation of all compounds was performed by Monika Schmidt.
- Manuscript was written by Monika Schmidt.
- Figures were made by Monika Schmidt.
- Cyclovoltammetric measurement of [Cp*Fe(η^5-As_5)] was performed by Dr. Hannes Krauss and is also part of his dissertation thesis (University of Regensburg 2011).
- Cyclovoltammetric measurement of [K(dme)$_2$][**2**] was performed and interpreted by Felix Riedlberger.
- Single crystal X-ray structure analyses of [K(dme)$_3$]$_2$[**1**] and [K(dme)$_2$]$_2$[**3**] and the refinements were performed by Dr. Eugenia V. Peresypkina, Dr. Alexander V. Virovets and Monika Schmidt.
- Single crystal X-ray structure analyses of [K(dme)$_2$][**2**], ([K(18-crown-6)(dme)$_2$]$_2$[**3'**]) and [K(dme)$_4$]$_2$[**4**] and the refinements were performed by Dr. Michael Bodensteiner and David Konieczny.
- DFT computations and their description regarding [K(dme)$_3$]$_2$[**1**] were performed by Dr. G. Balázs.
- EPR simulation of [K(dme)$_2$][**2**] and corresponding figures were performed/made by Dr. G. Balázs.
- Acknowledgement: The EPR spectrum of [K(dme)$_2$][**2**] was recorded by Moritz Modl.

8.2 Introduction

Ferrocene [Cp_2Fe] (**I**, Cp = η^5-C_5H_5) and its derivatives belong to the most frequently used compounds in organometallic chemistry, e.g. for catalysis[1] and bioorganometallic purposes.[2] Since **I** is redox active, it has also found application in redox switchable systems[3] or as a reference in cyclovoltammetry. While the oxidation of **I** to [**I**]$^+$ is a reversible one electron process, the electrochemical oxidation and reduction of the pentaphosphaferrocene derivative [Cp*Fe(η^5-P_5)] (**II**), which is isolobal to **I**, is more complex.[4] Both processes of oxidation and reduction are irreversible in nonaqueous solvents but reversible in bulk electrolysis. Furthermore, complex **II** is first oxidised to [**II**]$^+$ (17 VE) followed by a rapid dimerisation into the dication [$\mathbf{II}_2$]$^{2+}$. The same dimerisation behaviour has been observed for the reduction of **II** to [**II**]$^-$ (19 VE) followed by its rapid dimerisation to [$\mathbf{II}_2$]$^{2-}$. In 2013, the proposed compounds [$\mathbf{II}_2$]$^{2+}$ and [$\mathbf{II}_2$]$^{2-}$ as well as the dianionic doubly reduced [**II**]$^{2-}$ could be fully characterised and the structures of [$\mathbf{II}_2$]$^{2+}$ and [$\mathbf{II}_2$]$^{2-}$

have been determined by single crystal X-ray diffraction analysis (Scheme 8.1).[5] Besides the reduction with elementary potassium or potassium hydride the reduction of **II** by divalent lanthanide complexes has also been realised, leading to the formation of mixed d/f triple decker complexes[6] and reductive P-P bond formation.[7]

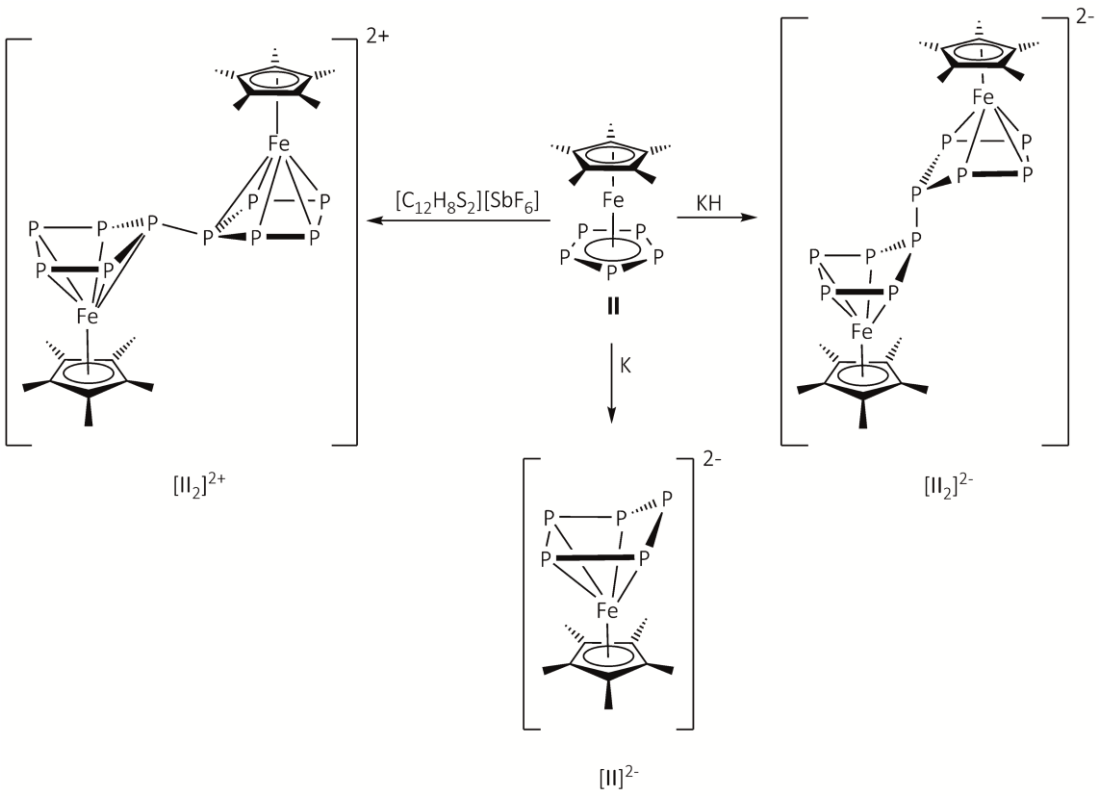

Scheme 8.1 Reduction and oxidation of **II**.[5]

In contrast to the relatively well investigated redox chemistry of **II**, little is known about the redox chemistry of the heavier congener [Cp*Fe(η^5-As$_5$)] (**III**). Although DFT calculations[8] and comparative studies on the charge distribution[9] based on Mössbauer spectroscopy exist and show only small differences between **II** and **III**, the experimentally found coordination behaviour of **II** is in sharp contrast to that of **III**. While **III** tends to form π-coordination through As-As bonds (η^2-fashion), its lighter congener **II** favours a σ-coordination *via* the lone pairs (η^1-fashion), opening an access to fullerene like spherical aggregates and one and/or two dimensional polymers.[8,10] The results of the DFT calculations show a reversed ordering of the unoccupied orbitals (LUMO, LUMO+1) for **III** compared to **II**. However, the HOMO is localised at the *cyclo*-E$_5$ ring (E = P (**II**), As (**III**)) in both cases. Therefore, it is not surprising that the reduction of **III** by the divalent samarium complex [Cp''$_2$Sm(thf)] (Cp'' = η^5-1,3-C$_5$H$_3$^{t}Bu$_2$) leads to the formation of complexes containing different As$_n$ units instead of the expected dianionic complex [**III**$_2$]$^{2-}$.[11] While reduction of **II** enables the formation of new P-P bonds, **III** is completely rearranged by the

reduction with [Cp''$_2$Sm(thf)]. Depending on the solvent used, either [(Cp''$_2$Sm)(μ,η$^{4:4}$-As$_4$)(Cp*Fe)] (toluene) or [(Cp''$_2$Sm)$_2$As$_7$(Cp*Fe)] (*n*-pentane) is obtained.

Therefore, it has been of fundamental interest whether an electrochemical redox reaction of **III** would first lead to the formation of the ionic species [Cp*Fe(η^5-As$_5$)]$^{+/-}$ followed by dimerisation to [**III**$_2$]$^{2+}$ and [**III**$_2$]$^{2-}$, respectively. Furthermore, the question arose whether the reactivity of **III** towards elemental potassium or KH proceeds analogously to that of **II** or similar to the reduction with [Cp''$_2$Sm(thf)]. Herein, we report on the reduction of **III** with K and KH, which leads to an unprecedented rearrangement of the former *cyclo*-As$_5$ moiety to yield [(Cp*Fe)$_2$(μ,η$^{4:4}$-As$_{10}$)]$^{2-}$ ([**1**]$^{2-}$ ≡ [**III**$_2$]$^{2-}$) and [{Cp*Fe(μ,η$^{2:2}$-As$_2$)}$_2$]$^-$ ([**2**]$^-$) as well as the arsenic rich ligand complexes [(Cp*Fe)$_2$(μ,η$^{4:4}$-As$_{14}$)]$^{2-}$ ([**3**]$^{2-}$) and [(Cp*Fe)$_4${μ$_4$,η$^{4:4:4:4}$-As$_{18}$)]$^{2-}$ ([**4**]$^{2-}$), which is the largest one reported so far.

8.3 Results and Discussion

Since the redox chemistry of **III** has not been studied by electrochemical methods, cyclic voltammetry has been used to get insight in its redox behaviour. In Figure 8.1, the cyclic voltammogram of **III** in CH_2Cl_2 is depicted.

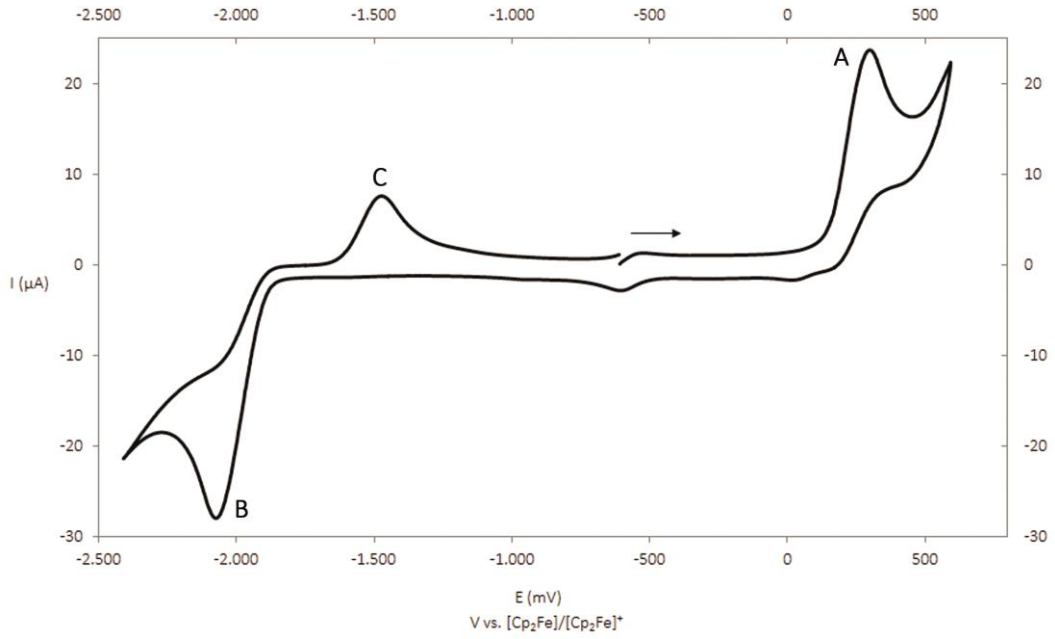

Figure 8.1 Cyclic voltammogram of **III** recorded at a platinum disc electrode in CH_2Cl_2 at 0.1 Vs^{-1} and referenced against [Cp_2Fe]/[Cp_2Fe]$^+$; supporting electrolyte [^{n}Bu$_4$N][PF$_6$] (0.1 mol/L).

Here, **III** shows an irreversible reduction (peak **B**: E_B= -2.08 V; **II**: E = -2.05 V) and an irreversible oxidation (peak **C**, E_c = -1.48 V; **II**: E = -1.34 V). Consequently, it could be expected that **III** undergoes reduction to [**III**]$^-$ and subsequent dimerisation to [**III**$_2$]$^{2-}$ as well as reoxidation to **III**, as

the cyclic voltammogram (CV) shows close similarity to the CV of the pentaphosphaferrocene derivative **II**.[4] Moreover, complex **III** exhibits an irreversible oxidation (peak **A**, E_A = +0.29 V). However, if the electrochemical oxidation (peak **A**) is studied only in the relevant range at different scan rates (v = 0.02 Vs^{-1} to v = 1.2 Vs^{-1}), the oxidation of **III** to [**III**]$^+$ appears to be reversible especially for higher scan rates (approximately $E_{1/2}$= +0.29 V, v = 0.8 Vs^{-1} to v = 1.2 Vs^{-1}) (Figure 8.2). In summary, the reduction behaviour of **III** is similar to that of **II**, whereas the oxidation process of **III** differs to **II**.

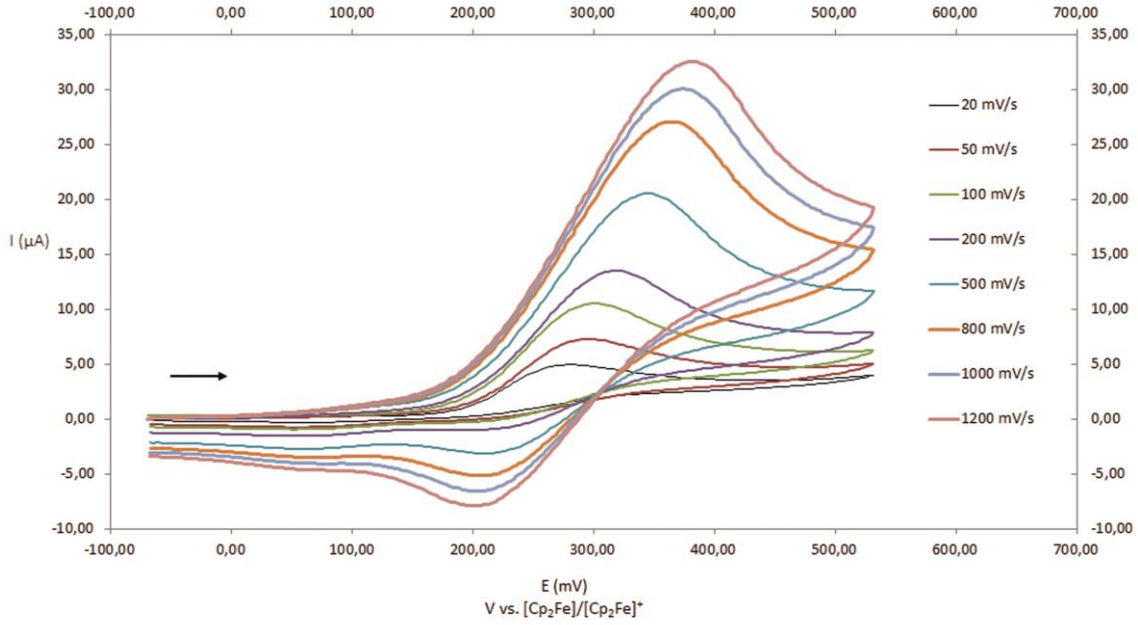

Figure 8.2 Cyclic voltammogram of the reversible oxidation (peak **A**) of **III** recorded at a platinum disc electrode in CH_2Cl_2 at different scan rates and referenced against $[Cp_2Fe]/[Cp_2Fe]^+$; supporting electrolyte $[^nBu_4N][PF_6]$ (0.1 mol/L).

The reaction of **III** with KH in dme at room temperature results in the formation of a mixture of $[\mathbf{1}]^{2-}$, $[\mathbf{2}]^{-}$, $[\mathbf{3}]^{2-}$ and $[\mathbf{4}]^{2-}$ (Scheme 8.2). In contrast, the reaction of **III** with elemental K at analogous reaction conditions yields $[\mathbf{2}]^{-}$.

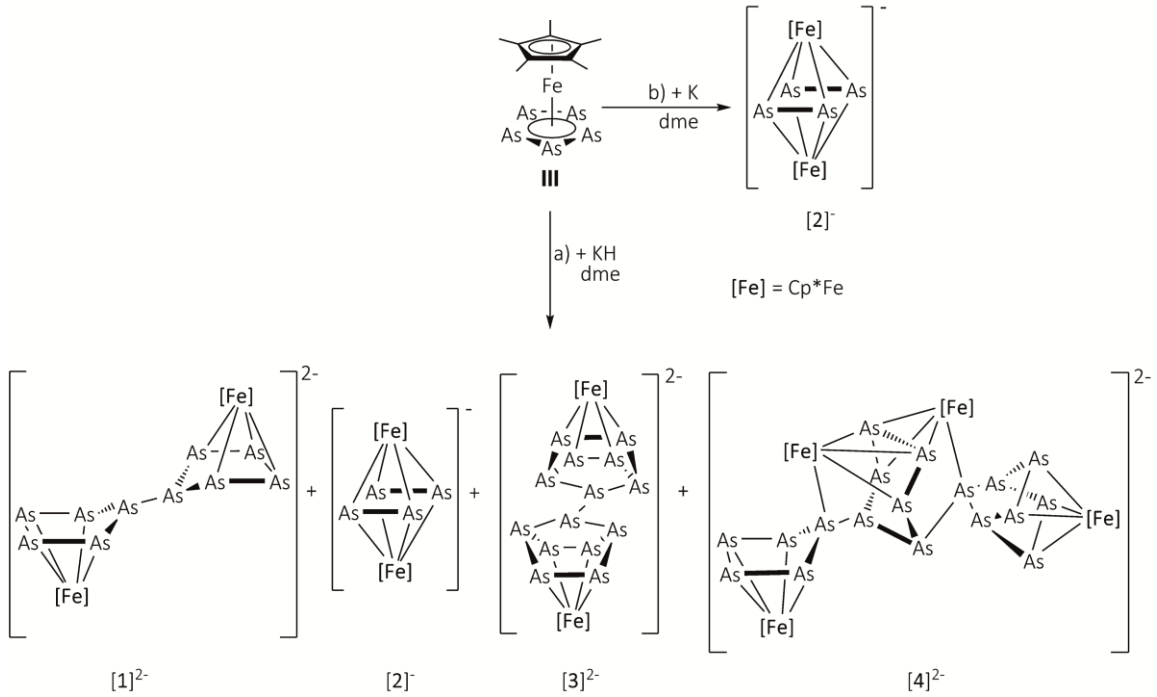

Scheme 8.2 Reactivity of **III** towards a) KH in dme and b) K in dme. Both reactions are performed at room temperature.

Crystals suitable for single crystal X-ray diffraction analysis can be obtained by layering the reaction mixture with *n*-hexane after complete diffusion at 0 °C. However, $[\mathbf{1}]^{2-}$, $[\mathbf{2}]^{-}$, $[\mathbf{3}]^{2-}$ and $[\mathbf{4}]^{2-}$ crystallise simultaneously as potassium salts. Hitherto, the separation of a sizeable amount of analytically pure samples was not possible due to their similar physical properties, colour and crystal shape. Nevertheless, few crystals of $[\mathbf{1}]^{2-}$, $[\mathbf{2}]^{-}$, $[\mathbf{3}]^{2-}$ and $[\mathbf{4}]^{2-}$ could be separated under the microscope from the reaction mixture. Consequently, the signals in the ^{1}H NMR spectra of all polyarsenide complexes could be tentatively assigned (Figure S8.1-S8.4, see supplementary information). All compounds are well soluble in dme or thf, slightly soluble in CH_3CN and insoluble in n-hexane, n-pentane or toluene. Solutions of $[\mathbf{1}]^{2-}$, $[\mathbf{2}]^{-}$, $[\mathbf{3}]^{2-}$ and $[\mathbf{4}]^{2-}$ in CH_2Cl_2 decompose over an extended period of time. Moreover, the formation of $[\mathbf{2}]^{-}$ is also observed by the reaction of **III** with elemental potassium. Although the ^{1}H NMR spectrum of the reaction mixture gives evidence for the presence of other polyarsenides in the reaction mixture, compound $[\mathbf{2}]^{-}$ is the only isolable product so far.

Complex $[\mathbf{1}]^{2-}$ can be obtained as dark brown blocks as the potassium salt $[K(dme)_3]_2[\mathbf{1}]$ and crystallises in the monoclinic space group $P2_1/n$. In Figure 8.3, the molecular structure of the

dianion $[\mathbf{1}]^{2-}$ in the solid state is depicted. Only half of the molecule can be found in the asymmetric unit, the other half is generated by symmetry.

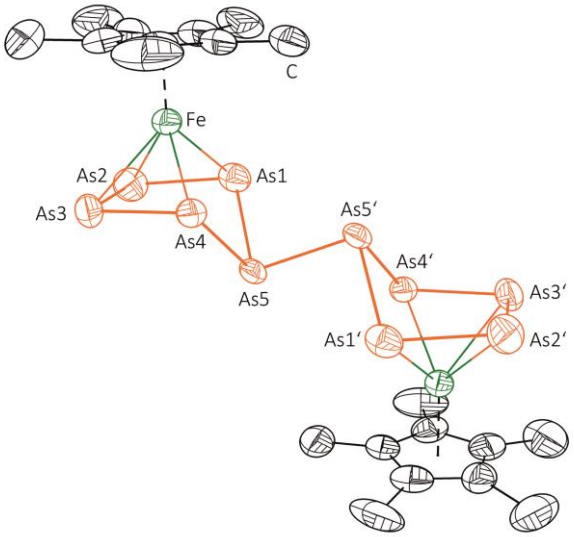

Figure 8.3 Molecular structure of $[\mathbf{1}]^{2-}$ in the solid state. Counterions, solvent molecules and H atoms are omitted for clarity. Thermal ellipsoids are drawn at 50 % probability level. Selected bond lengths [Å],angles [°] and torsion angles [°]: As1-As2 2.3712(14), As2-As3 2.37354(14), As3-As4 2.3691(12), As4-As5 2.4382(11), As1-As5 2.4367(13), As5-As5' 2.4398(16), As1-As5-As4 81.34(4), As1-As5-As5' 93.01(5), As4-As5-As5' 92.52(5), As1-As5-As5'-As4' 98.55(4), As4-As5-As5'-As4' 180.00(7).

The single crystal X-ray structure analysis of $[\mathbf{1}]^{2-}$ reveals a bridging As_{10} ligand consisting of two η^4-coordinating As_5 units in an envelope conformation, which are connected by an As-As single bond. The As-As bond lengths within the As_5 moiety of $[\mathbf{1}]^{2-}$ are in the range of an As-As double bond (2.245(1) Å in $[\{(Me_3Si)_3CAs\}_2]$),[12] but elongated in comparison to **III** (2.317(1) Å - 2.330(1) Å).[13] The remaining As-As bond lengths are in good agreement with an As-As single bond (electron diffraction: 2.435 Å in As_4,[14] DFT calculations: 2.4372 Å in As_4[15]). The As_{10} ligand of $[\mathbf{1}]^{2-}$ represents the all arsenic analogue of dihydrofulvalene and has only been found before in neutral transition metal complexes such as $[(Cp^RM)_4(\mu_4,\eta^{4:4:2:2:1:1}\text{-}As_{10})]$ (M = Co, Cp^R = Cp''',[19] Cp^{Bn};[16] M = Rh, Cp^R = Cp'' (η^5-1,3-$C_5H_3{}^tBu_2$)[17]). Although $[\mathbf{1}]^{2-}$ is expected to be isostructural to the phosphorus derivative $[\mathbf{II}_2]^{2-}$, its molecular structure differs especially in the conformation around the bridging E-E bond (E = P ($[\mathbf{II}_2]^{2-}$), As ($[\mathbf{1}]^{2-}$)). The bridging As-As bond (As5-As5') in $[\mathbf{1}]^{2-}$ points towards the [Cp*Fe] moieties representing an *exo* conformation of the η^4-As_5 moieties (Figure 8.4). In contrast, the bridging P1-P10 bond in $[\mathbf{II}_2]^{2-}$ points away from the [Cp*Fe] fragments which matches an *endo* arrangement of the η^4-P_5 unit. A similar conformation to $[\mathbf{1}]^{2-}$ has been observed for the oxidised phosphorus species $[\mathbf{II}_2]^{2+}$, however the envelope type P_5 units are less distorted from planarity than in $[\mathbf{II}_2]^{2-}$ and still η^5-coordinated to the [Cp*Fe] fragments (Figure 8.4).

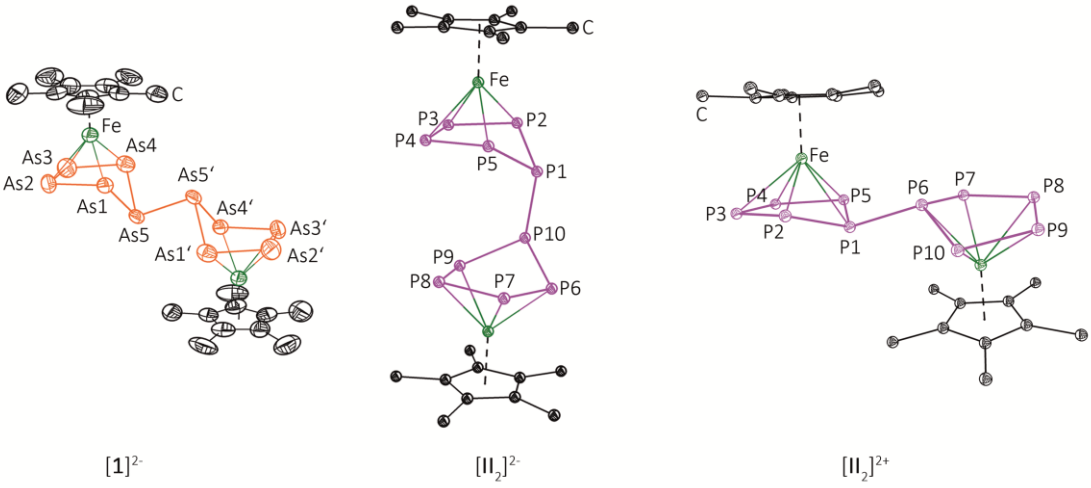

$[\mathbf{1}]^{2-}$ $[\mathbf{II}_2]^{2-}$ $[\mathbf{II}_2]^{2+}$

Figure 8.4 Comparison of the molecular structure of $[\mathbf{1}]^{2-}$ (left), $[\mathbf{II}_2]^{2-}$[5] (middle) and $[\mathbf{II}_2]^{2+}$[5] (right) in the solid state. Counterions, solvent molecules and H atoms are omitted for clarity. In case of disorder the main part is depicted. Thermal ellipsoids are drawn at 50 % probability level.

This feature is also apparent if the torsion angles of $[\mathbf{1}]^{2-}$, $[\mathbf{II}_2]^{2-}$ and $[\mathbf{II}_2]^{2+}$ are compared (Table 8.1). In $[\mathbf{1}]^{2-}$ the relevant torsion angle is 98.55(4)° (As4-As5-As5'-As1'), presenting an *anti* conformation of the $[Cp^*Fe(\eta^4\text{-}As_5)]^-$ units. In contrast, the corresponding torsion angle in $[\mathbf{II}_2]^{2-}$ are found to be 22.37(9)° (P5-P1-P10-P9) rather indicating a *syn* conformation of the $[Cp^*Fe(\eta^4\text{-}P_5)]^-$ moieties. In $[\mathbf{II}_2]^{2+}$, the relevant torsion angle is 67.75(10)° (P10-P6-P1-P2). Selected torsion angles of $[\mathbf{1}]^{2-}$, $[\mathbf{II}_2]^{2-}$ and $[\mathbf{II}_2]^{2+}$ are summarised in Table 8.1.

Table 8.1 Selected torsion angles [°] for **1**, $[\mathbf{II}_2]^{2-}$[5] and $[\mathbf{II}_2]^{2+}$.[5]

1		$[\mathbf{II}_2]^{2-}$		$[\mathbf{II}_2]^{2+}$	
As4-As5-As5'-As1'	98.55(4)	P5-P1-P10-P9	22.37(9)	P10-P6-P2-P1	67.75(10)
As4-As5-As5'-As4'	180.00(7)	P2-P1-P10-P9	-81.43(7)	P10-P6-P2-P1	-160.83(7)
		P6-P1-P10-P2	-80.66(7)	P7-P6-P1-P5	-27.67(9)
		P9-P1-P10-P2	175.55(5)	P7-P6-P1-P2	-159.09(7)

It has been expected that $[\mathbf{1}]^{2-}$ is the initial species formed by chemical reduction of **III** with KH, whereas compounds $[\mathbf{2}]^-$, $[\mathbf{3}]^{2-}$ and $[\mathbf{4}]^{2-}$ are established due to decomposition and reaggregation. To prove this, a sample of crystalline $[\mathbf{1}]^{2-}$ was dissolved in thf-d_8 and ^{1}H NMR spectra have been recorded over a period of one week. Within this time, the NMR tube has been exposed to light and stored at room temperature. Surprisingly, neither new signals, nor grey arsenic could be observed, indicating the decomposition of $[\mathbf{1}]^{2-}$. This is additionally confirmed by the fact that all compounds seem to crystallise simultaneously from the reaction mixture.

To get an insight into the electronic structure of [**1**]$^{2-}$, DFT calculations have been performed at the BP86/def2-TZVP level. The DFT results reveal a dimerisation of the presumably formed intermediate [Cp*Fe(η^5-As$_5$)]$^-$ to [**1**]$^{2-}$, which is with 42.0 kJ·mol^{-1} exothermic. Furthermore, in [Cp*Fe(η^5-As$_5$)]$^-$ 33% of the spin density is localised on the bent arsenic atom, indicating why a fast dimerisation to [**1**]$^{2-}$ occurs. The inspection of the molecular orbitals in [**1**]$^{2-}$ shows that the occupied frontier molecular orbitals are iron centred (d orbitals), which are basically nonbonding. Only starting with HOMO-4, the molecular orbitals contain atomic orbital contributions from arsenic (Figure 8.5). In contrast, the LUMO's are mainly localised on the As$_{10}$ unit. The natural population analysis (NPA) displays that the negative charge is spread over the Cp* and the As$_{10}$ ligand. In one As$_5$ unit in [**1**]$^{2-}$ the atom As5 bares the least negative charge (-0.08 e$^-$), followed by As1 and As4 (-0.10 e$^-$), while As3 and As4 carry the most negative charge (-0.14 e$^-$) (numbering according to the X-ray structure in Figure 8.3). The Wiberg Bond Indices (WBI) indicate the presence of As-As single bonds (WBI 0.95 to 1.13).

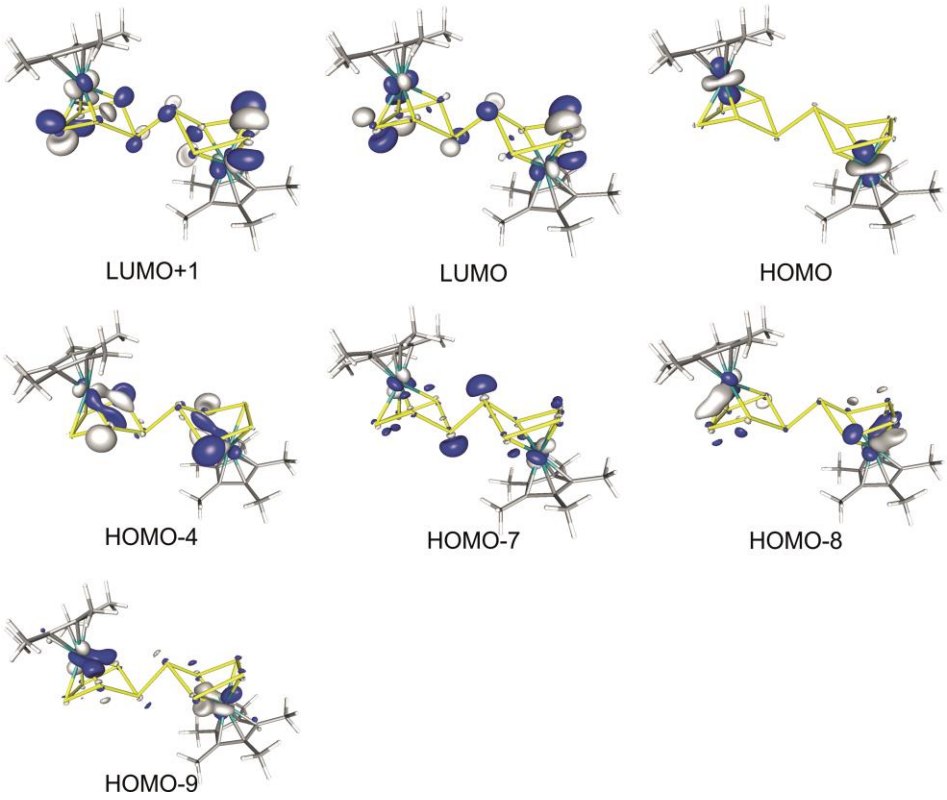

Figure 8.5 Selected molecular orbitals in [**1**]$^{2-}$, calculated at the BP86/def2-TZVP level.

Complex [**2**]$^-$ crystallises as dark brown blocks as the potassium salt [K(dme)$_4$][**2**] in the triclinic space group $P\bar{1}$. The central structural motif of [**2**]$^-$ in the solid state is a triple decker complex with two As$_2$ units as middle deck, which is severely disordered over four positions with

occupancy factors of 0.51, 0.41, 0.05 and 0.03 (Figure 8.6 for the main occupied part, for representation of the disorder of the two As_2 units see Figure S8.9, supplementary information).

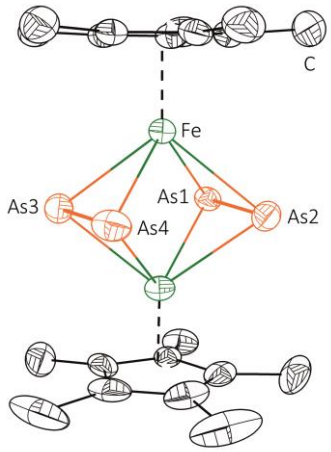

Figure 8.6 Molecular structure of [**2**]$^-$ (main part) in the solid state. Counterion, solvent molecules and H atoms are omitted for clarity. Due to disorder only the main part is depicted. Thermal ellipsoids are drawn at 50 % probability level. Selected bond lengths [Å] and angles [°]: As1-As2 2.333(3), As3-As4 2.334(3), As1···As3 3.169(5), As2···As4 3.007(4), As2-As1-As2 87.44(4), As1-As3-As4 88.56(7), As3-As4-As2 91.38(5), As4-As2-As1 92.59(2).

The As-As bond lengths of the As_2 ligands of [**2**]$^-$ lie between an As-As single and double bond (2.333(3) Å, 2.334(3) Å). Hence, the As-As bond lengths are in line with literature known neutral triple decker complexes of cobalt [{Cp^{R}Co(μ,η$^{2:2}$-As$_2$)}$_2$] (Cp^R = Cp*,[18] Cp' (η^5-C$_5$EtMe$_4$),[18] Cp''' (η^5-1,2,4-C$_5$H$_2$^{t}Bu$_3$),[19] Cp^{Bn} (η^5-C$_5${CH$_2$(C$_6$H$_5$)}$_5$)[20]). In contrast, the As1···As3 distances (3.169(5) Å) and As2···As4 (3.007(4) Å) distances are considerably longer in [**2**]$^-$, but nevertheless still shorter than the sum of the van der Waals radii of arsenic (3.7 Å),[21] indicating the presence of some weak interactions between the As_2 units. Interestingly, the chemical reduction of **III** by the divalent samarium complex [Cp''$_2$Sm(thf)] leads to [(Cp''$_2$Sm)(μ,η$^{4:4}$ -As$_4$)(Cp*Fe)], containing a *cyclo*-As_4 unit.[11]

As the As_2 ligand can be considered as a two π-electron donor, [**2**]$^-$ can be best described as a 31 VE complex. Accordingly, [**2**]$^-$ should exhibit paramagnetic behaviour due to the presence of at least one unpaired electron. Indeed, the EPR spectrum of [**2**]$^-$ in thf at 77 K shows an anisotropic signal indicating an unpaired electron which is expected to be localised on the central [Fe_2As_4] unit (see Figure S8.5 and simulated EPR spectra Figure S8.6, supplementary information). In the series of neutral triple decker complexes of iron [(Cp^{R}Fe)$_2$(μ,η$^{4:4}$-As$_4$)] (Cp^R = Cp''',[22] Cp^{Bn}[23]) and [(Cp^{R}Fe)$_2$(μ,η$^{4:4}$-*cyclo*-As$_4$)] (Cp^R = Cp''',[22] Cp^{BIG} (η^5-C$_5${4-^{n}BuC$_6$H$_4$}$_5$)[24]), [**2**]$^-$ can be regarded as the corresponding reduced onefold negatively charged analogue. Conversely, [**2**]$^-$ is expected to be oxidised by an appropriate oxidising agent to yield the neutral triple decker complex which likely

possesses a butadiene like As_4 ligand as realised in [$(Cp^RFe)_2(\mu,\eta^{4:4}\text{-}As_4)$] ($Cp^R$ = Cp''', Cp^{Bn}).[22,23] In fact, the cyclic voltammogram of [**2**]$^-$ gives evidence for the reversible electrochemical oxidation of [**2**]$^-$ in thf ($E_{1/2}$ = -1.2 V vs. [Cp_2Fe]/[Cp_2Fe]$^+$; see Figure S8.8, supplementary information). Unfortunately, the preparative chemical oxidation of [**2**]$^-$ could not be achieved regardless of several attempts.

Compound [**3**]$^{2-}$ crystallises as dark black prisms as the potassium salt [$K(dme)_2$]$_2$[**3**] in the monoclinic space group $P2_1/c$. Due to an inversion centre located in the middle of the As1-As1' bond, the As_{14} ligand is built up by only seven crystallographically independent arsenic atoms. In Figure 8.7, one of the two independent molecules of the asymmetric unit is depicted.

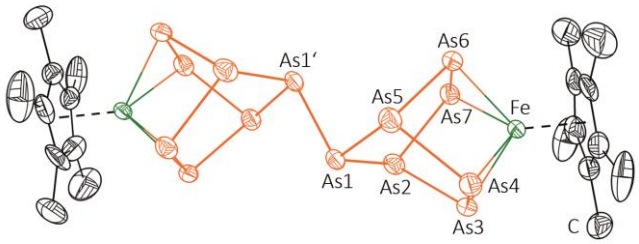

Figure 8.7 Molecular structure of [**3**]$^{2-}$ in the solid state. Only one of the two molecules of the asymmetric unit is depicted. Counterions, solvent molecules and H atoms are omitted for clarity. Thermal ellipsoids are drawn at 50 % probability level. Selected bond lengths [Å] and angles [°]: As1-As1' 2.4377(19), As1-As2 2.4026(16), As2-As3 2.4357(14), As3-As4 2.3563(14), As4-As5 2.4294(14), As5-As6 2.4423(15), As6-As7 2.3648(14), As1-As5 2.3901(15), As2-As7 2.4380(14), As1-As2-As3 106.30(6), As1-As5-As4 106.77(6), As1-As5-As6 98.55(5), As1-As2-As7 99.02(5), As2-As1-As5 102.15(5), As2-As1-As1' 97.50(7), As2-As3-As4 106.51(5), As3-As2-As7 80.60(4), As3-As4-As5 106.26(5), As4-As5-As6 81.82(5), As5-As1-As1' 97.39(6), As5-As6-As7 106.20(5).

The central structural motif of [**3**]$^{2-}$ exhibits an As_{14} ligand, which consists of two norbornadiene like As_7 moieties linked by an As-As bond. Each As_7 unit is η^4-coordinated to a [Cp*Fe] fragment. The As-As bond lengths within the coordinating arsenic atoms show double bond character (As3-As4 2.3563(14) Å, As6-As7 2.3648(14) Å) just like in the alkali metal derivative [Rb(18-crown-6)]$_4As_{14} \cdot 6\ NH_3$,[25] which has been synthesised by the use of Rb_4As_6 in liquid ammonia. Compared to [Rb(18-crown-6)]$_4As_{14} \cdot 6\ NH_3$ the As-As distances to the apical arsenic atom As1 (As1-As2 2.4026(16) Å, As1-As5 2.3901(15) Å) are slightly shortened due to delocalisation of the negative charge of the [Cp*Fe] fragments. The remaining As-As bond lengths range from 2.4294(14) Å to 2.4423(15) Å, which is in line with As-As single bond lengths. While [**3**]$^{2-}$ originates formally by the oxidative coupling of two norbornadiene like As_7^{3-} cages stabilised by [Cp*Fe] fragments, the reduction of **III** with [Cp''$_2$Sm(thf)] yielded to [(Cp''$_2$Sm)$_2As_7$(Cp*Fe)][11] inter alia, containing a norbornadiene like As_7 unit. Therefore, besides the alkali metal derivatives of the Zintl anion $[As_{14}]^{4-}$,[25,26] [**3**]$^{2-}$ represents the first characterised transition metal complex

containing an As_{14} ligand. Other neutral or charged As_{14} ligand complexes are not known in literature so far, although the norbornadiene structural motif has been realised in some transition metal complexes.[11,19,27,28]

The potassium salt $[K(dme)_4]_2$[**4**] crystallises as black brown blocks in the monoclinic space group $P2_1/c$ with two independent molecules of [**4**]$^{2-}$ in the asymmetric unit. The dianion [**4**]$^{2-}$ displays an unprecedented As_{18} ligand, consisting of three As_n subunits. Therein, a chair like *cyclo*-As_6 subunit (As6 to As11) is connected through two adjacent arsenic atoms to an envelope like As_5 unit and a norbornadiene like As_7 moiety *via* As-As single bonds (As5-As6 2.453(4) Å, As11-As12 2.442(3) Å), (Figure 8.8).

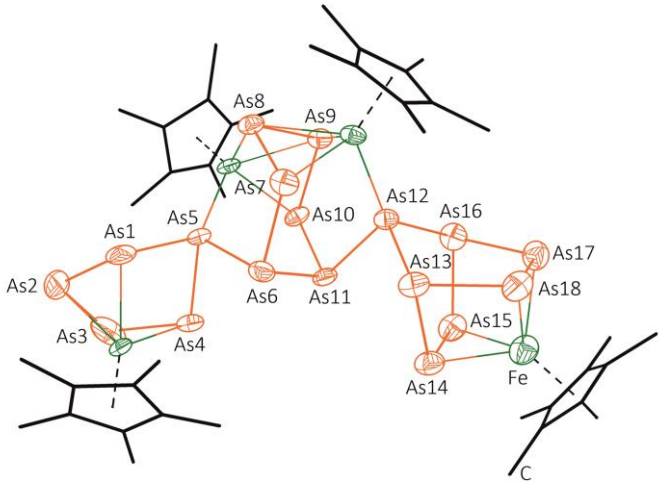

Figure 8.8 Molecular structure of [**4**]$^{2-}$ in the solid state. Only one of the two molecules of the asymmetric unit is displayed. Counterions, solvent molecules and H atoms are omitted for clarity. Cp* ligands are drawn in wire or frame model. Thermal ellipsoids are depicted at 50 % probability level. Selected bond lengths [Å] and angles [°]: As1-As2 2.360(6), As3-As2 2.353(8), As1-As5 2.447(4), As3-As4 2.357(4), As4-As5 2.441(3), As5-As6 2.453(4), As6-As7 2.451(4), As6-As11 2.419(4), As7-As8 2.384(4), As8-As9 2.570(4), As9-As10 2.384(3), As10-As11 2.439(4), As11-As12 2.442(3), As12-As13 2.469(4), As12-As16 2.445(4), As13-As14 2.416(4), As13-As18 2.438(4), As14-As15 2.374(5), As15-As16 2.432(4), As16-As17 2.429(4), As17-As18 2.358(5), As1-As5-As4 85.81(12), As1-As5-As6 90.77(15), As2-As1-As5 106.3(2), As2-As3-As4 101.42(18), As3-As4-As5 107.23(16), As4-As5-As6 86.29(12), As5-As6-As7 96.30(13), As5-As6-As11 90.68(13), As6-As7-As8 101.94(13), As6-As11-As10 104.31(13), As6-As11-As12 90.64(12), As7-As6-As11 102.79(12), As7-As8-As9 100.81(13), As8-As9-As10 100.75(12), As9-As10-As11 102.55(12), As11-As12-As13 95.05(12), As11-As12-As16 95.23(12), As12-As13-As14 101.46(14), As12-As13-As18 106.30(15), As12-As16-As15 100.79(14), As12-As16-As17 107.16(15), As13-As12-As16 99.46(14), As13-As14-As15 106.21(15), As13-As18-As17 106.55(15), As14-As13-As18 79.85(13), As14-As15-As16 106.73(14), As15-As16-As17 79.55(14), As16-As17-As18 106.65(15).

The As-As bond lengths within the envelope like As_5 moiety and the As_7 unit are similar to those of [**1**]$^{2-}$ and [**3**]$^{2-}$, respectively. The As-As bond distances in the *cyclo*-As_6 unit alternate, exhibiting two shorter As-As bond lengths (As7-As8 2.384(4) Å, As9-As10 2.384(3) Å) and four longer As-As bond lengths (As6-As7 2.451(4) Å, As6-As11 2.419(4) Å, As8-As9 2.570(4) Å,

As10-As11 2.439(4) Å). The latter are in the range of As-As single bond lengths. Merely, the As8-As9 distance is elongated but still in the range of single bonds. Considerably longer As-As distances, up to approximately 2.87 Å, have been reported in literature.[19,29] Among [**3**]$^{2-}$, the dianionic cluster [**4**]$^{2-}$ represents the largest As$_n$ ligand complex reported so far. Larger arsenic clusters are only reported for Zintl anions.[26,30]

In summary, we report on the electrochemical investigation of [Cp*Fe(η^5-As$_5$)] (**III**) by cyclic voltammetry. Thereby, **III** displays similar oxidation and reduction properties as the pentaphosphaferrocene derivative **II**, suggesting the formation of [**III**$_2$]$^{2-}$. Subsequent chemical reduction of **III** by KH or K leads to the unprecedented degradation and rearrangement of the former *cyclo*-As$_5$ ligand of **III** to yield different polyarsenic ligands stabilised by [Cp*Fe] fragments. Here, [(Cp*Fe)$_2$(μ,η$^{4:4}$-As$_{10}$)]$^{2-}$ ([**1**]$^{2-}$ ≡ [**III**$_2$]$^{2-}$), as well as the novel As$_n$ ligand complexes with n = 4 ([{Cp*Fe(μ,η$^{2:2}$-As$_2$)}$_2$]$^-$ ([**2**]$^-$)), 14 ([(Cp*Fe)$_2$(μ,η$^{4:4}$-As$_{14}$)]$^{2-}$ ([**3**]$^{2-}$)) and 18 ([(Cp*Fe)$_4${μ$_4$,η$^{4:4:4:4}$-As$_{18}$}]$^{2-}$ ([**4**]$^{2-}$)) are obtained. DFT calculations reveal a fast dimerisation of the presumably formed intermediate [Cp*Fe(η^5-As$_5$)]$^-$ to [**1**]$^{2-}$, which contains the centrosymmetric As$_{10}$ ligand. Remarkably, [**2**]$^-$, [**3**]$^{2-}$ and [**4**]$^{2-}$ are not formed due to decomposition of [**1**]$^{2-}$ followed by aggregation as assumed. The triple decker complex [**2**]$^-$ contains two As$_2$ units, representing the once reduced analogue of neutral triple decker complexes of the type [{Cp^{R}Fe}$_2$(μ,η$^{4:4}$-As$_4$)] (Cp^R = Cp’’’, Cp^{Bn}). Furthermore, [**2**]$^-$ exhibits paramagnetic behaviour due to at least one unpaired electron, which is localised on the central [Fe$_2$As$_4$] unit and confirmed by EPR spectroscopy. Additionally, [**3**]$^{2-}$ and [**4**]$^{2-}$ were isolated, displaying the largest As$_n$ ligand complexes up to date. Thereby, [**3**]$^{2-}$ contains two norbornadiene like As$_7$ units which are linked together to form an As$_{14}$ ligand, whereas [**4**]$^{2-}$ consists of a chair like As$_6$ subunit which is connected through adjacent arsenic atoms to an envelope like As$_5$ unit as well as to a norbornadiene like As$_7$ cage to give the unprecedented As$_{18}$ ligand. These observations show the potential of **III** for the formation of novel As$_n$ ligand complexes, which will be investigated further on.

8.4 Experimental Part

General Remarks

All reactions were performed under an atmosphere of dry argon using glovebox or Schlenk techniques. Solvents were purified, degassed and dried prior to use. [Cp*Fe(η^5-As$_5$)] was prepared according to literature procedure.[31] Elementary potassium and KH are commercially available and were used without further purification.

The ^{1}H NMR spectra were recorded on an Avance III HD 400 spectrometer. For this, a small amount of crystalline [K(dme)$_3$]$_2$[**1**], [K(dme)$_2$][**2**], [K(dme)$_2$]$_2$[**3**] or [K(dme)$_4$]$_2$[**4**] was isolated in the glovebox and washed with n-pentane The X-band EPR measurements of [K(dme)$_2$][2] were carried out with a MiniScope MS400 device with a frequency of 9.5 GHz and rectangular resonator TE102 of the company Magnettech GmbH. The EPR spectrum has been fitted using the program EasySpin.[32]

Synthesis of [K(dme)$_3$]$_2$[1], [K(dme)$_2$][2], [K(dme)$_2$]$_2$[3] and [K(dme)$_4$]$_2$[4]

To a mixture of [Cp*Fe(η^5-As$_5$)] (60 mg, 0.106 mmol) and KH (4 mg, 0.1 mmol) dme (20 mL) was added at room temperature. The reaction mixture turned brown immediately and little gas evolution was observed. After 24 h, the solvent was reduced to 10 mL and filtered into a thin Schlenk tube. The dark brown mixture was layered with *n*-hexane (20 mL) and stored at 0 °C under the exclusion of light. After complete diffusion, crystals of [K(dme)$_3$]$_2$[**1**], [K(dme)$_2$][**2**], [K(dme)$_2$]$_2$[**3**] and [K(dme)$_4$]$_2$[**4**] were obtained.

Crystalline yield: 37 mg (mixture of [K(dme)$_3$]$_2$[**1**], [K(dme)$_2$][**2**], [K(dme)$_2$]$_2$[**3**] and [K(dme)$_4$]$_2$[**4**]).

Alternatively, [K(dme)$_2$][**2**] can be also obtained by reacting [Cp*Fe(η^5-As$_5$)] (60 mg, 0.106 mmol) with K (17 mg, 0.424 mmol) in dme (15 mL) at room temperature. Within 1 h, the mixture turned from green to brown. After 4 h, the solution was filtered and the solvent was reduced to approximately 5 mL. Layering with *n*-hexane and storage at 0 °C lead to the formation of crystalline [K(dme)$_2$][**2**] as dark brown blocks.

Crystalline yield: 32 mg (mixture of [K(dme)$_2$][**2**] and unidentified products).

Analytical data of [K(dme)$_3$]$_2$[**1**]

^{1}H NMR (CD_2Cl_2): δ [ppm] = 1.39 (s, 30 H, $C_5(CH_3)_5$).

Analytical data of [K(dme)$_2$][**2**]

^{1}H NMR (CD_2Cl_2): δ [ppm] = 1.38 (s, 30H, $C_5(CH_3)_5$).

X-band EPR (77 K, CD_2Cl_2): g_{iso} = 2.008.

Analytical data of [K(dme)$_2$]$_2$[**3**]

^{1}H NMR (CD_2Cl_2): δ [ppm] = 1.39 (s, 30 H, $C_5(CH_3)_5$).

Analytical data of [K(dme)$_4$]$_2$[**4**]

^{1}H NMR (CD_2Cl_2): δ [ppm] = 1.44 (s, 60 H, $C_5(CH_3)_5$).

8.5 Supplementary Information

NMR Investigations

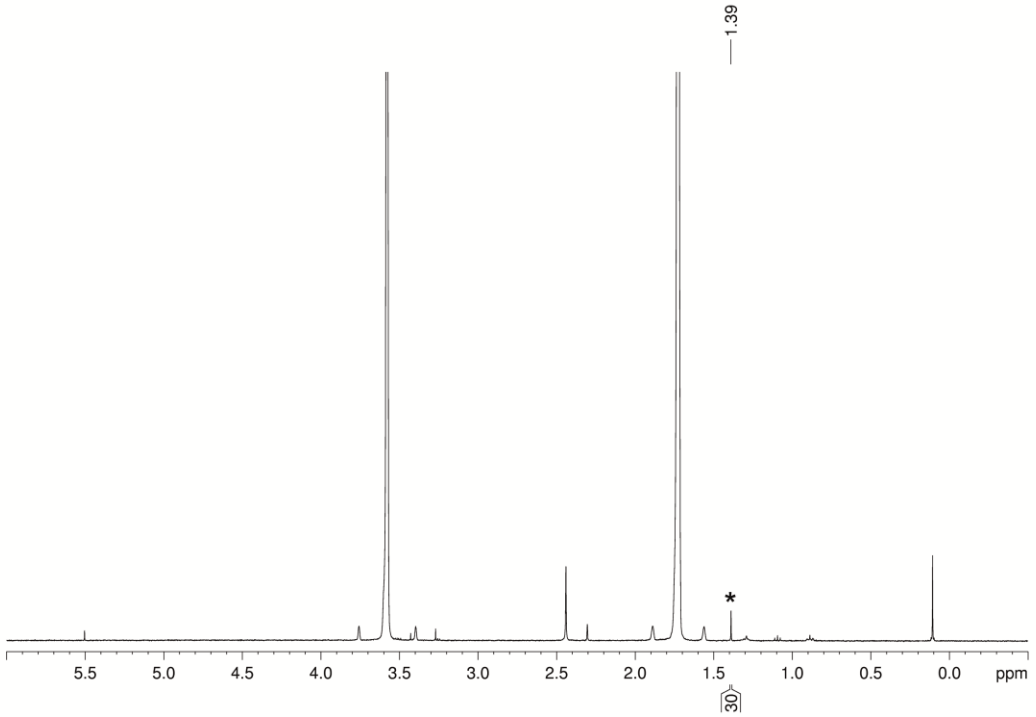

Figure S8.1 ^{1}H NMR spectrum of [K(dme)$_3$]$_2$[**1**] in thf-d$_8$ at 300 K. Signal of [K(dme)$_3$]$_2$[**1**] is marked with an asterisk. All other signals are due to different solvents and silicon grease.

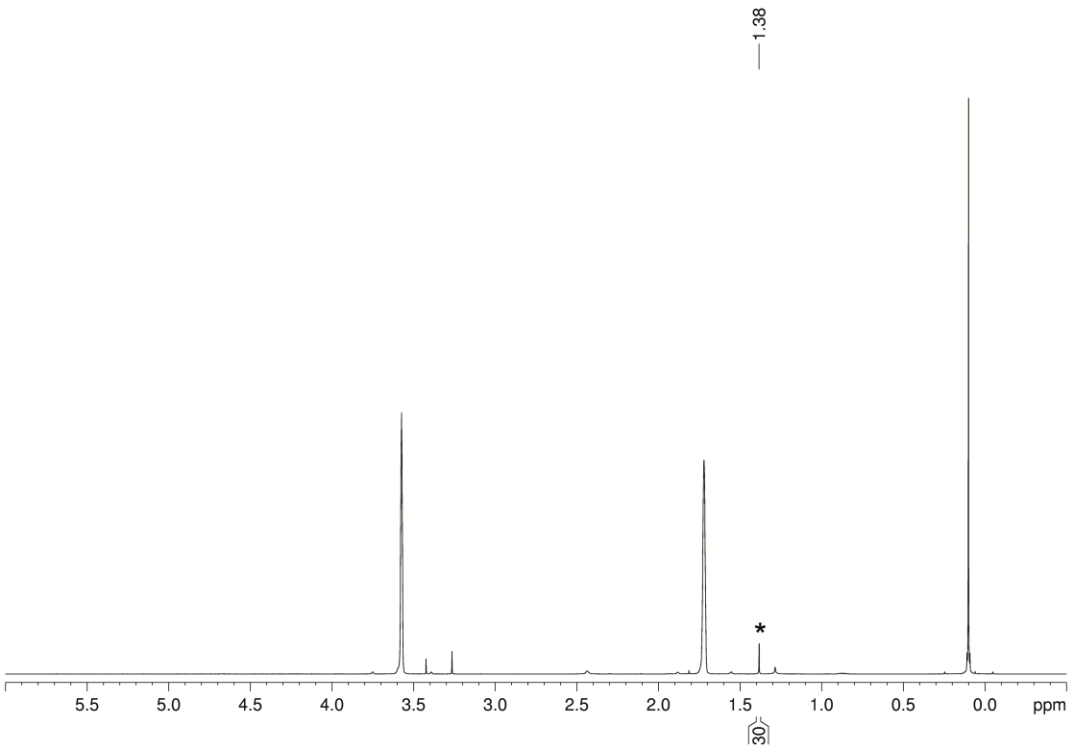

Figure S8.2 ^{1}H NMR spectrum of [K(dme)$_2$][**2**] in thf-d$_8$ at 300 K. Signal of [K(dme)$_2$][**2**] is marked with an asterisk. All other signals are due to different solvents and silicon grease.

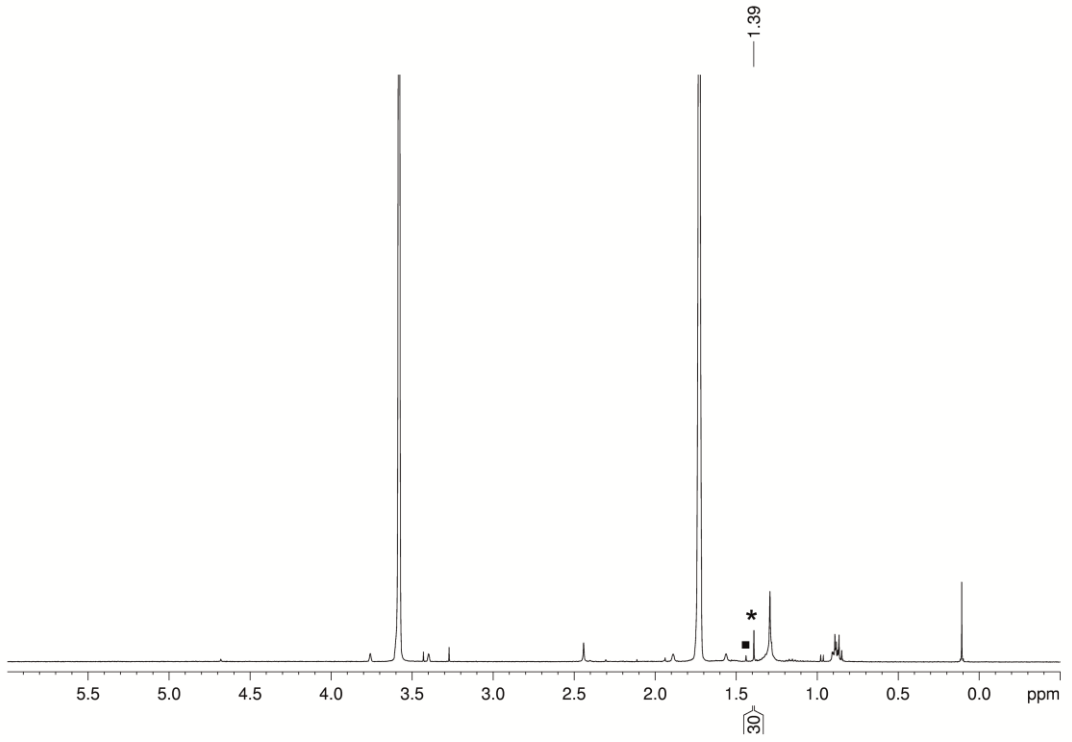

Figure S8.3 ^{1}H NMR spectrum of [K(dme)$_2$]$_2$[**3**] in thf-d$_8$ at 300 K. Signal of [K(dme)$_2$]$_2$[**3**] is marked with an asterisk. The signal marked with a square is due to impurities of [K(dme)$_4$]$_2$[**4**]. All other signals are due to different solvents and silicon grease.

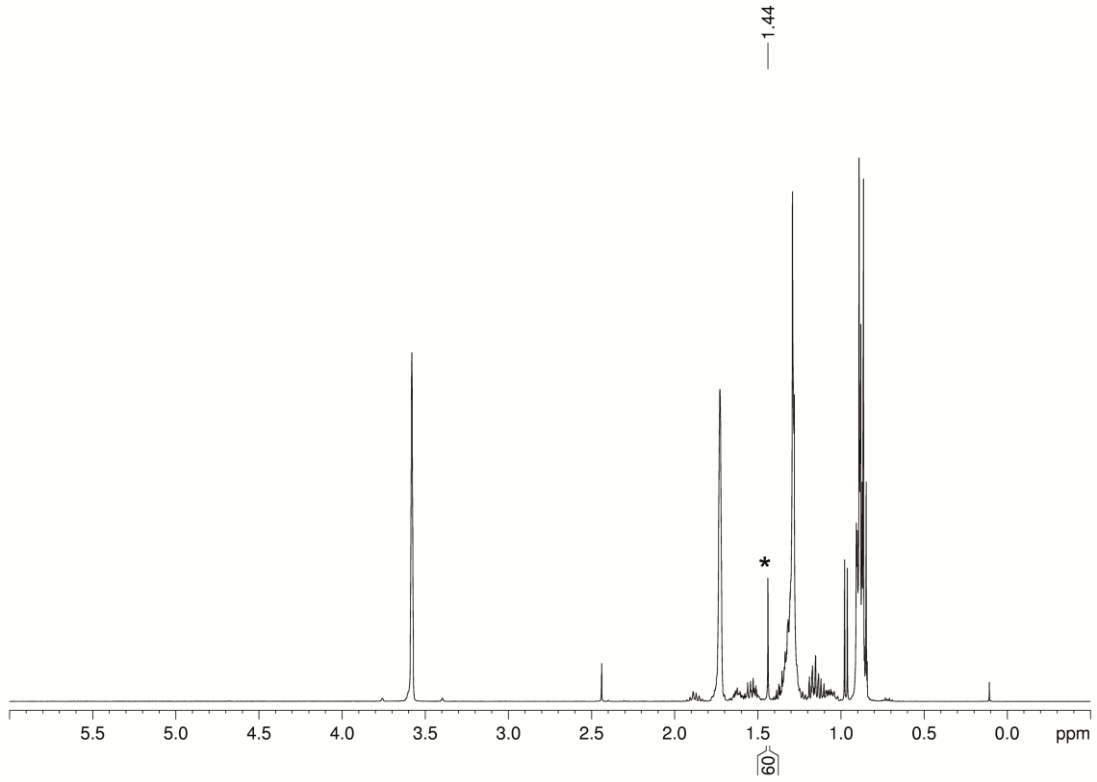

Figure S8.4 ^{1}H NMR spectrum of [K(dme)$_4$]$_2$[**4**] in thf-d$_8$ at 300 K. Signal of [K(dme)$_4$]$_2$[**4**] is marked with an asterisk. All other signals are due to different solvents and silicon grease.

Representation of the X-Band EPR spectra of [K(dme)$_2$][2]

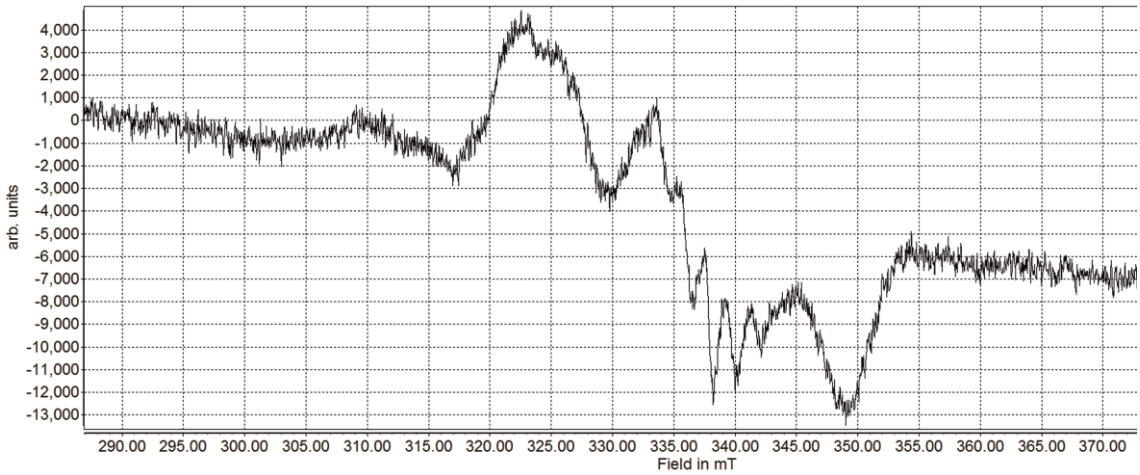

Figure S8.5 EPR spectrum of [K(dme)$_2$][**2**] in thf at 77 K.

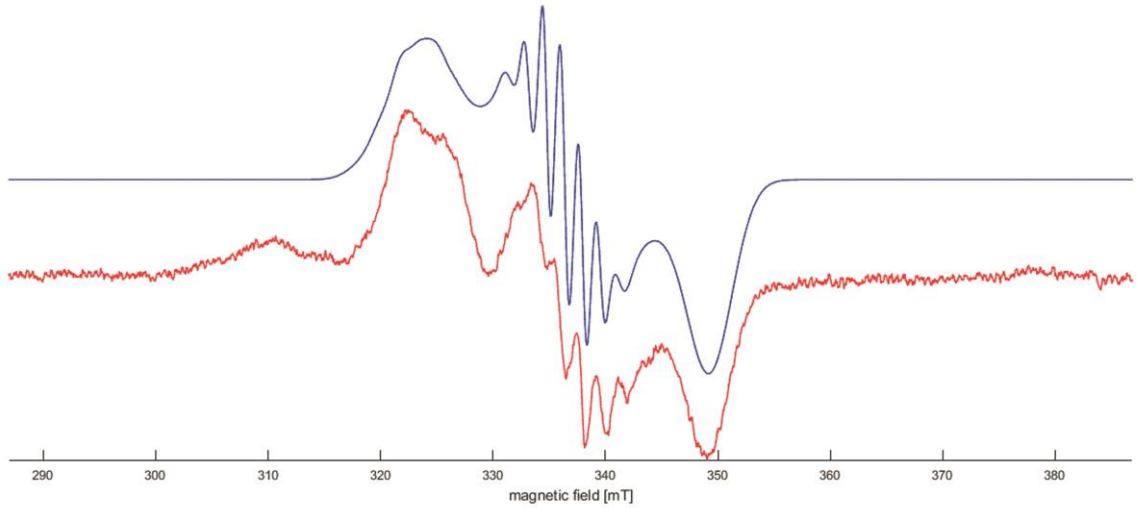

Figure S8.6 Experimental (red) and fitted EPR spectrum (blue) of [K(dme)$_2$][**2**] in thf at 77 K. Parameters used for the fitting: g_x = 1.93146, g_y = 2.00505, g_z = 2.08603; g_{iso} = 2.0075 (g_{iso}(experimental) = 2.008); A_{11} = 15.5 MHz, A_{12} = 44.5 MHz, A_{13} = 45.4 MHz, A_{21} = 15.5 MHz, A_{22} = 44.5 MHz, A_{23} = 45.4 MHz.

Details on DFT calculations

All DFT calculations have been performed with the TURBOMOLE program package[33] at the RI[34]-BP86[35]/def2-TZVP[36] level of theory, followed by single point calculations without the RI approximation. For the determination of relative energies, single point calculation have been performed on the geometries optimised in the gas phase, in which the solvent effects were incorporated *via* the Conductor like Screening Model (COSMO),[37] using THF (ε = 7.580) as solvent. The Multipole Accelerated Resolution of Identity (MARI-J)[38] approximation was used in the geometry optimisation steps.

Table S8.1 Cartesian coordinates of the optimised geometry of [**1**]$^{2-}$ at the BP86/def2-TZVP level of theory.

Atom	x	y	x
As	-2.1105637	-0.3604923	1.8534671
As	-0.4727360	1.0062508	0.5788199
As	-2.3827883	1.1571099	-1.0024660
As	-3.9916883	2.3973204	0.2839371
As	-3.7902640	1.2685518	2.4051387
Fe	-4.0065190	-0.0906959	0.3321639
As	2.1105637	0.3604923	-1.8534671
As	0.4727360	-1.0062508	-0.5788199
As	2.3827883	-1.1571099	1.0024660

As	3.7902640	-1.2685518	-2.4051387
As	3.9916883	-2.3973204	-0.2839371
Fe	4.0065190	0.0906959	-0.3321639
C	4.3448208	-2.1659355	0.1303239
C	5.3421987	-1.5693978	0.9789443
C	-5.4461814	-0.5276684	-1.1078321
C	-6.0184223	-0.5430079	0.2197771
C	-4.4063394	-1.5245278	-1.1548779
C	-5.8980540	0.3160502	-2.2617797
H	-6.3659121	1.2481128	-1.9136855
H	-6.6312885	-0.2162768	-2.8975522
H	-5.0496396	0.6021799	-2.9007631
C	-3.4721477	-3.3328136	0.4832034
H	-2.5238852	-3.3078346	-0.0707994
H	-3.9770845	-4.2903628	0.2526878
H	-3.2163045	-3.3363705	1.5520051
C	-7.1858299	0.2730895	0.6875991
H	-7.1228615	0.4689616	1.7679307
H	-8.1503404	-0.2331583	0.4900349
H	-7.2083705	1.2520131	0.1873868
C	-3.6110389	-1.9146845	-2.3645026
H	-3.4801755	-1.0649572	-3.0484566
H	-4.1116591	-2.7272186	-2.9252865
H	-2.6048213	-2.2609329	-2.0911125
C	-5.6651989	-1.9986936	2.3789593
H	-4.7604386	-2.3216482	2.9144937
H	-6.3807181	-2.8432293	2.3934309
H	-6.1036457	-1.1733697	2.9577188
C	4.3448208	2.1659355	-0.1303239
C	5.3421987	1.5693978	-0.9789443

C	5.4461814	0.5276684	1.1078321
C	6.0184223	0.5430079	-0.2197771
C	4.4063394	1.5245278	1.1548779
C	5.8980540	-0.3160502	2.2617797
H	6.3659121	-1.2481128	1.9136855
H	6.6312885	0.2162768	2.8975522
H	5.0496396	-0.6021799	2.9007631
C	3.4721477	3.3328136	-0.4832034
H	2.5238852	3.3078346	0.0707994
H	3.9770845	4.2903628	-0.2526878
H	3.2163045	3.3363705	-1.5520051
C	7.1858299	-0.2730895	-0.6875991
H	7.1228615	-0.4689616	-1.7679307
H	8.1503404	0.2331583	-0.4900349
H	7.2083705	-1.2520131	-0.1873868
C	3.6110389	1.9146845	2.3645026
H	3.4801755	1.0649572	3.0484566
H	4.1116591	2.7272186	2.9252865
H	2.6048213	2.2609329	2.0911125
C	5.6651989	1.9986936	-2.3789593
H	4.7604386	2.3216482	-2.9144937
H	6.3807181	2.8432293	-2.3934309
H	6.1036457	1.1733697	-2.9577188

ENERGIES [a.u.]:
Total energy = -25670.7774510844
Total energy + OC corr. = -25670.7859918989

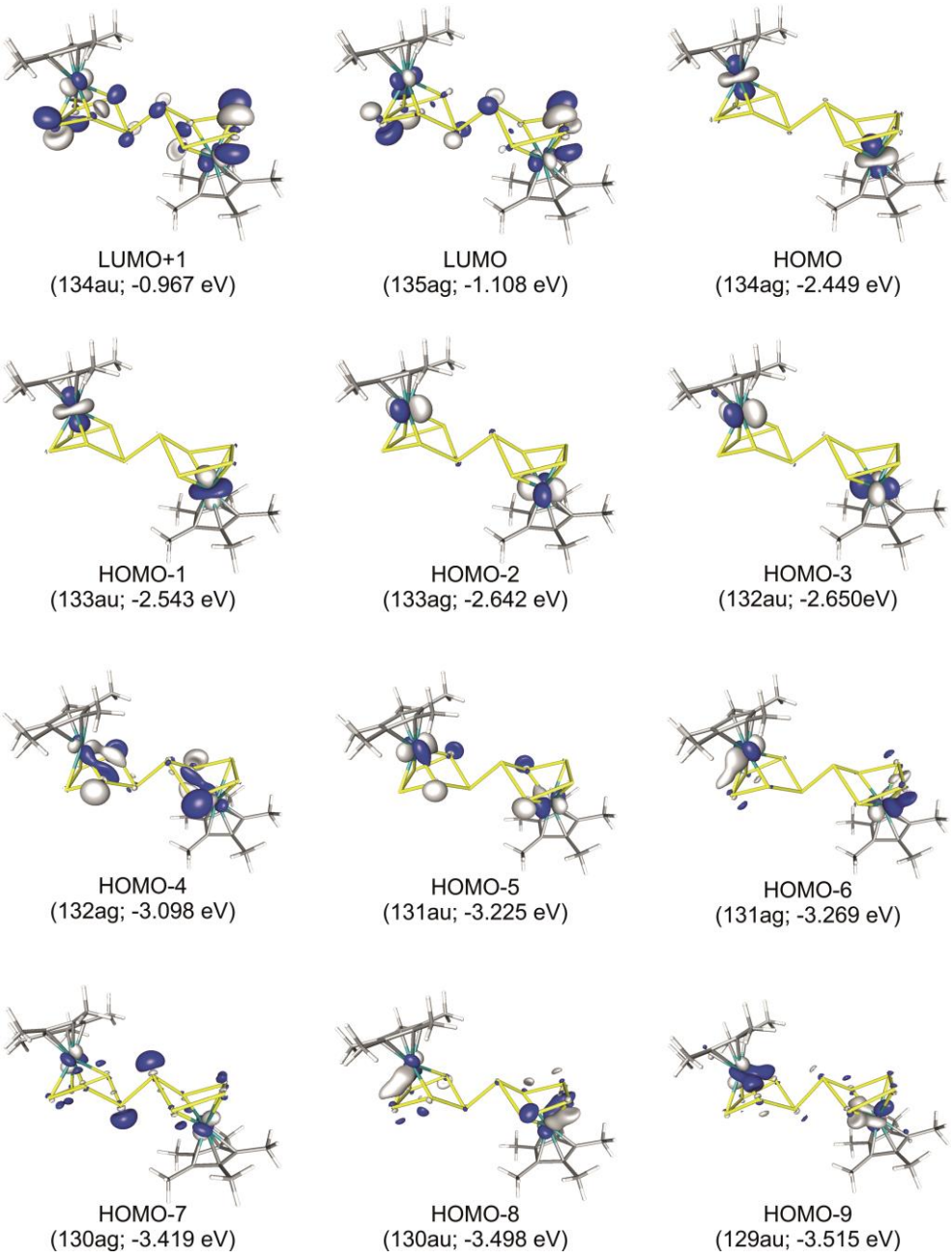

Figure S8.7 Selected molecular orbitals in [**1**]$^{2-}$, calculated at the BP86/def2-TZVP level.

Representation of the cyclic voltammogram of [K(dme)$_2$][2]

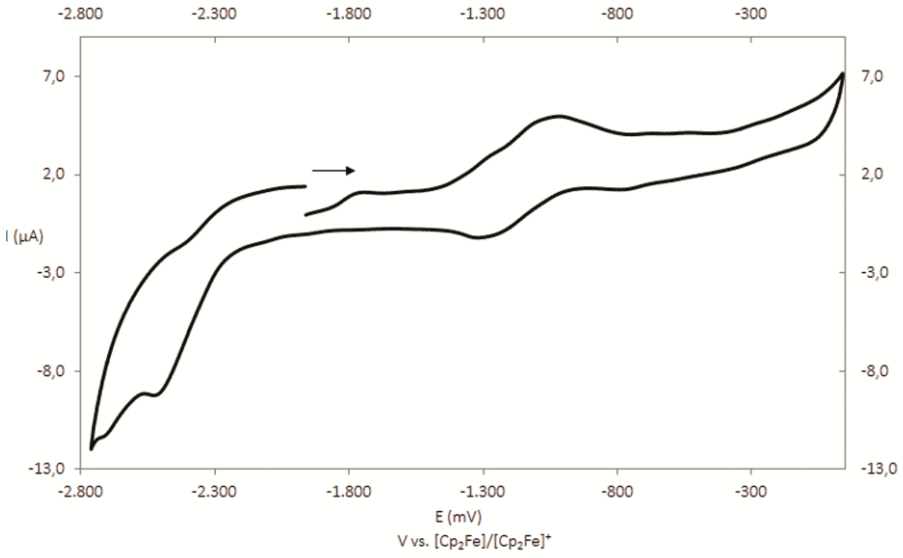

Figure S8.8 Cyclic voltammogram of [K(dme)$_2$][**2**] recorded at a platinum disc electrode in thf at 0.1 Vs^{-1} and referenced against [Cp$_2$Fe]/[Cp$_2$Fe]$^+$; supporting electrolyte [^{n}Bu$_4$N][PF$_6$] (0.1 mol/L).

Crystallographic Details

The data for [K(dme)$_3$]$_2$[**1**] and [K(dme)$_2$]$_2$[**3**] were collected on an Oxford Diffraction GV50 diffractometer equipped with Titan^{S2} CCD detector and a CuK$_\alpha$ microfocus source (λ = 1.54178 Å). The data for [K(dme)$_2$][**2**], [K(18-crown-6)(dme)$_2$]$_2$[**3'**] and [K(dme)$_4$]$_2$[**4**] were collected on an Agilent Technologies diffractometer equipped with an Atlas CCD detector and a SuperNova CuK$_\alpha$ ([K(dme)$_2$][**2**] and [K(dme)$_4$]$_2$[**4**]) or MoK$_\alpha$ microfocus source ([K(18-crown-6)(dme)$_2$]$_2$[**3'**]) (λ = 0.71073 Å). The crystal structure analyses were performed at 123 K. Crystallographic data and details of the diffraction experiments are given in Table S8.2-S8.4. Using Olex2,[39] the structures were solved by direct methods with the program ShelXT[40] and refined with least square method on F^2 employing the ShelXL[40] refinement package with anisotropic displacements for non H atoms. H atoms were located in idealised positions and refined isotropically according to the riding model. A semi-empirical numerical absorption correction based on gaussian[41] integration over a multifaceted crystal model was applied for all compounds. Figures were created with DIAMOND3.0.[42]

Table S8.2 Crystallographic data for $[K(dme)_3]_2$[**1**] and $[K(dme)_2]$[**2**].

	$[K(dme)_3]_2$[**1**]	$[K(dme)_2]$[**2**]
Chemical formula	$C_{44}H_{90}Fe_2As_{10}K_2O_{12}$	$C_{72}H_{137}Fe_4As_8K_2O_{16}$
M/g·mol^{-1}	1750.25	2159.77
T/K	123	123
Crystal system	monoclinic	triclinic
Space group	$P2_1/n$	$P\bar{1}$
a/Å	10.1319(4)	11.48414(16)
b/Å	14.9825(6)	20.8778(3)
c/Å	22.3987(10)	22.4231(3)
α/°	90.00	115.7830(14)
β/°	100.465(4)	91.6895(11)
γ/°	90.00	102.3095(13)
V/Å³	3343.6(2)	4683.87(13)
Z	2	2
ρ_{cal}/g·cm^{-3}	1.738	1.531
μ/mm^{-1}	10.489	9.246
F(000)	1734.0	2206.0
Crystal size/mm^3	0.1 × 0.087 × 0.059	0.4049 × 0.1554 × 0.0914
Radiation	CuK_α	CuK_α
2θ range/°	7.136 to 134.158	7.91 to 147.236
Index ranges	-12 ≤ h ≤ 10, -15 ≤ k ≤ 17, -19 ≤ l ≤ 26	-14 ≤ h ≤ 14, -25 ≤ k ≤ 25, -27 ≤ l ≤ 27
Reflections collected	11395	133430
Independent reflections	5905 [R_{int} = 0.0534, R_{sigma} = 0.0624]	18712 [R_{int} = 0.0599, R_{sigma} = 0.0286]
Data/restraints/parameters	5905/483/297	18712/1031/1266
Goodness-of-fit on F^2	1.034	1.023
Final R indexes [I>2σ(I)]	R_1 = 0.0640, wR_2 = 0.1611	R_1 = 0.0359, wR_2 = 0.0948
Final R indexes [All Data]	R_1 = 0.0803, wR_2 = 0.1715	R_1 = 0.0401, wR_2 = 0.0978
Largest diff. peak/hole/eA^{-3}	1.50/-1.26	1.18/-0.70

Table S8.3 Crystallographic data [K(dme)$_2$]$_2$[**3**] and [K(18-crown-6)(dme)$_2$]$_2$[**3'**].

	[K(dme)$_2$]$_2$[**3**]	[K(18-crown-6)(dme)$_2$]$_2$[**3'**]
Chemical formula	$C_{36}H_{70}Fe_2As_{14}K_2O_8$	$C_{60}H_{118}Fe_2As_{14}K_2O_{20}$
M/g·mol^{-1}	1869.70	1199.16
T/K	123	123
Crystal system	monoclinic	triclinic
Space group	$P2_1/c$	$P\bar{1}$
a/Å	25.2393(6)	11.8649(2)
b/Å	16.6711(3)	12.71961(19)
c/Å	14.5333(3)	16.5113(3)
α/°	90.00	109.0830(14)
β/°	92.847(2)	94.2938(14)
γ/°	90.00	105.1712(14)
V/Å³	6107.6(2)	2237.39(7)
Z	4	2
ρ_{cal}/g·cm^{-3}	2.033	1.780
μ/mm^{-1}	13.779	5.613
F(000)	3608.0	1190.0
Crystal size/mm^3	0.073 × 0.046 × 0.031	0.168 × 0.098 × 0.065
Radiation	CuK_α	MoK_α
2θ range/°	6.356 to 148.858	5.79 to 64.66
Index ranges	-24 ≤ h ≤ 31,	-17 ≤ h ≤ 17,
	-20 ≤ k ≤ 20,	-19 ≤ k ≤ 19,
	-17 ≤ l ≤ 17	-24 ≤ l ≤ 24
Reflections collected	21887	82999
Independent reflections	21887	15145
	[R_{int} = 0.06, R_{sigma} = 0.0382]	[R_{int} = 0.0412, R_{sigma} = 0.0293]
Data/restraints/parameters	21887/12/583	15145/0/480
Goodness-of-fit on F^2	1.071	1.042
Final R indexes [I>2σ(I)]	R_1 = 0.0553, wR_2 = 0.1619	R_1 = 0.0304, wR_2 = 0.0689
Final R indexes [All Data]	R_1 = 0.0705, wR_2 = 0.1748	R_1 = 0.0446, wR_2 = 0.0741
Largest diff. peak/hole/eA^{-3}	1.30/-1.21	1.10/-0.58

Table S8.4 Crystallographic data for $[K(dme)_4]_2$[**4**].

	$[K(dme)_4]_2$[**4**]
Chemical formula	$C_{128}H_{240}Fe_8As_{36}K_4O_{24}$
M/g·mol^{-1}	5463.51
T/K	123
Crystal system	monoclinic
Space group	$P2_1/c$
a/Å	15.9041(4)
b/Å	24.5448(5)
c/Å	51.0063(14)
α/°	90.00
β/°	109.348(3)
γ/°	90.00
V/Å³	18786.5(9)
Z	4
ρ_{cal}/g·cm^{-3}	1.932
μ/mm^{-1}	13.095
F(000)	10688.0
Crystal size/mm^3	0.285 × 0.099 × 0.009
Radiation	CuK_α
2θ range/°	7.204 to 145.558
Index ranges	-18 ≤ h ≤ 19,
	-28 ≤ k ≤ 30,
	-49 ≤ l ≤ 62
Reflections collected	64355
Independent reflections	30108
	[R_{int} = 0.0709, R_{sigma} = 0.0870]
Data/restraints/parameters	30108/0/1105
Goodness-of-fit on F^2	1.102
Final R indexes [I>2σ(I)]	R_1 = 0.1363, wR_2 = 0.3539
Final R indexes [All Data]	R_1 = 0.1679, wR_2 = 0.3762
Largest diff. peak/hole/eA^{-3}	2.64/-2.71

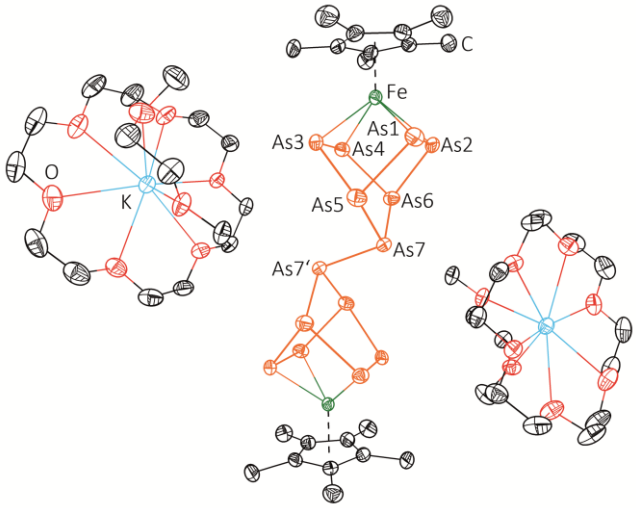

Figure S8.9 Molecular structure of $[K(18\text{-crown-6})(dme)_2]_2$[**3'**] in the solid state. H atoms and solvent molecules are omitted for clarity. Thermal ellipsoids are drawn at 50 % probability level. Selected bond lengths [Å] and angles [°]: As1-As2 2.3516(3), As3-As4 2.3722(4), As1-As5 2.4454(3), As3-As5 2.4470(3), As2-As6 2.4343(3), As4-As6 2.4475(3), As5-As7 2.4098(3), As6-As7 2.40066(3), As7-As7' 2.4425(5), As1-As2-As6 106.146(12), As1-As5-As3 79.945(10), As1-As5-As7 107.198(12), As2-As1-As5 106.392(12), As2-As6-As7 107.436(12), As2-As6-As4 81.521(10), As3-As4-As6 105.968(12), As3-As5-As7 99.491(12), As4-As6-As7 99.124(12), As4-As3-As5 105.968(12), As5-As7-As6 101.095(11), As5-As7-As7' 96.684(14), As6-As7-As7' 96.063(14).

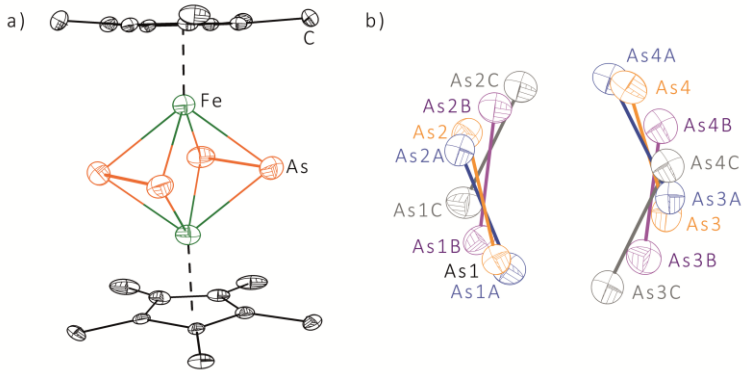

Figure S8.10 a) Molecular structure of $[2]^-$ (main part) in the solid state. The H atoms, counterion and solvent molecules are omitted for clarity. Thermal ellipsoids are drawn in 50 % probability level. b) Disordered core of compound $[2]^-$ (occupancy factors 0.51, 0.41, 0.05, 0.03). Cp* ligands as well as Fe atoms are omitted for clarity. Orange coloured As atoms belong to the main part. For selected bond lengths see Table S8.4.

Table S8.4 As-As bond lengths [Å] for compound [**2**]$^-$ within the disordered $(As_2)_2$ unit.

d(As-As)		occupancy factor	d(As-As)		occupancy factor
As1-As2	2.333(3)	0.51	As1B-As2B	2.413(7)	0.05
As1-As3	3.169(5)		As1B-As3B	2.989(8)	
As2-As4	3.007(4)		As2B-As4B	2.975(8)	
As3-As4	2.334(3)		As3B-As4B	2.336(7)	
As1A-As2A	2.319(4)	0.41	As1C-As2C	2.331(7)	0.03
As1A-As3A	3.169(6)		As1C-As3C	2.999(9)	
As2A-As4A	2.991(4)		As2C-As4C	2.968(9)	
As3A-As4A	2.335(4)		As3C-As4C	2.405(7)	

8.6 References

[1] a) N. Kataoka, Q. Shelby, J. P. Stambuli, J. F. Hartwig, J. *Org. Chem.* 2002, *67*, 5553-5566; b) R. Gómez Arrayás, J. Adrio, J. C. Carretero, *Angew. Chem. Int. Ed.* 2006, *45*, 7674-7715.

[2] a) D. R. van Staveren, N. Metzler-Nolte, *Chem. Rev.* 2004, *104*, 5931-5986; b) K. Kowalski, A. Koceva-Chyła, Ł. Szczupak, P. Hikisz, J. Bernasińska, A. Rajnisz, J. Solecka, B. Therrien, *J. Organomet. Chem.* 2013, *741–742*, 153-161.

[3] P. Neumann, H. Dib, A.-M. Caminade, E. Hey-Hawkins, *Angew. Chem. Int. Ed.* 2015, *54*, 311-314.

[4] R. F. Winter, W. E. Geiger, *Organometallics* 1999, *18*, 1827-1833.

[5] M. V. Butovskiy, G. Balazs, M. Bodensteiner, E. V. Peresypkina, A. V. Virovets, J. Sutter, M. Scheer, *Angew. Chem. Int. Ed.* 2013, *52*, 2972-2976.

[6] T. Li, J. Wiecko, N. A. Pushkarevsky, M. T. Gamer, R. Köppe, S. N. Konchenko, M. Scheer, P. W. Roesky, *Angew. Chem. Int. Ed.* 2011, *50*, 9491-9495.

[7] T. Li, M. T. Gamer, M. Scheer, S. N. Konchenko, P. W. Roesky, *Chem. Commun.* 2013, *49*, 2183-2185.

[8] H. Krauss, G. Balázs, M. Bodensteiner, M. Scheer, *Chem. Sci.* 2010, *1*, 337-342.

[9] R. H. Herber, O. J. Scherer, *Eur. J. Inorg. Chem.* 2000, *12*, 2451-2453.

[10] a) J. Bai, A. V. Virovets, M. Scheer, *Angew. Chem. Int. Ed.* 2002, *41*, 1737-1740; b) M. Scheer, J. Bai, B. P. Johnson, R. Merkle, A. V. Virovets, C. E. Anson, *Eur. J. Inorg. Chem.* 2005, 4023-4026; c) M. Scheer, *Dalton Trans.* 2008, *33*, 4321-4524; d) M. Scheer, A. Schindler, C. Gröger, A. V. Virovets, E. V. Peresypkina, *Angew. Chem.* 2009, *121*, 5148-5151.

[11] N. Arleth, M. T. Gamer, R. Köppe, S. N. Konchenko, M. Fleischmann, M. Scheer, P. W. Roesky, *Angew. Chem. Int. Ed.* 2016, *55*, 1557-1560.

[12] A. H. Cowley, N. C. Norman, M. Pakulski, *Dalton Trans.* 1985, *1*, 383-386.

[13] M. Fleischmann, S. Welsch, H. Krauss, M. Schmidt, M. Bodensteiner, E. V. Peresypkina, M. Sierka, C. Gröger, M. Scheer, *Chem. Eur. J.* 2014, *20*, 3759-3768.

[14] Y. Morino, T. Ukaji, T. Ito, *Bull. Chem. Soc. Jpn.* 1966, *39*, 64-71.

[15] H. A. Spinney, N. A. Piro, C. C. Cummins, *J. Am. Chem. Soc.* 2009, *131*, 16233-16243.

[16] Referring to [(Cp^{Bn}Co)$_4$(μ$_4$,η$^{4:4:2:2:1:1}$-As$_{10}$)] in chapter 9 (this work).

[17] O. J. Scherer, B. Höbel, G. Wolmershäuser, *Angew. Chem. Int. Ed. Engl.* 1992, *31*, 1027-1028.

[18] O. J. Scherer, K. Pfeiffer, G. Heckmann, G. Wolmershäuser, *J. Organomet. Chem.* 1992, *425*, 141-149.

[19] C. Graßl, M. Bodensteiner, M. Zabel, M. Scheer, *Chem. Sci.* 2015, *6*, 1379-1382.

[20] Referring to [{Cp^{Bn}Co(μ,η$^{2:2}$-As)$_2$}$_2$] in chapter 9 (this work).

[21] A. Bondi, *J. Phys. Chem.* **1964**, *68*, 441-451.

[22] M. Eckhardt, *Ph.D. thesis*, Universität Regensburg, **2014**.

[23] Referring to [(Cp^{Bn}Fe)$_2$(μ,η$^{4:4}$-As$_4$)] in chapter 5 (this work).

[24] S. Heinl, *Ph.D. thesis*, Universität Regensburg, **2014**.

[25] T. Hanauer, J. C. Aschenbrenner, N. Korber, *Inorg. Chem.* **2006**, *45*, 6723-6727.

[26] R. C. Haushalter, B. W. Eichhorn, A. L. Rheingold, S. J. Geib, *J. Chem. Soc., Chem. Commun.* **1988**, 1027-1028.

[27] B. W. Eichhorn, R. C. Haushalter, J. C. Huffman, *Angew. Chem. Int. Ed. Engl.* **1989**, *28*, 1032-1033.

[28] C. Knapp, B. Zhou, M. S. Denning, N. H. Rees, J. M. Goicoechea, *Dalton Trans.* **2010**, *39*, 426-436.

[29] a) A. L. Rheingold, M. J. Foley, P. J. Sullivan, *J. Am. Chem. Soc.* **1982**, *104*, 4727-4279; b) G. Friedrich, O. J. Scherer, G. Wolmershäuser, *Z. Anorg. Allg. Chem.* **1996**, *622*, 1478-1486.

[30] M. J. Moses, J. C. Fettinger, B. W. Eichhorn, *Science* **2003**, *300*, 778-780.

[31] O. J. Scherer, C. Blath, G. Wolmershäuser, *J. Organomet. Chem.* **1990**, *387*, C21-C24.

[32] S. Stoll, A. Schweiger, *J. Magn. Reson.* **2006**, *178*, 42-55.

[33] a) F. Furche, R. Ahlrichs, C. Hättig, W. Klopper, M. Sierka, F. Weigend, *WIREs Comput. Mol. Sci.* **2014**, *4*, 91-100; b) R. Ahlrichs, M. Bär, M. Häser, H. Horn, C. Kölmel, *Chem. Phys. Lett.* **1989**, *162*, 165–169; c) O. Treutler, R. Ahlrichs, *J. Chem. Phys.* **1995**, *102*, 346–354.

[34] a) K. Eichkorn, O. Treutler, H. Oehm, M. Häser, R. Ahlrichs, *Chem. Phys. Lett.* **1995**, *242*, 652–660; b) K. Eichkorn, F. Weigend, O. Treutler, R. Ahlrichs, *Theor. Chem. Acc.* **1997**, *97*, 119-124.

[35] a) P. A. M. Dirac, *Proc. Royal Soc. A*, 1929, 123, 714-733; b) J. C. Slater, *Phys. Rev.* **1951**, *81*, 385-390; c) S. H. Vosko, L. Wilk, M. Nusair, *Can. J. Phys.* **1980**, *58*, 1200-1211; d). A. D. Becke, *Phys. Rev. A*. **1988**, 38, 3098; e) J. P. Perdew, *Phys. Rev. B* **1986**, *33*, 8822-8824.

[36] a) F. Weigend, M. Häser, H. Patzelt, R. Ahlrichs, *Chem. Phys. Letters* **1998**, *294*, 143-152; b) F. Weigend, R. Ahlrichs, *Phys. Chem. Chem. Phys.* **2005**, *7*, 3297-3305.

[37] A. Klamt, G. Schüürmann, *J. Chem. Soc. Perkin Trans. 2* **1993**, *5*, 799–805. b) A. Klamt, V. Jonas, *J. Chem. Phys.* **1996**, *105*, 9972–9981.

[38] M. Sierka, A. Hogekamp, R. Ahlrichs, *J. Chem. Phys.* **2003**, *118*, 9136-9148.

[39] O.V. Dolomanov, L. J. Bourhis, R. J. Gildea, J. A. K. Howard, H. Puschmann, *J. Appl. Cryst.* **2009**, *42*, 339-341.

[40] G. M. Sheldrick, *Acta Cryst.* **2015**, *C71*, 3-8.

[41] a) CrysAlisPro, Version 1.171.38.41, Agilent Technologies UK Ltd, Oxford, UK (compound **1** and **3**); b) CrysAlisPro, Version 1.171.38.34, Agilent Technologies UK Ltd, Oxford, UK (compound **2**); c) CrysAlisPro, Version 1.171.38.37b, Agilent Technologies UK Ltd, Oxford, UK (compound **3'** and **4**).

[42] K. Brandenburg, H. Putz, Diamond3.0, Crystal and Molecular Structure Visualization, Crystal Impact GbR, Bonn, Germany, 2014.

9. Novel As_n Ligand Complexes of Cobalt

M. Schmidt, G. Balázs, F. Riedlberger and M. Scheer

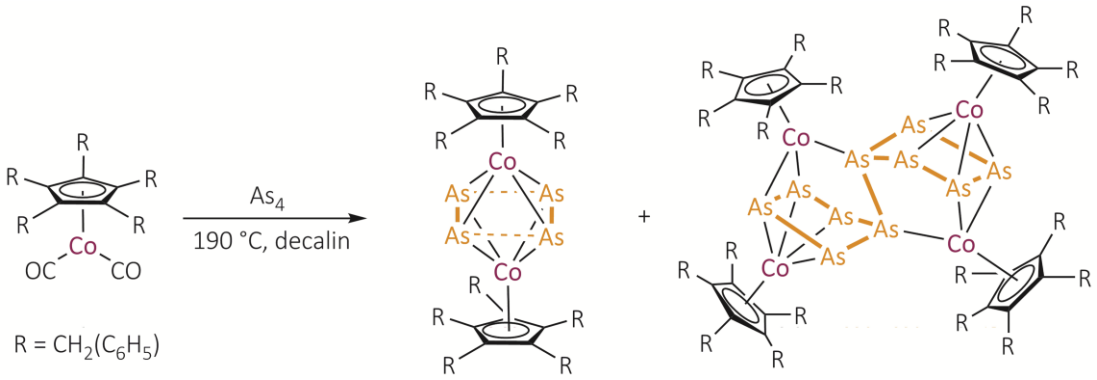

Abstract:

The co-thermolysis of $[Cp^{Bn}Co(CO)_2]$ ($Cp^{Bn} = \eta^5$-$C_5\{CH_2(C_6H_5)\}_5$) with yellow arsenic (As_4) in decalin afforded $[\{Cp^{Bn}Co(\mu,\eta^{2:2}\text{-}As_2)\}_2]$ (**1**) and $[(Cp^{Bn}Co)_4(\mu_4,\eta^{4:4:2:2:1:1}\text{-}As_{10})]$ (**2**) in a ratio of almost 1:1. Both As_n ligand complexes bear the Cp^{Bn} ligand. Complexes **1** and **2** were both fully characterised by NMR spectroscopy and mass spectrometry, elemental analysis as well as by single crystal X-ray diffraction analysis. To gain more insight into the bonding situation of **1**, DFT calculations were carried out and confirm the presence of two As_2 dumbbells as a middle deck. Furthermore, the redox behaviour of **1** has been investigated by cyclic voltammetry, showing two reversible oxidations.

9.1 Author contributions

- All syntheses and characterisations were performed by Monika Schmidt.
- Manuscript was written by Monika Schmidt.
- Figures were made by Monika Schmidt.
- Single crystal X-ray structure analyses and refinements were performed by Monika Schmidt.
- Cyclovoltammetric measurement of **1** was performed and interpreted by Felix Riedlberger.
- DFT computations and their description regarding **1** were performed by Dr. G. Balázs.

9.2 Introduction

Over the last few decades, many complexes with substituent free phosphorus ligands, the so called P_n ligand complexes, have been synthesised. Here, white phosphorus (P_4) is often used as a starting material due to its high reactivity and availability.[1] Interestingly, the first group 15 element ligands in organometallic chemistry were synthesised in the late 1960s by using $AsCl_3$ and $AsMe_5$ as starting materials (Figure 9.1).[2] However, the research area of As_n ligand complexes is only poorly investigated up to date.

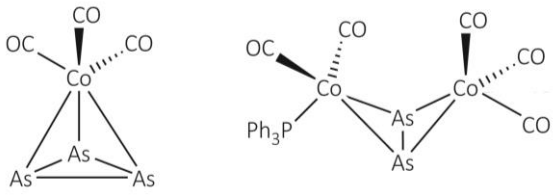

Figure 9.1 First reported As_n ligand complexes. $[Co(CO)_3(\eta^3\text{-}As_3)]$ (left) and $[Co_2(CO)_5(PPh_3)(\mu,\eta^{2:2}\text{-}As_2)]$ ($PPh_3 = P(C_6H_5)_3$) (right).

In the following years, especially Scherer and co-workers established the use of yellow arsenic (As_4) for the synthesis of As_n ligand complexes.[3] Cyclopentadienyl containing carbonyl complexes are usually suitable starting materials and novel As_n ligand complexes can be easily synthesised. The co-thermolysis of $[Cp^RCo(CO)_2]$ ($Cp^R = Cp^*(\eta^5\text{-}C_5Me_5)$, Cp' ($\eta^5\text{-}C_5EtMe_4$)) with As_4, for instance, afforded $[\{Cp^RCo(\mu,\eta^{2:2}\text{-}As_2)\}_2]$ (**I**/**II**) and $[(Cp^RCo)_2(\mu,\eta^{2:2}\text{-}As_6)]$ (**III**) as well as $[\{Cp^RCo(\mu,\eta^{2:2}\text{-}As_2)\}_3]$ (**IV**), containing a central As_6 prism like unit (Figure 9.2).[4]

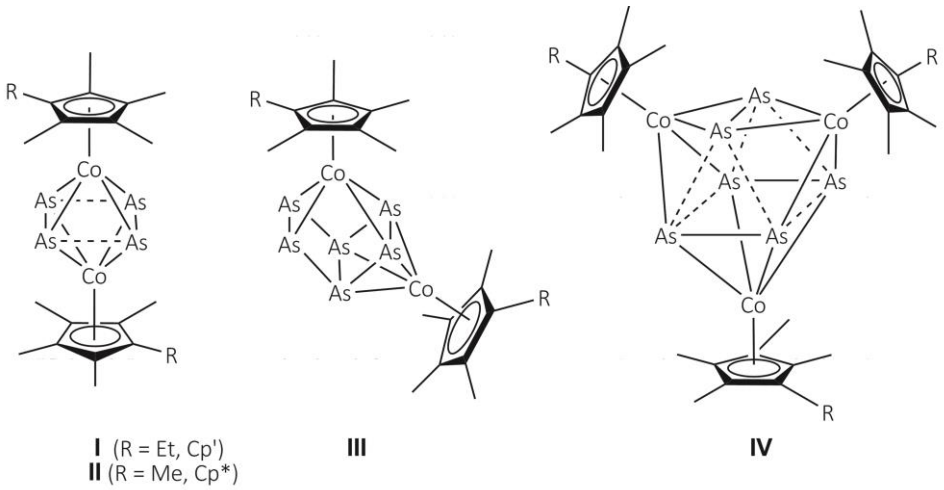

Figure 9.2 Products of the co-thermolysis of $[Cp^RCo(CO)_2]$ with As_4 (Cp^R = Cp*, Cp').[4]

An alternative source for As_n ligand complexes is the use of the $[As_7]^{3-}$ Zintl anion, which leads mostly to ionic complexes. For example, the reaction of the potassium salt K_3As_7 with $[Co(mes)_2(PEt_2Ph_2)]$ (mes = 2,4,6-trimethylphenyl) in ethylenediamine gives $[Co(\eta^3\text{-}As_3)\{\eta^4\text{-}As_4(mes)_2\}]^{2-}$, which consists of a *cyclo*-As_3 unit and a η^4-$As_4(mes)_2$ butadiene like ligand.[5] Furthermore, $[As_7(SiMe_3)_3]$ can also serve as a starting material for the synthesis of novel As_n ligand complexes.[6]

Recently, we reported on the mild activation of As_4 by $[(Cp'''Co)_2(\mu,\eta^{4:4}\text{-toluene})]$ ($Cp''' = \eta^5\text{-}1,2,4\text{-}C_5H_2{}^tBu_3$) at room temperature.[7] The reaction leads to the complexes $[\{Cp'''Co(\mu,\eta^{2:2}\text{-}As_2)\}_2]$ (**V**) and $[(Cp'''Co)_4(\mu_4,\eta^{4:4:2:2:1:1}\text{-}As_{10})]$ (**VI**) as well as to $[(Cp'''Co)_3(\mu_3,\eta^{4:4:2:1}\text{-}As_{12})]$ (**VII**), containing the largest neutral polyarsenic ligand reported so far (Figure 9.3).

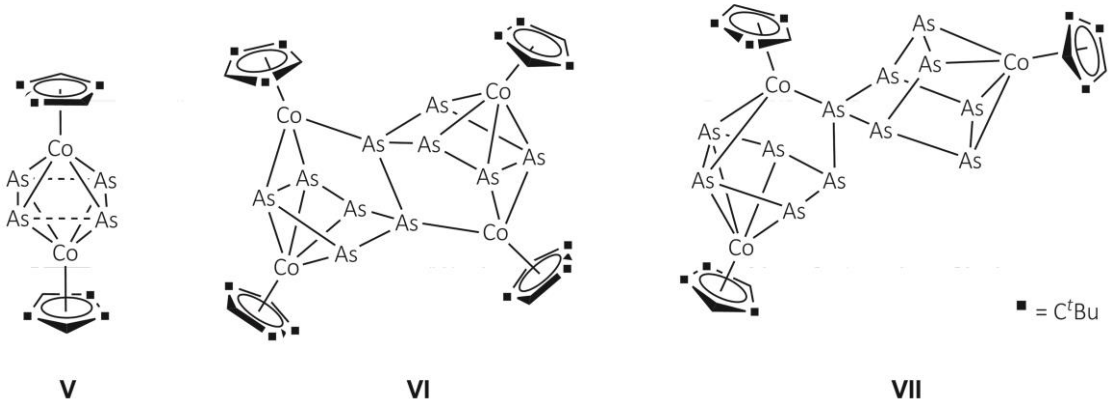

Figure 9.3 Products of the mild activation of yellow arsenic (As_4) by $[(Cp'''Co)_2(\mu,\eta^{4:4}\text{-toluene})]$.[7]

In respect to the previous results of As_4 activation by Cp^RCo complexes under mild activation conditions and co-thermolysis, the question arose if an introduction of the Cp^{Bn} ligand

(Cp^{Bn} = η^5-$C_5\{CH_2(C_6H_5)\}_5$) would lead to the formation of unprecedented As_n ligand complexes of cobalt. Herein, we report on the synthesis and characterisation of $[\{Cp^{Bn}Co(\mu,\eta^{2:2}\text{-}As_2)\}_2]$ (**1**) and $[(Cp^{Bn}Co)_4(\mu_4,\eta^{4:4:2:2:1:1}\text{-}As_{10})]$ (**2**). Here, **2** represents a new example of an arsenic rich As_n ligand complex which is available by a co-thermolysis reaction for the first time, from which smaller As_n ligand complexes are usually obtained.

9.3 Results and Discussion

Complexes **1** and **2** can be synthesised by the co-thermolysis of $[Cp^{Bn}Co(CO)_2]$ with As_4 in decalin (Scheme 9.1).

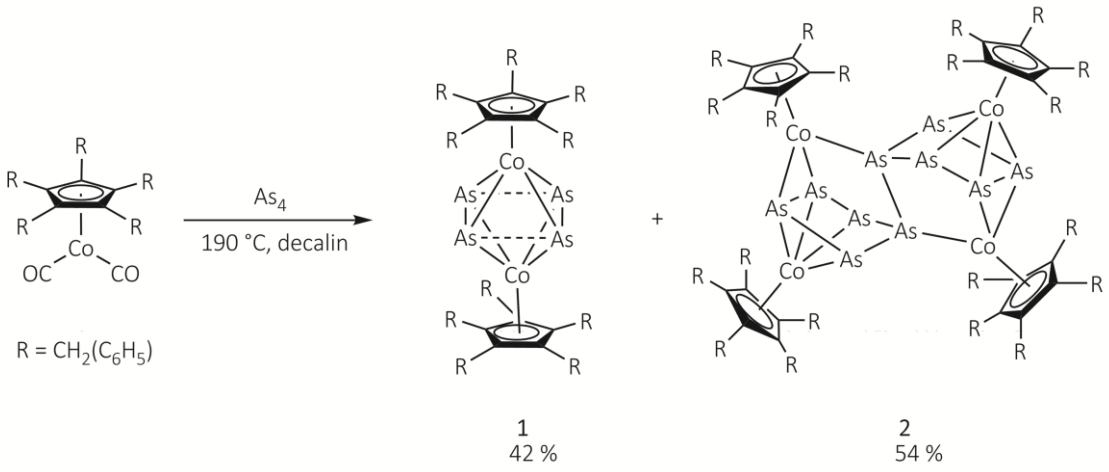

Scheme 9.1 Synthesis of $[\{Cp^{Bn}Co(\mu,\eta^{2:2}\text{-}As_2)\}_2]$ (**1**) and $[(Cp^{Bn}Co)_4(\mu_4,\eta^{4:4:2:2:1:1}\text{-}As_{10})]$ (**2**).

After column chromatographic workup, both products can be crystallised by layering a toluene solution with CH_3CN. Complexes **1** and **2** are soluble in CH_2Cl_2 and toluene, nearly insoluble in *n*-hexane and thf and insoluble in CH_3CN. The ^1H and $^{13}C\{^1H\}$ NMR spectra of **1** and **2** show the corresponding set of signals for the Cp^{Bn} ligands. In compound **2**, signals for two magnetically and chemically inequivalent Cp^{Bn} ligands are observed (Figure S9.1-S9.4, see supplementary information).

Complex **1** crystallises as dark green blocks in the monoclinic space group $P2_1/c$. The single crystal X-ray diffraction analysis reveals a triple decker structure with two As_2 units as the middle deck (Figure 9.4). Therefore, **1** is isostructural to **I** (Cp')/**II** (Cp*) and **V** (Cp''') [8]. In contrast to the afore mentioned complexes, the Cp^{Bn} ligands of **1** are aligned almost ecliptically. Moreover, the $(As_2)_2$ units appear to be disordered over four positions with occupancy factors of 0.16, 0.31, 0.42 and 0.11. The molecular structure of **1** (major component) is depicted in Figure 9.4. The bond lengths within the $(As_2)_2$ ligands (2.3764(19) Å and 2.389(2) Å) are shortened compared to an As-As single bond (electron diffraction: 2.435 Å in As_4,[8] DFT calculations: 2.4372 Å in As_4[9]) but the

distances are longer as expected for an As-As double bond (2.245(1) Å in $[\{(Me_3Si)_3CAs\}_2]$[10]). In contrast, the distances between the As_2 units As1···As2 (2.7439(19) Å) and As3···As4 (2.742(2) Å) are elongated, but nevertheless still shorter than the sum of the van der Waals radii of arsenic (3.7 Å).[11]

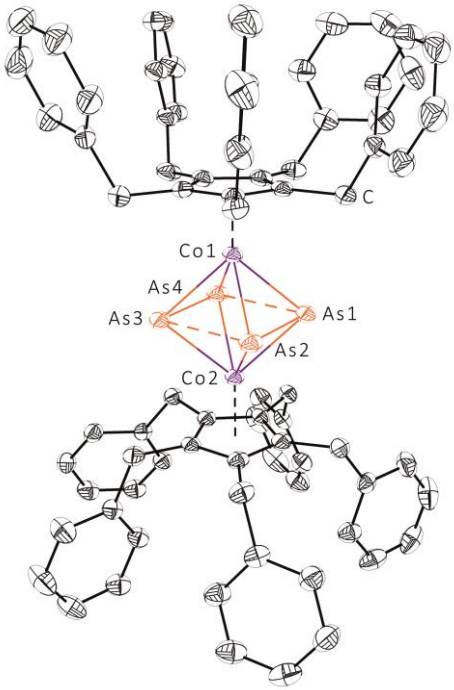

Figure 9.4 Molecular structure of **1** in the solid state. H atoms are omitted for clarity and due to disorder only the main part is depicted. Thermal ellipsoids are drawn at 50 % probability level. Selected bond lengths [Å] and angles [°]: As1···As2 2.7439(19), As2-As3 2.389(2), As3···As4 2.742(2), As4-As1 2.3764(19), As4-As1-As2 90.24(7), As1-As2-As3 89.72(7), As2-As3-As4 90.01(8), As3-As4-As1 90.03(7).

To get an insight into the disorder of the $(As_2)_2$ middle deck, DFT calculations (BP86/def2-TZVP) were carried out. They confirm the presence of As_2 dumbbells and eliminate the possibility of the existence of a *cyclo*-As_4 ligand or a butadiene like As_4 unit. Selected molecular orbitals are depicted in Figure 9.5 and show the bonding situation in the $(As_2)_2$ ligand. The HOMO represents the two shorter As-As bonds while the LUMO is bonding with respect to the longer As-As unit.

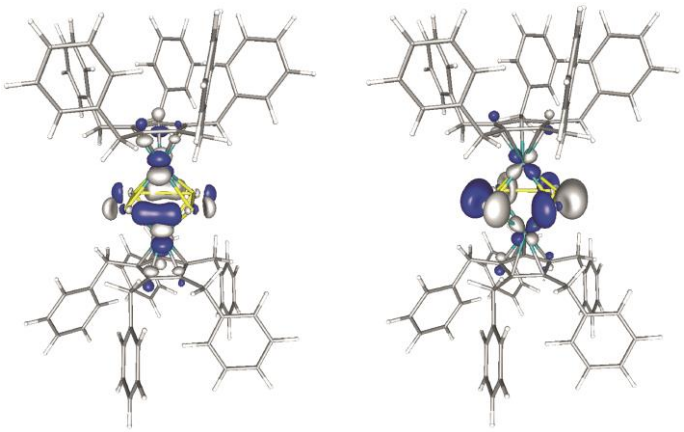

Figure 9.5 Selected molecular orbitals of **1** (LUMO: -2.731 eV (left); HOMO: -4.257 eV (right)). Calculated at the BP86/def2-TZVP level of theory.

While the As-As distances in the Cp' derivative **I** and Cp''' derivative **V** within and between the As_2 dumbbells are quite similar,[4,7] the bond lengths in **1** differ strongly from these isostructural complexes. This trend is also observed for the Co-As distances (2.4125(10) Å - 2.4545(10) Å) and reflects a slight distortion of the $[Co_4As_4]$ core. Table 9.1 summarises selected bond features of the isostructural complexes **1**, **I** and **V** for comparison.

Table 9.1 Selected bond lengths [Å] for **1**, **I**[4] and **V**.[7]

	1	**I**	**V**
d(As-As)	2.3764(19) / 2.389(2)	2.272(1)	2.2795(5)
d(As···As)	2.742(2) / 2.7439(19)	2.844(1)	2.8209(4)
$d(Co\text{-}As)_{min}$	2.4126(9)	2.414(1)	2.4211(5)
$d(Co\text{-}As)_{max}$	2.4547(10)	2.424(1)	2.4355(5)

Additionally, electrochemical investigations have been performed (Figure 9.6). The cyclic voltammetry data of **1** in CH_2Cl_2 showed up two reversible oxidations at a potential of $E_{1/2}$= -0.36 V (peak **A**) and $E_{1/2}$= +0.01 V (peak **B**). Accordingly, **1** should be oxidised by $[Cp_2Fe]^+$ to the monocation or by Ag^+ to the dication.[12] Unfortunately, all preparative attempts to oxidise **1** to the monocationic or dicationic species failed so far.

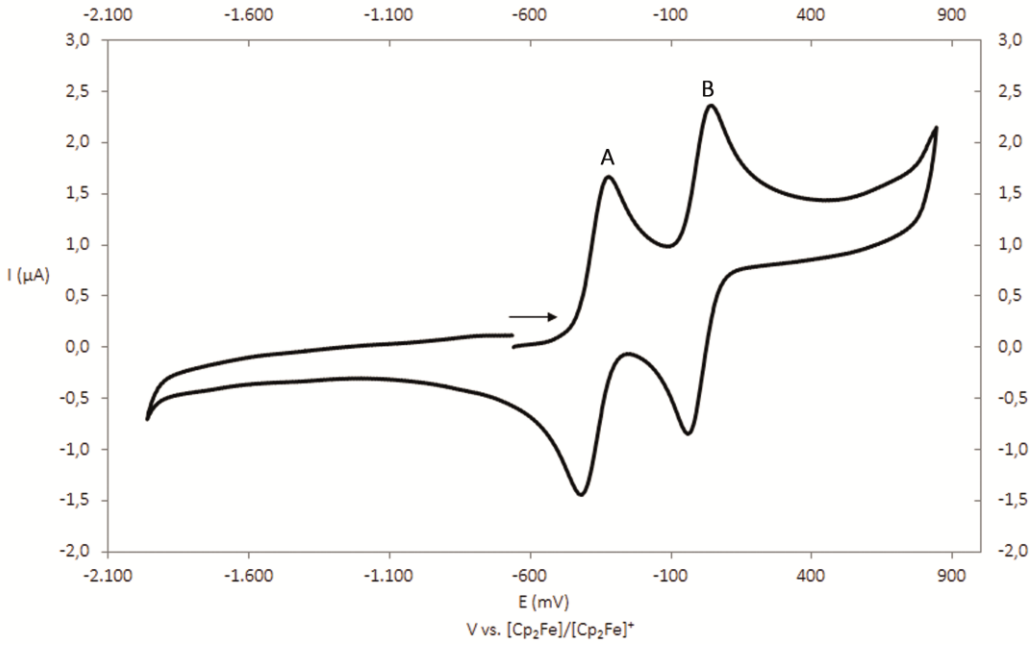

Figure 9.6 Cyclic voltammogram of **1** recorded at a platinum disc electrode in thf at 0.1 Vs^{-1} and referenced against $[Cp_2Fe]/[Cp_2Fe]^+$; supporting electrolyte $[^nBu_4N][PF_6]$ (0.1 mol/L).

Complex **2** crystallises as dark brown needles in the monoclinic space group $P2_1/n$ with one and a half molecules **2** and one solvent molecule toluene in the asymmetric unit. Figure 9.7 shows the molecular structure of **2** in the solid state, which is similar to the Cp''' derivative **VI**. The central structural motif of **2** consists of two envelope like As_5 units, which are connected through an As-As bond. Since arsenic is isolobal to CH, the As_{10} framework can be considered as the hypothetic As_{10} dihydrofulvalene analogue and serves as a 16 electron donor ligand. The two 4π systems bind to Co1 and Co4 resulting in 18 VE per cobalt atom, whereas Co2 and Co3 are both formally side-on coordinated to an As-As bond and by the lone pair of As5 and As6, respectively. This bonding situation leads unavoidably to an elongation of the As2-As3 bond (2.7003(7) Å) and the As8-As9 bond (2.7595(7) Å). Comparable As-As distances have been reported in **VI**[7] or in $[(CpMo)_2(\mu,\eta^4\text{-}As_5)]$ ($Cp = \eta^5\text{-}C_5H_5$).[13] All remaining bond lengths of the As_{10} ligand are in the range of a single bond or in-between a double and a single bond.

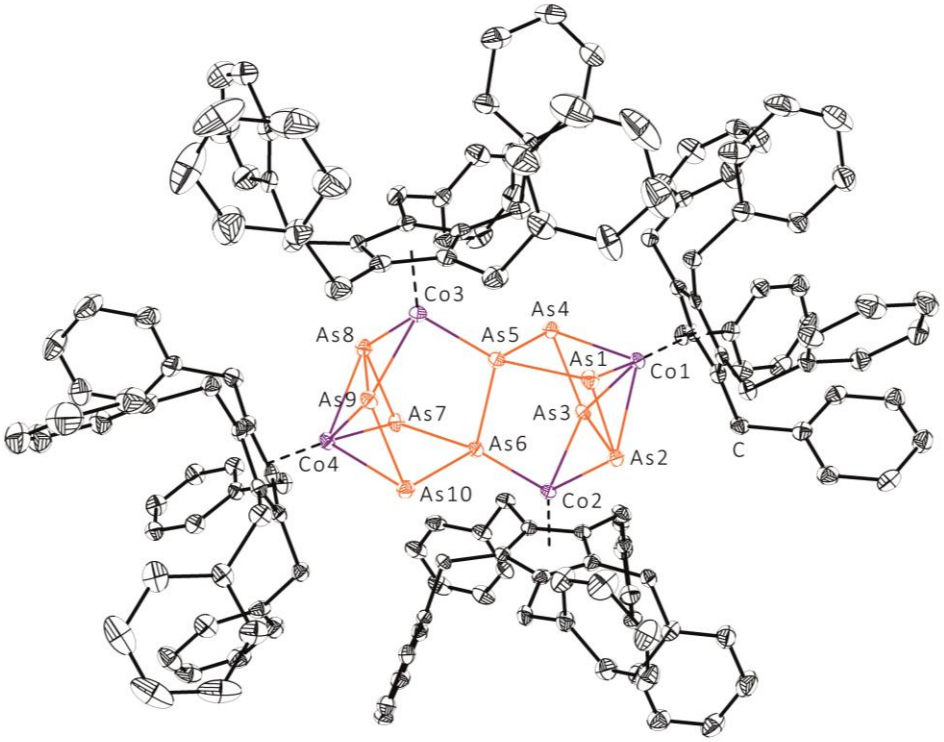

Figure 9.7 Molecular structure of **2** · 0.67 C_7H_8 in the solid state. Only one molecule of the two independent molecules of **2** is depicted. H atoms and solvent molecules are omitted for clarity and due to disorder only the main part is depicted. Thermal ellipsoids are drawn at 50 % probability level. Selected bond lengths [Å]: As1-As2 2.3733(7), As2-As3 2.7003(7), As3-As4 2.3746(7), As4-As5 2.4289(7), As5-As6 2.4080(7), As6-As7 2.4500(7), As6-As10 2.4276(7), As7-As8 2.3774(7), As8-As9 2.7595(7), As9-As10 2.3664(7), As1-As5 2.4311(7).

In summary, we reported on the synthesis and characterisation of two novel As_n ligand complexes of cobalt bearing the Cp^{Bn} ligand. Both complexes $[\{Cp^{Bn}Co(\mu,\eta^{2:2}\text{-}As_2)\}_2]$ (**1**) and $[(Cp^{Bn}Co)_4(\mu_4,\eta^{4:4:2:2:1:1}\text{-}As_{10})]$ (**2**) are isostructural to **I** (Cp')/**II** (Cp*), **V** (Cp''') and **VI** (Cp'''), respectively. In contrast to **V** and **VI**, complexes **1** and **2** can be received by co-thermolysis of $[Cp^{Bn}Co(CO)_2]$ with As_4 in high yields, while **I**/**II** (2%/6%) and **VI** (8%) present the minor products in the corresponding synthesis. For this reason and due to the good solubility, further studies will focus especially on the use of **1** in coordination chemistry to form soluble products. Further As_n ligand complexes with unprecedented structural motifs could not be obtained, but mild activation of yellow arsenic by the possible isostructural complex $[(Cp^{Bn}Co)_2(\mu,\eta^{4:4}\text{-toluene})]$ seems to be a promising way.

9.4 Experimental Part

General remarks:

All reactions were performed under an atmosphere of dry argon or nitrogen using glovebox or Schlenk techniques. Solvents were purified, degassed and dried prior to use. $[Cp^{Bn}Co(CO)_2]$[14] and As_4[15] were prepared according to literature procedures.

The NMR spectra were recorded on a Bruker Avance 300 or Avance III HD 400 spectrometer. EI MS spectra were measured on a Finnigan MAT SSQ 710A mass spectrometer and LIFDI MS spectra on a Finnigan MAT 95 mass spectrometer. The elemental analyses were performed on a Vario ELIII apparatus.

Synthesis of $[\{Cp^{Bn}Co(\mu,\eta^{2:2}\text{-}As_2)\}_2]$ (1) and $[(Cp^{Bn}Co)_4(\mu_4,\eta^{4:4:2:2:1:1}\text{-}As_{10})]$ (2)

A freshly prepared solution of As_4 (starting from 5 g grey arsenic) in 250 mL decalin was added to a suspension of $[Cp^{Bn}Co(CO)_2]$ (836 mg, 1.33 mmol) in 50 mL decalin. The mixture was heated to reflux and the reaction progress was monitored by IR spectroscopy. After 60 min, the carbonyl bands disappeared and the solvent was removed under vacuum. Column chromatographic work up (silica gel, *n*-hexane, 27 x 3 cm) with *n*-hexane/toluene (3:1) afforded a green fraction of **1**. Complex **2** was eluted as a brown zone by using toluene. Both complexes can be crystallised from toluene solutions layered with CH_3CN after complete diffusion.

Analytical data of **1**

Crystalline yield: 400 mg (0.28 mmol, 42 % referred to $[Cp^{Bn}Co(CO)_2]$).

^{1}H NMR (CD_2Cl_2): δ [ppm] = 4.02 (s, 20H, CH_2), 6.54-6.56 (m, 20H, C_6H_5), 6.85-6.89 (m, 20H, C_6H_5), 6.93-6.96 (m, 10H, C_6H_5).

$^{13}C\{^1H\}$ NMR (CD_2Cl_2): δ [ppm] = 33.66 (CH_2), 97.39 (C_5), 126.15 (C_6H_5), 128.25 (C_6H_5), 129.26 (C_6H_5), 140.08 (C_6H_5).

EI MS (70 eV, CH_2Cl_2): *m/z* (%) = 1447.9 (50) ($[(Cp^{Bn}Co)_2(As_2)_2]^+$), 514.4 (90) ($[Cp^{Bn}\text{-}H_2]^+$), 423.3 (100) ($[Cp^{Bn}\text{-}H_2\text{-}C_7H_7]^+$), 330.3 (40) ($[Cp^{Bn}\text{-}H_2\text{-}2\ C_7H_7]^+$), 241.2 (70) ($[Cp^{Bn}\text{-}H_2\text{-}3\ C_7H_7]^+$).

Elemental Analysis: Calculated (%) for $[C_{80}H_{70}Co_2As_4]$ (1448.96 g/mol): C 66.31, H 4.87; found C 66.40, H 4.88.

Analytical data of **2**

Crystalline yield: 550 mg (0.18 mmol, 54 % referred to $[Cp^{Bn}Co(CO)_2]$).

^{1}H NMR (CD_2Cl_2): δ [ppm] = 3.89 (s, 20H, CH_2), 4.16 (s, 20H, CH_2), 6.23-6.25 (m, 20H, C_6H_5), 6.67-6.72 (m, 20H, C_6H_5), 6.81-6.86 (m, 10 H C_6H_5), 6.94-7.09 (m, 50H, C_6H_5).

$^{13}C\{^1H\}$ NMR (CD_2Cl_2): δ [ppm] = 33.57 (CH_2), 34.24 (CH_2), 98.66 (C_5), 99.10 (C_5), 126.04 (C_6H_5), 126.39 (C_6H_5), 128.05 (C_6H_5), 128.54 (C_6H_5), 129.41 (C_6H_5), 129.71 (C_6H_5), 139.34 (C_6H_5), 139.43 (C_6H_5).

LIFDI MS (CH_2Cl_2): *m/z* (%) = 3046.7 (20) [$(Cp^{Bn}Co)_4As_{10}]^+$), 2173.3 (100) ([$(Cp^{Bn}Co)_3As_6]^+$).

Elemental Analysis: Calculated (%) for [$C_{160}H_{140}Co_4As_{10}$ · 0.67 C_7H_8] (3109.51 g/mol): C 63.61, H 4.71; found C 63.41, H 4.68.

9.5 Supplementary Information

NMR Investigations

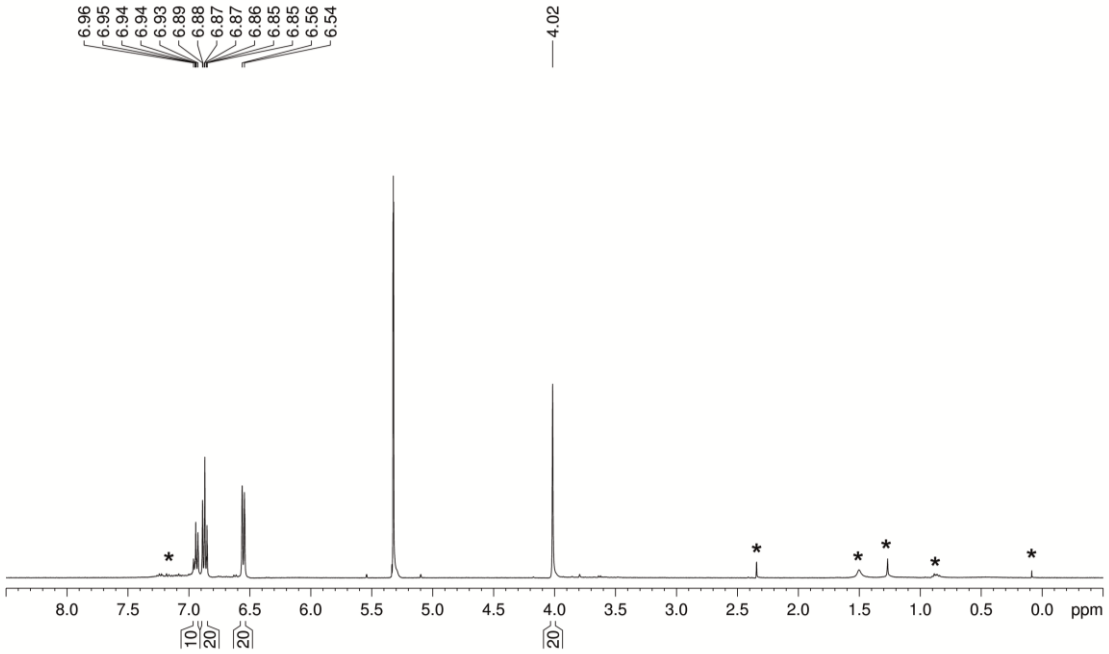

Figure S9.1 ^{1}H NMR spectrum of **1** in CD_2Cl_2 at 300 K. Signals marked with an asterisk are due to different solvents and silicon grease.

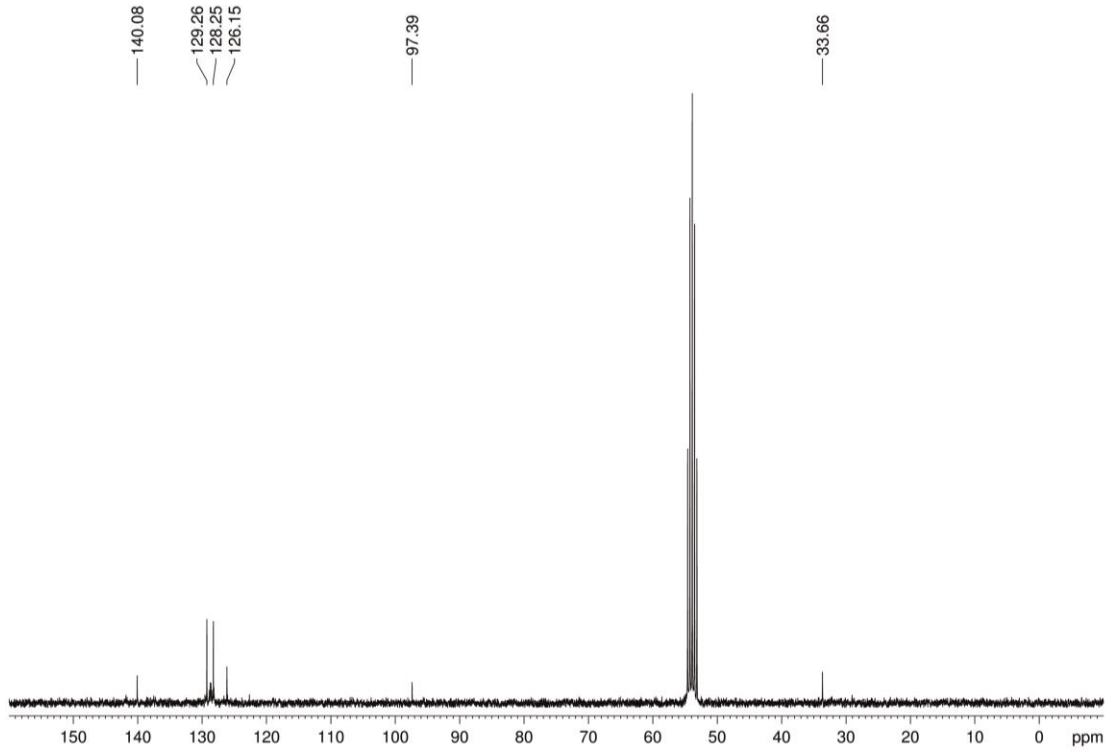

Figure S9.2 $^{13}C\{^{1}H\}$ NMR spectrum of **1** in CD_2Cl_2 at 300 K.

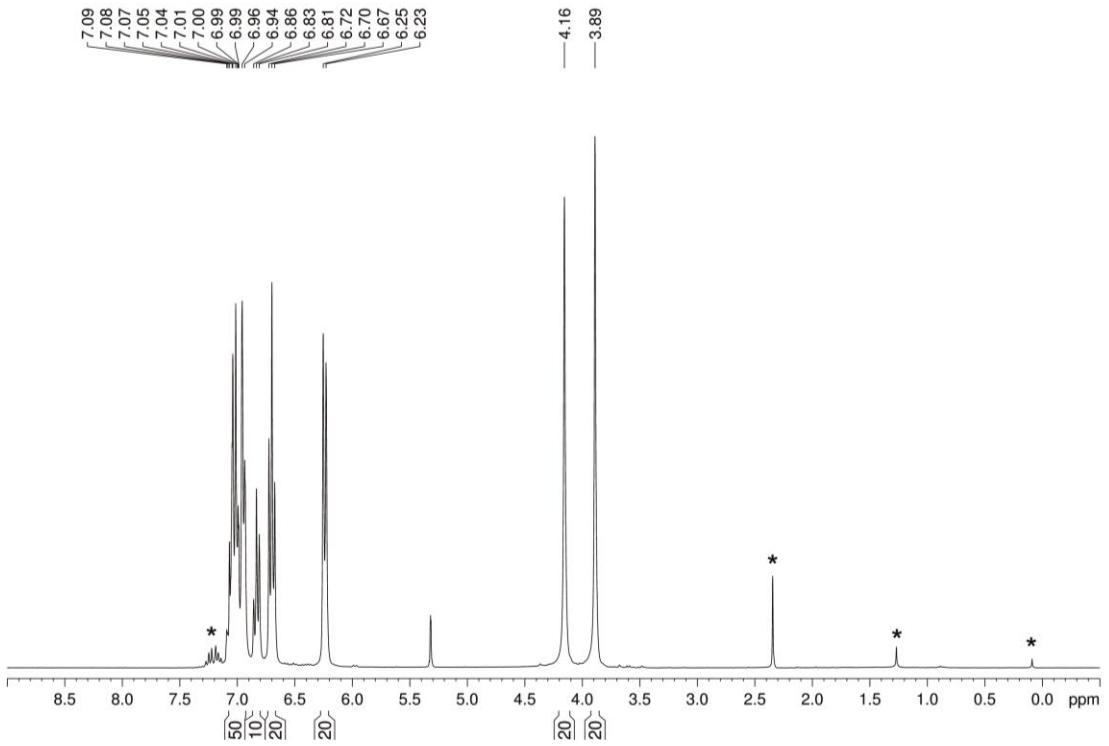

Figure S9.3 ^{1}H NMR spectrum of **2** in CD_2Cl_2 at 300 K. Signals marked with an asterisk are due to different solvents and silicon grease.

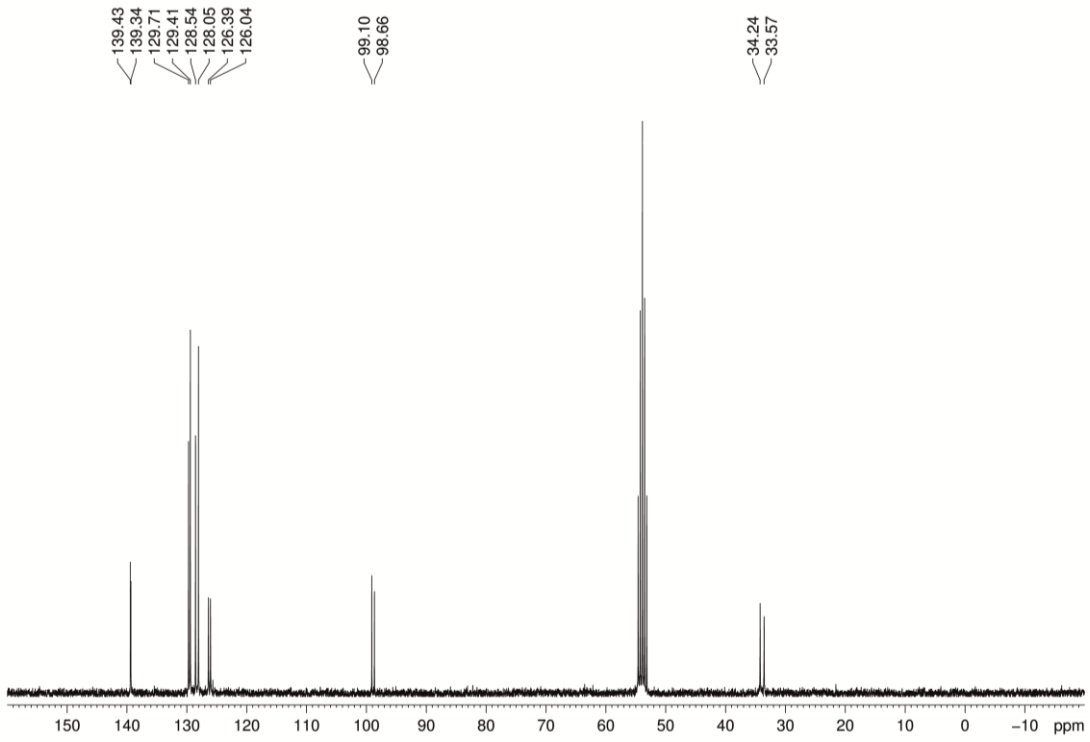

Figure S9.4 $^{13}C\{^{1}H\}$ NMR spectrum of **2** in CD_2Cl_2 at 300 K.

Crystallographic Details

The data for **1** were collected on an Oxford Diffraction GV50 diffractometer equipped with Titan^{S2} CCD detector and a CuK_α microfocus source (λ = 1.54178 Å) using 1° ω scans. The data for **2** · 0.67 C_7H_8 were collected on an Agilent Technologies diffractometer equipped with an Atlas CCD detector and a SuperNova CuK_α microfocus source using 0.25° ω scans. The crystal structure analyses were performed at 128 K (**1**) and 123 K (**2**). Crystallographic data and details of the diffraction experiments are given in Table S9.1.

Using Olex2,[16] the structures were solved by direct methods either with the program ShelXS[17] (**1**) or SIR97[18] (**2**) and refined with least square method on F^2 employing the ShelXL[19] refinement package with anisotropic displacements for non H atoms. The disordered $(As_2)_2$ units in **1** were refined to sum up to full occupancy applying distance and ellipsoid restraints (SUMP, SIMU, SADI). H atoms were located in idealised positions and refined isotropically according to the riding model. A semi-empirical numerical absorption correction based on gaussian[20] integration over a multifaceted crystal model (**1**) or an analytical[21] absorption correction from crystal faces (**2**) was applied. Figures were created with DIAMOND3.0.[22]

Table S9.1 Crystallographic data for **1** and **2**.

	1	**2** · 0.67 C_7H_8
Chemical formula	$C_{80}H_{70}Co_2As_4$	$C_{494}H_{436}Co_{12}As_{30}$
M/g·mol^{-1}	1448.90	9327.16
T/K	128	123
Crystal system	monoclinic	monoclinic
Space group	$P2_1/c$	$P2_1/n$
a/Å	24.5716(3)	12.57980(10)
b/Å	10.39797(13)	92.8970(7)
c/Å	25.6957(3)	17.2928(2)
α/°	90.00	90.00
β/°	105.5140(12)	91.2470(10)
γ/°	90.00	90.00
V/Å³	6325.93(14)	20204.0(3)
Z	4	2
ρ_{cal}/g·cm^{-3}	1.521	1.533
μ/mm^{-1}	6.778	6.931
F(000)	2944.0	9428.0
Crystal size/mm^3	0.1978 x 0.1466 x 0.1121	0.564 x 0.0792 x 0.0572
Radiation	CuK_α	CuK_α
2θ range/°	7.118 to 148.786	5.854 to 142.078
Index ranges	-30≤ h ≤30,	-15≤ h ≤11,
	-11≤ k ≤12,	-111≤ k ≤112,
	-32≤ l ≤31	-21≤ l ≤17
Reflections collected	67331	79296
Independent reflections	12756	37623
	[R_{int} = 0.0463, R_{sigma} = 0.0261]	[R_{int} = 0.0301, R_{sigma} = 0.0471]
Data/restraints/parameters	12756/284/883	37623/1807/2441
Goodness-of-fit on F^2	1.021	1.067
Final R indexes [I>2σ(I)]	R_1 = 0.0406, wR_2 = 0.0968	R_1 = 0.0464, wR_2 = 0.1076
Final R indexes [All Data]	R_1 = 0.0436, wR_2 = 0.0990	R_1 = 0.0558, wR_2 = 0.1102
Largest diff. peak/hole/eA^{-3}	1.22/-0.52	0.81/-0.75

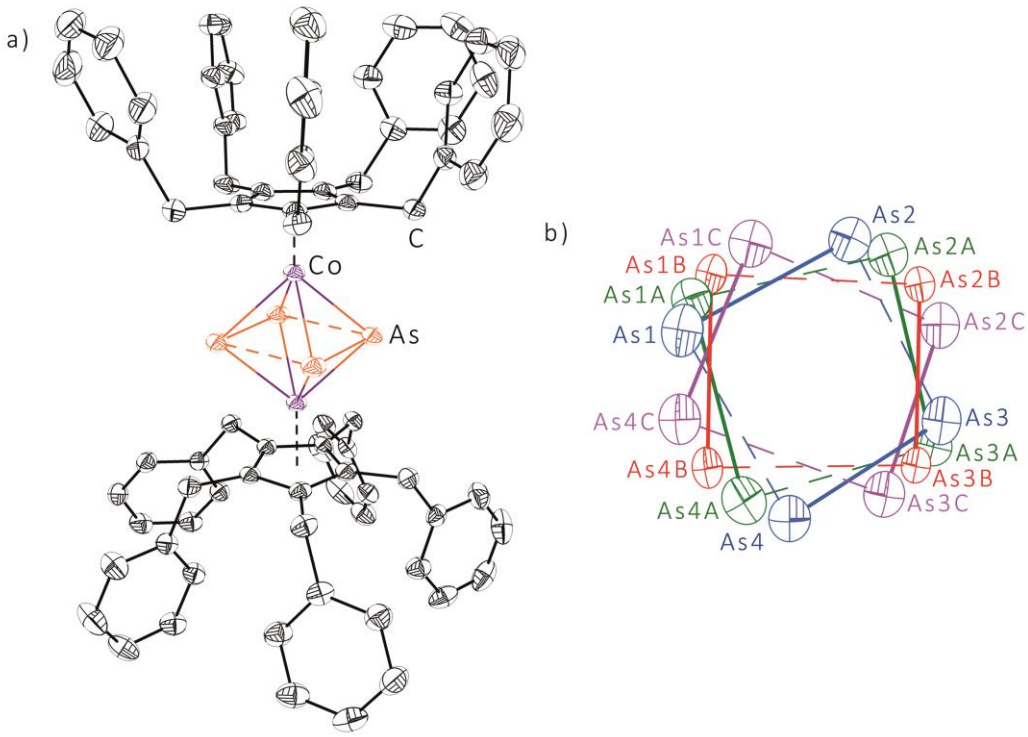

Figure S9.5 a) Molecular structure of **1** (main part) in the solid state. H atoms are omitted for clarity. Thermal ellipsoids are drawn at 50 % probability level. b) Disordered core of compound **1** (occupancy factors 0.16, 0.31, 0.42, 0.11). Cp^{Bn} ligands as well as Co atoms are omitted for clarity. Red coloured As atoms belong to the main part. For selected bond lengths see Table S9.2.

Table S9.2 As-As bond lengths [Å] for compound **1** within the disordered $(As_2)_2$ unit.

d(As-As)		occupancy factor	d(As-As)		occupancy factor
As1-As2	2.421(4)	0.16	As1B-As2B	2.7439(19)	0.42
As2-As3	2.666(4)		As2B-As3B	2.389(2)	
As3-As4	2.382(4)		As3B-As4B	2.742(2)	
As1-As4	2.700(4)		As1B-As4B	2.3764(19)	
As1A-As2A	2.602(2)	0.31	As1C-As2C	2.723(5)	0.11
As2A-As3A	2.599(3)		As2C-As3C	2.347(5)	
As3A-As4A	2.600(3)		As3C-As4C	2.815(5)	
As1A-As4A	2.568(3)		As1C-As4C	2.333(4)	

Details on DFT calculations

The DFT calculations were performed with the TURBOMOLE[23] program package at the RI[24]-BP86[25]/def2-TZVP[26] level of theory. The Multipole Accelerated Resolution of Identity (MARI-J)[27] approach was used to speed up the geometry optimisations which were performed without any symmetry restrains.

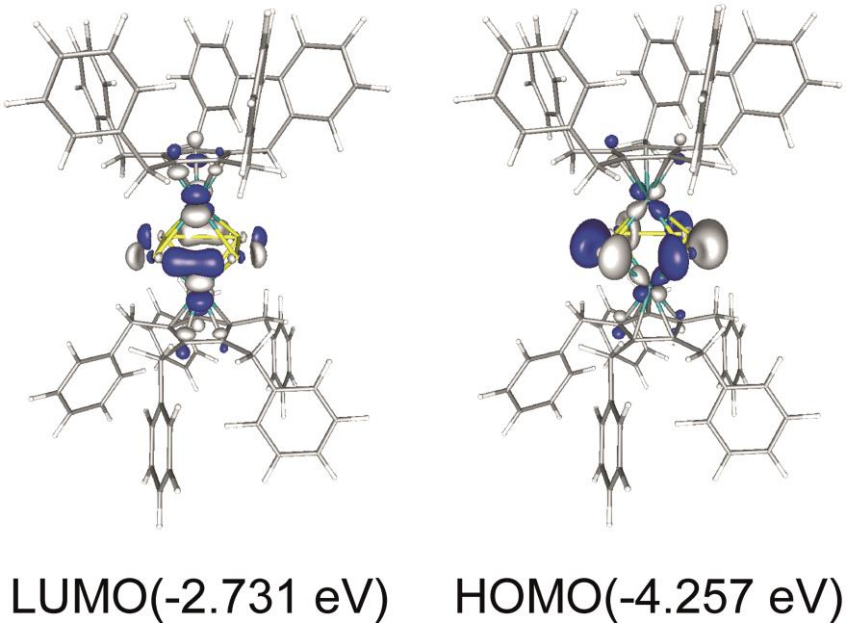

Figure S9.6 Selected molecular orbitals representing the bonding situation in the $(As_2)_2$ core of **1**. Calculated at the BP86/def2-TZVP level of theory.

9.6 References

[1] a) B. M. Crossairt, N. A. Piro, C. C. Cummins, *Chem. Rev.* 2010, *110*, 4164-4177; b) M. Caporali, L. Gonsalvi, A. Rossin, M. Peruzzini, *Chem. Rev.* 2010, *110*, 4178-4235. c) M. Scheer, G. Balázs, A. Seitz, *Chem. Rev.* 2010, *110*, 4236-4256; c) N. A. Giffin, J. D. Masuda, *Coord. Chem. Rev.* 2011, *255*, 1342-1359.

[2] a) A. S. Foust, M. S. Foster, L. F. Dahl, *J. Am. Chem. Soc.* 1969, *91*, 5631-5633; b) A. S. Foust, M. S. Foster, L. F. Dahl, *J. Am. Chem. Soc.* 1969, *91*, 5633-5635.

[3] a) O. J. Scherrer, H. Sitzmann, G. Wolmershäuser, *Angew. Chem. Int. Ed. Engl.* 1989, *28*, 212-213; b) O. J. Scherer, C. Blath, G. Wolmershäuser, *J. Organomet. Chem.* 1990, *387*, C21-C23; c) O. J. Scherer, C. Blath, G. Heckmann, G. Wolmershäuser, *Angew. Chem. Int. Ed. Engl.* 1991, *30*, 850-852.

[4] O. J. Scherer, K. Pfeiffer, G. Heckmann, G. Wolmershäuser, *J. Organomet. Chem.* 1992, *425*, 141-149.

[5] C. M. Knapp, B. H. Westcott, M. A. C. Raybould, J. E. McGrady, J. M. Goicoechea, *Chem. Commun.* 2012, *48*, 12183-12815.

[6] C. von Hänisch, D. Fenkse, F. Weigend, R. Ahlrichs, *Chem. Eur. J.* 1997, *3*, 1494-1498.

[7] C. Graßl, M. Bodensteiner, M. Zabel, M. Scheer, *Chem. Sci.* 2015, *6*, 1379-1382.

[8] Y. Morino, T. Ukaji, T. Ito, *Bull. Chem. Soc. Jpn.* 1966, *39*, 64-71.

[9] H. A. Spinney, N. A. Piro, C. C. Cummins, *J. Am. Chem. Soc.* 2009, *131*, 16233-16243.

[10] A. H. Cowley, N. C. Norman, M. Pakulski, *Dalton Trans.* 1985, *1*, 383-386.

[11] A. Bondi, *J. Phys. Chem.* 1964, *68*, 441-451.

[12] N. G. Connelly, W. E. Geiger, *Chem. Rev.* 1996, *96*, 877-910.

[13] A. L. Rheingold, M. J. Foley, P. J. Sullivan, *J. Am. Chem. Soc.* 1982, *104*, 4727-4279.

[14] M. D. Rausch, W. M. Tsai, J. W. Chambers, *Organometallics* 1989, *8*, 816-821.

[15] a) H. Erdmann, M. V. Unruh, *Z. Anorg. Chem.* 1902, *32*, 437-452; b) O. J. Scherer, H. Sitzmann, G. Wolmershäuser, *J. Organomet. Chem.* 1986, *309*, 77-86.

[16] O.V. Dolomanov, L. J. Bourhis, R. J. Gildea, J. A. K. Howard, H. Puschmann, *J. Appl. Cryst.* 2009, *42*, 339-341.

[17] G. M. Sheldrick, *Acta Cryst.* 2008, *A64*, 112-122.

[18] M. C. Burla, R. Caliandro, M. Camalli, B. Carrozzini, G. L. Cacarano, L. De Caro, C. Giacovazzo, G. Polidori, D. Siliqi, R. Spagna, *J. Appl. Cryst.* 2007, *40*, 609-613.

[19] G. M. Sheldrick, *Acta Cryst.* 2015, *C71*, 3-8.

[20] CrysAlisPro, Version 1.171.37.33, Agilent Technologies UK Ltd, Oxford, UK (compound 1).

[21] R. C. Clark, J. S. Reid, *Acta Cryst.* 1995, *A51*, 887-897.

[22] K. Brandenburg, H. Putz, Diamond3.0, Crystal and Molecular Structure Visualization, Crystal Impact GbR, Bonn, Germany, 2014.

[23] a) F. Furche, R. Ahlrichs, C. Hättig, W. Klopper, M. Sierka, F. Weigend, *WIREs Comput. Mol. Sci.* 2014, *4*, 91-100; b) R. Ahlrichs, M. Bär, M. Häser, H. Horn, C. Kölmel, *Chem. Phys. Lett.* 1989, *162*, 165–169; c) O. Treutler, R. Ahlrichs, *J. Chem. Phys.* 1995, *102*, 346–354.

[24] a) K. Eichkorn, O. Treutler, H. Oehm, M. Häser, R. Ahlrichs, *Chem. Phys. Lett.* 1995, *242*, 652–660; b) K. Eichkorn, F. Weigend, O. Treutler, R. Ahlrichs, *Theor. Chem. Acc.* 1997, *97*, 119-124.

[25] a) P. A. M. Dirac, *Proc. Royal Soc. A* 1929, *123*, 714–733; b) J. C. Slater, *Phys. Rev.* 1951, *81*, 385–390; c) S. Vosko; L. Wilk; M. Nusair, *Can. J. Phys.* 1980, *58*, 1200–1211; d) A. D. Becke, *Phys. Rev. A* 1988, *38*, 3098–3100; e) J. P. Perdew, *Phys. Rev. B* 1986, *33*, 8822–8824.

[26] a) A. Schäfer, C. Huber, R. Ahlrichs, *J. Chem. Phys.* 1994, *100*, 5829-5835; b) K. Eichkorn, F. Weigend, O. Treutler, R. Ahlrichs, *Theor. Chem. Acc.* 1997, *97*, 119-124; c) F. Weigend, R. Ahlrichs, *Phys. Chem. Chem. Phys.* 2005, *7*, 3297-3305; d) F. Weigend, *Phys. Chem. Chem. Phys.* 2006, *8*, 1057-1065.

[27] M. Sierka, A. Hogekamp, R. Ahlrichs, *J. Chem. Phys.* 2003, *118*, 9136-9148.

10. Synthesis and Characterisation of E_n Ligand Complexes (E = P, As) of Nickel

M. Schmidt, M. Eberl and M. Scheer

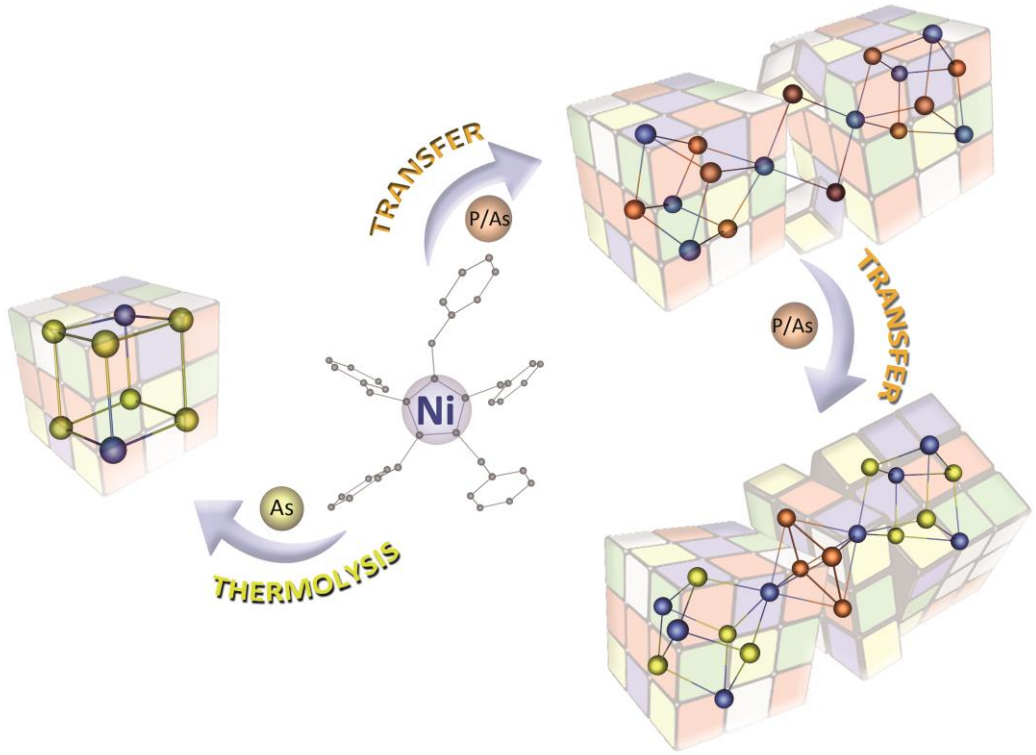

Abstract:

The reaction of *in situ* generated $[Cp^{Bn}Ni(\mu\text{-}Br)]_2$ (**1**) ($Cp^{Bn} = \eta^5\text{-}C_5(CH_2\{C_6H_5\})_5$) with the transfer reagent $[Cp''_2Zr(\eta^{1:1}\text{-}E_4)]$ (E = P, As; $Cp'' = \eta^5\text{-}1,3\text{-}C_5H_3{}^tBu_2$) at room temperature afforded $[(Cp^{Bn}Ni)_3(\mu_3\text{-}E)_4\{Ni(\mu\text{-}Br)\}]_2$ (E = P (**2**), As (**3**)). The structural core motif of **2** and **3** consist of two adjacent, distorted $[Ni_4(\mu\text{-}E)_4]$ cubes, which are connected by bromide bridges (μ_2-mode). The subsequent transfer reaction of **3** with $[Cp''_2Zr(\eta^{1:1}\text{-}E_4)]$ at room temperature leads to the selective formation of $[\{(Cp^{Bn}Ni)_3(\mu_3\text{-}As)_4Ni\}_2(\mu,\eta^{4:4}\text{-}E_4)]$ (E = P (**4**), E = As (**5**)), exhibiting a *cyclo*-E_4 ligand between the distorted cubic $[Ni_4(\mu\text{-}As)_4]$ moieties. In contrast, the co-thermolysis of $[Cp^{Bn}Ni(\mu\text{-}CO)]_2$ (**6**) with As_4 at elevated temperatures exclusively results in the formation of $[(Cp^{Bn}Ni)_2(\mu,\eta^{3:3}\text{-}As_6)]$ (**7**), which is obtained in moderate yields. Complex **7** shows an unprecedented $[Ni_2As_6]$ cuban structural core motif whose composition is unknown for As_n ligand complexes of nickel so far. Beside the synthesis of novel E_n ligand complexes either by transfer reaction or co-thermolysis, a synthetic route for the preparation of **1** and **6** has been developed, yielding both compounds in high yields.

10.1 Author contributions

- Syntheses and characterisations of **1**-**5** and **7** were performed by Monika Schmidt.
- Synthesis and IR spectroscopy of **6** was first performed by Dr. Miriam Eberl during her Ph.D. thesis and the characterisation was completed by Monika Schmidt.
- Manuscript was written by Monika Schmidt.
- Figures were made by Monika Schmidt.
- Single crystal X-ray structure analyses and refinements were performed by Monika Schmidt.

10.2 Introduction

The synthesis of unsubstituted group 15 element ligand complexes is of great interest in current research. Accordingly, a large library of different E_n ligand complexes (E = P, As) has been developed since their establishment in the 1970s.[1] The majority of these complexes has been prepared by co-thermolysis or photolysis of the corresponding transition metal precursor with E_4. Especially in the case of thermolysis, the reactions usually lead to the formation of the thermodynamically favoured complexes. Thus, compounds with different structural core motifs are obtained, since the E_4 tetrahedron often undergoes a successive degradation, yielding smaller E_n ligand complexes. However, subsequent aggregation to larger E_n ligand complexes can also occur. In case of nickel for example, distorted cubanes $[Cp^RNi(\mu_3\text{-}E)]_4$ (**I**) (E = P, As; $Cp^R = Cp^{Me}$ ($\eta^5\text{-}C_5H_4Me$), Cp^+ ($\eta^5\text{-}C_5H_4{}^tBu$))[2] or $[(Cp^RNi)_3(\mu_3\text{-}E)(E_4)]$ (**II**) (E = P, As; $Cp^R = Cp^*$ ($\eta^5\text{-}C_5Me_5$)),[3] the sandwich complex $[Cp^RNi(\eta^3\text{-}E_3)]$ (**III**) (E = P, Cp^R = Cp'' ($\eta^5\text{-}1,3\text{-}C_5H_3{}^tBu_2$),[2] Cp*,[3] Cp^{4iPr} ($\eta^5\text{-}C_5{}^iPr_4H$);[4] E = As, $Cp^R = Cp^{4iPr}$[4]) or prismatic complexes $[(Cp^RNi)_2(\mu,\eta^{3:3}\text{-}E_4)]$ (**IV**) (E = P, As; $Cp^R = Cp^{4iPr}$)[4] are often the favoured structural motifs (Figure 10.1).

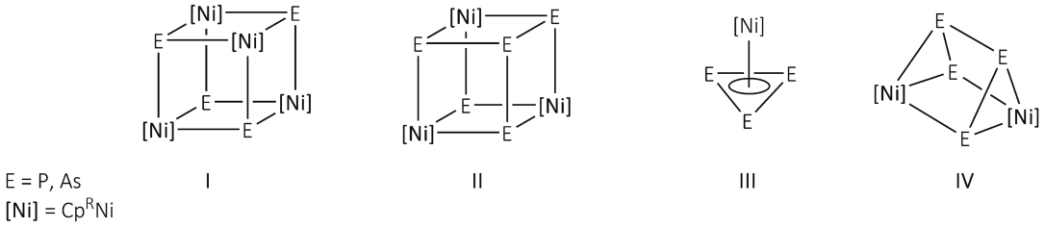

Figure 10.1 Selected representation of favoured structural motifs (**I**-**IV**) in E_n ligand complexes of nickel.

However, the isolation of metastable E_n ligand complexes seems to be a challenging task in the last years. Therefore, E_4 activation by unsaturated transition metal complexes has attracted substantial interest. These compounds bear β-diketiminato ligands or Cp^R ligands as well as labile ligands (e.g. toluene), which can be easily replaced by P_4 or As_4. Recently, we reported on the reaction of $[(L^{iPr}Ni)_2(toluene)]$ (L^{iPr} = CH[CMeN(2,6-$^iPr_2C_6H_3$)]$_2$) with E_4 (E = P, As) yielding

$[(L^{iPr}Ni)_2(\mu,\eta^{3:3}\text{-}E_3)]$ and $[(L^{iPr}Ni)_2(\mu,\eta^{3:3}\text{-}E_4)]$.[5] The P_4 ligand complex was also obtained by the Driess group in 2010.[6] Besides the mentioned nickel precursors, the 17 VE nickel(I) compound [CpNi(IDipp)] (Cp = η^5-C_5H_5, IDipp = $CH[NCH(2,6\text{-}^iPr_2C_6H_3)]_2$) has also been used for the transition metal mediated P_4 transformation, resulting in the formation of the butterfly like P_4 complex $[\{CpNi(IDipp)\}_2(\mu,\eta^{1:1}\text{-}P_4)]$.[7]

A further interesting approach to the synthesis of metastable compounds is the use of transfer reagents. Since the first report of Regitz on the synthesis of $[Cp_2Zr(\eta^2\text{-}C_2{}^tBu_2P_2)]$,[8] this complex was frequently used in salt metathesis reactions, yielding diverse heterocycles.[9] In recent years, especially the Cummins group extended the studies on the transfer of P_n units. These investigations are exemplary highlighted by the synthesis of AsP_3 using $[Na(thf)_3][(\eta^3\text{-}P_3)Nb(ODipp)_3]$ (Dipp = $2,6\text{-}^iPr_2C_6H_3$) and $AsCl_3$.[10] In contrast, the *cyclo*-P_3 unit can be also transferred unscathed from the niobium precursor to $[Rh(PPh_3)_3Cl]$ to form $[Rh(PPh_3)_3(\eta^3\text{-}P_3)]$.[11] Besides the synthesis of phosphorus containing transition metal complexes, transfer reactions also offer an access to the inorganic analogues of frequently used organic molecules like benzene or the cyclopentadienyl anion. Recently, the Cummins group reported on the synthesis of the $[P_2N_3]^-$ by the reaction of $[P_2(C_{14}H_{10})_2]$ with $[N^tBu_4][N_3]$.[12] Despite this progress in the transfer of P_n units, especially the transfer of As_n moieties has been neglected so far due to the lack of an appropriate transfer reagent. Just recently, the synthesis of the pnictogen silicon analogues of benzene $[(PhC(N^tBu)_2)_3Si_3E_3]$ (E = P, As) along with the pnictogen silicon congeners of cyclobutadiene $[(PhC(N^tBu)_2)_2Si_2E_2]$, starting from $[Cp''_2Zr(\eta^{1:1}\text{-}E_4)]$ and $[PhC(N^tBu)_2SiCl]$ at room temperature have been reported by our group. These examples can be seen as a benchmark in organometallic chemistry and in particular in the transfer of As_n units.[13]

These results prompted us to investigate the reactivity of $[Cp''_2Zr(\eta^{1:1}\text{-}E_4)]$ (E = P, As) towards transition metal complexes, especially in the case of nickel. Preliminary studies show a stoichiometry dependent reactivity of $[Cp''_2Zr(\eta^{1:1}\text{-}E_4)]$ towards $[Cp'''Ni(\mu\text{-}Br)]_2$ (Cp''' = η^5-$1,2,4\text{-}C_5H_2{}^tBu_3$),[14] resulting for E = P in the formation of $[(Cp'''Ni)_3(\mu_3\text{-}P)_4\{Ni(\mu\text{-}Br)\}]_2$ or $[Cp'''Ni(\eta^3\text{-}P_3)]$ and $[(Cp'''Ni)_2(\mu,\eta^{3:3}\text{-}P_4)]$.[14a] In contrast, for arsenic the hypothetic bromide bridged cubane dimer $[(Cp'''Ni)_3(\mu_3\text{-}As)_4\{Ni(\mu\text{-}Br)\}]_2$ is not observed, since the reaction yields $[(Cp'''Ni)_2(\mu,\eta^{3:3}\text{-}As_4)]$ and $[\{(Cp'''Ni)_3(\mu_3\text{-}As)_4Ni\}_2(\mu,\eta^{4:4}\text{-}As_4)]$ or $[(Cp'''Ni)_3(\mu_3\text{-}As)(As_4)]$.[14b] Therefore, the question arose whether a decrease in the steric demand of the Cp ligand by using Cp^{Bn} (Cp^{Bn} = η^5-$C_5\{CH_2(C_6H_5)\}_5$) would lead to the selective formation of the observed complexes or to unprecedented As_n ligand complexes of nickel. In addition, it is reasonable to consider whether

co-thermolysis of the corresponding nickel dimer $[Cp^{Bn}Ni(CO)]_2$ with As_4 yield other As_n ligand complexes in comparison to the transfer reaction.

Herein we report on the reaction of *in situ* generated $[Cp^{Bn}Ni(\mu\text{-}Br)]_2$ (**1**) with $[Cp''_2Zr(\eta^{1:1}\text{-}E_4)]$ (E = P, As) at room temperature, giving $[(Cp^{Bn}Ni)_3(\mu_3\text{-}E)_4\{Ni(\mu\text{-}Br)\}]_2$ (E = P (**2**), As (**3**)) in moderate yields. The subsequent reaction of **3** with $[Cp''_2Zr(\eta^{1:1}\text{-}E_4)]$ leads to the selective formation of $[\{(Cp^{Bn}Ni)_3(\mu_3\text{-}As)_4Ni\}_2(\mu,\eta^{4:4}\text{-}E_4)]$ (E = P (**4**), E = As (**5**)). In contrast, the co-thermolysis of $[Cp^{Bn}Ni(\mu\text{-}CO)]_2$ (**6**) with As_4 at elevated temperatures results in the formation of $[(Cp^{Bn}Ni)_2(\mu,\eta^{3:3}\text{-}As_6)]$ (**7**) exclusively.

10.3 Results and Discussion

Following the synthetic route for $[Cp^RNi(\mu\text{-}Br)]_2$ (Cp^R = Cp''', Cp^{3iPr} ($\eta^5\text{-}C_5H^iPr_3$), Cp^{4iPr} ($\eta^5\text{-}C_5H^iPr_4$)),[15] the Cp^{Bn} nickel derivative **1** can easily be prepared by reacting $Cp^{Bn}Li$[16] with $[NiBr_2\cdot dme]$ (for single crystal X-ray structure see Figure S10.14, supplementary information).[17] Subsequent reaction of *in situ* generated **1** with $[Cp''_2Zr(\eta^{1:1}\text{-}E_4)]$ (E = P, As) at room temperature results in the formation of $[(Cp^{Bn}Ni)_3(\mu_3\text{-}E)_4\{Ni(\mu\text{-}Br)\}]_2$ (E = P (**2**), As (**3**)) exclusively (Scheme 10.1). The driving force of the reaction is the formation of the thermodynamically stable complex $[Cp''_2ZrBr_2]$. Interestingly, a degradation of the E_4 unit of $[Cp''_2Zr(\eta^{1:1}\text{-}E_4)]$ to single E atoms is obtained, which are assembled in distorted $[Ni_4(\mu\text{-}E)_4]$ cubes. No unscathed transfer of the E_4 moiety is observed. Moreover, bromide bridges (μ_2-mode) remain in **2** and **3** building a linkage between two adjacent $[Ni_4(\mu\text{-}E)_4]$ units.

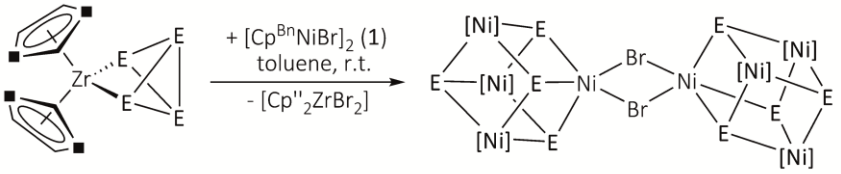

Scheme 10.1 Reactions of *in situ* generated **1** with $[Cp''_2Zr(\eta^{1:1}\text{-}E_4)]$ at room temperature.

After column chromatographic workup, crystals of **2** and **3** suitable for single crystal X-ray diffraction analysis can be obtained by layering a toluene solution with *n*-hexane. **2** and **3** are isostructural and crystallise as dark brown blocks in the triclinic space group $P\bar{1}$. Single crystal X-ray structure analysis of **2** and **3** reveals two distorted $[Ni_4(\mu\text{-}E)_4]$ cubanes, while those nickel atoms bearing no Cp^{Bn} ligands bridge the $[Ni_4(\mu\text{-}E)_4]$ moieties by $[Ni_2(\mu\text{-}Br)_2]$ four-membered rings.

In Figure 10.2, the molecular structure of **3** in the solid state is exemplarily depicted (for the molecular structure of **2** in the solid state see Figure S10.15, supplementary information).

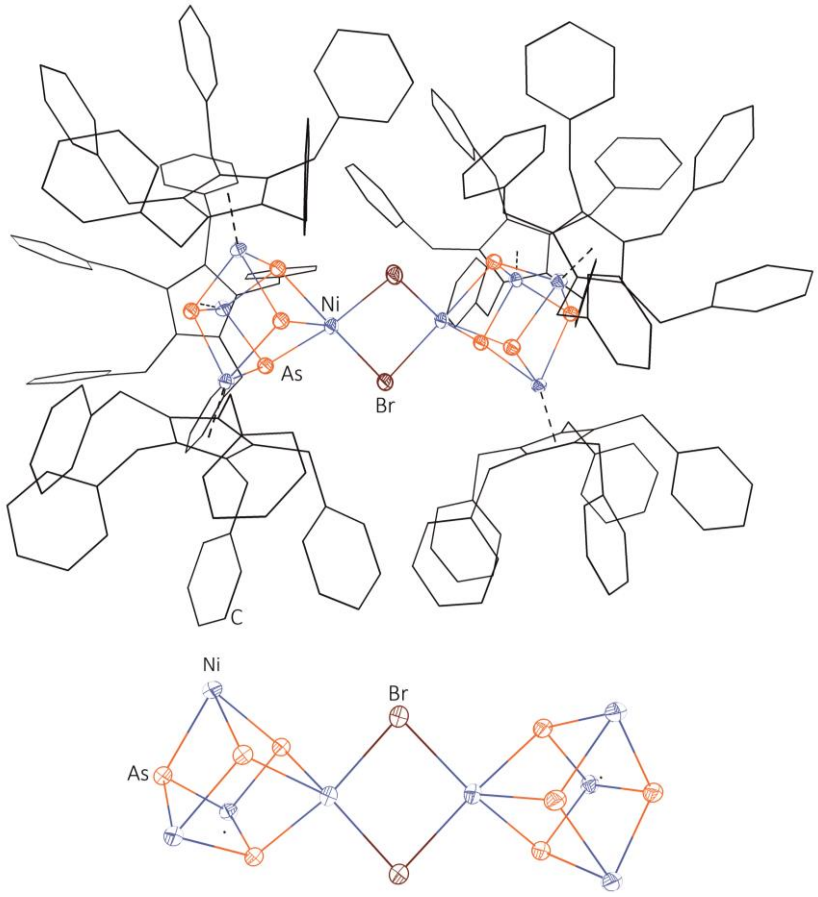

Figure 10.2 Molecular structure of **3** in the solid state (above). H atoms and solvent molecules are omitted for clarity. Cp^{Bn} ligands are drawn in wire or frame model and due to disorder only the main part is depicted. Central structural core motif of **3** (below). Cp^{Bn} ligands are omitted for clarity. Thermal ellipsoids are drawn at 50 % probability level. **2** and **3** are isostructural.

As it can be seen in Table 10.1, complexes **2** and **3** show similar trends in the observed bond lengths and bond angles, being in good agreement with reported bond distances and angles in the distorted cubanes $[Cp^{R}Ni(\mu_3\text{-}E)]_4$ (E = P, As; Cp^{R} = Cp^{Me}, Cp^{+})[2] and $[(Cp^{R}Ni)_3(\mu_3\text{-}E)(E_4)]$ (E = P, As; Cp^{R} = Cp*)[3] or the isostructural complex $[(Cp'''Ni)_3(\mu_3\text{-}P)_4\{Ni(\mu\text{-}Br)\}]_2$.[14a] For the arsenic derivative, the obtained structural core motif of **3** is unknown so far, since the transfer reaction of $[Cp'''Ni(\mu\text{-}Br)]_2$ with $[Cp''_2Zr(\eta^{1:1}\text{-}As_4)]$ yields the prismatic complex $[(Cp'''Ni)_2(\mu,\eta^{3:3}\text{-}As_4)]$ and $[\{(Cp'''Ni)_3(\mu_3\text{-}As)_4Ni\}_2(\mu,\eta^{4:4}\text{-}As_4)]$ or $[(Cp'''Ni)_3(\mu_3\text{-}As)(As_4)]$.[14b]

Table 10.1 Selected bond lengths [Å] and angles [°] of **2** and **3**. Whenever more than one bond is present in the asymmetric unit, the ranges of bond lengths are given.

	2 (E = P)	3 (E = As)
Ni-E	2.1898(5) - 2.2475(6)	2.2939(5) - 2.3581(5)
Ni-Br	2.4204(4) - 2.4585(4)	2.4054(5) - 2.4515(5)
Ni-E-Ni	101.77(2) - 106.92(2)	99.468(17) - 104.838(18)
E-Ni-E	71.558(19) - 75.154(19)	74.420(15) - 77.769(16)
Ni-Br-Ni	87.956(12) / 88.071(12)	84.541(16) / 84.825(16)

Compounds **2** and **3** are well soluble in CH_2Cl_2 and toluene, slightly soluble in *n*-hexane and insoluble in CH_3CN. The ^{1}H and $^{13}C\{^{1}H\}$ NMR spectra of **2** and **3** show the corresponding set of signals for the Cp^{Bn} ligands (Figure S10.1, S10.2 and S10.4, supplementary information). The $^{31}P\{^{1}H\}$ NMR spectrum of **2** shows two sharp singlets at δ = 194.1 ppm and δ = 130.8 ppm with an integral ratio of 3:1 (Figure S10.3 , supplementary information). In comparison to the isostructural derivative $[(Cp'''Ni)_3(\mu_3\text{-}P)_4\{Ni(\mu\text{-}Br)\}]_2$ the signals are downfield shifted (δ = 169.3 ppm and δ = 113.6 ppm).[14a] Unfortunately, the characterisation of **2** and **3** by mass spectrometry was not possible due to the high molecular weight. Several attempts and different spectrometric methods only led to peaks assignable to the Cp^{Bn} ligands.

Since **2** and **3** still contain bromide bridges, it has been reasonable to consider whether further reaction with $[Cp''_2Zr(\eta^{1:1}\text{-}E_4)]$ (E = P, As) can occur. Furthermore, it is also of current interest if a selective formation of $[\{(Cp^{Bn}Ni)_3(\mu_3\text{-}As)_4Ni\}_2(\mu,\eta^{4:4}\text{-}E_4)]$ would be possible, since in the case of the Cp''' derivative different As_n ligand complexes have been obtained. Indeed, the reaction of **3** with $[Cp''_2Zr(\eta^{1:1}\text{-}E_4)]$ at room temperature results in the selective formation of $[\{(Cp^{Bn}Ni)_3(\mu_3\text{-}As)_4Ni\}_2(\mu,\eta^{4:4}\text{-}E_4)]$ (E = P (**4**), E = As (**5**)) in moderate yields (Scheme 10.2).

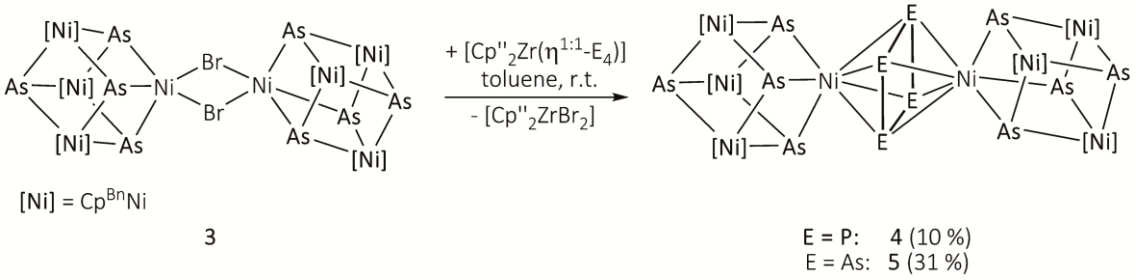

Scheme 10.2 Reactions of **3** with $[Cp''_2Zr(\eta^{1:1}\text{-}E_4)]$ at room temperature.

After column chromatographic workup, crystals of **4** and **5** suitable for single crystal X-ray diffraction analysis are obtained by layering a CH_2Cl_2 solution with CH_3CN (**4**) or *n*-hexane (**5**).

Complexes **4** and **5** are isostructural and crystallise as dark brown to black blocks in the monoclinic acentric space group *Cc* (Flack parameter: 0.030(15) (**4**); 0.06(3) (**5**)). Single crystal X-ray structure analysis of **4** and **5** reveal that the structural core motif of both complexes still consists of two distorted $[Ni_4(\mu\text{-}As)_4]$ cubanes. However, the adjacent $[Ni_4(\mu\text{-}As)_4]$ moieties are bridged by a *cyclo*-E_4 moiety, which is coordinated in a $\mu,\eta^{4:4}$-fashion. Unfortunately, the refinement for **4** and **5** is unstable so far, due to serious disorder of the Cp^{Bn} ligands, solvent molecules and the *cyclo*-E_4 ligands. Consequently, only a preliminary model is obtained, but trends in the bond lengths and bond angles could still be observed. In Figure 10.3 the molecular structure of **5** in the solid state is exemplarily depicted (for the molecular structure of **4** in the solid state see Figure S10.16, supplementary information).

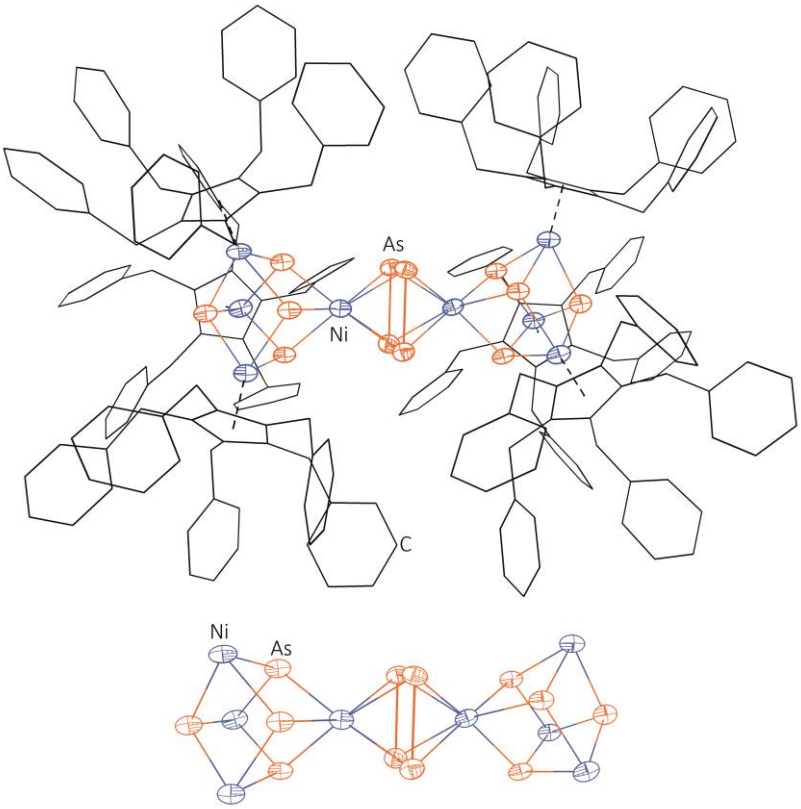

Figure 10.3 Preliminary molecular structure of **5** in the solid state (above). H atoms and solvent molecules are omitted for clarity. Cp^{Bn} ligands are drawn in wire or frame model. Central structural core motif of **5** (below). Cp^{Bn} ligands are omitted for clarity. Due to disorder only the main part is depicted. Thermal ellipsoids are drawn at 50 % probability level. **4** and **5** are isostructural.

The Ni-As bond lengths as well as the bond angles of **4** and **5** within the distorted $[Ni_4(\mu\text{-}As)_4]$ moieties are in the same range as observed for the starting complex **3** (Table 10.2). The average E-E bond length within the planar *cylco*-E_4 ligand of **4** and **5** (**4**: av. 2.21 Å, **5**: av. 2.46 Å) is in line with reported E-E single bond distances in E_4 (E = P: electron diffraction 2.1995 Å,[11] Raman spectroscopy 2.2228 Å,[18] DFT calculations 2.1994 Å;[11] E = As: electron diffraction 2.435 Å,[19] DFT

calculations 2.4372 Å[20]). In terms of simple formalism the *cyclo*-E_4 unit would be expected to be a *cyclo*-E_4^{2-} ligand. E_n ligand complexes exhibiting a *cyclo*-E_4^{2-} moiety are especially rare in the case of E = As.[21] However, the reported bond lengths in these complexes are usually in-between a double and a single bond and the majority contains end-on coordinated *cyclo*-E_4 ligands. The observed elongation of the E-E bond lengths of **4** and **5** to an E-E single bond might be due to the serious disorder of the *cyclo*-E_4 ligand and the bridging $\mu,\eta^{4:4}$-coordination to nickel, respectively. Nevertheless, in literature the 'free' cyclo-E_4^{2-} unit is known in [K@18-crown-6]$_2P_4 \cdot 3\ NH_3$ and [K@18-crown-6]$_2As_4$, showing similar elongation of the E-E bond distances (E = P: av. 2.21 Å; E = As: av. 2.39 Å), which suggests an E-E single bond.[22] Moreover, for E = As recent reports on $[(Cp^{BIG}Fe)_2(\mu,\eta^{4:4}\text{-}As_4)]$ ($Cp^{BIG} = \eta^5\text{-}C_5\{4\text{-}^n BuC_6H_4\}_5$, av. 2.43 Å)[23] and the isostructural Cp''' derivative $[\{(Cp'''Ni)_3(\mu_3\text{-}As)_4Ni\}_2(\mu,\eta^{4:4}\text{-}As_4)]$ (av. 2.43 Å)[14b] show similar trends in the described As-As bond distances within the *cyclo*-As_4 moiety. Besides the synthesis of new representatives of *cyclo*-E_4 ligand complexes, especially the formation of **4** reveals an access to mixed E_n ligand complexes. The latter are only rarely known and are supposed to show an interesting reactivity pattern in coordination chemistry.[10,11,21e]

Table 10.2 Selected preliminary bond lengths [Å] and angles [°] of **4** and **5**. Whenever more than one bond is presented in the asymmetric unit, the ranges of bond lengths are given. Due to disorder, the described bond lengths and bond angles correspond to the main part.

	4 (E = P)	5 (E = As)
Ni-As	2.301(3) - 2.365(3)	2.301(2) - 2.364(2)
Ni-E	2.334(9) - 2.373(9)	2.401(6) - 2.508(8)
E-E	2.198(14) - 2.222(12)	2.438(6) - 2.464(6)
Ni-As-Ni	98.97(10) - 106.02(10)	99.18(9) - 105.80(8)
As-Ni-As	73.17(9) - 78.43(9)	73.21(7) - 78.30(7)
E-E-E	89.8(5) – 90.3(5)	88.3(3) – 91.5(3)

Compounds **4** and **5** are well soluble in CH_2Cl_2 and toluene, slightly soluble in *n*-hexane and insoluble in CH_3CN. The ^1H and $^{13}C\{^1H\}$ NMR spectra of **4** and **5** show the corresponding set of signals for the Cp^{Bn} ligands (Figure S10.5-S10.6 and S10.8-S10.9, supplementary information). The $^{31}P\{^1H\}$ NMR spectrum of **4** shows a sharp singlet at δ = 148.3 ppm for the *cyclo*-P_4 unit (Figure S10.7, supplementary information). Unfortunately, characterisation of **4** and **5** by mass spectrometry was not possible due to the high molecular weight.

While transfer reactions at room temperature lead to metastable compounds inter alia, co-thermolysis results in the formation of the thermodynamically favoured product. Under these

conditions the co-thermolysis of $[Cp^{Bn}Ni(\mu\text{-}CO)]_2$ (**6**) with As_4 at elevated temperatures has been investigated. Since the synthesis of **6** has not been reported in literature, a synthetic strategy was developed, following the preparation of $[Cp^*Ni(\mu\text{-}CO)]_2$.[24] Compound **6** can be obtained in high yields by starting from $Cp^{Bn}Li$[16] with $[NiBr_2{\cdot}dme]$[17] in the presence of CO and subsequent reduction (Scheme 10.3).

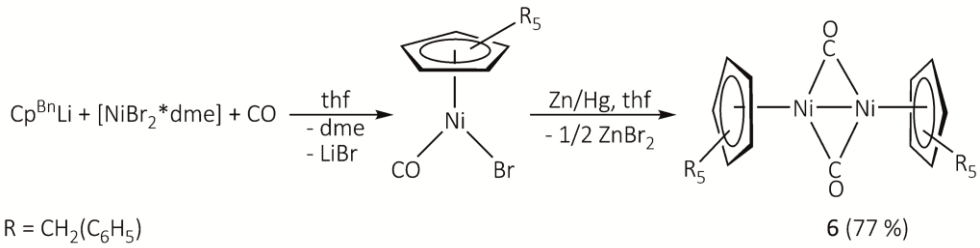

Scheme 10. 3 Synthesis of **6**.

Compound **6** is soluble in CH_2Cl_2 and toluene, slightly soluble in *n*-hexane and insoluble in CH_3CN. By layering a CH_2Cl_2 solution with CH_3CN, **6** crystallises in the triclinic space group $P\bar{1}$ as dark red blocks. Single crystal X-ray structure analysis of **6** reveals a dinuclear complex with bridging CO ligands (μ_2-fashion) as well as a staggered conformation of the Cp^{Bn} ligands (Figure 10.4). Two halves of molecules of **6** can be found in the asymmetric unit, the other halves are generated by symmetry.

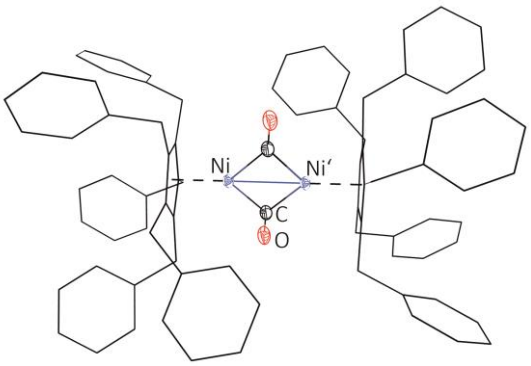

Figure 10.4 Molecular structure of **6** in the solid state. Only one molecule of the two independent molecules of **6** is depicted. H atoms and solvent molecules are omitted for clarity and Cp^{Bn} ligands are drawn in wire or frame model. Thermal ellipsoids are drawn at 50 % probability level. Selected bond lengths [Å] and angles [°]: Ni-Ni' 2.3983(3), Ni-C 1.845(2), Ni-C' 1.866(3), C-O 1.171(3), Cp_{cent}-Ni-Ni' 176.034(26), Ni-C-O 141.8(2), Ni-C'-O' 138.2(3), Ni-C-Ni' 79.98(10).

The bridging μ_2-coordination mode of the carbonyl ligands is in line with the CO stretching bands of **6** in the IR spectrum (ν_{CO}(KBr) = 1813 cm^{-1}, 1863 cm^{-1}). The Ni-Ni single bond in **6** is typically short (Ni-Ni' 2.3983(3) Å) and similar to reported Ni-Ni distances in $[Cp^RNi(\mu\text{-}CO)]_2$ (Cp^R = Cp''': 2.396(4) Å,[25] Cp^{4iPr}: 2.387(4) Å,[25] Cp^{Me} (η^5-C_5H_4Me): 2.3901(1) Å[26]). The ^1H and $^{13}C\{^1H\}$ NMR spectra of **6** show the corresponding set of signals for the Cp^{Bn} ligands as well as a signal for the

carbonyl ligands in the $^{13}C\{^1H\}$ NMR spectrum (δ $[CD_2Cl_2]$ = 237.41 ppm) (see Figure S10.10-S10.11, supplementary information).

Subsequent reaction of **6** with yellow arsenic in decalin for 35 minutes leads to the formation of **7** exclusively (Scheme 10.4).

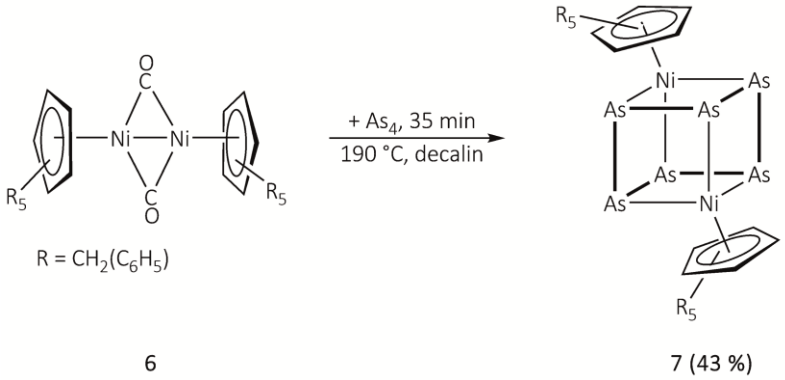

6 **7 (43 %)**

Scheme 10.4 Co-thermolysis of **6** with As_4 in decalin.

Compound **7** is soluble in CH_2Cl_2 and toluene and insoluble in *n*-hexane and CH_3CN. The ^1H and $^{13}C\{^1H\}$ NMR spectra of **7** show the corresponding set of signals for the Cp^{Bn} ligands (Figure S10.12-S10.13, supplementary information). By layering a CH_2Cl_2 solution with CH_3CN, **7** crystallises in the triclinic space group $P\bar{1}$ as dark green plates. Single crystal X-ray structure analysis of **7** reveals a cubic $[Ni_2As_6]$ structural core motif (Figure 10.5). Two halves of molecules of **7** can be found in the asymmetric unit, the other halves are generated by symmetry.

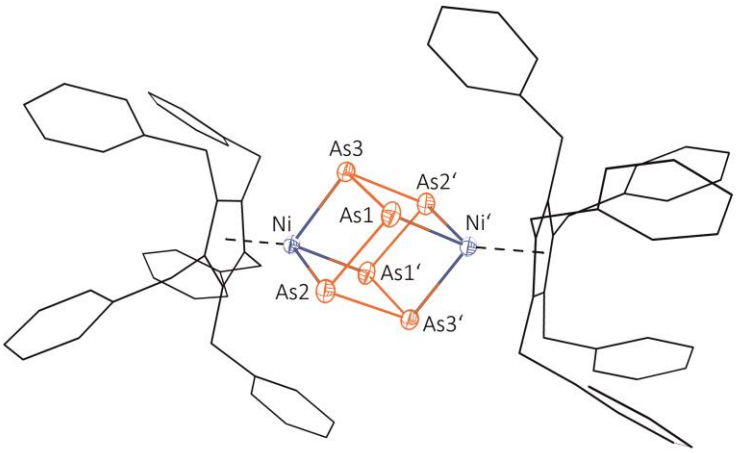

Figure 10.5 Molecular structure of **7** in the solid state. Only one molecule of the two independent molecules of **7** is depicted. H atoms and solvent molecules are omitted for clarity and Cp^{Bn} ligands are drawn in wire or frame model. Thermal ellipsoids are drawn at 50 % probability level. Selected bond lengths [Å] and angles [°]: As1-As2 2.4488(6), As1-As3 2.4371(6), As2-As3' 2.4374(6), Ni-As1 2.3352(7), Ni-As2 2.3455(8), Ni-As3 2.3518(8), As1-As3-As2' 82.241(19), As2-As1-As3 80.44(2), As1-As2-As3' 80.776(19).

Complex **7** can be alternatively considered as a chair like As_6 ligand stabilised by two $[Cp^{Bn}Ni]$ fragments ($\eta^{3:3}$-coordination). All As-As bond lengths within the chair like As_6 unit in **7** are in good agreement with an As-As single bond length (av. 2.44 Å). The $[Ni_2As_6]$ structural core motif of **7** is unknown in literature, since only the distorted cubanes $[Cp^RNi(\mu_3\text{-As})]_4$ (Cp^R = Cp^{Me}, Cp^+)[2] and $[(Cp^*Ni)_3(\mu_3\text{-As})(As_4)]$[3] have been observed so far, which are also obtained by co-thermolysis of $[Cp^RNi(\mu\text{-CO})]_2$ with As_4.

In summary, the syntheses of novel E_n ligand complexes (E = P, As) of nickel bearing the Cp^{Bn} ligand are presented. The reaction of *in situ* generated $[Cp^{Bn}Ni(\mu\text{-Br})]_2$ (**1**) with $[Cp''_2Zr(\eta^{1:1}\text{-}E_4)]$ leads to the selective formation of $[(Cp^{Bn}Ni)_3(\mu_3\text{-}E)_4\{Ni(\mu\text{-Br})\}]_2$ (E = P (**2**), As (**3**)). Here, the degradation of the former E_4 unit of the Zr precursor to single E atoms is observed. This fact is displayed in the distorted $[Ni_4(\mu_4\text{-}E_4)]$ cubanes, which are linked *via* bromide bridges (μ_2-mode). Furthermore, the bromide atoms in **2** and **3** are available to subsequently react with $[Cp''_2Zr(\eta^{1:1}\text{-}E_4)]$. To achieve this, **3** has been reacted with $[Cp''_2Zr(\eta^{1:1}\text{-}E_4)]$ to give $[\{(Cp^{Bn}Ni)_3(\mu_3\text{-As})_4Ni\}_2(\mu,\eta^{4:4}\text{-}E_4)]$ (E = P (**4**), E = As (**5**)) in moderate yields exclusively. In complexes **4** and **5** the two distorted $[Ni_4(\mu_4\text{-}As_4)]$ cubes remain, which are now connected by a *cyclo*-E_4 ligand ($\mu,\eta^{4:4}$-coordination). Consequently, we succeeded in the selective synthesis of **2** and **5**, being isostructural to $[(Cp'''Ni)_3(\mu_3\text{-P})_4\{Ni(\mu\text{-Br})\}]_2$[14a] and $[\{(Cp'''Ni)_3(\mu_3\text{-As})_4Ni\}_2(\mu,\eta^{4:4}\text{-}As_4)]$,[14b] which were previously only obtained in a stoichiometrically dependent reaction of $[Cp'''Ni(\mu\text{-Br})]_2$ with $[Cp''_2Zr(\eta^{1:1}\text{-}E_4)]$. Moreover, the arsenic analogue **3** and the phosphorus congener **4** could be isolated, which could not be observed in the case of the Cp''' ligand. Especially **4** represents an access to mixed E_n ligand complexes, which are only rarely known so far. In contrast, co-thermolysis of $[Cp^{Bn}Ni(\mu\text{-CO})]_2$ (**6**) with As_4 at high temperatures results in the formation of $[(Cp^{Bn}Ni)_2(\mu,\eta^{3:3}\text{-}As_6)]$ (**7**) exclusively. Complex **7** exhibits an unknown cubic $[Ni_2As_6]$ structural core motif, consisting of a chair like As_6 ligand. Thereby, the As_6 moiety is stabilised by two $[Cp^{Bn}Ni]$ fragments. Altogether **2**-**5** and **7** show the preference of nickel to form cubic structural motifs to give novel E_n ligand complexes bearing the Cp^{Bn} ligand.

10.4 Experimental Part

All reactions were performed under an atmosphere of dry argon or nitrogen using glovebox or Schlenk techniques. Solvents were purified, degassed and dried prior to use. As_4,[27] $Cp^{Bn}Li$,[16] $[NiBr_2 \cdot dme]$[17] and $[Cp''_2Zr(\eta^{1:1}\text{-}E_4)]$ (E = P,[28] As[14b]) were prepared according to literature procedure. ^{n}BuLi (c = 1.6 mmol/L, solution in *n*-hexane) was commercially available and was used without further purification.

The NMR spectra were recorded on a Bruker Avance 300 or Avance III HD 400 spectrometer. The EI MS spectra were measured either on a ThermoQuest Finnigan MAT SSQ 710A mass spectrometer or on a Jeol AccuTOF GCX spectrometer. The LIFDI MS spectra were measured on a Jeol AccuTOF GCX spectrometer or on a Finnigan MAT 95 mass spectrometer. The elemental analyses were determined with a Vario ELIII apparatus. The IR spectrum was measured on a VARIAN FTS-800 FT-IR spectrometer.

Synthesis of $[Cp^{Bn}Ni(\mu\text{-}Br)]_2$ (1)

A solution of ^{n}BuLi in *n*-hexane (0.65 mL, c = 1.6 mol/L, 1.04 mmol) was added dropwise to a solution of $Cp^{Bn}H$ (520 mg, 1.01 mmol) in thf at -30 °C. The solution became purple and was stirred for 15 minutes. Then, the reaction mixture was added to a -30 °C cold suspension of $[NiBr_2 \cdot dme]$ (313 mg, 1.01 mmol) in thf. The resulting brownish orange solution was stirred for 1 h at this temperature and for 1 h at room temperature. The solvent was removed under reduced pressure. Subsequent column chromatographic workup (silica gel, *n*-hexane, 14 x 2.5 cm) with n-hexane/toluene (1:1) afforded a red fraction of **1**. The solvent was removed and pure **1** can be obtained as red powder or crystallised by layering a toluene solution with *n*-hexane.

Analytical data of **1**

Crystalline yield: 265 mg (0.20 mmol, 40 % referred to $Cp^{Bn}H$).
LIFDI MS (toluene): *m/z* (%) = 1308.3 (2) ($[Cp^{Bn}NiBr]_2]^+$), 514.3 (100) ($[Cp^{Bn}H\text{-}H_2]^+$).
Elemental Analysis: Calculated (%) for $[C_{80}H_{70}Ni_2Br_2]$ (1308.61 g/mol): C 73.43, H 5.39; found C 72.84, H 5.50.

Synthesis of $[(Cp^{Bn}Ni)_3(\mu_3\text{-}E)_4\{Ni(\mu\text{-}Br)\}]_2$ (E = P (2), As (3))

A solution of ^{n}BuLi in *n*-hexane (**2**: 0.65 mL, c = 1.6 mol/L, 1.04 mmol, **3**: 0.6 mL, c = 1.6 mol/L, 0.96 mmol) was added dropwise to a solution of $Cp^{Bn}H$ (**2**: 516 mg, 0.999 mmol, **3**: 502 mg, 0.97 mmol) in thf at -30 °C. The resulting purple solution was stirred for 1 h at -30 °C and for 1 h

at room temperature. Then, the reaction mixture was added dropwise to a suspension of [$NiBr_2$·dme] (**2**: 308 mg, 0.999 mmol, **3**: 300 mg, 0.97 mmol) in thf at -30°C. The orange brownish reaction mixture was stirred for 1 h at this temperature and for 1 h at room temperature. The solvent was removed under reduced pressure, the brown oily residue was dissolved in toluene and filtered into a solution of [$Cp''_2Zr(\eta^{1:1}\text{-}E_4)$] (E = P: 142 mg, 0.25 mmol, E = As: 181 mg, 0.24 mmol) in toluene. After stirring for 7 days at room temperature, the solvent was removed *in vacuo.* Subsequent column chromatographic workup (silica gel, *n*-hexane, **2**: 14 x 2 cm, **3**: 26 x 2 cm) afforded [Cp''_2ZrBr_2] as first fraction. A mixture of *n*-hexane/toluene (1:2) yielded a green fraction of **2** and **3**, respectively. Crystals of **2** and **3** suitable for single crystal X-ray diffraction analysis can be obtained by layering a CH_2Cl_2 or toluene solution with *n*-hexane.

Analytical data of **2**

Crystalline yield: 95 mg (0.02 mmol, 19 % referred to [$Cp''_2Zr(\eta^{1:1}\text{-}P_4)$]).

^{1}H NMR (CD_2Cl_2): δ [ppm] = 4.14 (s, 60H, CH_2), 6.61 (d, 60H, C_6H_5), 6.81-6.92 (m, 90H, C_6H_5).

^{13}C{^{1}H} NMR (CD_2Cl_2): δ [ppm] = 32.44 (CH_2), 108.47 (C_5), 125.50 (C_6H_5), 127.77 (C_6H_5), 128.73 (C_6H_5), 139.45 (C_6H_5).

^{31}P{^{1}H} NMR (CD_2Cl_2): δ [ppm] = 194.08 (s), 130.79 (s).

^{31}P NMR (CD_2Cl_2): δ [ppm] = 194.08 (s), 130.79 (s).

Positive ion ESI MS (CH_2Cl_2): *m/z* (%) = 655.3 (45) $[Cp^{Bn}Ni(CH_3CN)_2]^+$, 614.2 (100) $[Cp^{Bn}Ni(CH_3CN)]^+$, 573.1 (65) $[Cp^{Bn}Ni]^+$.

Elemental Analysis: Calculated (%) for [$C_{240}H_{210}Ni_8P_8Br_2$] (3971.38 g/mol): C 72.58, H 5.32; found C 72.43, H 5.47.

Analytical data of **3**

Crystalline yield: 196 mg (0.05 mmol, 42 % referred to [$Cp''_2Zr(\eta^{1:1}\text{-}As_4)$]).

^{1}H NMR (CD_2Cl_2): δ [ppm] = 4.09 (s, 60H, CH_2), 6.56 (d, 60H, C_6H_5), 6.77-6.91 (m, 90H, C_6H_5).

EI MS (70 eV, toluene): *m/z* (%) = 514.2 (47) ($[Cp^{Bn}\text{-}H_2]^+$), 423.2 (17) ($[Cp^{Bn}\text{-}H_2\text{-}C_7H_7]^+$), 331.1 (10) ($[Cp^{Bn}\text{-}H_2\text{-}2\ C_7H_7]^+$), 242.1 (4) ($[Cp^{Bn}\text{-}H_2\text{-}3\ C_7H_7]^+$, 91.1 (100) ($[C_7H_7]^+$).

Elemental Analysis: Calculated (%) for [$C_{240}H_{210}Ni_8As_8Br_2 \cdot 2\ CH_2Cl_2$] (4492.83 g/mol): C 64.69, H 4.80; found C 64.82, H 4.77.

Synthesis of $[\{(Cp^{Bn}Ni)_3(\mu_3\text{-}As)_4Ni\}_2(\mu,\eta^{4:4}\text{-}E_4)]$ (E = P (4), E = As (5))

$[(Cp^{Bn}Ni)_3(\mu_3\text{-}As)_4\{Ni(\mu\text{-}Br)\}]_2$ (**4**: 20 mg, 4.63 µmol, **5**: 25 mg, 5.78 µmol) and $[Cp''_2Zr(\eta^{1:1}\text{-}E_4)]$ (E = P: 10 mg, 0.02 mmol, E = As: 20 mg, 0.03 mmol) were dissolved in toluene. After stirring the reaction mixture for approximately 1 day at room temperature, the solvent was removed *in vacuo*. Subsequent column chromatographic workup (silica gel, *n*-hexane, **4**: 8 x 2 cm, **5**: 10 x 2 cm) afforded $[Cp''_2ZrBr_2]$ as first fraction and with toluene or CH_2Cl_2 a brown fraction of **4** and **5**, respectively. Crystals of **4** suitable for single crystal X-ray diffraction analysis can be obtained by layering a CH_2Cl_2 solution with CH_3CN. For **5** crystals are obtained by layering a CH_2Cl_2 solution with *n*-hexane.

Analytical data of **4**

Crystalline yield: 2 mg (0.47 µmol, 10 % referred to **3**).

^{1}H NMR (CD_2Cl_2): δ [ppm] = 4.24 (s, 60H, CH_2), 6.58 (d, 60H, C_6H_5), 6.75-6.90 (m, 90H, C_6H_5).

$^{13}C\{^1H\}$ NMR (CD_2Cl_2): δ [ppm] = 33.47 (CH_2), 107.50 (C_5), 126.02 (C_6H_5), 128.29(C_6H_5), 129.31 (C_6H_5), 140.41 (C_6H_5).

$^{31}P\{^1H\}$ NMR (CD_2Cl_2): δ [ppm] = 148.29 (s).

^{31}P NMR (CD_2Cl_2): δ [ppm] = 148.29 (s).

EI MS (70 eV, toluene): *m/z* (%) = 514.2 (45) ($[Cp^{Bn}\text{-}H_2]^+$), 423.2 (20) ($[Cp^{Bn}\text{-}H_2\text{-}C_7H_7]^+$), 331.1 (11) ($[Cp^{Bn}\text{-}H_2\text{-}2\ C_7H_7]^+$), 241.1 (18) ($[Cp^{Bn}\text{-}H_2\text{-}3\ C_7H_7]^+$, 91.1 (100) ($[C_7H_7]^+$).

Elemental Analysis: Calculated (%) for $[C_{240}H_{210}Ni_8As_8P_4 \cdot CH_2Cl_2]$ (4371.98 g/mol): C 66.21, H 5.32; found C 66.29, H 5.02.

Analytical data of **5**

Crystalline yield: 8 mg (1.79 µmol, 31 % referred to **3**).

^{1}H NMR (CD_2Cl_2): δ [ppm] = 4.24 (s, 60H, CH_2), 6.58 (d, 60H, C_6H_5), 6.75- 6.90 (m, 90H, C_6H_5).

$^{13}C\{^1H\}$ NMR (CD_2Cl_2): δ [ppm] = 32.89 (CH_2), 106.52 (C_5), 125.40 (C_6H_5), 127.67 (C_6H_5), 128.72 (C_6H_5), 139.89 (C_6H_5).

EI MS (70 eV, toluene): *m/z* (%) = 514.2 (58) ($[Cp^{Bn}\text{-}H_2]^+$), 423.2 (17) ($[Cp^{Bn}\text{-}H_2\text{-}C_7H_7]^+$), 331.1 (10) ($[Cp^{Bn}\text{-}H_2\text{-}2\ C_7H_7]^+$), 241.1 (16) ($[Cp^{Bn}\text{-}H_2\text{-}3\ C_7H_7]^+$, 91.1 (100) ($[C_7H_7]^+$).

Elemental Analysis: Calculated (%) for $[C_{240}H_{210}Ni_8As_{12} \cdot 2\ CH_2Cl_2]$ (4632.71 g/mol): C 62.74, H 4.66; found C 62.69, H 4.75.

Synthesis of $[Cp^{Bn}Ni(\mu\text{-}CO)]_2$ (6)

A solution of ^{n}BuLi in *n*-hexane (8 mL, c = 1.6 mol/L, 0.01 mol) was added dropwise to a solution of $Cp^{Bn}H$ (5.3 g, 0.01 mol) in thf (25 mL) at -20 °C. The solution became purple and was stirred for 2 h at -20 °C and for 2 h at room temperature. The solvent was removed under vacuum and the purple residue was washed with *n*-hexane (3 x 10 mL). Then $Cp^{Bn}Li$ in thf was added to a -30 °C cold suspension of $[NiBr_2 \cdot dme]$ (2.56 g, 0.01 mol) in thf. The resulting brownish red solution was stirred overnight and was warmed to room temperature. The next day, CO gas was discharged in the reaction mixture at -20 °C. After 3.5 h, a mixture of zinc-mercury alloy (4.6 g Zn, 0.5 µL Hg) was added to the reaction mixture and it was stirred over night at room temperature. The following day the solvent was removed *in vacuo.* The red residue was extracted with toluene and filtered (Al_2O_3, 8 x 3 cm). The solvent was removed and pure **6** was obtained as red powder or crystallised by layering a CH_2Cl_2 solution with CH_3CN.

Analytical data of **6**

Crystalline yield: 4.75 g (3.94 mmol, 77 % referred to $Cp^{Bn}H$).

^{1}H NMR (CD_2Cl_2): δ [ppm] = 3.59 (s, 20H, CH_2), 6.84-6.87 (m, 20H, C_6H_5), 7.04-7.06 (m, 30H, C_6H_5).

^{13}C{^{1}H} NMR (CD_2Cl_2): δ [ppm] = 30.99 (CH_2), 107.34 (C_5), 126.18 (C_6H_5), 128.43 (C_6H_5), 129.09 (C_6H_5), 133.30 (C_6H_5), 140.09 (C_6H_5), 237.41 (CO).

IR (KBr): ν_{CO} [cm^{-1}] = 1813 (s), 1863 (w).

EI MS (70 eV, CH_2Cl_2): *m/z* (%) = 1204.3 (20) ($[Cp^{Bn}Ni(CO)]_2]^+$), 1088.6 (90) ($[Cp^{Bn}{}_2Ni]^+$), 516.3 (80) ($[Cp^{Bn}H]^+$), 425.3 (60) ($[Cp^{Bn}\text{-}C_7H_7]^+$), 91.1 (100) ($[C_7H_7]^+$).

Elemental Analysis: Calculated (%) for $[C_{82}H_{70}Ni_2O_2]$ (1204.82 g/mol): C 81.74, H 5.85; found C 81.70, H 5.69.

Synthesis of $[(Cp^{Bn}Ni)_2(\mu,\eta^{3:3}\text{-}As_6)]$ (7)

A freshly prepared solution of As_4 (starting from 4.8 g grey arsenic) in 250 mL decalin was added to a suspension of $[Cp^{Bn}Ni(\mu\text{-}CO)]_2$ (315 mg, 0.26 mmol) in 50 mL decalin. The mixture was heated to reflux and the reaction progress was monitored by IR spectroscopy. After 35 min, the carbonyl bands disappeared and the solvent was removed *in vacuo*. The green residue was dissolved in CH_2Cl_2 and filtered through diatomaceous earth. The eluate was concentrated and layered with CH_3CN. After complete diffusion, complex **2** was obtained as dark green needles.

Analytical data of **7**

Crystalline yield: 177 mg (0.11 mmol, 43 % referred to **6**).

^{1}H NMR (CD_2Cl_2): δ [ppm] = 3.37 (s, 20H, CH_2), 6.82-7.09 (m, 50H, C_6H_5).

$^{13}C\{^1H\}$ NMR (CD_2Cl_2): δ [ppm] = 31.15 (CH_2), 105.76 (C_5), 126.05 (C_6H_5), 128.46 (C_6H_5), 129.01 (C_6H_5), 139.89 (C_6H_5).

LIFDI MS (CH_2Cl_2): *m/z* (%) = 1613.8 (39) ($[\{Cp^{Bn}Ni\}_2As_6+O]^+$, 1597.7 (53) ($[\{Cp^{Bn}Ni\}_2As_6]^+$), 1448.0 (100) ($[\{Cp^{Bn}Ni\}_2As_4]^+$), 1371.3 (11) ($[\{Cp^{Bn}Ni\}_2As_3]^+$), 1088.9 (6) ($[Cp^{Bn}{}_2Ni]^+$), 798.1 (82) ($[Cp^{Bn}NiAs_3]^+$).

Elemental Analysis: Calculated (%) for [$C_{80}H_{70}Ni_2As_6 \cdot 0.5\ CH_2Cl_2$] (1640.79 g/mol): C 58.93, H 4.36; found C 59.37, H 4.43.

10.5 Supplementary Information

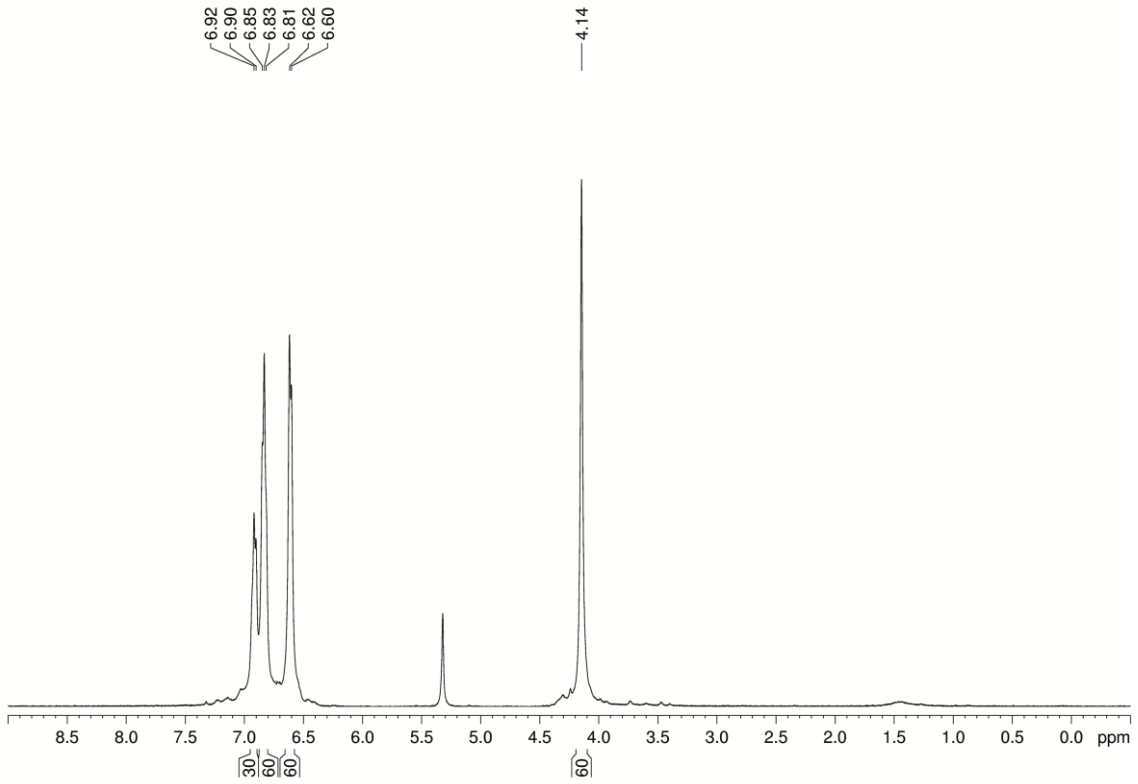

Figure S10.1 ^{1}H NMR spectrum of **2** in CD_2Cl_2 at 300 K.

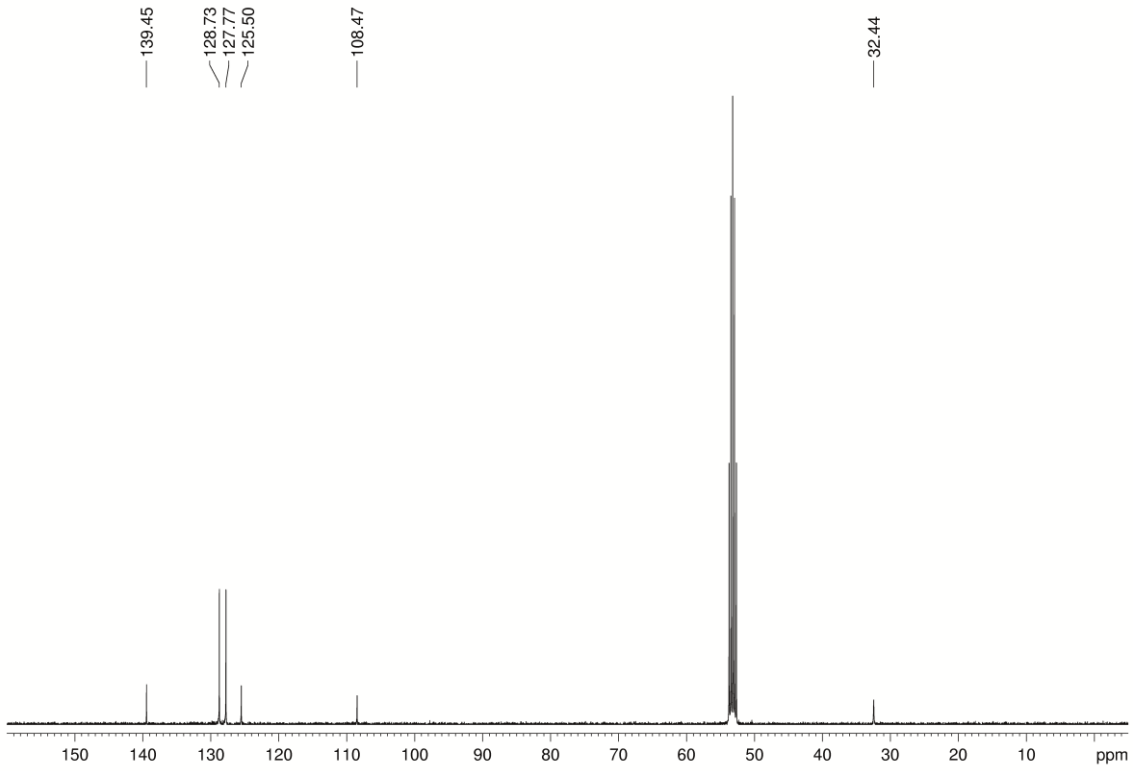

Figure S10.2 $^{13}C\{^{1}H\}$ NMR spectrum of **2** in CD_2Cl_2 at 300 K.

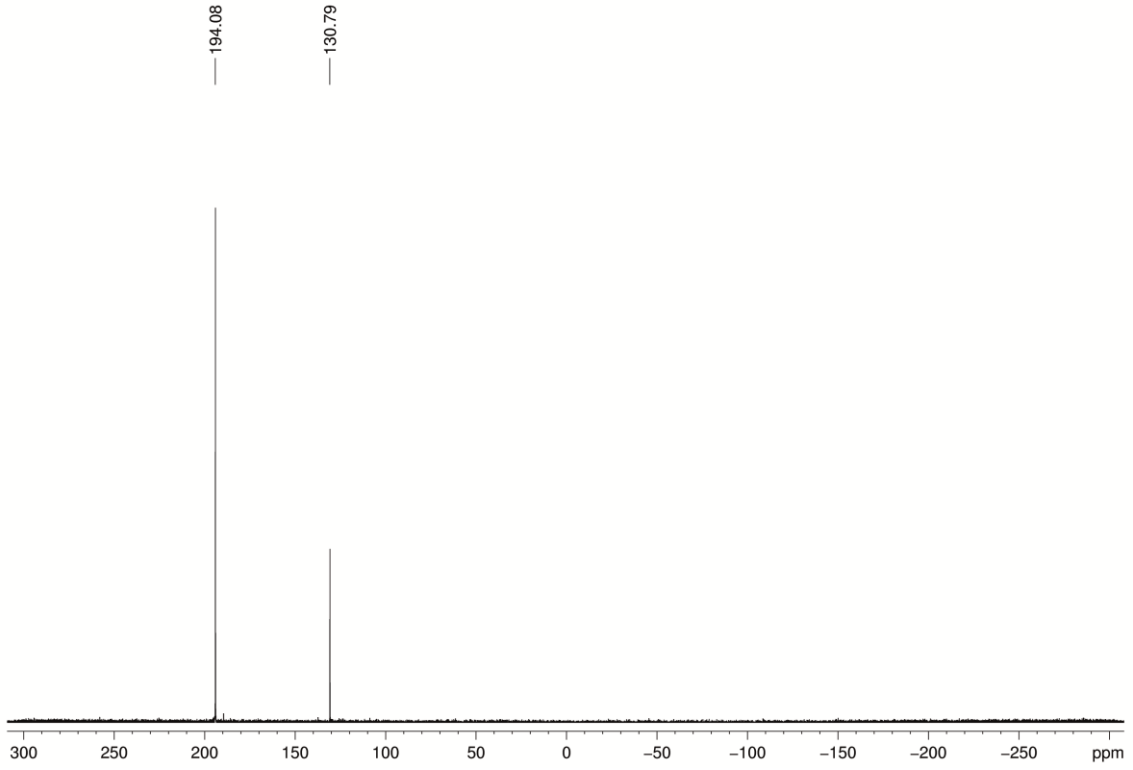

Figure S10.3 $^{31}P\{^{1}H\}$ NMR spectrum of **2** in CD_2Cl_2 at 300 K.

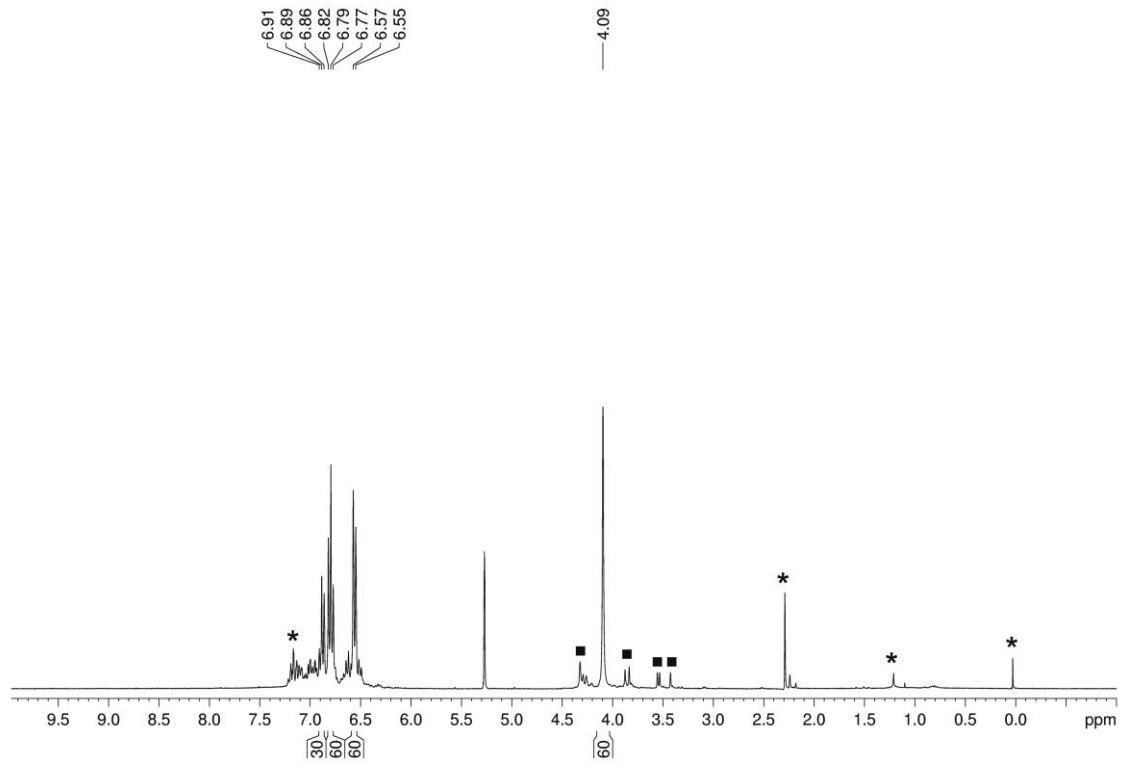

Figure S10.4 ^{1}H NMR spectrum of **3** in CD_2Cl_2 at 300 K. Signals marked with an asterisk are due to different solvents and silicon grease. Signals marked with a square are due to unidentified impurities.

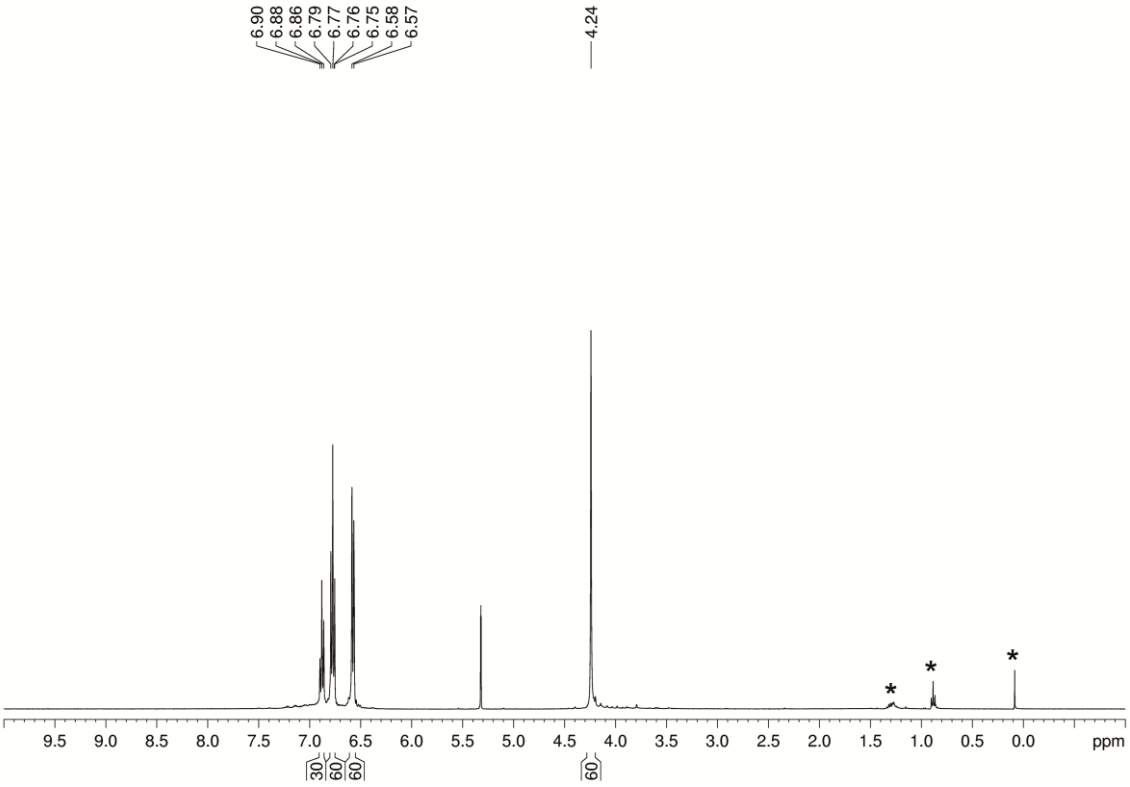

Figure S10.5 ^{1}H NMR spectrum of **4** in CD_2Cl_2 at 300 K. Signals marked with an asterisk are due to different solvents and silicon grease.

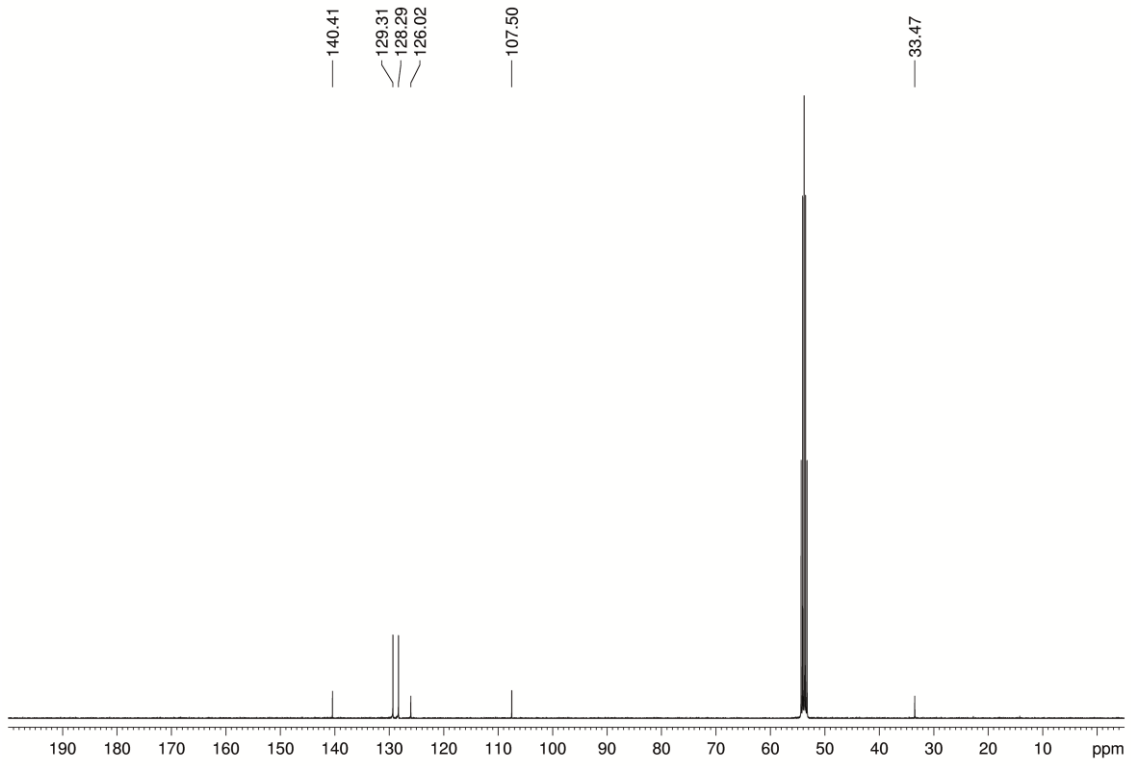

Figure S10.6 $^{13}C\{^{1}H\}$ NMR spectrum of **4** in CD_2Cl_2 at 300 K.

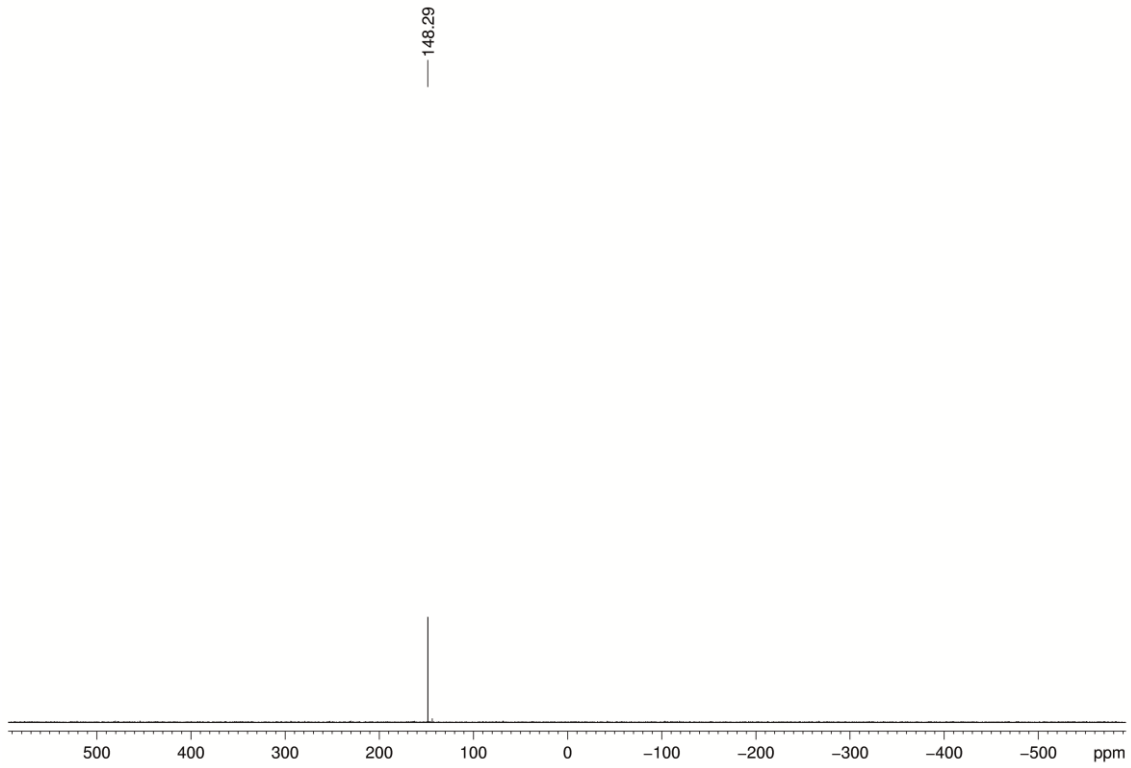

Figure S10.7 $^{31}P\{^{1}H\}$ NMR spectrum of **4** in CD_2Cl_2 at 300 K.

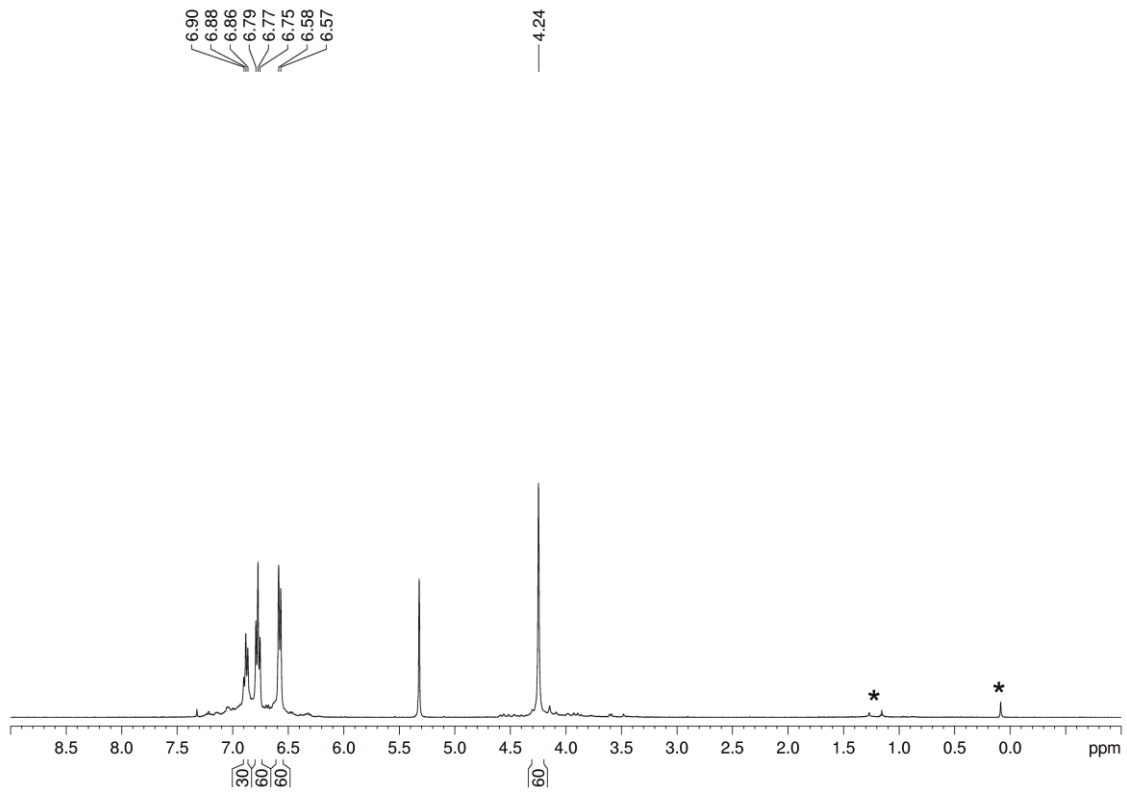

Figure S10.8 ^{1}H NMR spectrum of **5** in CD_2Cl_2 at 300 K. Signals marked with an asterisk are due to different solvents and silicon grease.

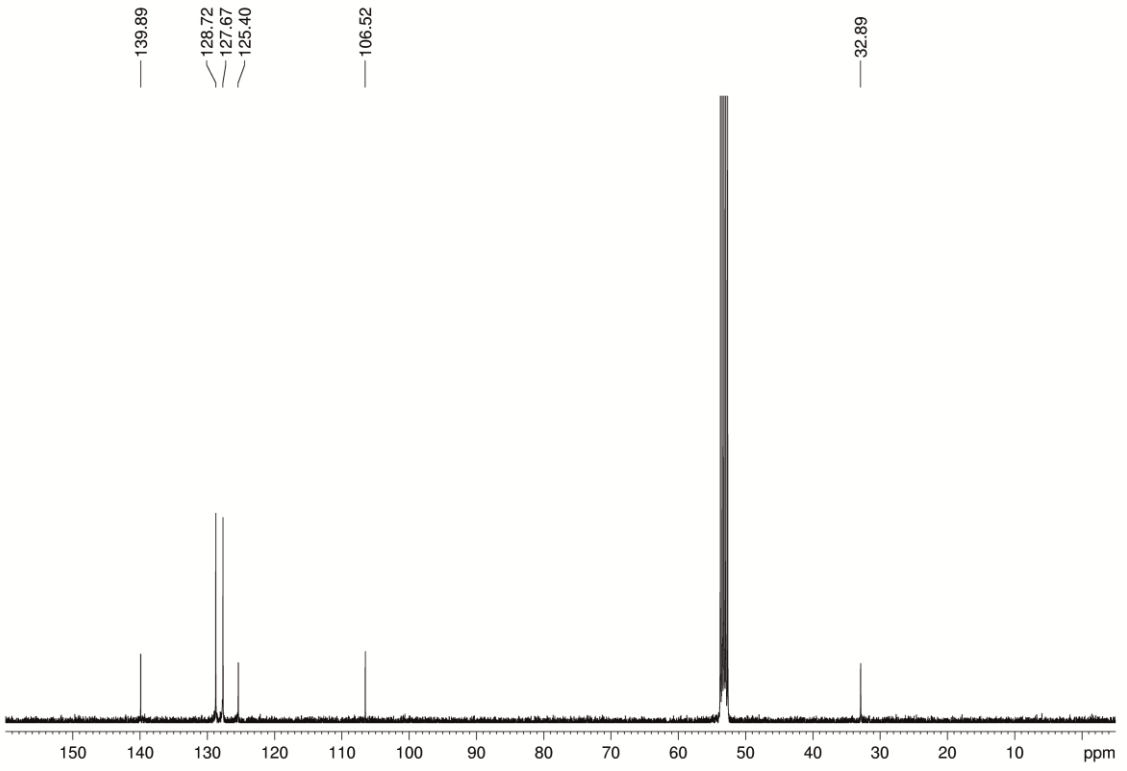

Figure S10.9 $^{13}C\{^{1}H\}$ NMR spectrum of **5** in CD_2Cl_2 at 300 K.

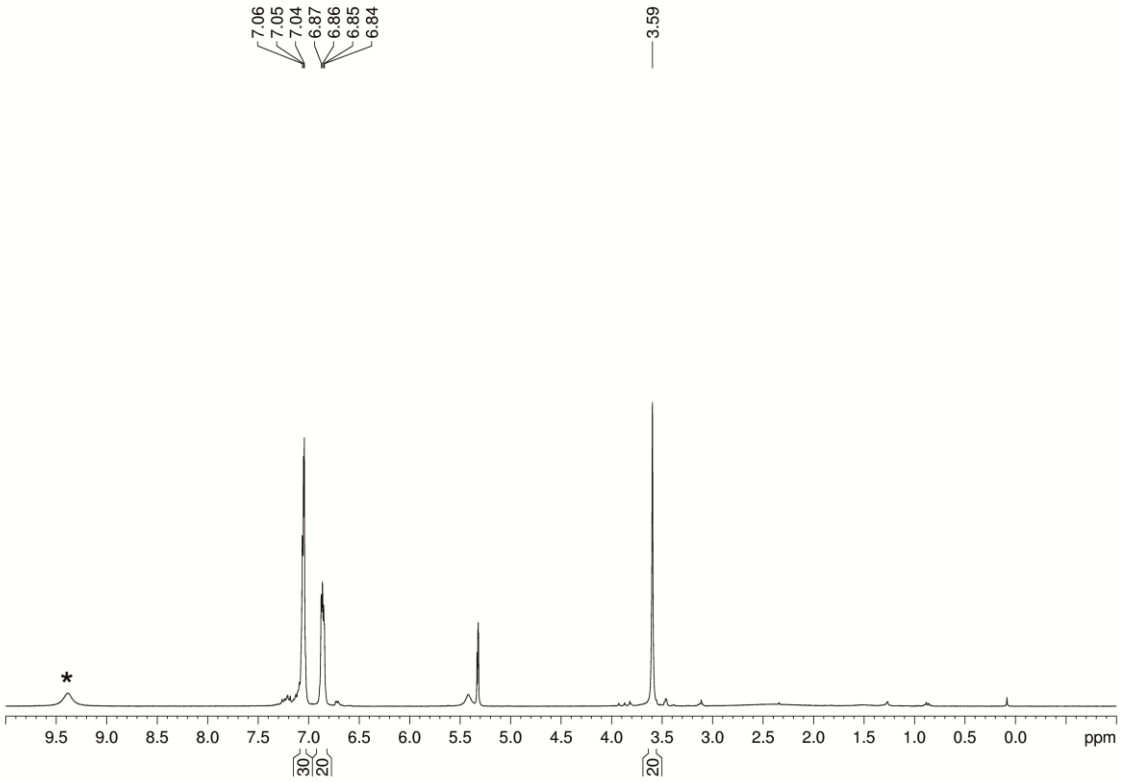

Figure S10.10 ^{1}H NMR spectrum of **6** in CD_2Cl_2 at 300 K. Signal marked with an asterisk is probably due to an impurity.

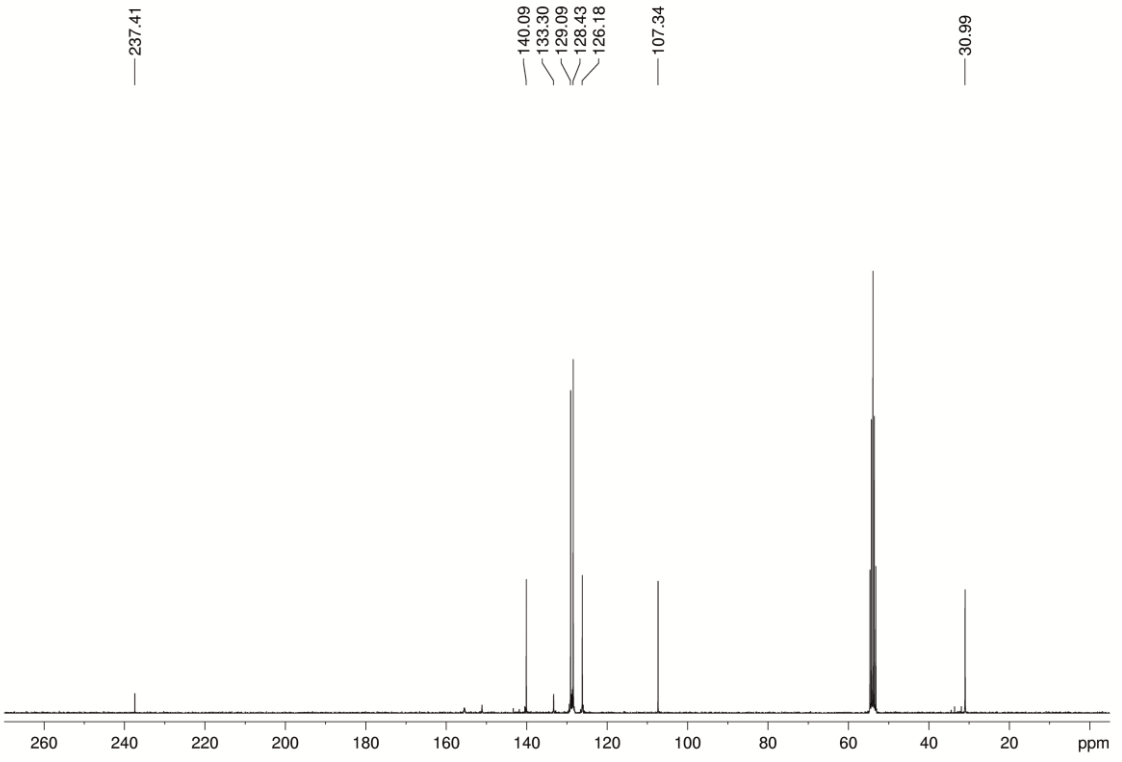

Figure S10.11 $^{13}C\{^{1}H\}$ NMR spectrum of **6** in CD_2Cl_2 at 300 K.

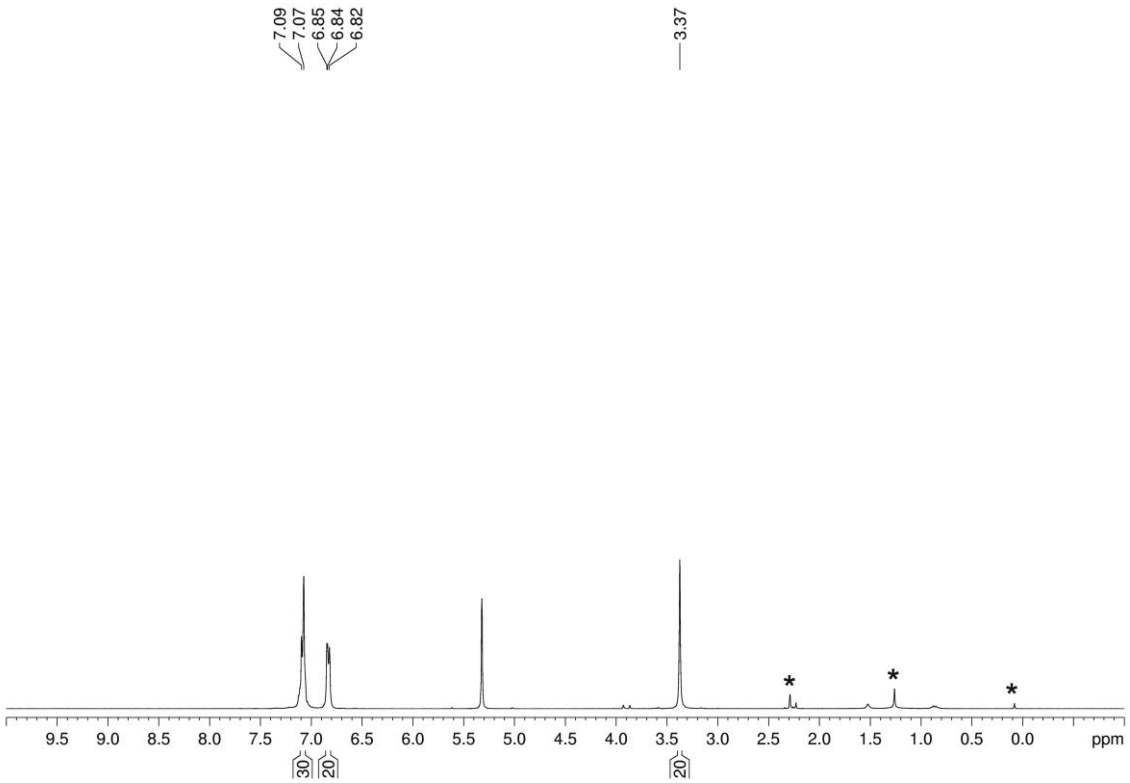

Figure S10.12 ^{1}H NMR spectrum of **7** in CD_2Cl_2 at 300 K. Signals marked with an asterisk are due to different solvents and silicon grease.

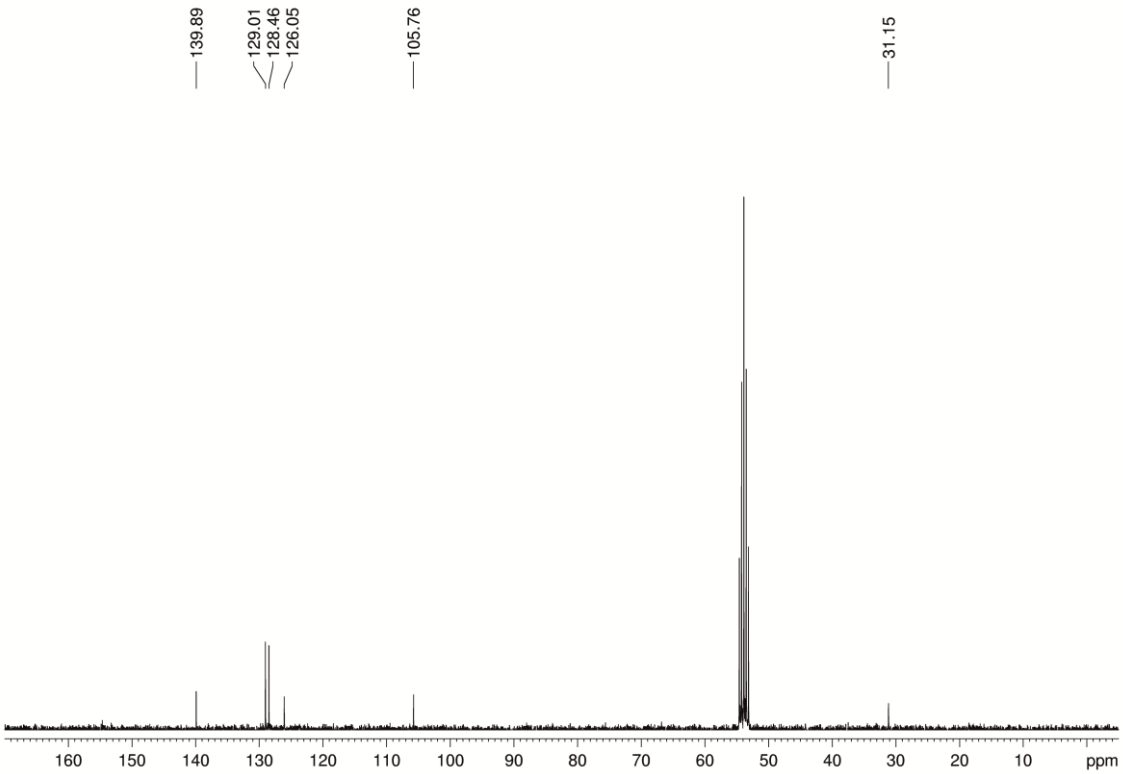

Figure S10.13 $^{13}C\{^{1}H\}$ NMR spectrum of **7** in CD_2Cl_2 at 300 K.

Crystallographic Details

The data for **1**, **2** and **4** were collected on an Agilent Technologies Gemini R-Ultra diffractometer equipped with an Atlas^{S2} CCD detector and using an Enhanced Ultra CuK_α (λ = 1.54178 Å) sealed tube. The data for **3** were collected on an Agilent Technologies diffractometer equipped with an Atlas CCD detector and a SuperNova CuK_α microfocus source. The data for **5**, **6** and **7** were collected on an Oxford Diffraction GV50 diffractometer equipped with Titan^{S2} CCD detector and a CuK_α microfocus source. All measurements were performed at 123 K. Crystallographic data and details of the diffraction experiments are given in Table S10.1-S10.4. Using Olex2,[29] the structures were solved either with the ShelXT[30] (**1-5** and **7**) or SUPERFLIP[31] (**6**) structure solution program using Direct Methods and refined with the ShelXL[32] refinement package using Least Squares minimisation. Especially in case of disorder, commonly used restraints for the ShelXL program were applied (SIMU). Since several solvent molecules are seriously disordered, the EADP constraint was used. Furthermore, the refinements for **4** and **5** are unstable so far due to severe disorder of the Cp^{Bn} ligands, solvent molecules and the *cyclo*-E_4 ligands. Consequently, a preliminary model is obtained. Moreover, H atoms were located in idealised positions and refined isotropically according to the riding model. A semi-empirical numerical absorption correction based on gaussian[33] integration over a multifaceted crystal model (**1**-**3** and **7**), an analytical[34] absorption correction from crystal faces (**4** and **6**) or a semi-empirical numerical absorption correction (multiscan for **5**) was applied.[35] Figures were created with DIAMOND3.0.[36]

Table S10.1 Crystallographic data for **1** and **2**.

	1	**2** · 7 C_7H_8
Chemical formula	$C_{80}H_{70}Ni_2Br_2$	$C_{289}H_{266}Ni_8P_8Br_2$
M/g·mol^{-1}	1308.60	4616.26
T/K	123	123
Crystal system	triclinic	triclinic
Space group	$P\bar{1}$	$P\bar{1}$
a/Å	9.9438(2)	17.71184(9)
b/Å	12.1351(2)	22.61704(12)
c/Å	14.6374(3)	29.89807(18)
α/°	93.4576(16)	95.0607(5)
β/°	107.0166(19)	90.6755(4)
γ/°	112.904(2)	104.5530(5)
V/Å³	1525.06(6)	11540.23(11)
Z	1	2
ρ_{cal}/g·cm^{-3}	1.425	1.328
μ/mm^{-1}	2.646	2.060
F(000)	676.0	4828.0
Crystal size/mm^3	0.243 × 0.119 × 0.084	0.763 × 0.392 × 0.338
Radiation	CuK_α	CuK_α
2θ range/°	8.068 to 133.448	6.87 to 134.16
Index ranges	-11 ≤ h ≤ 11,	-21 ≤ h ≤ 21,
	-14 ≤ k ≤ 14,	-27 ≤ k ≤ 27,
	-17 ≤ l ≤ 17	-34 ≤ l ≤ 35
Reflections collected	33451	580698
Independent reflections	5386	41091
	[R_{int} = 0.0328, R_{sigma} = 0.0198]	[R_{int} = 0.0517, R_{sigma} = 0.0187]
Data/restraints/parameters	5386/0/379	41091/642/2951
Goodness-of-fit on F^2	1.023	1.091
Final R indexes [I>2σ(I)]	R_1 = 0.0228, wR_2 = 0.0564	R_1 = 0.0350, wR_2 = 0.0881
Final R indexes [All Data]	R_1 = 0.0245, wR_2 = 0.0577	R_1 = 0.0357, wR_2 = 0.0886
Largest diff. peak/hole/eA^{-3}	0.34/-0.32	0.71/-0.70

Table S10.2 Crystallographic data for **3** and **4**.

	3 · 6 C_7H_8	**4** ·3 CH_2Cl_2
Chemical formula	$C_{282}H_{258}As_8Ni_8Br_2$	$C_{483}H_{426}As_{16}Ni_{16}P_8Cl_6$
M/g·mol^{-1}	4875.73	8828.75
T/K	123	123
Crystal system	triclinic	monoclinic
Space group	$P\bar{1}$	*Cc*
a/Å	17.7192(2)	28.9845(4)
b/Å	22.6405(2)	16.8386(3)
c/Å	29.9422(3)	43.0838(9)
α/°	94.9583(8)	90.00
β/°	91.1153(8)	100.396(2)
γ/°	104.6084(9)	90.00
V/Å³	11569.5(2)	20682.2(6)
Z	2	2
ρ_{cal}/g·cm^{-3}	1.400	1.418
μ/mm^{-1}	2.792	3.259
F(000)	5016.0	9044.0
Crystal size/mm^3	0.187 × 0.159 × 0.055	0.306 × 0.111 × 0.056
Radiation	CuK_α	CuK_α
2θ range/°	6.342 to 134.16	6.622 to 133.428
Index ranges	-21 ≤ h ≤ 21,	-29 ≤ h ≤ 34,
	-27 ≤ k ≤ 27,	-20 ≤ k ≤ 19,
	-35 ≤ l ≤ 35	-51 ≤ l ≤ 51
Reflections collected	142925	76172
Independent reflections	41028	31449
	[R_{int} = 0.0285, R_{sigma} = 0.0251]	[R_{int} = 0.0554, R_{sigma} = 0.0714]
Data/restraints/parameters	41028/986/2928	31449/161/2494
Goodness-of-fit on F^2	1.059	1.097
Final R indexes [I>2σ(I)]	R_1 = 0.0328, wR_2 = 0.0850	R_1 = 0.0764, wR_2 = 0.1904
Final R indexes [All Data]	R_1 = 0.0366, wR_2 = 0.0875	R_1 = 0.0827, wR_2 = 0.1942
Largest diff. peak/hole/eA^{-3}	1.20/-0.63	1.65/-1.07
Flack parameter	-	0.030(15)

Table S10.3 Crystallographic data for **5** and **6**.

	5 · 3 CH_2Cl_2	**6** ·1.15 CH_2Cl_2 · 0.85 CH_3CN
Chemical formula	$C_{483}H_{426}As_{24}Ni_{16}Cl_6$	$C_{84.85}H_{74.85}Ni_2O_2Cl_{2.3}N_{0.85}$
M/g·mol^{-1}	9180.35	1337.36
T/K	123	123
Crystal system	monoclinic	triclinic
Space group	*Cc*	$P\bar{1}$
a/Å	29.0686(4)	11.7408(4)
b/Å	16.8745(2)	15.2992(3)
c/Å	43.0146(6)	21.0463(6)
α/°	90.00	71.269(2)
β/°	100.7428(13)	84.588(2)
γ/°	90.00	69.505(2)
V/Å³	20729.7(5)	3352.93(17)
Z	2	2
ρ_{cal}/g·cm^{-3}	1.471	1.325
μ/mm^{-1}	3.669	1.927
F(000)	9332.0	1402.0
Crystal size/mm^3	0.221 × 0.143 × 0.11	0.1059 × 0.0589 × 0.0465
Radiation	CuK_α	CuK_α
2θ range/°	6.084 to 146.074	6.484 to 148.612
Index ranges	-35 ≤ h ≤ 25,	-14 ≤ h ≤ 14,
	-20 ≤ k ≤ 19,	-18 ≤ k ≤ 14,
	-53 ≤ l ≤ 52	-26 ≤ l ≤ 26
Reflections collected	56395	36426
Independent reflections	27766	13083
	[R_{int} = 0.0324, R_{sigma} = 0.0390]	[R_{int} = 0.0645, R_{sigma} = 0.0594]
Data/restraints/parameters	27766/131/2458	13083/18/854
Goodness-of-fit on F^2	1.045	1.023
Final R indexes [I>2σ(I)]	R_1 = 0.0759, wR_2 = 0.2033	R_1 = 0.0531, wR_2 = 0.1352
Final R indexes [All Data]	R_1 = 0.0767, wR_2 = 0.2042	R_1 = 0.0652, wR_2 = 0.1461
Largest diff. peak/hole/eA^{-3}	1.79/-1.09	1.02/-1.24
Flack parameter	0.06(3)	-

Table S10.4 Crystallographic data for **7**.

	7 · CH_2Cl_2
Chemical formula	$C_{81}H_{72}As_6Ni_2Cl_2$
M/g·mol^{-1}	1683.22
T/K	123
Crystal system	triclinic
Space group	$P\bar{1}$
a/Å	13.3409(3)
b/Å	16.3105(5)
c/Å	18.4309(5)
α/°	111.660(3)
β/°	103.196(2)
γ/°	92.687(2)
V/Å³	3590.58(17)
Z	2
ρ_{cal}/g·cm^{-3}	1.557
μ/mm^{-1}	4.738
F(000)	1692.0
Crystal size/mm^3	0.312 × 0.072 × 0.065
Radiation	CuK_α
2θ range/°	5.35 to 134.152
Index ranges	-15 ≤ h ≤ 11,
	-18 ≤ k ≤ 19,
	-22 ≤ l ≤ 20
Reflections collected	20936
Independent reflections	12593
	[R_{int} = 0.0215, R_{sigma} = 0.0303]
Data/restraints/parameters	12593/346/931
Goodness-of-fit on F^2	1.027
Final R indexes [I>2σ(I)]	R_1 = 0.0488, wR_2 = 0.1447
Final R indexes [All Data]	R_1 = 0.0537, wR_2 = 0.1502
Largest diff. peak/hole/eA^{-3}	2.33/-0.97

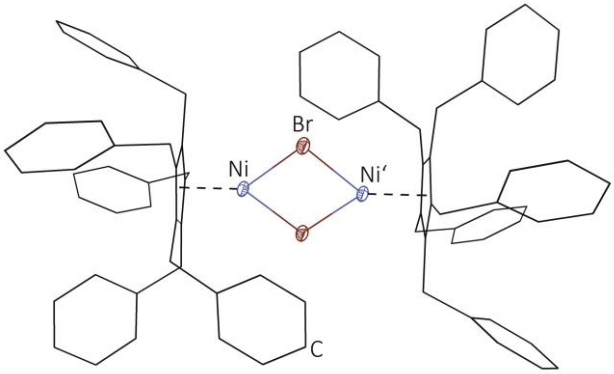

Figure S10.14 Molecular structure of **1** in the solid state. H atoms are omitted for clarity. Cp^{Bn} ligands drawn in wire or frame model. Thermal ellipsoids are drawn at 50% probability level. Selected bond lengths [Å] and angles [°]: Ni···Ni' 3.4191(4), Ni-Br 2.4593(4), Ni'-Br 2.5236(3), Ni-Br-Ni' 89.141(12), Cp_{cent}-Ni-Ni' 177.427(13).

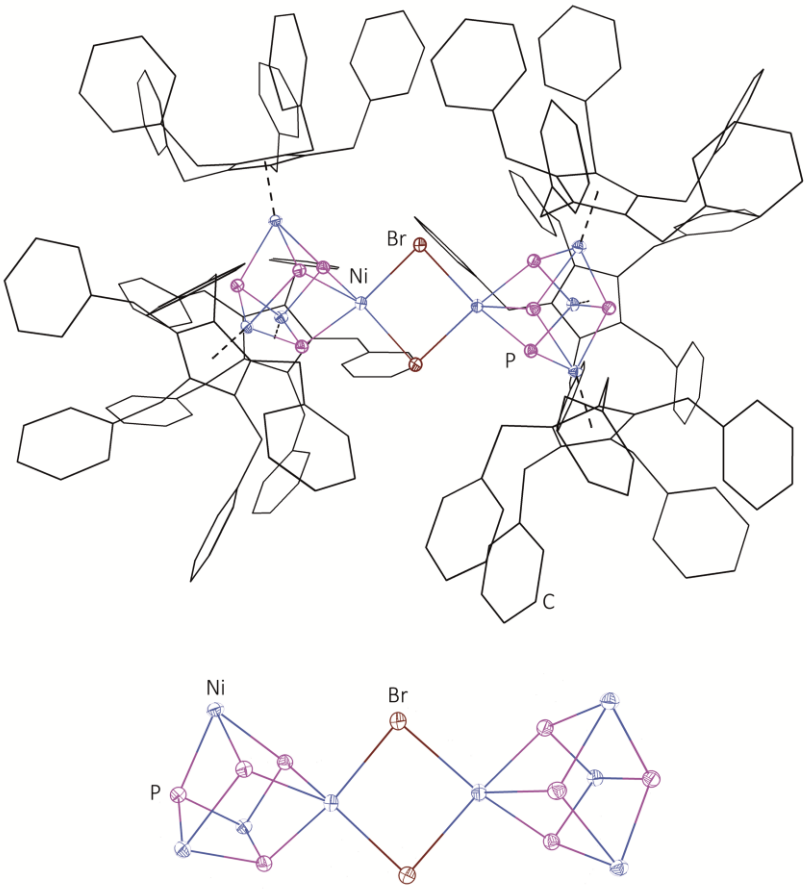

Figure S10.15 Molecular structure of **2** in the solid state (above). H atoms and solvent molecules are omitted for clarity. Cp^{Bn} ligands are drawn in wire or frame model and due to disorder only the main part is depicted. Central structural core motif of **2** (below). Cp^{Bn} ligands are omitted for clarity. Thermal ellipsoids are drawn at 50 % probability level. **2** and **3** are isostructural.

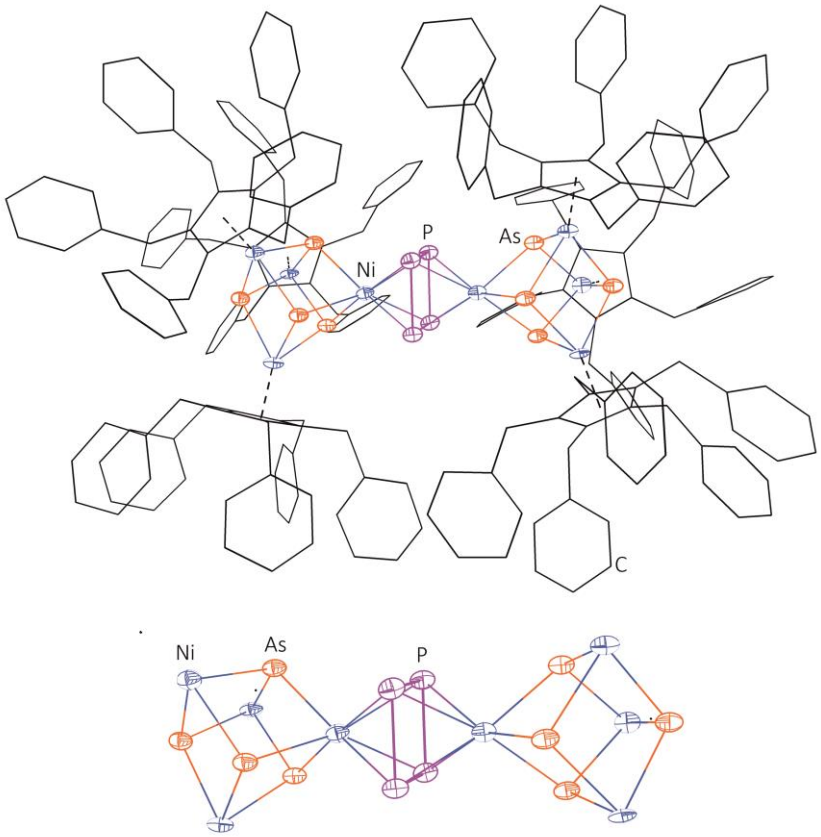

Figure S10.16 Molecular structure of **4** in the solid state (above). H atoms and solvent molecules are omitted for clarity. Cp^{Bn} ligands are drawn in wire or frame model and due to disorder only the main part is depicted. Central structural core motif of **4** (below). Cp^{Bn} ligands are omitted for clarity. Thermal ellipsoids are drawn at 50 % probability level. **4** and **5** are isostructural.

10.6 References

[1] a) O. J. Scherer, *Angew. Chem. Int. Ed. Engl.* 1985, *24*, 924-943; b) O. J. Scherer, *Acc. Chem. Res.* 1999, *32*, 751-762; c) B. M. Crossairt, N. A. Piro, C. C. Cummins, *Chem. Rev.* 2010, *110*, 4164-4177; d) M. Caporali, L. Gonsalvi, A. Rossin, M. Peruzzini, *Chem. Rev.* 2010, *110*, 4178-4235; e) M. Scheer, G. Balázs, A. Seitz, *Chem. Rev.* 2010, *110*, 4236-4256; c) N. A. Giffin, J. D. Masuda, *Coord. Chem. Rev.* 2011, *255*, 1342-1359.

[2] O. J. Scherer, T. Dave, J. Braun, G. Wolmershäuser, *J. Organomet. Chem.* 1988, *350*, C20-C24.

[3] O. J. Scherer, J. Braun, G. Wolmershäuser, *Chem. Ber.* 1990, *123*, 471-475.

[4] O. J. Scherer, J. Braun, P. Walther, G. Wolmershäuser, *Chem. Ber.* 1992, *125*, 2661-2665.

[5] F. C. Graßl, *Ph.D. thesis*, Universität Regensburg, 2013.

[6] S. Yao, Y. Xiong, C. Milsmann, E. Bill, S. Pfirrmann, C. Limberg, M. Driess, *Chem. Eur. J.* 2010, *16*, 436-439.

[7] S. Pelties, D. Herrmann, B. de Bruin, F. Hartl, R. Wolf, *Chem. Commun.* 2014, *50*, 7014-7016.

[8] P. Binger, T. Wettling, R. Schneider, F. Zurmühlen, U. Bergsträsser, J. Hoffmann, G. Maas, M. Regitz, *Angew. Chem.Int. Ed. Engl.* 1991, *30*, 207-210.

[9] selected publications: a) T. Wettling, B. Geissler, R. Schneider, S. Barth, P. Binger, M. Regitz, *Angew. Chem. Int. Ed. Engl.* 1992, *31*, 758-759; b) J. M. Lynam, M. C. Copsey, M. Green, J. C. Jeffery, J. E. McGrady, C. A. Russell, J. M. Slattery, A. C. Swain, *Angew. Chem.Int. Ed. Engl.* 2003, *42*, 2778-2782; c) M. D. Francis, P. B. Hitchcock, *Organometallics* 2003, *22*, 2891-2896; d) C. Fish, M. Green, J. C. Jeffery, R. J. Kilby, J. M. Lynam, C. A. Russell, C. E. Willans, *Organometallics* 2005, *24*, 5789-5791; e) C. Fish, M. Green, J. C. Jeffery, R. J. Kilby, J. M. Lynam, J. E. McGrady, D. A. Pantazis, C. A. Russell, C. E. Willans, *Angew. Chem. Int. Ed. Engl.* 2006, *45*, 6685-6689; f) C. Fish, M. Green, J. C. Jeffery, R. J. Kilby, J. M. Lynam, J. E. McGrady, D. A. Pantazis, C. A. Russell, C. E. Willans, *Chem. Commun.* 2006, 1375-1377; g) C. Fish, M. Green, R. J. Kilby, J. E. McGrady, D. A. Pantazis, C. A. Russell, *Dalton Trans.* 2008, 3753-3758.

[10] B. M. Cossairt, M.-C. Diawara, C. C. Cummins, *Science* 2009, *323*, 602.

[11] B. M. Cossairt, C. C. Cummins, *Angew. Chem. Int. Ed.* 2010, *49*, 1595-1598.

[12] A. Velian, C. C. Cummins, *Science* 2015, *348*, 1001-1004.

[13] A. E. Seitz, M. Eckhardt, A. Erlebach, E. V. Peresypkina, M. Sierka, M. Scheer, *J. Am. Chem. Soc.* 2016, *138,* 10433-10436.

[14] a) M. Eberl, *Ph.D. thesis*, Universität Regensburg, 2011; b) M. Eckhardt, *Ph.D. thesis*, Universität Regensburg, 2014.

[15] M. Schär, D. Saurenz, F. Zimmer, I. Schädlich, G. Wolmershäuser, S. Demeshko, F. Meyer, H. Sitzmann, O. M. Heigl, F. H. Köhler, *Organometallics* 2013, *32*, 6298-6305.

[16] C. Dohmeier, E. Baum, A. Ecker, R. Köppe, H. Schnöckel, *Organometallics* 1996, *15*, 4702-4706. (^{n}BuLi (c = 1.6 mmol/L, solution in *n*-hexane) was used instead of ^{t}BuLi)

[17] M. Scheer, G. Balázs, *Präparative Metallorganische Chemie Für Fortgeschritttene* 2013, Institut für Anorganische Chemie der Universität Regensburg.

[18] N. J. Brassington, H. G. M. Edwards, D. A. Long, *J. Raman Spectrosc.* 1981, *11*, 346-348.

[19] Y. Morino, T. Ukaji, T. Ito, *Bull. Chem. Soc. Jpn.* 1966, *39*, 64-71.

[20] H. A. Spinney, N. A. Piro, C. C. Cummins, *J. Am. Chem. Soc.* 2009, *131*, 16233-16243.

[21] selected publications: a) O. J. Scherer, J. Vondung, G. Wolmershäuser, *J. Organomet. Chem.* 1989, *376*, C35-C38; b) M. Scheer, E. Herrmann, J. Sieler, M. Oehme, *Angew. Chem.* 1991, *103*, 1023-10251; c) O. J. Scherer, R. Winter, G. Wolmershäuser, *Z. Anorg. Allg. Chem.* 1993, *619*, 827-835; d) M. Herberhold, G. Frohmader, W. Milius, *J. Organomet. Chem.* 1996, *522*, 185-196; e) C.Schwarzmaier, A. Noor, G. Glatz, M. Zabel, A. Y. Timoshkin, B. M. Cossairt, C. C. Cummins, R. Kemp, M. Scheer, *Angew. Chem. Int. Ed.* 2011, *50*, 7283-7286.

[22] F. Kraus, T. Hanauer, N. Korber, *Inorg. Chem.* 2006, *45*, 1117-1123.

[23] S. Heinl, *Ph.D. thesis*, Universität Regensburg, 2014.

[24] N. M. Boag, A. J. Goodby, R. Quyoum, *Organometallics* 1992, *11*, 3135-3136.

[25] H. Sitzmann, G. Wolmershäuser, *Z. Naturforsch.* 1995, *50b*, 750-756.

[26] L. B. Byers, L. F. Dahl, *Inorg. Chem.* 1980, *19*, 680-692.

[27] a) H. Erdmann, M. V. Unruh, *Z. Anorg. Chem.* 1902, *32*, 437-452; b) O. J. Scherer, H. Sitzmann, G. Wolmershäuser, *J. Organomet. Chem.* 1986, *309*, 77-86.

[28] O. J. Scherer, M. Swarowsky, H. Swarowsky, G. Wolmershäuser, Angew. Chem. Int. Ed. 1988, 27, 694-695.

[29] O. V. Dolomanov, L. J. Bourhis, R. J. Gildea, J. A. K. Howard, H. Puschmann, *J. Appl. Cryst.* 2009, *42*, 339-341.

[30] G. M. Sheldrick, *Acta Cryst.* 2015, *A71*, 3-8.

[31] L. Palatinus, G. Chapuis, *J. Appl. Cryst.* 2007, *40*, 786-790.

[32] G. M. Sheldrick, *Acta Cryst.* 2015, *C71*, 3-8.

[33] a) CrysAlisPro, Version 1.171.38.41, Agilent Technologies UK Ltd, Oxford, UK (**1** and **7**); b) CrysAlisPro, Version 1.171.38.42b, Agilent Technologies UK Ltd, Oxford, UK (**2** and **3**)

[34] R. C. Clark, J. S. Reid, *Acta Cryst.* 1995, *A51*, 887-897.

[35] CrysAlisPro, Version 1.171.37.35e, Agilent Technologies UK Ltd, Oxford, UK.

[36] K. Brandenburg, H. Putz, Diamond3.0, Crystal and Molecular Structure Visualization, Crystal Impact GbR, Bonn, Germany, 2014.

11. Conclusion

This work deals with the preparation of transition metal complexes bearing the Cp^{Bn} ligand (Cp^{Bn} = η^5-$C_5(CH_2\{C_6H_5\})_5$), which are used as starting materials for the synthesis of As_n ligand complexes. The latter are obtained either by co-thermolysis of the corresponding cyclopentadienyl containing carbonyl complexes with As_4 at elevated temperatures or by transfer reaction using $[Cp''_2Zr(\eta^{1:1}\text{-}As_4)]$ (Cp'' = η^5-1,3-$C_5H_3{}^tBu_2$) as an arsenic source under mild reaction conditions. In addition, the reactivity of selected As_n ligand complexes towards coinage metal salts and the redox chemistry of $[Cp^*Fe(\eta^5\text{-}As_5)]$ (Cp^* = η^5-C_5Me_5) has been investigated. Within this thesis, the introductory part (chapter 1) gives a brief overview of the relevance of As_n ligand complexes in organometallic chemistry as well as of its reactivity. Furthermore, the research objectives (chapter 2) and some general aspects of the Cp^{Bn} ligand and its transition metal complexes have been discussed (chapter 3), followed by the obtained results which are presented in the chapters 4-10.

11.1 Synthesis of Transition Metal Precursors Bearing the Cp^{Bn} Ligand

A major part of this work deals with the synthesis of novel As_n ligand complexes of the transition metals chromium, molybdenum, iron, cobalt and nickel bearing the Cp^{Bn} ligand. Here, suitable precursors have been prepared for the co-thermolyses and transfer reactions. While co-thermolysis requires cyclopentadienyl containing carbonyl complexes of the general formula $[Cp^{Bn}M(CO)_x]_y$, for transfer reactions $[Cp^{Bn}M(\mu\text{-}Br)]_2$ is used (M = Fe (**1**), Ni (**2**)). Therefore, a simple synthesis for **1** and **2** is presented (Scheme 11.1). Unfortunately, **1** could not be isolated within the scope of this thesis. Consequently, **1** has usually been generated *in situ* for the subsequent reactions. In contrast, **2** is obtained in moderate yields. In the case of thermolysis, for M = Mo and Co, the preparation of $[Cp^{Bn}Mo(CO)_2]_2$ and $[Cp^{Bn}Co(CO)_2]$ is reported in the literature, whereas $[Cp^{Bn}Cr(CO)_2]_2$ (**3**) and $[Cp^{Bn}Ni(CO)]_2$ (**4**) are obtained in good yields by following the synthetic route for $[Cp^{Bn}Mo(CO)_2]_2$ (for M = Cr) and $[Cp^*Ni(\mu\text{-}CO)]_2$ (M = Ni), respectively (Scheme 11.1). For iron, the original synthesis for $[Cp^{Bn}Fe(CO)_2]_2$ (**5**) has been improved, providing **5** in 87 % yield (literature: 8%).

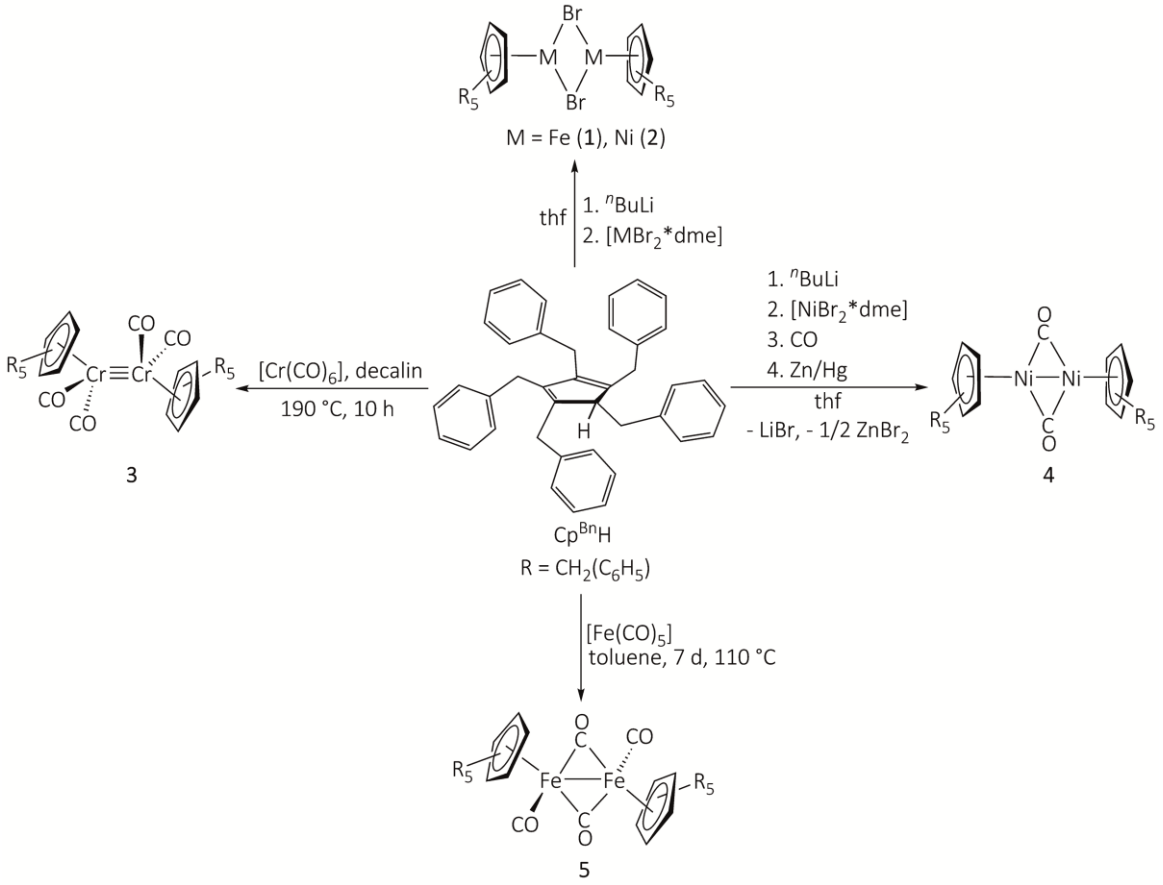

Scheme 11.1 Syntheses of the transition metal precursors **1**-**5**.

11.2 Synthesis of As_n Ligand Complexes

Although a variety of As_n ligand complexes has been described so far, the preparation of these compounds are much more challenging than the synthesis of P_n ligand complexes. Moreover, arsenic complexes bearing the Cp^{Bn} ligand are not reported to date, whereas some Cp^{Bn} derivatives of the lighter congener phosphorus are known. Accordingly, it has been the scope of this thesis to synthesise novel As_n ligand complexes carrying the Cp^{Bn} ligand. Furthermore, to compare the influence of the reaction conditions on the overall yield of these compounds, the latter has been prepared in some cases by co-thermolysis at elevated temperatures as well as by transfer reaction with $[Cp''_2Zr(\eta^{1:1}\text{-}As_4)]$ at room temperature. In the following, all As_n ligand complexes are summarised according to the type of synthetic strategy: (a) is referred to co-thermolysis at higher temperatures and (b) describes a comparison between co-thermolysis and transfer reaction.

(a) Co-Thermolysis of $[Cp^{Bn}M(CO)_x]_y$ (M = Cr (3), Mo, x = y = 2; M = Co, x = 2, y = 0) with As_4 at Elevated Temperatures

Under thermolytic conditions, usually the thermodynamically favoured complexes are obtained. In Scheme 11.2, the As_n ligand complexes formed by the reaction of $[Cp^{Bn}M(CO)_x]_y$ (M = Cr (**3**), Mo, x = y = 2; M = Co, x = 2, y = 0) with As_4 in decalin are summarised.

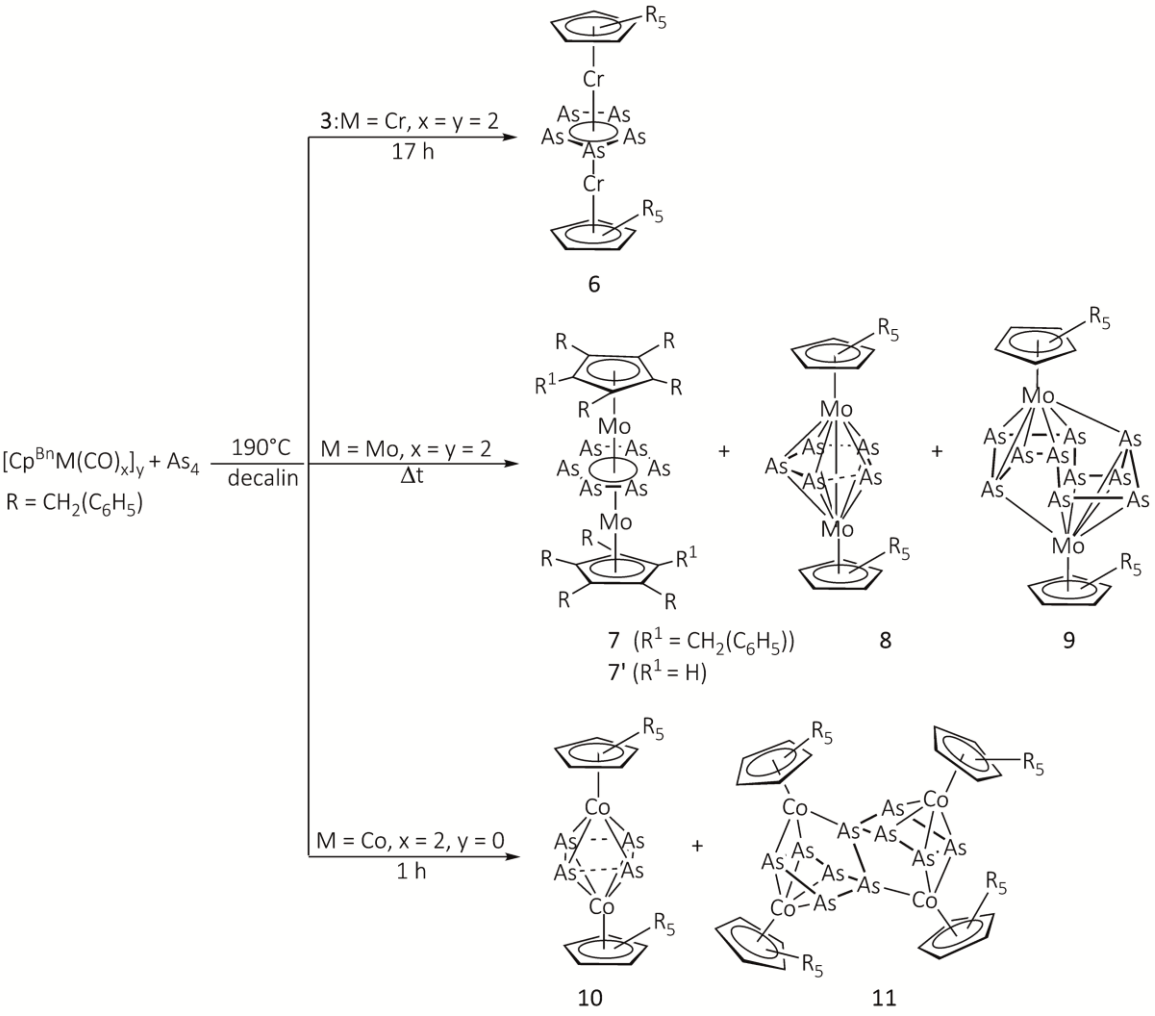

Scheme 11.2 Syntheses of the As_n ligand complexes **6**-**11**.

Starting from **3**, the reaction with As_4 exclusively leads to the formation of the triple decker complex $[(Cp^{Bn}Cr)_2(\mu,\eta^{5:5}\text{-}As_5)]$ (**6**) in moderate yields, exhibiting a *cyclo*-As_5 middle deck. In the case of the molybdenum derivative, several different triple decker complexes are obtained. Thereby, $[(Cp^{Bn}Mo)_2(\mu,\eta^{6:6}\text{-}As_6)]$ (**7**) and $[(Cp^{TetraBn}Mo)_2(\mu,\eta^{6:6}\text{-}As_6)]$ (**7'**) ($Cp^{TetraBn}$ = η^5-$C_5H(CH_2\{C_6H_5\})_4$) display the main product, co-crystallising in a 1:1 ratio. Both **7** and **7'** contain a *cyclo*-As_6 unit, which is stabilised in-between two $[Cp^{Bn}Mo]^+$ fragments. The presence of the $Cp^{TetraBn}$ ligand probably arises from impurities during the synthesis of the $Cp^{Bn}H$ ligand. Unfortunately, the formation of $Cp^{TetraBn}H$ cannot be eliminated and the separation by column

chromatographic workup failed. Moreover, the by-products $[(Cp^{Bn}Mo)_2(\mu,\eta^2\text{-}As_2)(\mu,\eta^3\text{-}As_3)]$ (**8**) and $[(Cp^{Bn}Mo)_2(\mu,\eta^{5:5:1:1}\text{-}As_{10})]$ (**9**) could be obtained in traces, depending on reaction time and stoichiometry of As_4. While **8** shows a distorted pseudo five-membered ring, consisting of a η^3-As_3 unit and a η^2-As_2 moiety, the *cyclo*-As_{10} ligand of **9** represents the largest known cyclic arsenic ligand reported so far. Changing to cobalt, the co-thermolysis of $[Cp^{Bn}Co(CO)_2]$ with As_4 results in the formation of $[\{Cp^{Bn}Co(\mu,\eta^{2:2}\text{-}As_2)\}_2]$ (**10**) and $[(Cp^{Bn}Co)_4(\mu_4,\eta^{4:4:2:2:1:1}\text{-}As_{10})]$ (**11**) in good yields. Complex **10** reveals a triple decker structure with two As_2 units as middle deck, whereas **11** shows an As_{10} framework, which can be considered as the hypothetic As_{10} dihydrofulvalene analogue.

(b) Co-Thermolysis Versus Transfer Reaction

Until now, the majority of As_n ligand complexes have been synthesised by co-thermolysis, leading to the thermodynamically most stable arsenic compounds. However, it has also been a subject of this thesis to investigate transfer reactions, since the reaction of $[Cp''_2Zr(\eta^{1:1}\text{-}As_4)]$ with $[Cp^{Bn}M(\mu\text{-}Br)]_2$ (M = Fe (**1**), Ni (**2**)) at room temperature is expected to give metastable arsenic complexes in good yields. In the case of nickel, the reactivity of **2** has also been studied towards $[Cp''_2Zr(\eta^{1:1}\text{-}P_4)]$, as preliminary studies on the Cp''' derivative $[Cp'''Ni(\mu\text{-}Br)]_2$ (Cp''' = η^5-1,2,4-$C_5H_2{}^tBu_3$) have shown an interesting reactivity pattern. In addition, it is reasonable to study the corresponding co-thermolysis of $[Cp^{Bn}M(CO)_x]_y$ (**4**: M = Ni, x = 0, y = 2; **5**: M = Fe, x = y = 2) with As_4 in comparison to the transfer reactions (Scheme 11.3).

The co-thermolysis of **4** with yellow arsenic at elevated temperatures leads to in the selective formation of $[(Cp^{Bn}Ni)_2(\mu,\eta^{3:3}\text{-}As_6)]$ (**12**), showing a $[Ni_2As_6]$ cubane structural core motif, whose composition is unknown for As_n ligand complexes of nickel so far. In contrast, the mild activation of *in situ* generated **2** with $[Cp''_2Zr(\eta^{1:1}\text{-}E_4)]$ (E = P, As) results in the formation of $[(Cp^{Bn}Ni)_3(\mu_3\text{-}E)_4\{Ni(\mu\text{-}Br)\}]_2$ (E = P (**13**), As (**14**)), displaying adjacent, distorted $[Ni_4(\mu\text{-}E_4)]$ cubanes, which are connected *via* bromide bridges (μ_2-fashion). Interestingly, the degradation of the E_4 unit of the Zr precursor to E atoms is observed, instead of a transfer of the intact E_4 moiety. Since **13** and **14** still contain bromide ligands, the question arose whether a further transfer reaction can take place. To confirm this assumption, **14** has been reacted with $[Cp''_2Zr(\eta^{1:1}\text{-}E_4)]$ to yield $[\{(Cp^{Bn}Ni)_3(\mu_3\text{-}As)_4Ni\}_2(\mu,\eta^{4:4}\text{-}E_4)]$ (E = P (**15**), E = As (**16**)). In complexes **15** and **16** the two distorted cubic $[Ni_4(\mu\text{-}As_4)]$ unit remain, but a connection of both occurs *via* a newly formed *cyclo*-E_4 ligand. Moreover, **15** represents an access to mixed E_n ligand complexes, which have been scarcely known up to now.

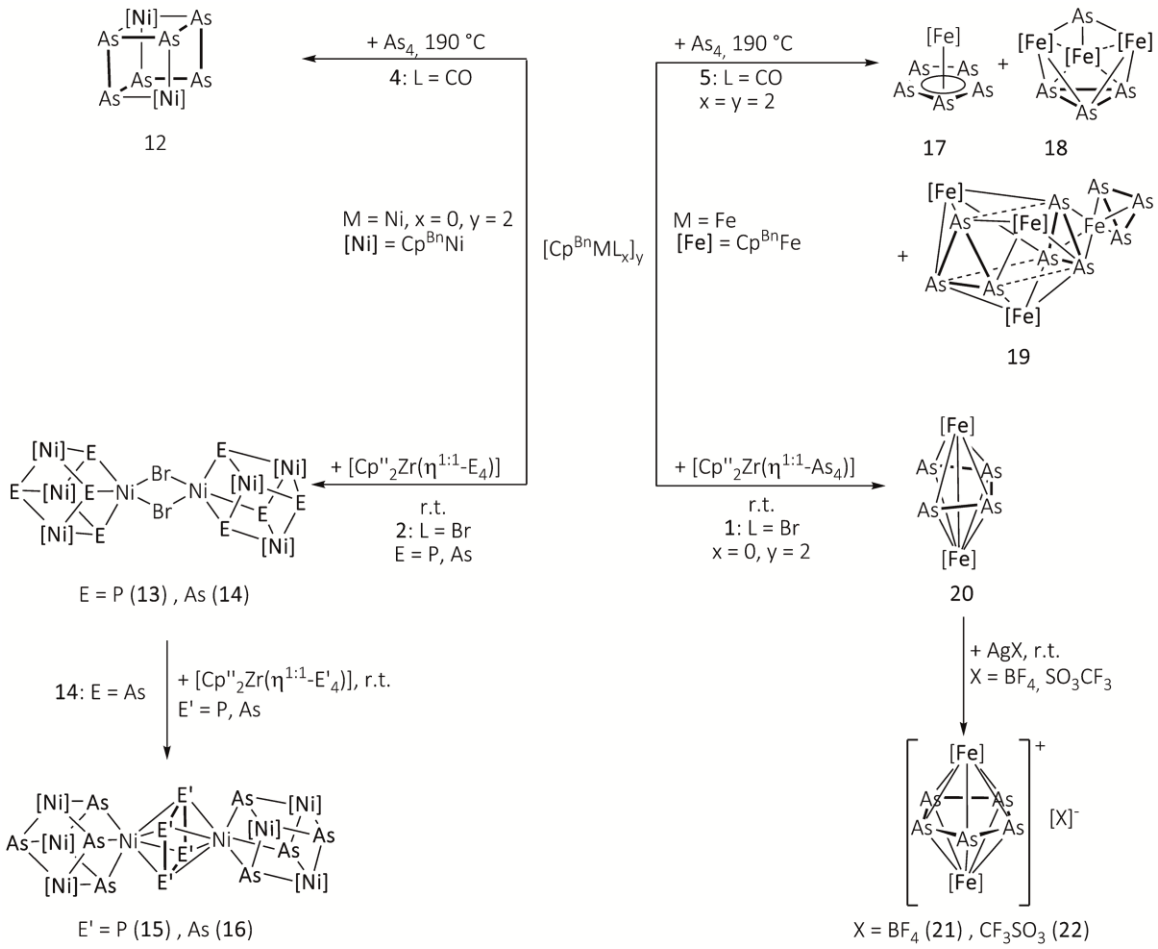

Scheme 11.3 Syntheses of the As_n ligand complexes 12-22.

In the case of iron, the reaction of 5 with As_4 affords a mixture of diverse As_n ligand complexes, consisting of the sandwich complex $[Cp^{Bn}Fe(\eta^5\text{-}As_5)]$ (17), $[(Cp^{Bn}Fe)_3(\mu_3,\eta^{2:2:2}\text{-}As_3)(\mu_3\text{-}As)]$ (18) and $[(Cp^{Bn}Fe)_3(\mu_3,\eta^{4:4:4}\text{-}As_6)\{Fe(\eta^3\text{-}As_3)\}]$ (19). Complex 17 is a representative of pentaarsaferrocene derivatives, whose Cp* congener has already been frequently used in coordination chemistry. In contrast, 18 and 19 display unprecedented iron containing arsenic clusters, which are unknown so far. The central structural core motif of 18 can formally be described by an insertion of $[Cp^{Bn}Fe]$ fragments into three As-As bonds of the As_4 tetrahedron, while 19 shows a prismatic As_6 ligand as well as an end-on coordinated *cyclo*-As_3 unit. However, transfer reaction of *in situ* generated 1 with $[Cp''_2Zr(\eta^{1:1}\text{-}As_4)]$ yields the triple decker complex $[(Cp^{Bn}Fe)_2(\mu,\eta^{4:4}\text{-}As_4)]$ (20), showing a *cisoid*-As_4 moiety. Since the redox chemistry of 20 has been investigated by CV, also chemical oxidation has been performed. Interestingly, the reaction of 20 with AgX ($X^- = BF_4^-$, $CF_3SO_3^-$) leads to an expansion of the four-membered tetraarsabutadiene moiety, resulting in the formation of $[(Cp^{Bn}Fe)_2(\mu,\eta^{5:5}\text{-}As_5)][X]$ ($X^- = BF_4^-$ (21), $CF_3SO_3^-$ (22)). Thereby, 21 and 22 possess a new formed *cyclo*-As_5 middle deck. In general, the complexes 6-22 show the versatility of the structural core motifs of As_n ligands in combination with transition metal complexes. On one hand the As_4

tetrahedron can often go through successive degradation, yielding smaller arsenic complexes, but on the other hand a subsequent aggregation to larger As_n units stabilised by transition metal fragments can also occur.

11.3 Reactivity of Selected As_n Ligand Complexes Towards Coinage Metal Salts

[Cp*Fe(η^5-As_5)] has been frequently used as a building block in coordination chemistry. Mainly its reactivity towards different monovalent metal salts, e.g. Cu^I halides, has been investigated and different coordination compounds have been obtained. In this context, the question arose whether the nature of the Cp ligand as well as the central metal atom of the pentaarsaferrocene derivatives of the general formula [Cp^RM(η^5-As_5)] (M = Fe, Cp^R = Cp^{Bn} (**17**); M = Ru, Cp^R = Cp*) influence the reactivity towards Cu^I halides. Furthermore, so far the use of copper(I) salts has been limited to Cu^I halides exclusively. Therefore, it was also part of this thesis to investigate the coordination behaviour of [Cp*Fe(η^5-As_5)] towards other Cu^I sources, e.g. $Cu(CF_3SO_3) \cdot 0.5\ C_7H_8$ (Scheme 11.4).

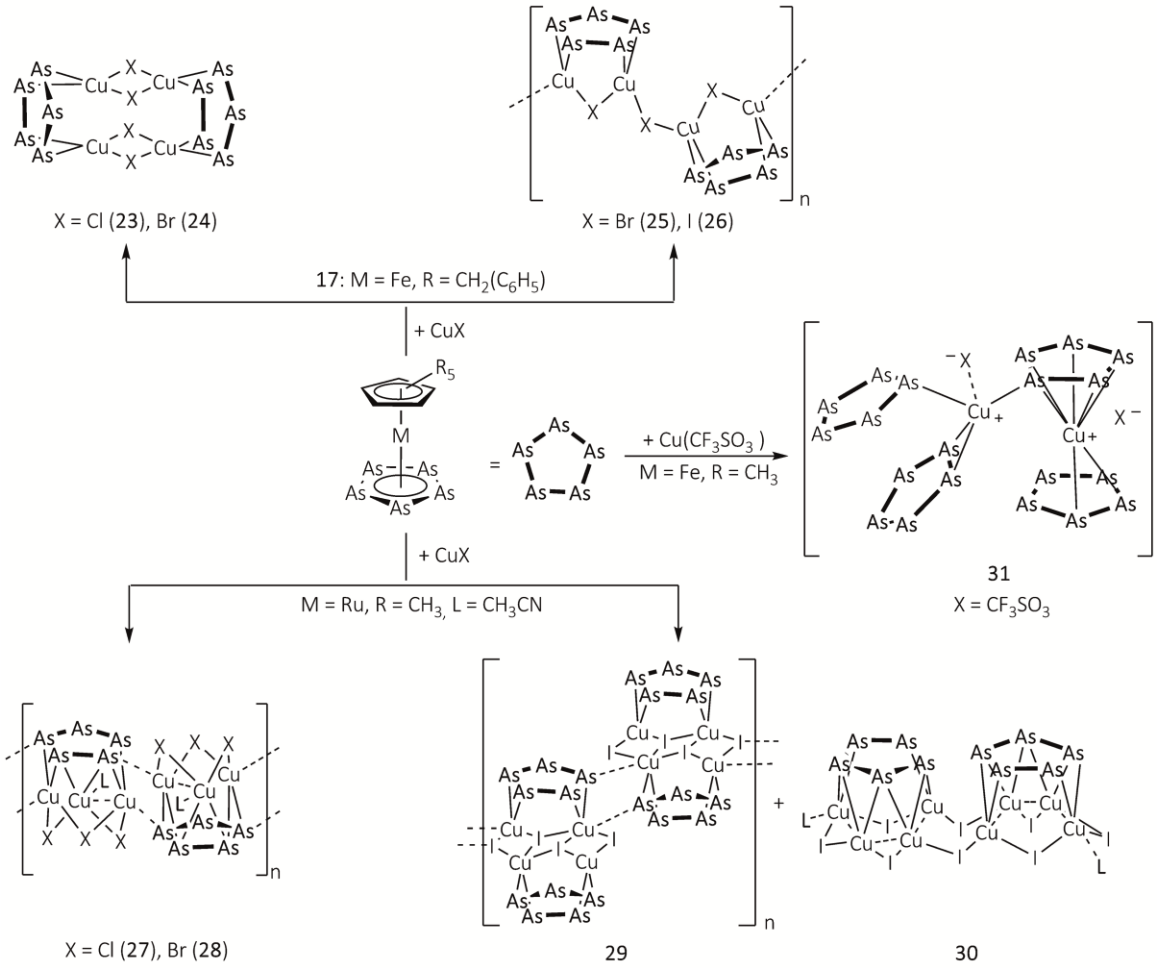

Scheme 11.4 Reactions of selected pentaarsaferrocene derivatives with copper(I) salts.

The diffusion reaction of the Cp^{Bn} derivative **17** with CuX (X = Cl, Br) leads to the formation of the discrete dimer $[\{Cp^{Bn}Fe(\eta^{5:2:2}\text{-}As_5)\}\{Cu(\mu\text{-}X)\}_2]_2$ (X = Cl (**23**), Br (**24**)). Complexes **23** and **24** show two adjacent moieties of **17**, coordinating Cu^I atoms by an As-As bond (η^2-coordination), which are part of a $\{Cu_2(\mu\text{-}X)_2\}$ four-membered linking unit. In the case of the CuCl derivative, **23** is the only observed dimer. However, using CuBr also yields the one dimensional polymer $[\{Cp^{Bn}Fe(\eta^{5:2:2}\text{-}As_5)\}\{Cu(\mu\text{-}Br)\}_2]_n$ (**25**). Here, one molecule of **17** is coordinating two copper atoms (η^2-fashion), which are bridged by bromide atoms (μ_2-mode) to form the scarcely reported zigzag structural core motif. By reacting **17** with CuI, the isostructural compound $[\{Cp^{Bn}Fe(\eta^{5:2:2}\text{-}As_5)\}\{Cu(\mu\text{-}I)\}_2]_n$ (**26**) is obtained. Consequently, an increase of complexity from dimers to one dimensional polymers is observed for coordination compounds containing **17** and CuX by going from CuCl to CuI. In contrast, the diffusion reaction of $[Cp^*Ru(\eta^5\text{-}As_5)]$ with CuX (X = Cl, Br) results in the selective formation of $[\{Cp^*Ru(\eta^{5:2:2:2}\text{-}As_5)\}\{Cu(\mu\text{-}X)\}_3(CH_3CN)]_n$ (X = Cl (**27**), Br (**28**)). Both **27** and **28** are isomorphs to $[\{Cp^*Fe(\eta^{5:2:2:2}\text{-}As_5)\}\{Cu(\mu\text{-}X)\}_3(CH_3CN)]_n$ (X = Cl, Br), displaying a π-coordination of the Cu^I atoms, which are part of a six-membered chair like $\{CuX\}_3$ ring. Additionally, the moieties are linked *via* intermolecular Cu···As interactions to give a one dimensional polymer. In this context, the obtained coordination products **23**-**28** seem to be independent of the metal atom or the used Cp^R ligand, but a strong dependency on the Cu^I halide occurs. This is also demonstrated by using CuI, which affords the one dimensional polymer $[\{Cp^*Ru(\eta^{5:2:2}\text{-}As_5)\}\{Cu(\mu\text{-}I)\}\{Cu(\mu_3\text{-}I)\}]_n$ (**29**) and the dimer $[\{Cp^*Ru(\eta^{5:2:2:2:2}\text{-}As_5)\}\{Cu(\mu\text{-}I)\}_4(CH_3CN)]_2$ (**30**). The central structural motif in **29** reveals a $\{CuI\}_4$ ladder, which is connected either by Cu···As or Cu···I interactions, resulting in a one dimensional strand. Polymer **29** shows close structural similarity to the reported one dimensional polymer containing the Cp* iron derivative. In contrast, the dimer **30** exhibits an unknown modified crown like structural core motif, built up by four moieties of Cu^I (η^2-coordination) which are connected by weak Cu···Cu interactions or by iodide atoms (μ_2-fashion). In the coordination compounds **23**-**30** the preference of As_n ligand complexes for π-coordination is obvious, while σ-coordination plays a minor role. However, the reaction of $[Cp^*Fe(\eta^5\text{-}As_5)]$ with $Cu(CF_3SO_3) \cdot 0.5\, C_7H_8$ exclusively yields the soluble discrete dimer $[Cu_2\{Cp^*Fe(\eta^{5:5:1}\text{-}As_5)\}\{Cp^*Fe(\eta^{5:2}\text{-}As_5)\}_2\{Cp^*Fe(\eta^{5:1}\text{-}As_5)\}\{CF_3SO_3\}_2]$ (**31**), revealing an unprecedented η^5-coordination mode, an uncommon σ-coordination of the *cyclo*-As_5 complex to Cu^I as well as the favoured π-coordination of two adjacent *cyclo*-As_5 units. In addition, one triflate anion interacts with Cu^+, while the other counterion is separated. Moreover, $[Cp^*Fe(\eta^5\text{-}As_5)]$ has been reacted with AgX (X^- = ClO_4^-, BF_4^-), which bears a coordinating anion. This is of interest, since not much is known about the coordination behaviour of the pentaarsaferrocene derivative towards Ag^I salts. These reactions lead to the formation of $[Ag\{Cp^*Fe(\eta^{5:2:2}\text{-}As_5)X]_2$ ($X^- = ClO_4^-$

(**32a**), BF_4^- (**33a**)) and $[Ag\{Cp^*Fe(\eta^{5:3:2}\text{-}As_5)\}X]_2$ ($X^- = ClO_4^-$ (**32b**), BF_4^- (**33b**)), which crystallise as co-crystals in the solid state (Scheme 11.5). Both **32** and **33** show either an unexpected $\eta^{3:2}$-coordination (**32b**/**33b**) or $\eta^{2:2}$-coordination (**32a**/**33a**) and an additional interaction of the ClO_4^- or BF_4^- anions with the Ag^+ centre. Interestingly, short Ag···Ag distances are observed, being sometimes even shorter than the sum of the covalent radii of silver. Moreover, **33** can be used as a transfer reagent of As_n units by reacting the latter with $[Cp'''Co(\mu\text{-}Cl)]_2$. Surprisingly, here the *cyclo*-As_5 ligand is degraded and rearranged to give $[(Cp'''Co)_3(\mu_3,\eta^{4:4:4}\text{-}As_6)][BF_4]_2$ (**34**) as well as the by-product $[(Cp'''Co)_2(\mu_2\text{-}Cl)_3][BF_4]$ (**35**).

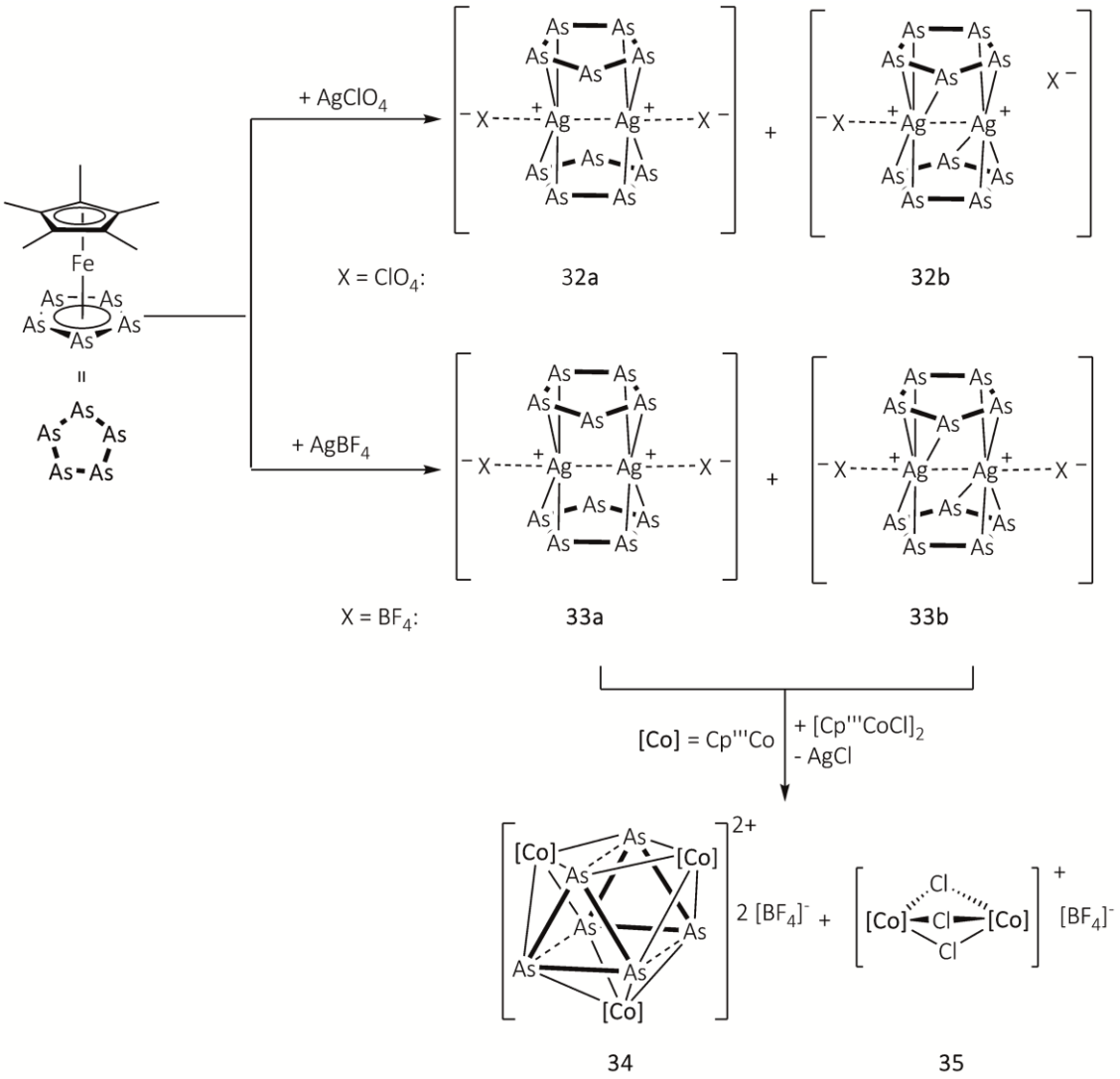

Scheme 11.5 Reaction of **33** with $[Cp'''Co(\mu\text{-}Cl)]_2$ at room temperature.

11.4 Investigation on the Redox Chemistry of [Cp*Fe(η^5-As_5)]

A minor part of this thesis has been the investigation of the redox chemistry of [Cp*Fe(η^5-As_5)]. Within this context, the chemical reduction with KH or K leads to the unprecedented degradation and rearrangement of the former *cyclo*-As_5 ligand to give a mixture of diverse anionic polyarsenide complexes (Scheme 11.6). Besides the triple decker complex [{Cp*Fe(μ,$\eta^{2:2}$-As_2)}$_2$]$^-$ ([**36**]$^-$) and the dianion [(Cp*Fe)$_2$(μ,$\eta^{4:4}$-As_{10})]$^{2-}$ ([**37**]$^{2-}$) even larger polyarsenide As_n frameworks - up to n = 14 and n = 18 – stabilised by [Cp*Fe] fragments could be obtained. This includes [(Cp*Fe)$_2$(μ,$\eta^{4:4}$-As_{14})]$^{2-}$ ([**38**]$^{2-}$) as well as [(Cp*Fe)$_4${μ$_4$,$\eta^{4:4:4:4}$-As_{18}}]$^{2-}$ ([**39**]$^{2-}$). Compound [**38**]$^{2-}$ possesses two connected norbornadiene like As_7 moieties, whereas [**39**]$^{2-}$ consists of a chair like As_6 subunit, which is connected through adjacent arsenic atoms to an envelope like As_5 ligand as well as to a norbornadiene like As_7 cage. Remarkably, [**36**]$^-$, [**38**]$^{2-}$ and [**39**]$^{2-}$ are not formed due to decomposition and reaggregation of [**37**]$^{2-}$, which has been confirmed by ^{1}H NMR spectroscopy. Moreover, [**38**]$^{2-}$ and [**39**]$^{2-}$ represent the largest anionic As_n ligand complexes reported, which are obtained in coordination chemistry so far.

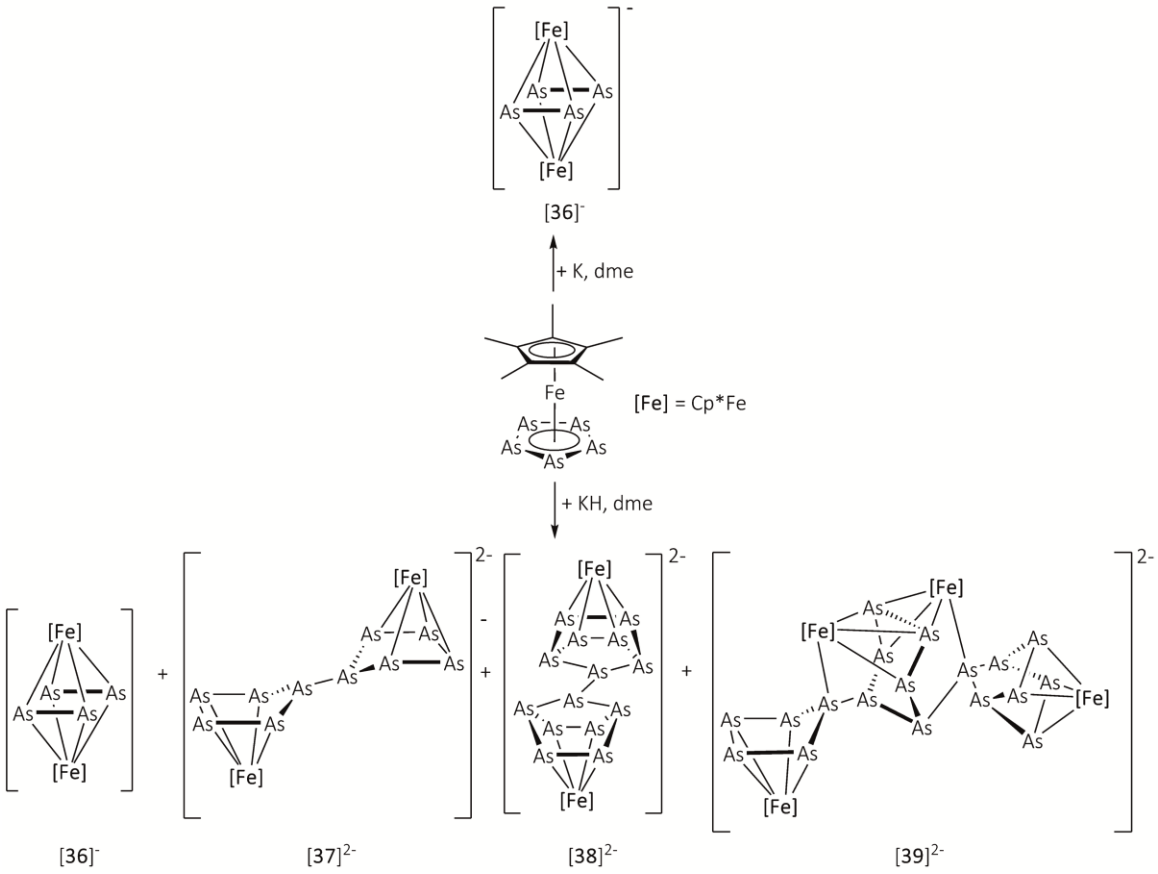

Scheme 11.6 Chemical reduction of [Cp*Fe(η^5-As_5)] with KH or K in dme.

12. Appendices

12.1 Alphabetic List of Abbreviations

Å	Angstroem, 1 Å = $1 \cdot 10^{-10}$ m
°C	degree Celsius
AO	atomic orbital
av.	average
^{n}Bu	*n*-butyl, C_4H_9
^{t}Bu	*tert*-butyl, C_4H_9
butterfly	*bicyclo*[1.1.0]butane
c	concentration
CAAC	cyclic (alkyl)(amino)carbenes
^{c}Hex	*cyclo*-hexyl, C_6H_{10}
COSY	correlation spectroscopy
COD	cycloocta-1,5-diene, C_8H_{12}
Cp	cyclopentadienyl, η^5-C_5H_5
Cp’	ethyltetramethylcyclopentadienyl, η^5- C_5EtMe_4
Cp’’	1,3-di-*tert*-butylcyclopentadienyl, η^5-$C_5H_3{}^{t}Bu_2$
Cp’’’	1,2,4-tris-*tert*-butylcyclopentadienyl, η^5-$C_5H_2{}^{t}Bu_3$
Cp*	pentamethylcyclopentadienyl, η^5-C_5Me_5
Cp^{BIG}	pentakis-4-*n*-butylphenylcyclopentadienyl, η^5-$C_5(4\text{-}{}^{n}BuC_6H_4)_5$
Cp^{Bn}	pentabenzylcyclopentadienyl, η^5-$C_5(CH_2\{C_6H_5\})_5$
$Cp^{TetraBn}$	tetrabenzylcyclopentadienyl, η^5-$C_5H(CH_2\{C_6H_5\})_4$
Cp^{3iPr}	triisopropylcyclopentadienyl, η^5-$C_5H^{i}Pr_3$
Cp^{4iPr}	tetraisopropylcyclopentadienyl, η^5-$C_5H^{i}Pr_4$
Cp^{Pr}	tetramethylpropylcyclopentadienyl, η^5-$C_5Me_4{}^{n}Pr$
Cp^{3Me}	trimethylcyclopentadienyl, η^5-$C_5H_2Me_3$
Cp^{Me}	methylcyclopentadienyl, η^5-C_5H_4Me
Cp^{tBu}	tetramethyltertbutylcyclopentadienyl, η^5-$C_5Me_4{}^{t}Bu$
Cp^{+}	*tert*-butylcyclopentadienyl, η^5-$C_5H_4{}^{t}Bu$
Cp^{R}	substituted cyclopentadienyl ligand
CV	cyclic voltammetry

d(NMR)	doublet
δ	chemical shift
dd(NMR)	doublet of doublets
decalin	decahydronaphthalene, $C_{10}H_{18}$
DFT	density functional theory
Dipp	2,6-diisopropylphenyl
DIP_2pyr	2,5-bis{N-(2,6-diisopropylphenyl)iminomethyl}pyrrolyl
IDipp	1,3-bis(2,6-diisopropylphenyl)imidazol-2-ylidene,
dme	1,2-dimethoxyethane, $C_4H_{10}O_2$
dpmp	bis(diphenylphosphinomethyl)phenylphosphine
dppe	1,2-bis(diphenylphosphino)ethane
DSC	differential scanning calorimetry
E	heavier element of the 15^{th} group, E = P, As
E(CV)	potential
e^-	electron
EI MS	electron impact mass spectrometry
EPR	electron paramagnetic resonance
Et	Ethyl, C_2H_5
ESI MS	electron spray ionisation mass spectrometry
f	frequency
FAL	$[FAl\{OC_6F_{10}(C_6F_5)\}_3]$
FD MS	field desorption ionization mass spectrometry
h	hour(s)
HMBC	heteronuclear multiple bond correlation
HOMO	highest occupied molecular orbital
HSQC	heteronuclear single quantum coherence
Hz	Hertz
IR	infrared spectroscopy
J(NMR)	coupling constant
K	Kelvin
L	ligand (specified in text)
L	litre
L^{iPr}	$CH[CMeN(2,6\text{-}^iPr_2C_6H_3)]_2)$

LMO	localised molecular orbital
LUMO	lowest unoccupied molecular orbital
M	metal
μ_B	Bohr magneton
μ_{eff}	effective magnetic moment
m(NMR)	multiplet
m/z	mass to charge ratio
Me	methyl, CH_3
MHz	megahertz, 10^6 Hz
mg	milligram, 10^{-3} g
mL	milliliter, 10^{-3} L
menthyl	1-*iso*-propyl-1-methylcyclohexane, $C_{10}H_{20}$
Mes	mesityl, 2,4,6-trimethylphenyl, C_9H_{11}
MOF	metal organic framework
NMR	nuclear magnetic resonance
N_3N	$(Me_3SiNCH_2CH_2)_3N$
NPA	natural population analysis
ν	frequency/wavenumber
OTf	triflate, $CF_3SO_3^-$
Ph	phenyl, C_6H_5
^{i}Pr	*iso*-propyl, C_3H_7
^{n}Pr	*n*-propyl, C_3H_7
PPh_3	triphenylphosphine, $P(C_6H_5)_3$
ppm	parts per million
R	organic substituent
r.t.	room temperature
s(NMR)	singlet
s(CV)	second(s)
TEF	$[Al\{OC(CF_3)_3\}_4]$
T	temperature
t(NMR)	triplet
thf	tetrahydrofurane, C_4H_8O
V(CV)	Volt
VE	valence electron

vs(IR)	very strong
w(IR)	weak
WBI	wiberg bond index
χ_m	molar susceptibility

12.2 Acknowledgments

At this point I want to thank…

- Prof. Dr. Manfred Scheer for giving me the opportunity to work in his group on such an interesting project and the excellent working conditions.
- My family for their support during the last years.
- Dr. Gábor Balázs for his help in all points of daily (lab) life and for the DFT calculations.
- Dr. Eugenia Peresypkina, Prof. Dr. Alexander V. Virovets and Dr. Michael Bodensteiner for their help with the single crystal X-ray structure analyses, although I 'produce' every crystallographic problem one can imagine.
- Andreas Seitz for just being my best friend in every situation and for the patience you have shown during several periods of 'Ich muss noch schnell aufs Klo' and since 'I'm a Pfloatsch'.
- Felix for all the funny moments on the balcony between 'I need a Schoki' and 'despair'.
- Andi, Eva-Maria, Fabi, Claudi and Sebi for all the funny evenings, partys and 'discussions'.
- The girl's lab (Andrea and Claudia) for a great time also beyond research.
- Andreas Seitz, Eva-Maria Rummel, Felix and Dr. Gábor Balázs for accurate proof reading.
- Eric Mädl and Felix Riedlberger for the cyclovoltammetric measurements.
- Moritz Modl for the EPR measurements and for his help in all points of technic.
- Dr. Ilya Shenderovich, Anette Schramm, Georgine Stühler and Fritz Kastner for the measurement of the NMR spectra.
- Josef Kiermaier and Wolfgang Söllner for the mass spectrometric analyses.
- Helmut Schüller and Barbara Baumann for elemental analyses.
- The staff of glass blowing, electronic and mechanic facilities of the University of Regensburg
- all present and former members of the research group: Barbara B., Barbara, Bianca, Bodi, Christoph, Dani, David, Eric, Helena, Hias, Jens, Julian, Karin, Küken, Liese, Luis, Luigi, Marcella, Martin, Martina, Matthias, Mehdi, Mia, Michi, Miriam, ML, Moartl, Moritz, Musch, Muschine, Olli, Petra, Rebecca, Reini, Robert, Rudi, Sabine, Sμ, Schotti, Stubi, Susanne, Thomsi, Tobi, Valentin, Walter, Wast, Wurzl.